Australian Government

Geoscience Australia

Proceedings of the 2012 Australian Geothermal Energy Conference

Edited by C. Huddlestone-Holmes, E. Gerner

2012 Australian Geothermal Energy Conference
www.ausgeothermal.com
14–16 November – Coogee Beach, Sydney
Unleashing the Heat

Proceedings of the 2012 Australian Geothermal Energy Conference

Australian Government
Geoscience Australia

2012 Australian Geothermal Energy Conference
14-16 November – Coogee Beach, Sydney
Unleashing the Heat

1. CSIRO
2. Geoscience Australia

Department of Resources, Energy and Tourism
Minister for Resources and Energy: The Hon. Martin Ferguson, AM MP
Secretary: Mr Drew Clarke

Geoscience Australia
Chief Executive Officer: Dr Chris Pigram

This paper is published with the permission of the CEO, Geoscience Australia

Geoscience Australia has tried to make the information in this product as accurate as possible. However, it does not guarantee that the information is totally accurate or complete. Therefore, you should not solely rely on this information when making a commercial decision.

Sponsors

petra**therm**

Government of South Australia
Department for Manufacturing,
Innovation, Trade, Resources and Energy

CSIRO

GreenRock
Energy

HR
hot rock

GT
Power

Greenearth Energy Ltd.

TRADE EXHIBITOR	MEDIA PARTNER

Government of **Western Australia**
Department of **Mines and Petroleum**

ecogeneration
The voice for Australia's clean energy industry
www.ecogeneration.com.au

Organising Committee

Peter Reid – Chair	Petratherm Ltd
Susan Jeanes	Chief Executive, AGEA
Vicki Cleveland	AGEA
Graeme Beardsmore	Hot Dry Rocks Pty Ltd
Betina Bendall	South Australian DMITRE
Anthony Budd	Geoscience Australia
Hal Gurgenci	University of Queensland
Cameron Huddlestone-Homles	CSIRO

Technical Committee

Cameron Huddlestone-Holmes	CSIRO
Betina Bendall	South Australian DMITRE
Ed Gerner	Geoscience Australia
Hal Gurgenci	University of Queensland
Chris Matthews	Panax Ltd
Doone Wyborn	Geodynamics Ltd

Conference secretariat

Lisa Beckham	Sapro Conference Management

Introduction

This volume is a compilation of the Extended Abstracts presented at the 2012 Australian Geothermal Energy Conference, 14-16 November 2012, Crowne Plaza, Coogee Beach, Sydney, organised by the Australian Geothermal Energy Association and the Australian Geothermal Energy Group.

As editors of these proceedings we are very grateful for the generosity of the Technical Committee. Their assistance in reviewing abstracts and working with authors was an essential contribution to the preparation of the quality technical program for this conference.

We would also like to thank the Conference Chair Peter Reid and the rest of the Organising Committee who stepped up to arrange this event on behalf of the Australian Geothermal Energy Association and the Australian Geothermal Energy Group for the benefit of the whole Australian geothermal sector.

Lisa Beckham and Sapro Conference Management have done an excellent job in assisting the Organising Committee.

We also thank again the sponsoring organisations for their generous support.

We thank Geoscience Australia for publishing these proceedings, and Dan Rawson for his production work.

Most importantly, we thank the delegates for their interest and attendance, which makes this all worthwhile. Their continued dedication to exploring the potential of geothermal energy in Australia will be critical if we are to succeed in unleashing the heat.

Cameron Huddlestone-Holmes

Ed Gerner

Contents

Natural fracture networks enhancing geothermal producibility, mapping or predicting!

Abul Khair, H.[1], Cooke, D.[1], & Hand, M.[2]

[1]Centre for Tectonics, Resources and Exploration (TRaX), Australian School of Petroleum, University of Adelaide, North Terrace, Adelaide SA 5005. [2]SA Centre for Geothermal Energy Research, University of Adelaide, SA 5005, Australia.

Hani.Abulkhair@adelaide.edu.au

Abstract

Subsurface natural fracture networks that act as conduits for thermal fluids play an important role in geothermal reservoirs. The success of enhanced geothermal systems is mainly reliant on modelling the orientation of the pre-existing natural fracture networks within the reservoir. This will help modelling the direction of movement of the hydrothermal fluids, and in locating sweet spots and/or possible orientation of susceptible fractures for further stimulation programs. We applied both mapping and predicting techniques on sand and shale intervals in the Cooper Basin/South Australia and calibrated these techniques using image logs, well data, and quality seismic in order to validate their ability to model subsurface fracture networks.

We used most positive curvature attribute to generate a workflow for modelling subsurface fractures with high confidence. As the curvature attributes are known to be sensitive to the acquisition direction, we reduced all acquisition artefacts using structural smoothening and generated a seismic cube that is free of data acquisition artifacts. A final curvature volume was produced after eliminating low values that don't reflect any structural features. A validation procedure was applied using image logs, well data, and seismic sections and a high correlation was found between the curvature mapped fractures and the image logs fractures.

Another technique used in this study was to integrate geological and geophysical data extracted from fault and horizon seismic interpretation with geomechanical analyses of stress, strain, and displacements associated the structural development of the basin. Finite element method (FEM) and boundary element method (BEM) are two ways used to predict fractures generated during the tectonic events of basins. FEM provides a physically-based soluiton for subsurface issues related to fractures and basin evolution taking into consideration horizon geometry, heterogeneous rock properties and stresses generated from structural features. The BEM method considers the effect of fault displacement on generating stress and near the fault. One of the disadvantages of BEM is that it doesn't consider rock heterogeneity or the effect of intra-seismic relaxation on fracture generation. Also, BEM ignores far field stress data, and thus does not predict fracture generation away from the major faults.

The validation procedure was applied on fractures predicted from FEM and BEM, and a good correlation was found between the predicted fracture network and the image logs fractures next to the major faults in both methods as fractures in these areas were mostly generated due to strain exerted during fault displacement. FEM succeeded in predicting fractures close to and away from major faults with higher accuracy while BEM didn't map fractures away from faults. Thus, both FEM and enhanced most positive curvature attributes can be used successfully to model subsurface fracture networks that will locate productive spots with good permeability.

Introduction

Geothermal energy is increasingly attracting the interest of the governments as a strategic green energy source for electricity generation, especially with the gradual depletion of conventional reservoirs. The traditional geothermal systems consist of injection and production wells drilled to subsurface hot reservoirs. Cold water is pumped to the target reservoir, heated, and returned to the surface via production wells. The success of this type of geothermal systems is highly reliant on water

circulation within a network of fractures between the injection and production wells. Accurate detection or prediction of pre-existing fracture network and current day stress regime, is of high importance for enhanced geothermal systems well planning, and fracture stimulation programs.

Cooper Basin is a potential Australian geothermal basin, it is a Late Carboniferous to Middle Triassic basin located in the eastern part of central Australia (Fig. 1). The Cooper Basin floor was carved out of the ground uplifted after the end of the formation of Warburton Basin rocks (Preiss, 2000). Following the deposition of the Cambrian-Ordovician sequences of the eastern Warburton Basin underlying the Cooper Basin, NW-SE compression caused a partial inversion of the Warburton Basin, deformation of the pre-existing sequence and the subsequent intrusion of Middle to Late Carboniferous granites (Gatehouse et al., 1995; Gravestock and Flint, 1995; Alexander and Jensen-Schmidt, 1996). From Early to Late Permian, the basin was filled with around 1200 m of clastic sediments and coals deposited in glacio-fluvial to fluvial to open basin environments (Paten, 1969; Stuart, 1979; Thornton, 1979; Powell and Veevers, 1987).
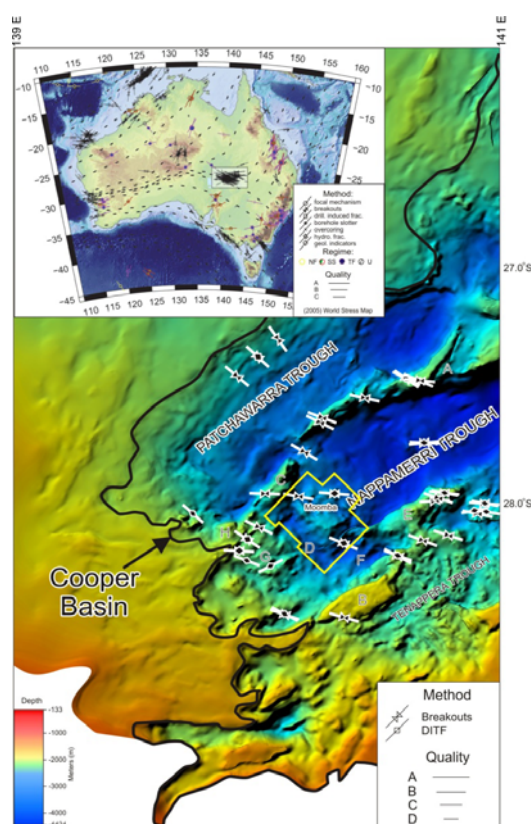
Figure 1: Top Warburton Basin (Pre-Permian Basement, seismic horizon Z) in the Cooper Basin. Map shows NE-SW major troughs separated by ridges. Study area is located at the south-western termination of the Nappamerri trough (Moomba-Big Lake 3D seismic cube outlined in yellow). A: Innamincka Ridge; B: Murteree Ridge; C: Gidgealpa-Merrimelia Ridge; Wooloo Trough; E:Della-Nappacoongee Ridge; F: Allunga Trough; H: Warra Ridge. Top left: Australian stress map (Modified after Hillis and Reynolds, 2000 and World Stress Map, 2010).

The granites bodies underlying the 4 km thick Cooper Basin sediments in some areas are believed to be the source of high temperatures and high geothermal gradients recognized in deep sediments within the basin (Deighton & Hill 1998). This led to considering the basin as the most significant Australian geothermal basin recognized to date (Somerville et al. 1994).

Curvature attributes

Seismic attributes are currently used and abused in mapping fracture networks. In the current study, we used seismic attributes and validated them using seismic and well controls. Among the many seismic attributes used in geophysical studies, structurally smoothed, non-steered and dip steered curvature attributes including most-positive curvature (MPC) and most negative (MNC), have proven most successful in delineating features that are mostly folds, faults and/or fractures (Fig. 2). Ant tracking and automatic fault extraction were used in order to help modelling the mapped features in 3D for better validation.
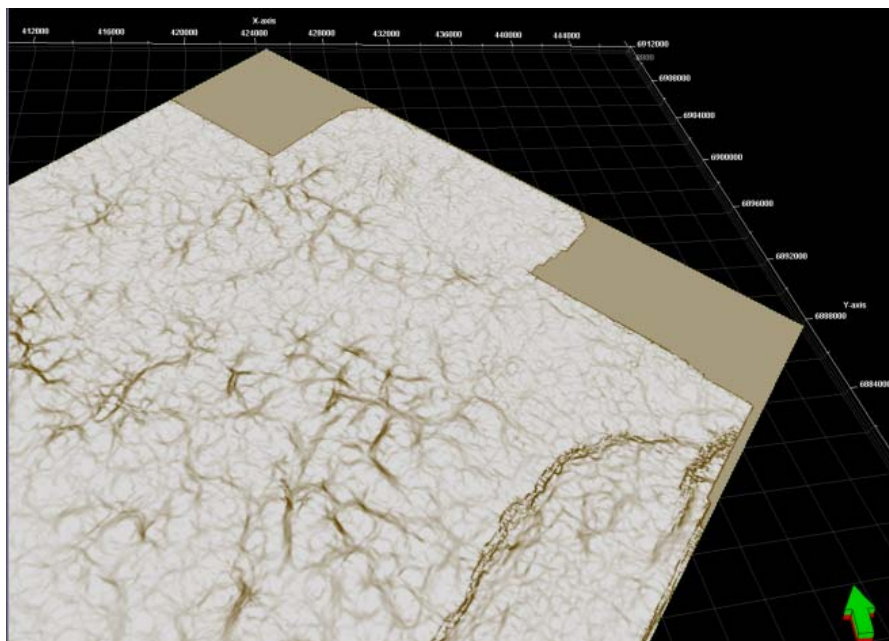
Figure 2: Most positive curvature attribute of the Moomba-Big lake fields. Features represent faults, accompanying large fractures ,and anticlines.

Curvature is defined as the reciprocal of the radius of a circle that is tangent to the given curve at a point (Chopra and Marfurt, 2007). An observed high value of curvature corresponds to a curved sufrace, whereas curvature will be zero for a straight line). The curvature attribute enables mapping of geological structures, such as folds or faults, which are characterized by high curvature (Backe et al., 2011; Abul Khair et al., 2012). MPC attribute delineates up-thrown fault blocks and crests of antiforms, whilst MNC attributes delineates the down-thrown faulted blocks of faults in addition to synclines (Chopra and Marfurt, 2007). In this study we used around 300 wells to calibrate the curvature results.

Image logs

A total of 7 wells containing image logs were analysed and compared with the curvature signatures. More than 70% of fractures interpreted using image logs were found to correspond to the seismic curvature attribute. By comparing the structures that appear on seismic, it was clear that whenever an anticline is present, the signature on the curvature will be reflecting the fold axis, and the fractures on image logs will mostly be perpendicular to the fold hinge with less percentage parallel to it (Fig. 3).
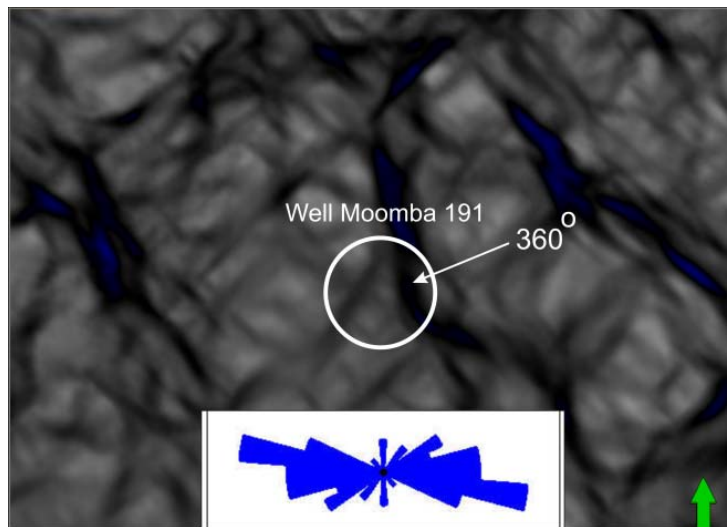
Figure 3: *Most positive curvature attribute at the depth of 8776 ft showing a main signature striking north-south, and a rose diagram of image log fractures showing east-west.*

During the formation of an anticline, the maximum horizontal stress (SHmax) is perpendicular to the fold axis, this will cause the rocks to fracture in the direction of SHmax if the rock reached failure conditions and if the deviatoric stress was relatively high. Due to the maximum bending at the hinge of the anticline, weakness of rocks will generate a new set of fractures parallel to the hinge and perpendicular to the old set. If we added to this scenario the existence of an old set of fractures that was generated due to an older tectonic event in a direction other than the event that caused the formation of the fold, then we will have a group of fractures as in figure 4. Thus, curvature attributes will map fractures caused by the formation of the current fold and faults, in addition to other tectonic events.
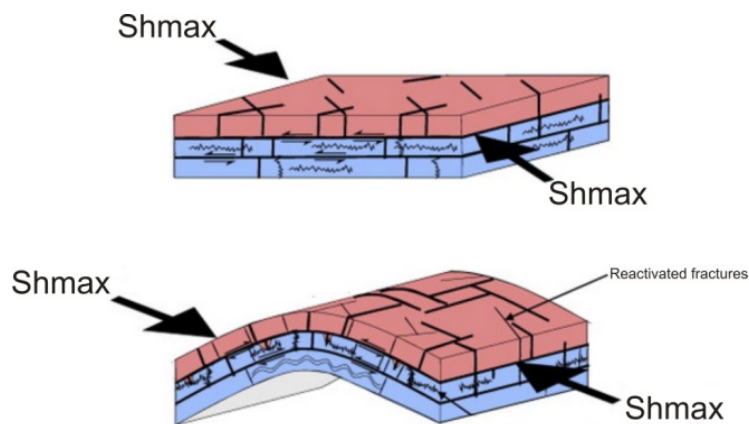
Figure 4: *Schematic figure showing the generation of different sets of fractures at different tectonic stages.*

Seismic amplitudes

By comparing the curvature signatures to the seismic structures, a high correlation was found with more than 70% of the curvature signatures presented in seismic as either anticlines or small faults with offsets 1 ms or more. A new seismic volume was generated using all the curvature signatures more than a cut-off value that doesn't map any structure. This value should be examined for every survey by comparing the curvature values to seismic structures before generating the new volume that represents only the available structures (Fig. 5)
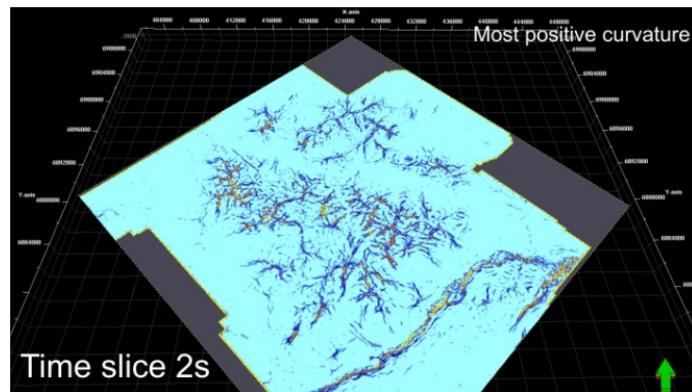
Figure 5: Most positive curvature attribute calculated after eliminating the values less or equal to 0.2, which is the cut off for Moomba field.

Well control

Considering the fact that any fault cutting a well will cause thickness change, isopach maps were generated and compared to seismic and curvature signatures.

A consistent relationship was found between the isopach anomalies and the seismic and curvature signatures. It was found that whenever an anomalie exists, a deep fault will be seen on seismic, although it may not cut target horizon, and a strong curvature signature will be obvious. This indicates that the fault is present, but because of the seismic resolution, faults with small offsets aren`t apparent, on the other hand, curvature will map it (Fig. 6).
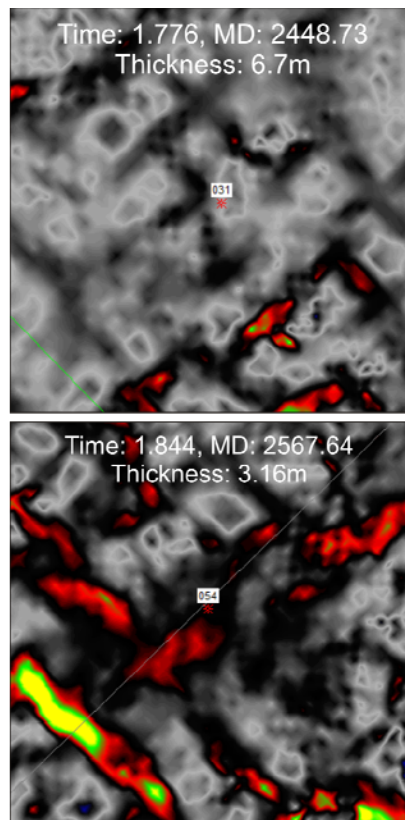
Figure 6: Time slice showing weak MPC signature due to normal formation thickness (upper photo), and strong MPC signature due to thickness reduction (lower photo). Normal thickness is measured to be 7 m.

Elastic Dislocation (ED)

Elastic dislocation theory (ED) predicts the distribution of strain and stress in the rocks surrounding major faults by using mapping of fault geometry and slip distribution in 3D data sets (Dee et al, 2007). ED is a BEM in which faults are represented as dislocations in an isotropic elastic medium (Crouch and Starfield, 1983). It addresses the effect of large faults displacements on the distribution of strain in the rocks surrounding them using the algorithms of Okada 1992, and software Traptester (Fig. 7).
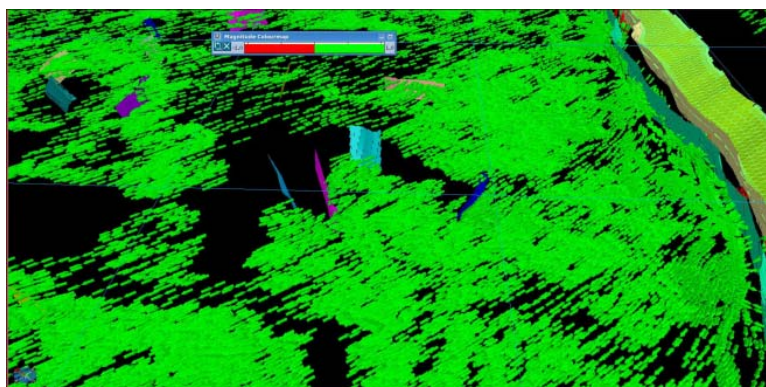
Figure 7: Variation of maximum principle stress around Big Lake fault. Notice the major stress disruption close to the fault and the consistency away from the fault.

Like other modelling techniques, ED doesn`t consider all factors that might influence fracture generation particularly variations in rock properties. Another point in ED is that considering an elastic rheology for the medium is valid for "infinitesimal" strains rather than finite strains (Ramsay, 1967). Also, experiments proved that better results can be achieved in reverse and normal faults stress regimes compared with strike-slip stress regimes as in Cooper Basin (Dee et al, 2007).

Comparing the predicted fractures from ED method with image logs fractures showed a clear correlation within the wells close to the major fault (Fig. 8). Whereas, wells away from the major fault didn`t succeed in predicting the fractures that can be seen in the image logs. This is clear as most of the fractures close to big faults are likely to be generated due to stresses exerted from the faults during major slip movements rather than other factors.

Other fracture trends seen in image logs (Fig. 8), which are not correlating with predicted fractures, emphasise the fact that generation of fractures is controlled by combination of factors rather than one specific methodology.
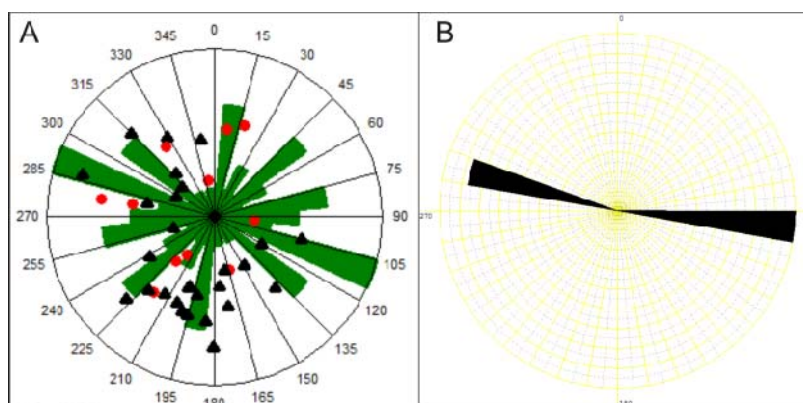
Figure 8: Rose diagram of well Big Lake 54 showing A: fractures interpreted from image logs, B: fractures predicted from ED method.

Finite element method

Using FEM for modelling the behaviour of complex geological structures such as folds, fractures, and faults is proved to be the most powerful tool for mimicking the tectonic history of sedimentary basins. We used software Dynel 3D for geomechanically restoring the interpreted horizons in the Moomba-Big Lake field in order to predict the fracture network generated during the major tectonic events.

The methodology allows the reconstruction of the current day structural and geometrical placement and the prediction of fractures generated due to stresses released during tectonic events. Input parameters include interpreted faults and horizons, rock elastic properties, fault displacements, and structural relationships (Maerten and Maerten, 2006). Lateral heterogeneity is not considered during restoration, although it affects transit of stresses and thus the generation of failure planes.

Predicted fractures succeeded in mapping sweet spots in Big Lake field, that are the main gas production spots in South Australia (Fig. 9). On the other hand, high variation of fracture trends in predicted sets, compared with low control points, made it hard to validate all the results, although the current predicted fractures are correlating well with the image log fractures.
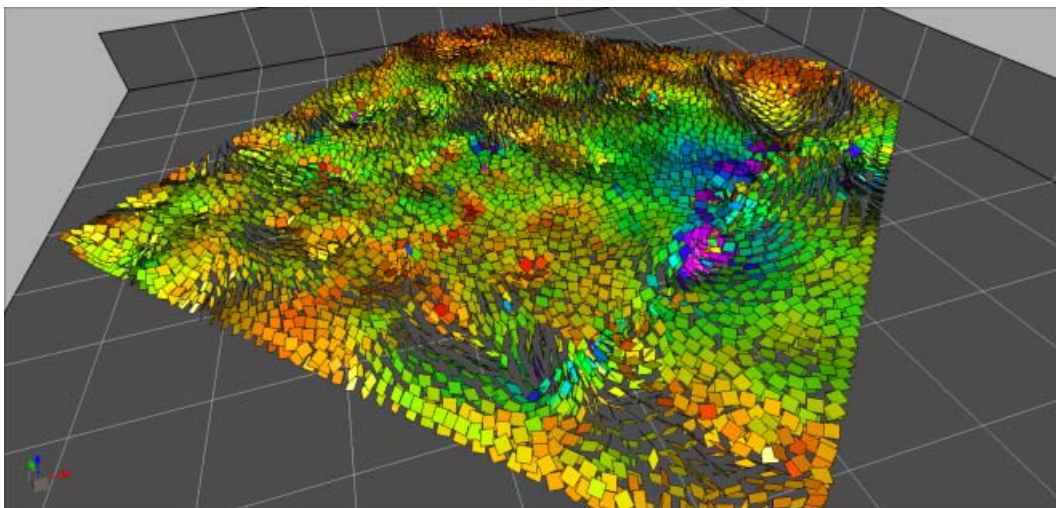
Figure 9: Predicted fractures using geomechanical restoration showing sweet sots (purple colours).

Summary

We have compared several methods for mapping and predicting fracture networks and validated them using 3D seismic an dense well control in the Moomba-Big Lake field. MPC attributes can be used for mapping fractures, but after relating their signatures to folds and faults for better understanding the trends. If folds exist, then the attribute signature will be mapping the fold axis and fractures are expected to be parallel or perpendicular to the fold axis. However, if the curvature signature is mapping a fault, then the fractures are most likely to be parallel or in the direction of the mapped curvature signature as they might be fractures in the damage zone of the fault.

ED can be used for predicting most of the fractures generated close to major faults. Caution must be taken while applying this method away from major faults, as fractures mostly will be generated due to other controllers in these areas. FEM can be used for predicting fracture networks generated during tectonic events. The method succeeded in locating fractured sweet spots for potential production in the Big Lake field. The method was found to be very sensitive to any change in the input parameters, so caution needs to be taken during the process. No single method succeeded completely in mapping or predicting fractures taking into consideration all the affecting factors.

References

Abul Khair, H., Backe, G., King, R., Holford, S., Tingay, M., Cooke, D., Hand, M., 2012, *Factors influencing fractures networks within permian shale intervals in the cooper basin, south australia*, APPEA p. 213-228.

Alexander, E.M. And Jensen-Schmidt, B., 1996, "*Structural and Tectonic history*". In: The petroleum Geology of South Australia, Volume 2: Eromanga Basin. Petroleum Division, SA Department of Mines and Energy, Report Book, 96/20.

Backé, G., Abul Khair, H., King, R., and Holford, S., 2011, *Fracture mapping and modelling in shale-gas target in the Cooper basin*, South Australia, APPEA p. 397-410

Chopra, S., And Marfurt, K., 2007, "*Volumetric Curvature Attributes adding value to 3D seismic data interpretation*"; The Leading Edge, 26, 856-867.

Crouch, S. L. & Starfield, A. M. 1983. *Boundary Element Methods in Solid Mechanics: with Applications in Rock Mechanics and Geological Engineering.* Allen and Unwin, Winchester, MA.

Dee, S., Yielding, G., Freeman, B., Healy, D., Kusznir, N., Grant, N., and Ellis, P., 2007. *Elastic dislocation modelling for prediction of small-scale fault and fracture network characteristics*. Geological Society, London, Special publications, 270, 139-155.

Deighton, I., and Hill, A.J., 1998. *Thermal and burial history. In:* Gravestock, D. I., Hibburt, J.E. and Drexel, J.F. (Eds), Petroleum Geology of South Australia, Volume 4: Cooper Basin, Primary Industries and Resources South Australia, 143–156.

Gatehouse, C., Fanning, C. And Flint, R., 1995, *Geochronology of the Big Lake Suite, Warburton Basin, northeastern South Australia.* South Australia Geological Survey. Quarterly Geological Notes, 128:8-16.

Gravestock, D.I. And Flint, R.B., 1995, "*Post-Delamerian compressive deformation. In: Drexel, J.F. and Preiss, W.V. (Eds), The geology of South Australia. Vol. 2, The Phanerozoic. South Australia. Geological Survey. Bulletin, 54, 60–1.

Heidbach, O., Tingay, M.R.P., Barth, A., Reinecker, J., Kurfeβ, D., Müller, B., 2010, "*Global crustal stress pattern based on the 2008 World Stress Map database release*". Tectonophysics 482, 3–15.

Hillis R. R. and Reynolds S. D. 2000, *The Australian stress map,* Journal of the Geological Society of London 157, 915-921.

Maerten, L., and Maerten, F., 2006. Chronologic modelling of faulted and fractured reservoirs using geomicjanically based restoration: Technique and industry applications. AAPG, vol. 90, no. 8, 1201-1226.

Okada, Y. 1992. *Internal deformation due to shear and tensile faults in a half-space.* Bulletin of the Seismological Society of America, 82, 1018– 1040.

Paten, R.J., 1969, "*Palynologic contributions to petroleum exploration in the Permian formations of the Cooper Basin, Australia*". APEA Journal, 9(2):79-87.

Powell, C.Mca. And Veevers, J.J., 1987, "*Namurian uplift in Australia and South America triggered the main Gondwanan glaciation*". Nature, 326:177-179.

Preiss, W.V., 2000, "*The Adelaide Geosyncline of South Australia and its significance in Neoproterozoic continental reconstruction*". Precambrian Research, 100, 21–63.

Ramsay, J. G. 1967. *Folding and Fracturing of Rocks.* McGraw-Hill, New York.

Somerville, M., Wyborn, D., Chopra, P., Rahman, S., Estrella, D., and Van Der Meulen, T., 1994. *Hot Dry Rocks Feasibility Study, Energy Research And Development Corporation* (Erdc) Report 243, 133p.

Stuart, W.J., 1976, "*The genesis of Permian and lower Triassic reservoir sandstones during phases of southern Cooper Basin development*". APEA Journal, 16:37-47.

Thornton, R.C.N., 1979, "*Regional stratigraphic analysis of the Gidgealpa Group, southern Cooper Basin, Australia*". South Australia. Geological Survey. Bulletin, 49.

Research into drilling fluid rheology and behaviour at extremely high temperatures and pressures

Atrens, A. D.[1], Rudolph, V.[1], Stokes, J.R.[1]

[1]The Queensland Geothermal Energy Centre of Excellence, The University of Queensland

aleks.atrens@uq.edu.au

Introduction

Role of drilling fluids

Drilling fluids must contain components to meet a number of fluid property requirements. These include cuttings-lifting, well pressure control, wellbore surface stabilisation, drill string lubrication, and minimal pumping requirements (Mitchell and Ravi 2006; West et al. 2006). Many of these requirements necessitate either specific fluid rheological properties, or the introduction of fluid components that alter rheological properties in a manner that must be counteracted. Overall, drilling fluids typically combine a yield stress or gelling behaviour under low shear conditions with shear thinning and thixotropic behaviour. A yield stress assists with the task of lifting cuttings, by reducing their settling velocity, and maintaining their suspension within the drilling fluid if circulation is reduced or halted. Fluid yield stress can also assist in maintaining dispersion of dense particles used to increase fluid density (weighting agents). Shear thinning and thixotropic properties reduce frictional pressure losses and thereby minimise pumping power requirements. Deviation from optimal rheology properties leads to a reduction in drilling performance, reducing rate of penetration, and can increase the risk of 'trouble' occurring down-hole. Maintaining rheological properties within a favourable range of values is therefore critical to drilling wells safely and cost-effectively.

Rheological properties can change substantially with increased temperature and pressure. Individual fluid components can also become thermally unstable. This can lead to unpredictable behaviour of drilling fluids at high pressure and temperature conditions, which can pose a major challenge for accessing deep underground resources, particularly engineered geothermal systems.

Temperature-pressure exposure in EGS wells

These problems are substantially exacerbated by increasing well depth, which is a contributor to the comparative difficulty of accessing deep enhanced geothermal systems. Figure 1 depicts the modelled pressure-temperature conditions for wells of identical bottom-hole temperature and heat transfer properties of 1000 m and 4000 m total depth, showing the much wider range of conditions that deeper wells experience.

A comprehensive method for determining circulating temperature profiles is available in the literature (Raymond 1969). Figure 1 illustrates why, despite more than 100 years of development of geothermal power generation capabilities, drilling under extremely high temperatures and pressures is a new and important challenge. Although reservoir temperatures may be similar, deeper wells have much greater surface for heat transfer, thereby leading to a closer approach of drilling fluid temperatures to reservoir temperatures. Design and formulation of drilling fluids therefore becomes increasingly complex for deeper geothermal resources. This is coupled with an expanded range of operating pressures over the length of the well. Ideally, drilling fluid components would be chemically and physically stable up to the highest temperatures to which they are exposed, and the drilling fluid would provide desired rheological properties across the full range of temperature and pressure conditions experienced within the wellbore.
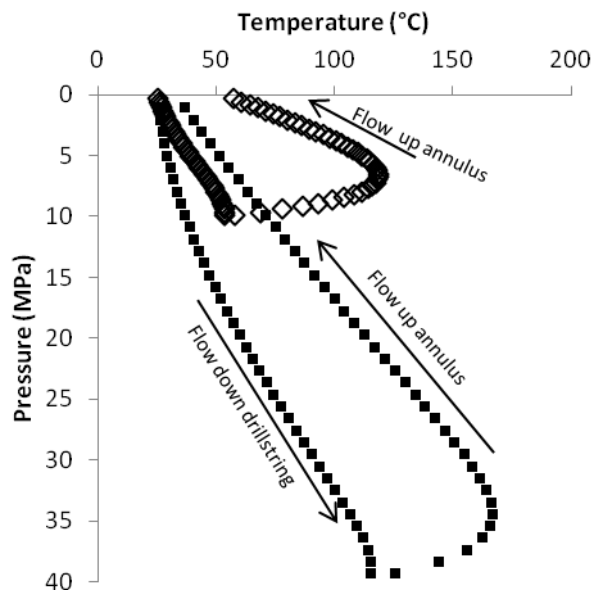
Figure 1: Temperature-pressure conditions for wells of 1000 m (open diamonds) and 4000 m (solid squares) depths, for a linear gradient reaching a bottom-hole temperature of 225 °C, a well diameter of 8", a drill string diameter of 4", overall heat transfer coefficients of 200 W/m^2/K, and a fluid circulation rate of 20 L/s; pressure in this model is linearly proportional to depth (and can thereby be used to interpret position of each fluid data point in the well).

The challenge posed by the depth of Australian geothermal resources is compounded by various additional interactions, which further amplify the need for consistent rheological performance. Figure 2 depicts some of the major interrelations.
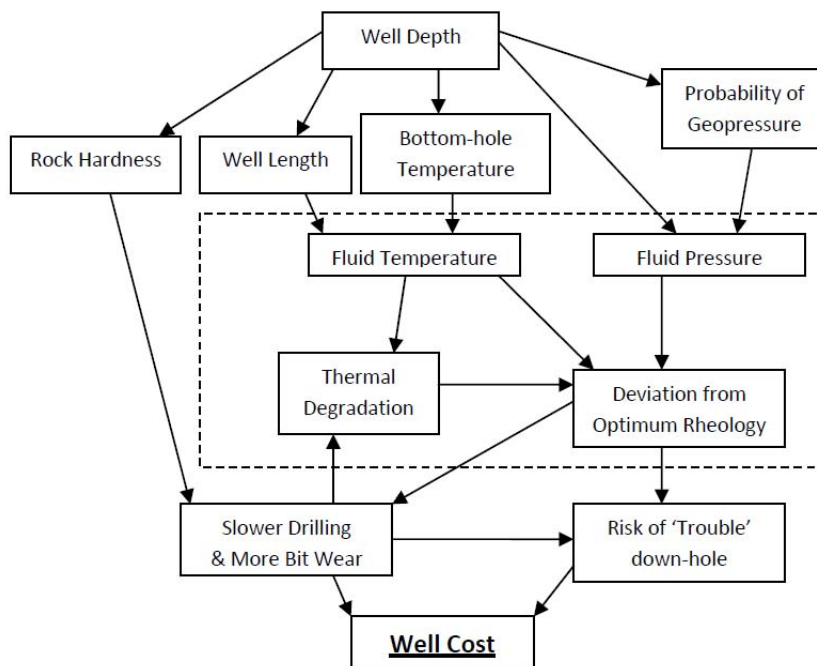
Figure 2: The interaction of fluid rheology with other well characteristics; dashed box indicates the area of the QGECE's interest.

Development of Australian geothermal resources will invariably require deeper wells than 'conventional' geothermal development of shallow resources present in shallow reservoirs in regions of high tectonism and volcanism. All deep EGS well developments except for Soultz-sous-Forêts have experienced substantial challenges related to drilling operations, and arguably exacerbated by drilling fluid design (e.g. (Nuckois et al. 1981)). This is reflected in the higher costs of deep geothermal wells compared to the average oil & gas well costs as a function of depth (Augustine et al. 2006). Current drilling fluid formulations can be successful at a technical level in accessing Australia's deep geothermal resources, but if dramatic reductions in cost are desired, there is a need for improvement in fluid design.

Rheology effects of temperature and pressure on drilling fluid components

Historically, drilling fluid designs have largely developed iteratively, where new fluid formulations have been created based on modifications of previous designs. This has lead to a wide array of different designs tailored to drilling through different geological formations and different in situ conditions. That approach will not provide the most effective fluids for the extremely high temperature and pressure needs of deep geothermal wells.

Drilling fluids fundamentally meet their desired performance criteria by straddling the boundary between liquid-like conditions and solid-like behaviour when the fluid gels. It is the sensitivity of that interface, and the forces between fluid components that mediate it, which make drilling fluid behaviour susceptible to changes in conditions. Understanding the relationships that govern the boundary – the interactions between suspended minerals, clays, bulk fluid, and surface-active components – will provide the basis for predictive models of fluid of different compositions. Such an approach can provide a capacity for rational design of drilling fluids for the spectrum of conditions present in HPHT wells.

An example of preliminary work conducted at the QGECE towards this goal is shown in Figure 3, where the dependence of the yield stress of Mn3O4, a drilling fluid weighting agent, on fluid composition and conditions is assessed.
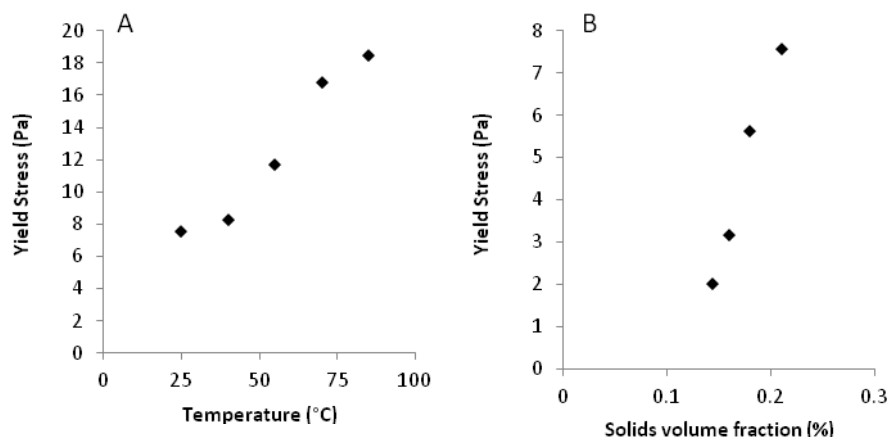
Figure 3: Preliminary analysis of an aqueous mineral suspension of Mn_3O_4, a potential HPHT-stable weighting agent; (A) the dependence of yield stress of a 21 vol% Mn_3O_4 aqueous suspension on temperature; and (B) the dependence of yield stress on Mn_3O_4 content at 25 °C.

Figure 3 shows the delicate boundary – delineated to an extent by the yield stress of the suspension – and its sensitivity to changes in conditions or composition. Increases in temperature or solids content increase the extent of solid-like behaviour. Results of this type – although covering the full range of actually temperature and pressure conditions – can feed into predictive models of fluid rheology behaviour, to determine compositions needed to provide desired fluid properties.

Many typical drilling fluid components undergo substantial rheological changes at elevated temperatures. For example, Bentonite, the most common clay used in drilling fluids tends to gel at high temperatures, leading to excessive yield stresses and to higher viscosities under flow conditions (Carney et al. 1982; Briscoe et al. 1994). These issues can be exacerbated by elevated pressures (Briscoe et al. 1994). Many of the rheological properties of suspensions such as drilling fluids are mediated by the interactions between individual particles and between the particles and the bulk solvent, all of which are affected by elevated temperatures. This is combined with increasing thermal degradation of drilling fluid components with increasing temperature, particularly of organic thickeners, surfactants, and dispersing agents. Degradation of these components can lead to separation of fluid components and substantial loss of performance.

One approach to handling these challenges when iteratively developing new drilling fluids based on older designs has been to incorporate additional components to attempt to mitigate decline in rheological performance at elevated temperature and pressure conditions. These additional components can take the form of rheologically-active components that supplement performance drops under particular T-P ranges, or of stabilising agents which reduce thermal degradation of other fluid components (e.g. polyglycols (van Oort et al. 1997)). With increasing temperatures and pressures however, this approach becomes increasingly problematic: stabilisers and other rheological components reduce in effectiveness, and may become unstable themselves. Other approaches such as the use of oil-based drilling fluids (Shaughnessy et al. 2003; Bland et al. 2006) may not be applicable for the development of Australian resources.

Ideally, this stop-gap approach could be supplanted with alternative drilling fluids that use thermally stable components as the basis for their formulation, which either directly, or through a mixture of multiple different components, provide a relatively constant set of rheological properties throughout the desired temperature and pressure range.

The QGECE's role

Understanding the physical-chemical mechanisms that cause the change in rheological behaviour of drilling fluids is key to developing ways to mitigate loss of rheological performance, or alternative fluid formulations that maintain consistent behaviour. The Queensland Geothermal Energy Centre of Excellence (QGECE) plans to develop a capability in HPHT rheology research to determine the mechanisms that lead to alteration of drilling fluid properties up to 250 °C and 60 MPa. Initially, an assessment of the actual in situ performance of typical drilling fluids will enable determination of the specifics of current shortcomings. This will inform approaches to research into fluid additives that may supplement or replace existing fluid components to provide optimum fluid rheology for drilling process at the elevated conditions.

This will focus on understanding the fundamental behaviours that alter properties such as yield stress and gel strength, viscosity over a range of relevant sustained shear conditions, and zeta potential or zero electric point. It will also include stability testing of fluids via sustained exposure to HPHT conditions, with physical and chemical examination – before and afterwards – to understand the basis for property changes.

References

Augustine, C., Tester, J. W., Anderson, B., Petty, S.Livesay, B., 2006. A comparison of geothermal with oil and gas well drilling costs. Thirty-First Workshop on Geothermal Reservoir Engineering, Stanford University, Stanford, California. p.

Bland, R., Mullen, G., Gonzalez, Y., Harvey, F.Pless, M., 2006. HP/HT Drilling Fluids Challenges. IADC/SPE Asia Pacific Drilling Technology Conference and Exhibition, Bangkok, Thailand. p.

Briscoe, B. J., Luckham, P. F.Ren, S. R. 1994.The properties of drilling muds at high pressures and high temperatures. Philosophical Transactions: Physical Sciences and Engineering v. 348, no. 1687: p. 197-207.

Carney, L. L., Guven, N.McGrew, G. T., 1982. Investigation of high-temperature fluid loss control agents in geothermal drilling fluids. SPE California Regional Meeting, San Francisco, California. p.

Mitchell, R. F.Ravi, K. 2006. Fluid Mechanics for Drilling. Petroleum Engineering Handbook, Volume 2: Drilling Engineering. R. F. Mitchell and L. W. Lake. Richardson, TX, Society of Petroleum Engineers.

Nuckois, E. B., Miles, D., Laney, R., Polk, G., Friddle, H.Simpson, G., 1981. Drilling fluids and lost circulation in hot dry rock geothermal wells at Fenton Hill. Geothermal Resource Council Annual Meeting, Houston, Texas. p.

Raymond, L. R. 1969.Temperature distribution in a circulating drilling fluid. Journal of Petroleum Technology v. 21, no. 3: p. 333-341.

Shaughnessy, J. M., Romo, L. A.Soza, R. L., 2003. Problems of ultra-deep high-temperature, high-pressure drilling. SPE Annual Technical Conference and Exhibition, Denver, Colorado. p.

van Oort, E., Bland, R. G., Howard, S. K., Wiersma, R. J.Roberson, L., 1997. Improving HPHT stability of water based drilling fluids. SPE/IADC Drilling Conference, Amsterdam, Netherlands. p.

West, G., Hall, J.Seaton, S. 2006. Drilling Fluids. Petroleum Engineering Handbook, Volume 2: Drilling Engineering. R. F. Mitchell and L. W. Lake. Richardson, TX, Society of Petroleum Engineers.

Geochemical tracers: capabilities and potential for geothermal reservoir characterisation in Australia

Ayling, B.F.[1,2], Rose, P.E.[2], and Budd, A.R.[1]

[1]Geoscience Australia, GPO Box 378, ACT 2601, Australia,
[2]Energy and Geoscience Institute, The University of Utah, Salt Lake City, UT 84108, USA

Bridget.Ayling@ga.gov.au

Abstract

In Australia to date, there are only a handful of projects that have drilled deep wells to intersect geothermal reservoir targets, and limited flow tests have been performed. Consequently, the characteristics and behaviour of geothermal reservoirs in Australia (geometries, fluid chemistry, mineralogy, permeability type and distribution, temperature distribution etc.) are not well understood. It is clear that the geological variability in the geothermal plays targeted to date (and in the future) will result in diverse reservoir types, but regardless of setting, all geothermal reservoirs must have sufficient permeability to enable fluid flow and heat extraction.

Geochemical tracers have been used internationally for many years to improve the understanding of reservoir dynamics in conventional geothermal systems. Their application in Australia is yet to be widely demonstrated however they provide an attractive opportunity to learn more about geothermal reservoirs in Australian geological settings. Tracers can be classified as either conservative or reactive, and can be used in liquid-phase, vapour-phase or two-phase reservoirs. Tracer tests can provide information on inter-well connectivity, fluid mean residence time, recharge areas, swept pore volumes, temperatures, fracture surface area, flow-storage capacity relationships and volumetric fluid sweep efficiencies. In addition, tracer data can be used with numerical transport codes to help validate 3D reservoir models. This paper presents an overview of existing tracers and their capabilities, and new research directions in tracer science internationally.

Introduction

Geothermal reservoirs in conventional geothermal systems are typically dominated by fracture permeability with high fracture permeabilities and low matrix permeabilities, and with the exception of porous hot sedimentary aquifer systems, this will likely be the case for most enhanced or engineered geothermal systems that are stimulated by hydraulic, chemical or thermal means. Understanding the distribution, aperture, orientation, and connectivity of new and existing fractures in a geothermal reservoir is important to both assess the effectiveness of a stimulation effort, or to manage the field over the longer term and minimize thermal breakthrough or too-rapid thermal drawdown (Bodvarsson and Stefansson, 1989). Down-hole tools such as borehole televiewers can provide some of this information: fracture aperture and orientation, stress regime and lithologic-associations (e.g. Davatzes and Hickman, 2009) and micro-seismic monitoring during hydraulic stimulation can map out the location of fractures around a well (e.g. Asanuma et al., 2005), but ultimately fracture connectivity (and thus inter-well-connectivity) can only be assessed by direct measurements.

The two key methods for determining whether hydraulic conductivity exists between wells include pressure-transient testing, and tracer testing. Pressure-transient testing includes both interference and pulse testing: both provide an indication of whether a connection exists between wells. With some assumptions of flow models between the wells (e.g. radial flow or linear flow), transmissivity and storativity of the formation in the interval between the wells can be estimated (Leaver, 1986; Fan et al., 2005). It typically involves initiating a pressure change at the active well (either by shutting-in or opening the well) and monitoring the pressure response in the shut-in observation well.

Tracer testing of flow between geothermal (or groundwater) wells is an effective tool to map fluid flow pathways in a reservoir, and break-through curves (BTC) can provide a variety of useful, quantitative

data depending on the type of tracer used (conservative or reactive). In many instances, this data can be used to provide insight into projected thermal drawdown in the reservoir or thermal breakthrough of re-injected fluids (e.g. Robinson et al., 1984; Pruess and Bodvarsson, 1984; Axelsson et al., 2001). A benefit of tracer testing (compared to pressure-transient testing) is that wells do not need to be shut in to assess connectivity – shutting-in wells is likely to be less desirable for commercially-producing fields.

Background

Tracer testing basics

A tracer is a chemical indicator present in the fluid system that can used to track flow pathways in the sub-surface. Tracers can be naturally present in the system (e.g. ^{14}C, tritium or δ^{18}O) and used to track water movements over long timescales (years to thousands of years) from source to reservoir, however the tracers discussed here are artificially-injected into the system and used to track fluid movements over shorter timescales (days to a few years at most) and distances (typically no more than 10's of kilometres).

Geochemical tracer testing has been performed at many geothermal fields around the world for several decades. In a typical geothermal tracer test, a chemical tracer is injected into the reservoir to track the movement of fluid, and monitored either in one or more production wells or during flow-back from the same injection well (single-well injection-backflow testing). In the reservoir, various transport processes affect the return of the tracer: solutes will be affected by advection, dispersion and diffusion as they move through the reservoir, and these processes will be reflected in the character of the tracer break-through curve that is measured in the injection well(s). Most tracer-tests performed to-date in geothermal reservoirs have used solute tracers, however current research is also investigating the use of nano-colloids as 'smart' geothermal tracers (discussed later).

Geochemical tracers in either groundwater or geothermal applications should not affect the water flow regime (by changing fluid density or viscosity), and they are ideally not present in the reservoir or aquifer of interest (i.e. have a low background level). In addition, they should be environmentally benign, have low toxicity, be detectable at low concentrations and be affordable (100's of kilograms may need to be injected). A key requirement for geothermal tracers is that they are stable at reservoir temperatures, or have well-characterised decay-kinetics.

Types of tracers

Geochemical tracers (geothermal or groundwater) can be divided into those that are believed to behave in a conservative manner (i.e. all tracer that is injected is eventually returned), and those that are not conserved, either through interactions with the reservoir rock (e.g. adsorption/desorption or thermal degradation) or natural decay (e.g. radioactive decay). These reactive or 'smart' tracers have the potential to provide additional information about the reservoir, and are best used in conjunction with a conservative tracer to provide constraints on reservoir hydraulic properties.

Different tracers are used depending on the fluid phase in the reservoir (i.e. liquid phase, two-phase or vapour-dominated). Most reservoirs in Australia could be expected to be liquid-dominated given their temperatures and geological setting, and thus liquid-phase tracers are discussed here.

Commonly-used conservative liquid-phase tracers include the UV-fluorescent polyaromatic-sulfonate family that have demonstrated thermal stability at temperatures of 200°C and above (Rose et al., 2001). There are 9 compounds in this family that have been identified as suitable geothermal tracers, and these have been used successfully to map fluid flow pathways and provide insight into reservoir properties at many geothermal fields around the world over the last 10 years (e.g. Philippines (Nogara and Sambrano, 2005), Japan (Watanabe et al., 2005), New Zealand (Rose,1998, Rose et al., 2000), Mexico (Iglesias et al., 2011), Germany (Behrens et al., 2006) and the USA (Rose et al., 1998, 1999, 2000)). In late 2008, they were used at Geodynamics Ltd's Habanero project to map flow properties of the reservoir between the Habanero #1 and #3 wells (Yanagisawa et al., 2009). The naphthalene sulfonates are detectable at very low levels in the reservoir (100 ppt), and they are mutually

compatible, meaning that any number of the family can be used simultaneously in a tracer test. They are analysed using conventional high-performance liquid chromatography (HPLC) with fluorescence detection (Rose et al., 2001).

A method of estimating inter-well volumes and flow geometries in liquid-phase geothermal reservoirs using conservative tracer tests was presented by Shook (2003). This approach is centred on moment analysis and analysis of tracer residence times (Robinson and Tester, 1984) and assuming that steady-state conditions are met and the tracer is conservative, it enables quantitative information to be derived from tracer break-through curves including mean residence time, flow geometry, swept pore volume, and volumetric-fluid sweep efficiency (Shook and Forsmann, 2005).

The idea of using tracers that are temperature-sensitive (and thus reactive) has been explored for a couple of decades (e.g. Robinson et al., 1984; Tester et al., 1986). Popular groundwater tracers (e.g. Rhodamine-WT and fluorescein) are usable in low-temperature geothermal reservoirs as conservative tracers, but at higher temperatures (>160°C for Rhodamine-WT and 250°C for fluorescein), they are thermally unstable (Adams and Davis, 1991; Adams et al., 1992; Rose and Adams, 1994; Behrens et al., 2006).

Similarly, the idea of using tracers that undergo adsorption/desorption reactions in the reservoir has been proposed in earlier studies (e.g. Shan and Pruess, 2005). Developing such tracers is no easy feat and this is the focus of several current research projects in the USA (discussed in Section 4.0).

When to use tracer tests – opportunities for Australia's geothermal projects

Tracer tests can provide different information depending at what phase of a project they are utilised. Although they are often used to map flow pathways in established geothermal fields, tracer tests can provide useful information at many stages of project development and new 'smart' tracers may be able to be used with a single well (via an injection-backflow test) to evaluate changes in fracture surface area following reservoir stimulation (e.g. Ghergut et al., 2007, 2010). Currently, tracer tests can be used to:

- determine whether any connections exist between a newly-drilled injection-production well doublet, and if so, hydraulic properties of the connected reservoir (fluid residence time, velocity, how 'open' the system is, flow capacity- storage capacity relationships, thermal sweep efficiencies);

- evaluate the success of a hydraulic or chemical stimulation effort – either identifying whether new hydraulic connections exist between an injector and producer or between an existing field and a previously 'dry' or isolated well, or, whether fracture surface area in the reservoir has changed (heat exchange area); or

- map flow pathways in a larger field between multiple injectors and producers, to manage injection returns and identify areas where thermal breakthrough might occur in the future if left unmanaged.

Future capabilities will hopefully involve the use of 'smart' tracers in geothermal tracer testing.

Smart tracers: new research directions (USA and Europe)

Overview

Through the US Department of Energy's (DOE) Geothermal Technologies Program, there are several research projects in progress in the USA that are aiming to develop new technologies and techniques in tracer science. These research projects are typically focussing on the development and validation of 'smart' tracers: tracers that have the ability to provide additional information about the reservoir beyond hydraulic properties. Reservoir characteristics of interest include (1) fracture surface area, (2) matrix-fracture relationships, and (3) distributed temperature regime along a flow pathway. The ability to measure changes in fracture surface area (and thus the area available for heat exchange) is particularly important for EGS, and creating and maintaining connectivity of an engineered fracture

network is one of the major challenges in EGS development. Thermally-sensitive and sorbing tracers may both have the capability to assess changes in fracture surface area.

Reactive tracers (solute tracer)

Solute tracers that undergo sorption/desorption reactions are currently being explored for their potential to measure changes in fracture surface areas in enhanced geothermal reservoirs (Shan and Pruess, 2005). These include cation-exchange tracers such as lithium ion (Reimus et al., 2012) and fluorescent compounds that exhibit both sorption behaviour and thermal decay (such as Safranin-T) (Leecaster et al., 2012; Rose et al., 2012). Sorption of a reactive tracer onto geothermal reservoir surfaces results in the delay (or retardation) of the reactive tracer relative to the bulk water velocity as measured by a conservative tracer. Laboratory tests with flowing column studies have demonstrated that Safranin-T reversibly sorbs at high temperatures and that its retardation is positively correlated with amount of surface area that it interrogates relative to the conservative tracer 1,5 naphthalene sulfonate (Leecaster et al., 2012). The retardation (and thus inferred-sorption) decreases as temperatures increases. Safranin-T is also thermally-unstable at geothermal reservoir temperatures, and its thermal degradation has been characterised in auto-clave reactor and column flow-through experiments (Leecaster et al., 2012). A field test of the Safranin-T tracer at the Soda Lake geothermal field (Nevada, USA) between two wells, indicated that the Safranin-T breakthrough curve was retarded relative to the conservative naphthalene sulfonate tracer, and did show thermal decay (Rose et al., 2012).

Other solute tracers that are thermo-sensitive are being investigated by researchers in Germany. Reaction kinetics of esters derived from naphthol sulfonates are being explored and they appear to show promise as thermally-sensitive tracers under a range of reservoir conditions (temperature and pH) and tracer test durations (Nottebohm et al., 2010).

Nano-tracers (colloidal geothermal tracers: reactive and conservative)

Colloidal tracers may be able to provide additional information about geothermal reservoir properties. Particle transport in physically heterogeneous and fractured systems deviates significantly from the transport of solute species; breakthrough of colloids is often found to occur ahead of the breakthrough of solute tracers (Redden et al., 2010). Several research projects are investigating colloid tracers, including both conservative and reactive tracers.

A team at the University of Utah is developing a method for the fabrication of quantum dots that have potential for use in conventional and engineered geothermal systems (Bartl and Siy, 2009a; 2009b; Rose et al., 2010). Importantly, quantum dots may have the capability to perform as either conservative tracers (with customisable diffusivities) when fabricated a particular way, or as reactive tracers, either through temperature-sensing capability or sorption capabilities. Quantum dots are small crystallites of semiconductors in the size range of 1 to 20 nano-metres and composed of a few hundred to several thousands of atoms. As a result of quantum size effects and strongly confined excitons, quantum dots display unique size and shape-related electronic and optical properties. In particular, they can be made to fluoresce over a wide range, including the visible and near infrared (NIR) regions of light – regions where geothermal and EGS reservoir waters possess very little interference. The inorganic semi-conducting nano-crystal core of each quantum dot can be tuned to deliver various emission colours (ranging from the visible to the NIR). The surface chemistry of colloidal quantum dots can be adjusted independently, by varying the choice of ligands to optimize their interaction with the sensing environment (e.g., hydrophilic/ hydrophobic, functional chemical groups, positively/negatively charged surface, etc.). Thus, it is hoped that quantum dot tracers can be designed to possess all of the qualities of the conventional conservative tracers (i.e. the naphthalene sulfonates), or be converted to reactive tracers depending on the surface treatment (Rose et al., 2010). Currently, the quantum dots being fabricated and tested at the University of Utah are using a Cadmium selenide (CdSe) core (Siy et al., 2011) and this core is being protected by either a Cadmium sulphide (CdS) or a silica shell, or combination of both, to which ligands can be attached to modify the surface chemistry (Riassetto et al., 2011).

Researchers at Stanford University have investigated other temperature-sensitive nano-tracers including tin-bismuth alloy nano-particles and silica nano-particles with covalently linked dye (Alaskar et al., 2011; Ames, 2011). The tin-bismuth alloy has a melting temperature that varies between 139°C and 271°C depending on its composition: this is the premise for the temperature-sensing capability. Other temperature sensitive nano-tracers are being investigated at Idaho National Laboratory, incorporating temperature-dependent processes such as mineral thermo-luminescence, or racemisation in polymers of organic compounds. Workers are investigating the possibilities of encapsulating such temperature-sensitive minerals/compounds in a protective silica shell to protect them from alteration in the geothermal environment and enable them to be transported through the reservoir recording its thermal signature (Redden et al., 2010).

Summary

Geothermal tracers continue to be a useful tool for exploring and characterising geothermal reservoirs in active geothermal fields worldwide. As more Australian projects drill wells, tracer testing should become a fundamental part of the exploration/resource characterisation stage of project developments: the benefits are significant (qualitative data on flow pathways and quantitative data on reservoir hydraulic properties) and the tests are easy to perform. New research directions in 'smart' tracers have great potential to provide further insight into engineered and natural geothermal reservoirs in Australian geological settings.

Acknowledgements

References

Adams, M. C., Moore,J.N., Fabry, L.G., and Ahn, J.-H., 1992. Thermal stabilities of aromatic acids as geothermal tracers. Geothermics, Vol. 213, pp323-339.

Adams, M.C., and Davis, J., 1991. Kinetics of fluorescein decay and its application as a geothermal Tracer. Geothermics, Vol. 201-2, pp53-60.

Alaskar, M., Ames, M., Liu, C., Conor, S., Horne, R., Li, K., and Cui, Y., 2011. Smart nanosensors for in-situ temperature measurement in fractured geothermal reservoirs. Proceedings of the 36th Workshop on Geothermal Reservoir Engineering, Stanford University, Jan 31 – Feb 2, 2011.

Ames, M., 2011. Nanosensors as reservoir engineering tools to map in-situ temperature distributions in geothermal reservoirs. MSc Thesis, Stanford University, SGP-TR-192.

Asanuma, H., Soma, N., Kaieda, H., Kumano, Y., Izumi, T., Tezuka, K., Niitsuma, H., and Wyborn, D., 2005. Microseismic monitoring of hydraulic stimulation at the Australian HDR project in Cooper Basin. Proceedings of the World Geothermal Congress, Antalya Turkey, 24-29 April 2005.

Axelsson, G., Flovenz, O.G., Hauksdottir, S., Hjartarson, A., and Liu, J., 2001. Analysis of tracer test data, and injection-induced cooling, in the Laugaland geothermal field, N-Iceland. Geothermics, Vol. 30, pp697-725.

Bartl, M.H., and Siy, J.T., 2009a. Method for the Low-Temperature Synthesis of Colloidal Nanocrystals with Narrow Size Distribution, Patent Application 61/145,477, USA.

Bartl, M.H., and Siy, J.T., 2009b. Method for the Post-Synthesis Shape Modification of Colloidal Nanocrystals in Solution, Patent Application 61/145,925, USA.

Behrens, H., Ghergut, I., Licha, T., Lodemann, M., Orzol, J., and Sauter, M., 2006. Reactive behaviour of uranine fluorescein in a deep geothermal-reservoir tracer test. Geophysical Research Abstracts, Vol. 8, 10448, European Geosciences Union.

Bodvarsson, G., and Stefansson, V., 1989. Some theoretical and field aspects of reinjection in geothermal reservoirs. Water Resources Research, Vol. 256, pp1235-1248.

Davatzes, N.C. and Hickman, S., 2009. Fractures, stress and fluid flow prior to stimulation of well 27-15, Desert Peak, Nevada, EGS Project, Proceedings 34th Workshop on Geothermal Reservoir Engineering, Stanford University, Stanford, CA, SGP-TR-187.

Fan, K.C., Tom Kuo., M.C., Liang, K.F., Shu Lee, C., and Chiang, S.C., 2005. Interpretation of a well interference test at the Chingshui geothermal field, Taiwan. Geothermics, Vol. 34, pp99-118.

Gerghut, I., Sauter, M., Behrens, H., Licha, T., McDermott, C.I., Herfort, M., Rose, P., Zimmermann, G., Orzol, J., Jung, R., Huenges, E., Kolditz, O., Lodemann, M., Fischer, S., Wittig, U., Guthoff, F., and Kuhr, M., 2007. Tracer tests evaluating hydraulic stimulation at deep geothermal reservoirs in Germany. Proceedings of the 32nd Workshop on Geothermal Reservoir Engineering, Stanford University, Jan 22-24, 2007.

Gerghut, I., Behrens, H., and Sauter, M., 2010. Tracer properties and tracer test results from geothermal reservoir testing: Part 2. Proceedings of the 35th Workshop on Geothermal Reservoir Engineering., Stanford University, Feb 1-3, 2010.

Iglesias, E.R., Ramírez-Montes, M., Torres, R.J., Cruz-Grajales, I., and Reyes-Picasso, N. 2011. Tracer testing at the Los Humeros, Mexico, high-enthalpy geothermal field. Proceedings of the Australian Geothermal Energy Conference, 2011, GA Record 2011/043.

Leaver, J.D., 1986. A technical review of interference testing with application in the Ohaaki geothermal field. Stanford University Publication, SGP-TR-95, 199pp.

Leecaster, K., Ayling, B., Moffitt, G., and Rose, P., 2012. Use of Safranin-T as a reactive tracer for geothermal reservoir characterization. Proceedings of the 37th Workshop on Geothermal Reservoir Engineering, Stanford University, Jan 30 – Feb 1, 2012.

Nogara, J.B., and Sambrano, B.M.G., 2005. Tracer Tests Using Naphthalene Di-Sulfonates in Mindanao Geothermal Production Field, Philippines. Proceedings of the World Geothermal Congress; Antalya, Turkey, 24-29 April, 2005.

Nottebohm, M., Licha, T., and Sauter, M., 2010. Thermal decay of selected organic substances as "smart tracers" in geothermal reservoirs. Proceedings of the 35th Workshop on Geothermal Reservoir Engineering, Stanford University, Feb 1-3rd, 2010.

Pruess, K., and Bodvarsson, G.S., 1984.Thermal effects of reinjection in geothermal reservoirs with major vertical fractures, Journal of Petroleum Technology, Vol. 36, pp1567-1578.

Redden, G., Stone, M., Wright, K.E., Mattson, E., Palmer, C.D., Rollins, H., Harrup, M., and Hull, L.C., 2010. Tracers for characterizing enhanced geothermal systems. Proceedings of the 35th Workshop on Geothermal Reservoir Engineering., Stanford University, Feb 1-3, 2010.

Reimus, P., Williams, M., Vermeul, V., Rose, P., Leecaster, K., Ayling, B., Sanjuan, R., Ames, M., Dean, C., and Benoit, D., 2012. Use of tracers to interrogate fracture surface area in single-well tracer tests in EGS systems. Proceedings of the 37th Workshop on Geothermal Reservoir Engineering, Stanford University, Jan 30-Feb 1, 2012.

Riassetto, D., Ma, N., Amador, J., Benson, B., Briggs, A., Mella, M., Rose, P., Bartl, M., 2011. Biphasic Route to Silica-Encapsulation of Quantum Dots, Nanoscience and Nanotechnology Letters, Vol. 35, pp 655-658.

Robinson, B.A., and Tester, J.W., 1984, Dispersed fluid flow in fractured reservoirs: An analysis of tracer-determined residence time distributions. Journal of Geophysical Research, Vol. 89B12, pp10, 374-10,384.

Robinson, B.A., Tester, J.W., and Brown, L.F. 1984. Using chemically reactive tracers to determine temperature characteristics of geothermal reservoirs. Geothermal Resources Council Transactions, Reno, Nevada, August 26-29, 1984.

Rose, P.E. and Adams, M.C. 1994. The application of Rhodamine-WT as a geothermal tracer. Geothermal Resource Council Transactions, Vol.18, p. 237-240.

Rose, P.E., Benoit, W.R., and Adams, M.C., 1998. Tracer testing at Dixie Valley, Nevada, using pyrene tetrasulfonate, amino G, and fluorescein. Geothermal Resource Council Transactions, Vol. 22, 583-587.

Rose, P.E., 1998. The use of polyaromatic sulfonates as tracers in high temperature geothermal reservoirs. Proceedings 20th NZ Geothermal Workshop, 239-243.

Rose, P.E., Goranson, C., Salls, D., and Kilbourn, P.M., 1999. Tracer testing at Steamboat Hills, Nevada, using fluorescein and 1,5-naphthalene disulfonate. Proceedings of the 24th Workshop on Geothermal Reservoir Engineering, Stanford University, SGPTR-162.

Rose, P., Benoit, D., Lee, S.G., Tandia, B., and Kilbourn, P., 2000. Testing the naphthalene sulfonates as geothermal tracers at Dixie Valley, Ohaaki and Awibengkok. Proceedings of the 25th Workshop on Geothermal Reservoir Engineering, Stanford University, January 24-26th, 2000.

Rose, P., Benoit, D., and Kilbourn, P., 2001. The application of the polyaromatic sulfonates as tracers in geothermal reservoirs. Geothermics, Vol. 30, pp617-630.

Rose. P., Riasetto,D., Siy, J., Bartl, M.H., Reimus, P., Mella, M., Leecaster, K., and Petty, S., 2010. The Potential for the Use of Colloidal-Crystal Quantum Dots as Tracers in Geothermal and EGS Reservoirs. GRC Transactions, Vol. 34.

Rose, P., Leecaster, K., Clausen, S., Sanjuan, R., Ames, M., Reimus, P., Williams, M., Vermeul, V., and Benoit, D., 2012. A tracer test at the Soda Lake, Nevada geothermal field using a sorbing tracer. Proceedings of the 37th Workshop on Geothermal Reservoir Engineering, Stanford University, Jan 30 – Feb 1, 2012.

Shan, C., and Pruess, K., 2005. Sorbing tracers – A potential tool for determining effective transfer area in hot fractured rock systems. Proceedings of the 30th Workshop on Geothermal Reservoir Engineering, Stanford University, Jan 31- Feb 2, 2005.

Shook, M.G., 2003. A simple, fast method of estimating fractured reservoir geometry from tracer tests. Geothermal Resources Council Transactions, Vol. 27.

Shook, M.G., and Forsmann, J.H., 2005. Tracer interpretation using temporal moments on a spreadsheet. Idaho National Laboratory publication, INL/EXT-05-00400 Revision-1.

Siy, J.T., Brauser, E.M., and Bartl, M.H., 2011. Low-temperature synthesis of CdSe nanocrystal quantum dots. Chemical Communications, Vol. 47, pp364-366.

Tester, J.W., Robinson, B.A., and Ferguson, J.H., 1986. Inert and reacting tracers for reservoir sizing in fractured, hot dry rock systems. Proceedings of the 11th Workshop on Geothermal Reservoir Engineering, Stanford University, Jan 21-23rd, 1986.

Watanabe, M., Arai, F., Fukuda, D., Asanuma, M., Hishi, Y., and Tsutsumi, J., 2005. Tracer testing at Mori geothermal field Japan, using aromatic compounds. Proceedings of the 30th Workshop on Geothermal Reservoir Engineering, Stanford University, Jan 31 – Feb 2nd, 2005.

Yanagisawa, N., Rose, P.E., and Wyborn, D., 2009. First tracer test at Cooper-basin, Australia HDR reservoir. Geothermal Resources Council Transactions, Vol. 33, pp281-284.

Targeting Fracture Permeability for Geothermal Developments in the North Perth Basin[1]

Ballesteros, M.[1], Oppermann, R.[2], Meyer, G.[1], McDairimid, J.[1], and Larking, A.[1]

[1]Green Rock Energy Ltd, [2]OPPtimal Exploration and Development Pty Ltd

mballesteros@greenrock.com.au

Introduction

The North Perth Basin (NPB) offers one of the most attractive areas for Hot Sedimentary Aquifer (HSA) geothermal projects in Australia. Key geological ingredients for a working geothermal system include a heat source and a heat trap in the form of thermally insulating rocks such as coals or low thermal conductivity shales with underlying naturally permeable, cavernous or fractured reservoir rocks (Cooper and Beardsmore, 2008). Available data suggests that the NPB has all of these attributes.

The technical evaluation of the NPB has identified a number of attractive target areas, with permeability associated with open natural fractures providing the most attractive potential reservoir. The Upper Rhine Graben in Europe provides a valuable analogue for the NPB geological model (Larking et al, 2010). Germany currently hosts two commercial HSA geothermal power plants, including the Unterhaching plant near Munich in southern Germany, and one in Landau in the Upper Rhine Graben. A third plant is now under construction at Insheim, close to Landau. An additional facility, the Soultz Research and Development plant, is located nearby in the Upper Rhine Graben in France (Schindler et. al, 2010). Importantly, all of these HSA plants produce exclusively from fractures.

Regional Setting

The NPB target area is located at the northern end of the Perth Basin, a north-south trending 1,000 km long rift basin which formed during the Permian to Early Cretaceous. The area has a complex tectonic history resulting in the development of extensive fault and fracture networks. The regional geology of the area is discussed by Mory and Iasky (1996) and the geological setting of the project area is described in more detail by Larking et al (2010, 2011). The structural setting in the project area is shown in Figure 1.

The primary source of geological and thermal information about the sedimentary sequences in the Perth Basin comes from petroleum wells and shallower water bores. Over 250 wells have been drilled in the NPB, reaching depths up to 4,850m, resulting in the discovery of more than 13 oil and gas fields. Most of these discoveries are located in and around the Green Rock permits and as a result the area has the highest density of petroleum wells and seismic data in the Basin. Approximately 24,000 km of 2D seismic and over 2,800 km^2 of 3D seismic have been acquired to date and provide valuable assistance in understanding the detailed structural and stratigraphical history of the area (*figure 2*).

Heat Flow and Temperatures

Temperature gradients exceeding 5°C/100m and heat flows exceeding 100 mW/m^2 have been measured from wells and deep bores in the study area (*Larking, et al, 2011*). Modelled surface heat flows in the Perth Basin ranged from 60–140 mW/m^2, with a median value for all wells in the northern Perth Basin of 95 mW/m^2. This compares to a median value of around 76 mW/m^2 for the entire Perth Basin and 64.5 mW/m^2 for Australia as a whole (WADME, 2008; Waining, 2009; Beardsmore, 2010).

---

1 This article (or a version of it) was previously published in PESA News Resources, June/July Edition No 118 (www.pnronline.com.au)
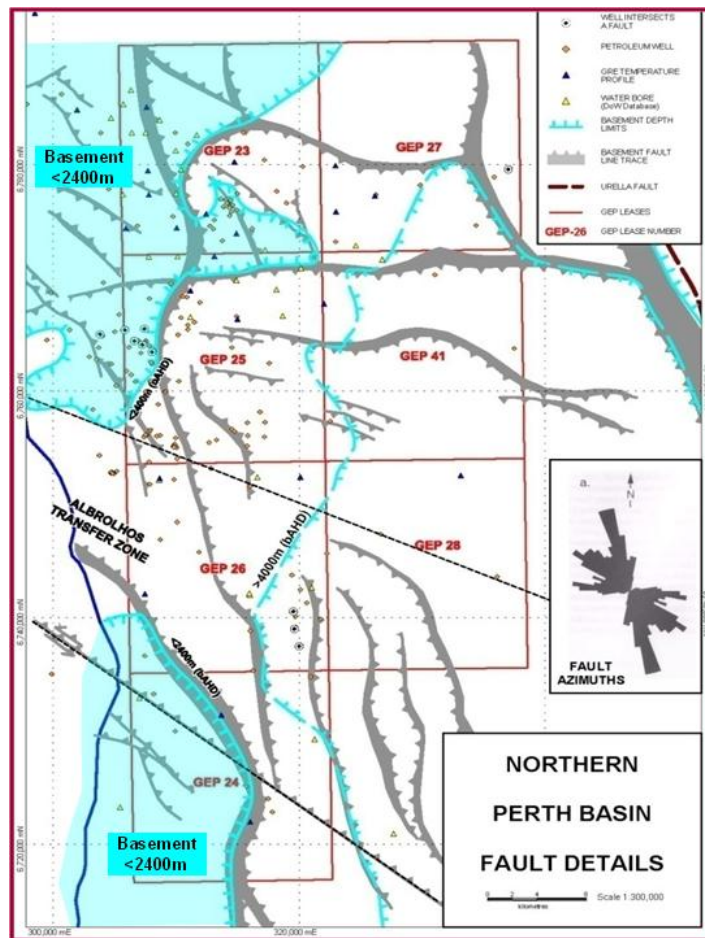
Figure 1: Location map of GreenRock Energy geothermal permits in the North Perth Basin.

Five wells within the Green Rock permit area have encountered bottom-hole temperatures greater than 150°C (Warradong-1, Redback-1 and -2, West Eregulla-1 and Mountain Bridge-1) at depths ranging from 3416m to 4065m. In addition, temperature and heat flow modelling for an additional 95 wells drilled in the area indicate locations where temperatures of 150°C should be reached at depths less than 3500m deep. Figure 2 shows the area within the Green Rock permits where there is 3D data coverage and temperatures are expected to reach 150°C within the sedimentary section at depths less than 3500m. This area represents our primary area of interest; west of this area basement is too shallow for HSA reservoirs and to the east deeper drilling would be required to reach the 150°C isotherm.

Reservoirs

HSA geothermal projects require relatively high water production rates to be commercially viable – generally in excess of 75 litres/sec (40,000 BPD) per well (Mortimer, 2010). Higher flow rates than these have been achieved from producing geothermal fields at Landau and Unterhaching in Germany and from shallow aquifers in the Perth Basin. Geothermal wells achieve this by producing from much thicker water saturated reservoir sections than typically encountered in petroleum wells.

A number of potential reservoirs are present in the Permit area; the most prospective of which are all Permian in age, including the Upper Permian Wagina Formation and the Caryngina Formation, Irwin River Coal Measures and High Cliff Sandstone (*Larking et al., 2011*). Younger formations in the Triassic exhibit good reservoir qualities, but appear to have more limited potential as geothermal reservoirs due to their relatively shallow depths and consequent lower temperatures within the permit areas. Nevertheless, despite examples of good reservoir quality at suitable depths locally, general

trends show that reservoir quality deteriorates significantly below 3000m (Laker, 2000), decreasing the probability of encountering a reservoir section with adequate matrix porosity and transmissivity to sustain the required flow rates. As a result, there is significant risk associated with relying solely on matrix permeability to supply adequate flow rates.
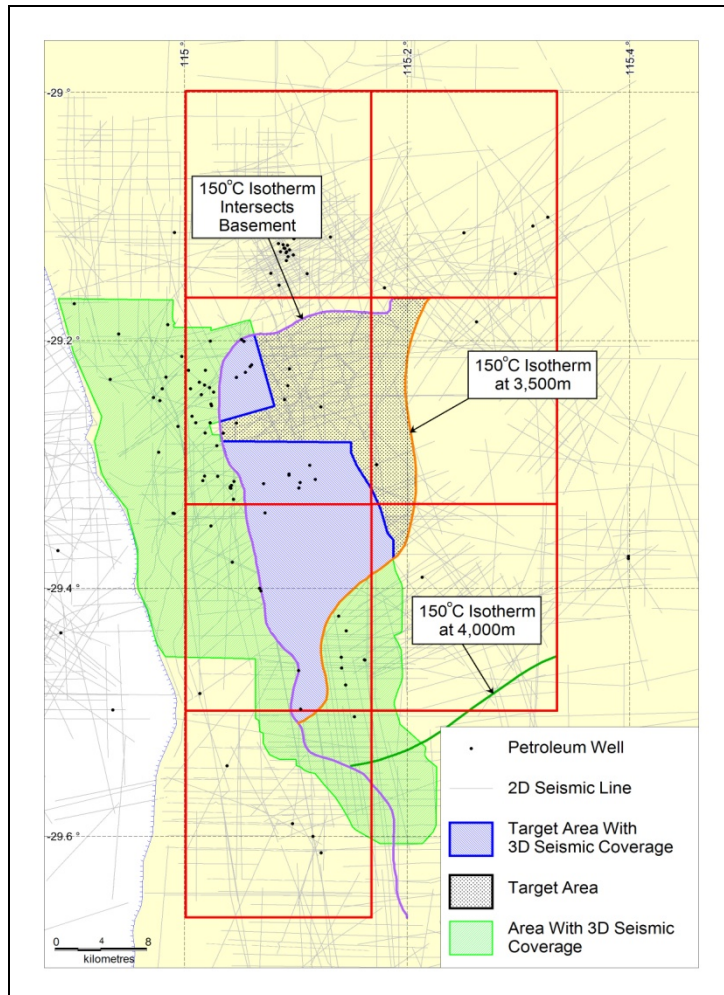
Figure 2: Geothermal permits showing primary target area.

Natural Open Fractures

As noted previously, geothermal developments in the Rhine Graben produce sustainable high flow rates exclusively from open natural fractures due to lack of any significant matrix permeability in the sediments or in basement rocks. In the NPB, available well data proves that open natural fractures occur frequently in all of the target formations. For example, a fracture at 3334m in Redback 1 had a measured *in situ* open thickness of 25cm (King et al, 2008). These fractures are an attractive mechanism for recovering hot geothermal fluids from the sub-surface.

Review of borehole breakouts, rock densities and formation testing results, particularly leak-off tests has shown that the current stress regime in the NPB is transitional between the reverse and strike-slip regimes. This is due to the vertical and minimum horizontal principal stress components having similar magnitude. Break-out analysis has also shown that the maximum horizontal stress direction (σH_{max}) is oriented in an east-west direction (N84^{o}E) (King et al, 2008).
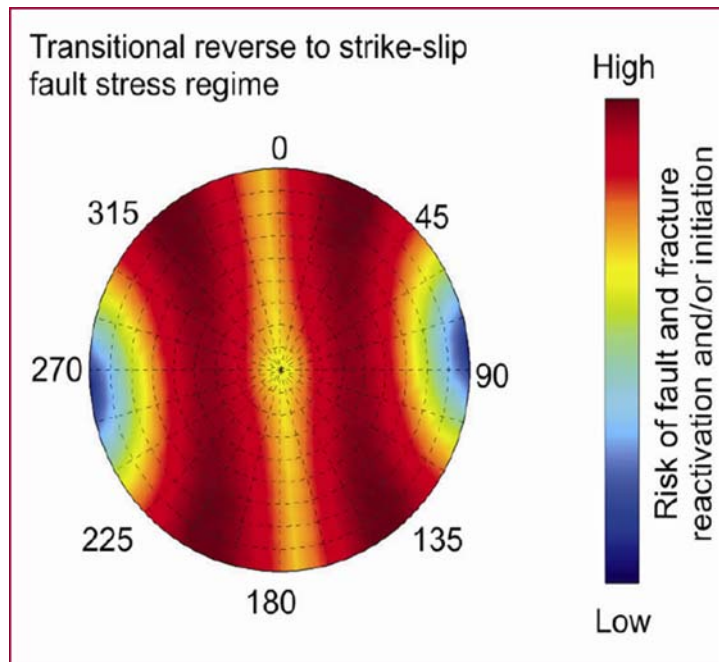
Figure 3: Theoretical calculation of probability that a particularly oriented fault (plotted as pole to plane) will be re-activated (and potentially permeable) in a stress regime similar to the modern day northern Perth basin (from King, 2011).
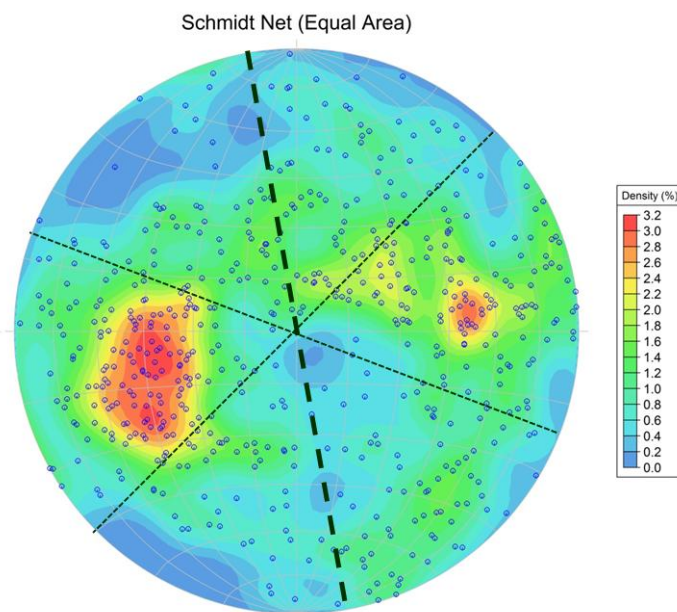
Figure 4: Distribution of orientations of conductive faults identified from image log interpretations of wells in the study area plotted as poles to plane. Most common orientations appear in red.

Figure 3 illustrates the probability that a fault or fracture in this stress regime is critically stressed according to its dip and azimuth (plotted as a pole to plane). Critically stressed fractures are most likely to currently experience dilation and therefore be open to fluid movement (King et al, 2011). A number of studies have been undertaken to establish the nature and orientation of fractures in the Permit areas using borehole image logs (King et al, 2008, 2011; Bailey, in press). These efforts have catalogued the orientation of the fractures and classified them as open (conductive) and therefore

likely to act as a conduit for fluid flow unless cemented with conductive minerals, or closed (resistive). Fractures generally tend to be oriented north, northwest and east depending on the local stress regime. There are examples of both resistive and conductive fractures in each orientation.

It is important to note that the dip of the fault or fracture is a critical variable. The most common azimuth for the fractures detected is approximately N10^{o}W, which is essentially perpendicular to the σH_{max}. Figure 3 illustrates that vertical fractures with this azimuth have the lowest probability of reactivation, and therefore of being permeable. In contrast, when fractures with this azimuth are dipping 20° to 50° to the east or west, they are among the most likely to be reactivated.

Figure 4 illustrates the composite orientation of all the conductive fractures identified in the borehole image logs analyzed. It shows that the most common orientation for conductive fractures in the study area is trending N10^{o}W with dips of 30° to 60°. This in turn suggests that fractures with this orientation are likely to be critically stressed and therefore permeable. This suggests that the reservoir risk can be significantly reduced by targeting areas where seismic data shows a high density of appropriately oriented fractures is present.
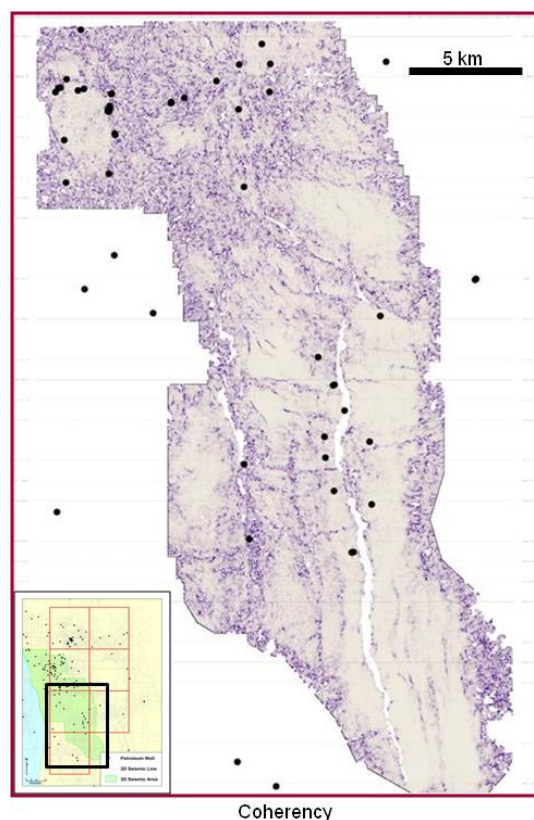
Coherency

Figure 5: Coherency extracted at top Permian from Hibbert-Hovea 3D seismic survey.

Fracture Detection from Seismic Data

A number of 3D seismic surveys are available in the public domain over the project area. These surveys provide coverage over a number of the areas identified by Green Rock as having good geothermal prospectivity.

In addition to conventional structural mapping, a number of volume interpretation techniques have been applied to North Perth Basin seismic data, allowing 3D sub-surface features to be identified, filtered, classified and extracted quickly and accurately using an automated process. Automated fracture extraction is based on the physical measurement of spatial variation in amplitude, phase and/or frequency content of 3D seismic data, and is as such free of bias and interpretation. Fracture

extraction allows to confidently identify small displacement faults in true 3D space that would often not be identified by manual interpretation (Oppermann 2010, 2012).

A key benefit of automated fracture extraction is that it facilitates the quantitative assessment of fracture properties such as distribution, orientation, size and intensity, as well as the confidence in the presence of a particular fracture. As the confidence value is often a proxy for fault throw or fracture aperture, it allows us to quickly visualise and separate larger (higher confidence) fractures from smaller (lower confidence) fractures (Oppermann, 2012). Results from unpublished studies show that fluid losses or fracture productivity are consistently linked with high confidence (larger) seismic fractures – though fracture orientation relative to present-day stress also plays a role.

Detailed correlation work in multiple study areas worldwide has demonstrated good matches between seismically identified fractures and fractures identified from well data (image logs, cores, correlation, well tests, productivity, fluid losses etc.). Automated fracture extraction helps to narrow or close the scale gap between seismic and well data (Oppermann 2010, 2012).
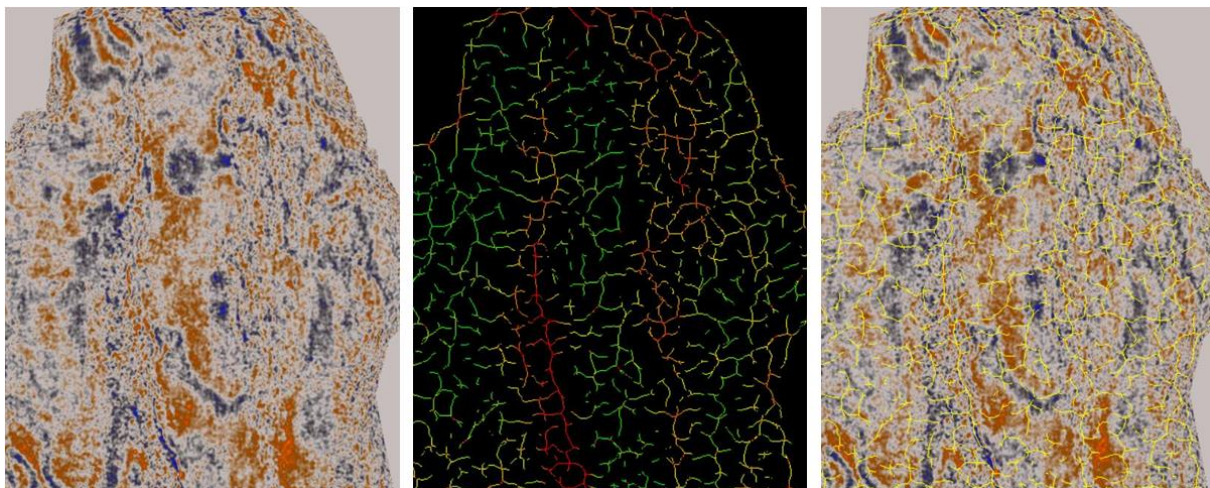
Figure 6: Comparison of reflectivity data with regional fault extraction results. Same time slice) through different volumes: (a) Reflectivity, (b) Fracture Network (red=high confidence, green=low confidence), (c) Fracture Network Reflectivity [Beharra Springs 3D seismic data set, time slices at 1,150 msec].

Unpublished studies have also revealed that varying fracture densities encountered in wells (identified from image logs) are primarily related to the orientation of a well relative to a seismic fracture zone, or fracture corridor. Higher image log fracture densities are usually encountered when drilling parallel or sub-parallel to seismic fractures/fracture corridors, suggesting that a simple geometrical relationship exists between fracture density and well orientation. This highlights that detailed well planning using seismic fracture network data can allow us to increase fracture intersections and target productive sweet spots.

In the NPB, coherency processing was undertaken to help delineate major fault trends (figure 5). However, this only shows the general trends of the faulting. This work is therefore being supplemented by both regional and high-resolution fracture processing that provide much greater detail regarding the orientation and density of the fracture networks (figure 6).

Analysis of the Redback-1 image logs reveals two conductive fractures within the Kockatea Shale between 3334 and 3335m (Figure 7). The orientation of the two fractures is azimuth 338 degrees with a dip of 37 degrees and 221 degrees with a dip of 29 degrees, respectively. The lower fracture displays a void of approximately 25 cm. Automated fracture detection results in the immediate vicinity of the well bore are shown in Figure 8 and illustrate two fractures were detected, one trending NW-SE, the other trending NE-SW; the features appear to intersect near the well bore (Figure 8a). Figure 8b

show that both of these fractures have low dip angles consistent with the orientation observed in the image log.

While full evaluation of these results is still underway, they provide encouragement about the potential to correlate well bore and seismic data to accurately detect fractures. These results are being evaluated in conjunction with the heat flow and temperature data to identify the most favourable drilling location to directly target favourably oriented fractures, thus maximising the chance of being able to produce a sufficient volume of hot water to sustain a geothermal development.
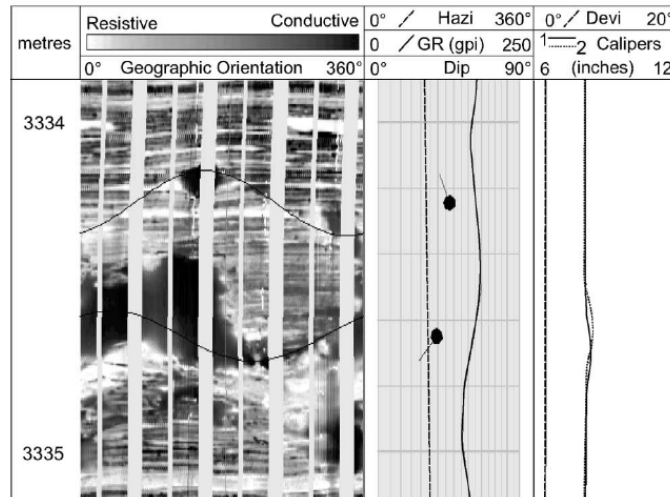
Figure 7: Image log from Redback-1 showing 2 conductive fractures, the lower one has contains a void of approximately 25cm. The upper fracture has an azimuth of 338 degrees and a dip of 37 degrees and the lower one an azimuth of 221 degrees and a dip of 29 degrees. (from King, et al, 2008)

Conclusions

The NPB displays all the necessary ingredients for successful development of a HSA geothermal development based on both matrix and fracture permeability type plays. Well data proves that temperatures in excess of 150°C can be reached at depths less than 3500m. The most significant risk is identifying a zone with sufficient transmissivity to allow geothermal waters to be produced at commercially viable flow rates.

Work completed to date shows naturally occurring open fractures provide the best opportunity for intersecting a reservoir with the required transmissivity. Fault and fracture orientations most likely to be critically stressed, and therefore open and permeable, have been modelled based on the local stress regime in the NPB. Interpretation of borehole image logs provides data on the orientation of resistive and conductive fractures observed in the area.

These results are now being utilised to focus the seismic interpretation in order to identify a low risk drilling target. The application of new structural volume interpretation techniques in the NPB has shown that fault and fracture networks can be delineated at high resolution from seismic data. The integration of these seismic fracture networks with well and other data allows identification of areas with favourable fault orientations and densities that will significantly increase the chances of intersecting a suitable conduit for geothermal fluid production and ensure the potential for a successful HSA geothermal project.
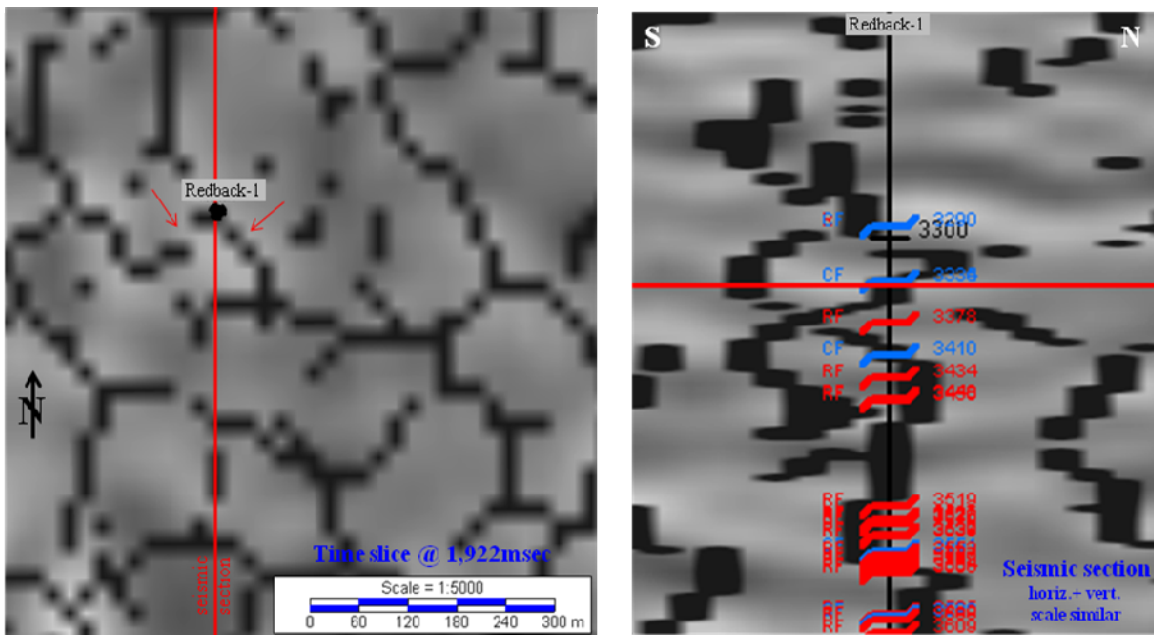
Figure 8: *Automated fracture analysis results showing high resolution results (low plus high confidence faults) in the Redback-1 area showing a) a time slice at 1922ms (~3334m) and b) seismic section through the well location.*

References

Bailey, A.H.E., King, R. C. And Backe, G., in press, Integration of Structural, Stress and Seismic Data to Define Secondary Permeability Networks Through Deep Comented Sediments in the Northern Perth Basin, *Proc of* APPEA Conference 2012.

Beardsmore, G., 2010, Northern Perth Basin Project (NPBP) Geothermal Play, Statement of Geothermal Resources, unpublished report for Green Rock Energy Ltd .

Cooper, G.T and Beardsmore, G.M., 2008, Geothermal systems assessment: understanding risks in geothermal exploration in Australia, Proc. PESA Eastern Australian Basins Symposium III, pp. 411-419.

King, R. C., Hillis, R. R. and Reynolds, S. D., 2008,'In situ stresses and natural fractures in the Northern Perth Basin, Australia', Australian Journal of Earth Sciences, 55:5,685 — 701.

King, R., Khair, A.A.,Bailey, A., Backe, G., Holford, S. and Hand, M., 2011, Integration of In-Situ Stress Analysis and Three-Dimensional Seismic Mapping to Understand Fracture Networks in Australian Basins, Australian Geothermal Energy Conference 2011, Melbourne.

Laker, N., 2000 Sedimentalogical and Petrographic Review of the Permo-Triassic Sandstones of the Northern Perth Basin, unpublished report by Oolithica Geoscience Ltd prepared for AWE.

Larking, A.L, 2010, Geothermal Energy in the Perth Basin, Australia: Comparisons with the Rhine Graben, *proc of* AGEA Conference, p. 30-34..

Larking, A.L., Meyer, Meyer, G., and Ballesteros, M., 2011, Mid West Geothermal Project, North Perth Basin, Australia, *proc of* AGEA Conference, p.139.

Mortimer, L., 2010, Geothermal Flow Rates in Australia – What Can We Expect and How We Can Mitigate Pre-Drill Risks, PESA News April/May 2010, pp 66-67.

Mory, A.J. and Iasky, R.P, 1996, Stratigraphy and Structure of the Onshore Northern Perth Basin, Western Australia, Geol. Survey W.A. Report 46.

Oppermann, R., 2010, A new method for high-resolution fault imaging delivers groundbreaking insights into drilling and production of resources, ASEG 21st International Geophysical Conference and Exhibition, Extended Abstract, Sydney.

Oppermann, R., 2012, High-resolution fracture recognition from seismic data - applying oil and gas technology to mining, In: Deep Mining 2012, Y. Potvin (ed), Australian Centre for Geomechanics, Perth.

Schindler, Baumgartner, M. J., Gandy, T., Hauffe, P., Hettkamp, T., Menzel, H., Penzkofer, P., Teza, D., Tischner, T., and Wahl, G., 2010, Successful Hydraulic Stimulation Techniques for Electic Power Production in the Upper Rhine Graben, Central Europe, *Proc World Geothermal Congress 2010*, Bali, Indonesia.

Sagasco, 1993, Mountain Bridge-1 Well Completion Report

Waining, B., 2009, Northern Perth Basin – extended heat flow analysis of wells for the GRK tenement areas. Unpublished report for Green Rock Energy Ltd.

Use of *In-situ* flow-through reactors to study mineral replacement reactions and associated permeability changes in hydrothermal systems

Brautigan, D[1,2,3.], Etschmann, B[1,2,3.], Pring [A.1,5.], O'Neil, B[4]., Ngothai, Y[2,4.]

[1]Department of Mineralogy, South Australian Museum, North Terrace, Adelaide, SA 5000 Australia
[2]South Australian Centre for Geothermal Energy Research, University of Adelaide, Adelaide, SA 5005, Australia
[3]School of Earth and Environmental Sciences, University of Adelaide, Adelaide, SA 5005, Australia
[4]School of Chemical Engineering, University of Adelaide, Adelaide, SA 5005, Australia
[5]School of Chemistry and Physics, University of Adelaide, Adelaide, SA 5005, Australia

david.brautigan@adelaide.edu.au

Mineral replacement reactions and permeability

When a mineral interacts with a fluid with which it is not in equilibrium, a chemical reaction occurs which may result in replacement of all or part of the original (parent) mineral and the formation of a new (product) material. This mineral replacement reaction occurs in 2 stages:

- Dissolution of the parent material until it comes into equilibrium with the fluid (thus changing the composition of the fluid).

- Precipitation of a new mineral assemblage from the fluid that replaces all or part of the parent assemblage.

Critically, the above process can result in new porosity generation at the reaction front (Putnis 2009). Changes in volume associated with mineral replacement reactions induce stress into the system, resulting in micro-fractures and porosity changes that change the permeability of the mineral assemblage (Xia *et al* 2009).

Hydrothermal mineral replacement reactions play an important role in controlling fluid transport in fluid flow environments such as geothermal energy systems. Their role has been studied principally via numerical modelling due to the widely held belief that the timescale of mineral replacement reactions are incompatible with laboratory experiments (Berkowitz 2002). Very little experimental research has been conducted and the relative contributions to permeability of micro-cracks and reaction generated porosity are not empirically verified.

In order to an attempt to explore this problem experimentally we have developed *in-situ* flow-through reactors (figure 1). The reactors are used to determine the effect of pressure, temperature, fluid flow rate, fluid composition and pH on mineral replacement reactions and associated changes in permeability.

In-situ flow through reactors

A high pressure high performance liquid chromatography (HPLC) pump was used to generate fluid flow rates of between 1 and 10 ml-min. The pump was capable of maintaining these flow rates at pressures of up to 400 bar (6,750 PSI). The HPLC pump was used in conjunction with a hand loaded back pressure regulator (BPR) providing pressures of up to 400 bar.

A heating jacket, capable of heating to 400^0C was used to heat fluid prior to its passing through the mineral sample. As heat transference into the BPR could result in increasing pressure over time, the fluid was cooled prior to reaching the BPR. Pressure transducers were placed before and after the sample holder and linked to a data logger so that pressure changes could be used to detect changes in porosity of the sample.

Ultra high pressure reactor

In order to simulate more extreme hydrothermal environments an ultra-high pressure flow-through reactor is being developed.

An ultra-high pressure HPLC pump will generate fluid flow rates of between 0.001 and 5 ml-min. The pump is capable of maintaining these flow rates at pressures of up to 1700 bar (25,000 PSI) in conjunction with a high performance BPR.

The reactor's tubing, sample holding cell and fittings will be constructed from high pressure nickel-alloy (Inconel 625 and Hastealloy C276). Conventional stainless steel components are incapable of withstanding the required temperatures/pressures and have poor corrosion resistance at high temperatures, particularly with saline fluids, resulting in the development of leaks after 24 hours of use. The nickel alloys are capable of withstanding very high pressures (>1500 bar) at high temperatures (>500°C). The alloys are also highly corrosion resistant allowing corrosive fluids such as chlorides to be used at elevated temperatures and pressures for extended periods.

Benefits gained from the reactors include the ability to simulate dynamic rather than static environments for study of mineral transformation reactions. The reactors allow us to independently control pressure, temperature and flow rate so the effect of each on mineral transformation and porosity can be independently assessed.
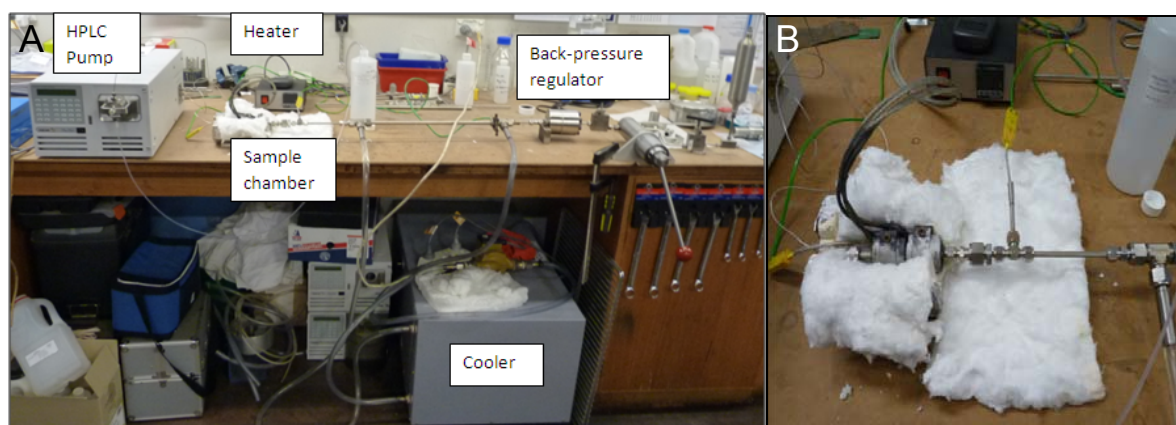
Figure 1: A: Flow through reactor showing (from left to right) HPLC pump, heating element, sample chamber, cooling unit and hand loaded back pressure regulator. Tubing and fittings are stainless steel. Pressure transducers are not fitted. B: A close up image of the heating unit (at left) and sample holder (immediately to the left of the heating unit).

Sample analysis

Samples were non-destructively analysed before and after treatments using a Philips XL40 scanning electron microscope (SEM), Cameca SX-51 electron microprobe with SAMX software and a Skyscan 1072 micro-computer tomography (MCT) analyser. Energy dispersive analysis X-ray (EDAX) analysis was used to determine changes in elemental composition of the samples. MCT analysis allowed construction of 3-dimensional x-ray images of samples from which porosity could be determined using grey-scale analysis.

Preliminary studies

Dolomitisation of marble

Pilot dolomitisation experiments were performed on a 12mm by 7 mm marble sample at 30 bar pressure and 200^{0}C. The sample was pre-cracked to allow fluid flow through the marble and provide a

region of interest to monitor for dolomitisation. Pressure transducers linked to a data logger were used to monitor for pressure changes across the marble sample resulting from changes in porosity. A magnesium/calcium solution was pumped through the sample at a flow-rate of 10 ml-min.

Initial results showed a 16 bar pressure difference across the marble sample over 10 days, indicating a significant change in porosity had occurred. Analysis using a SEM and electron microprobe showed dolomitisation occurred both at the front face of the marble sample and along the crack (figure 2). The dolomitisation extended from the crack into the marble along the calcite grain boundaries.
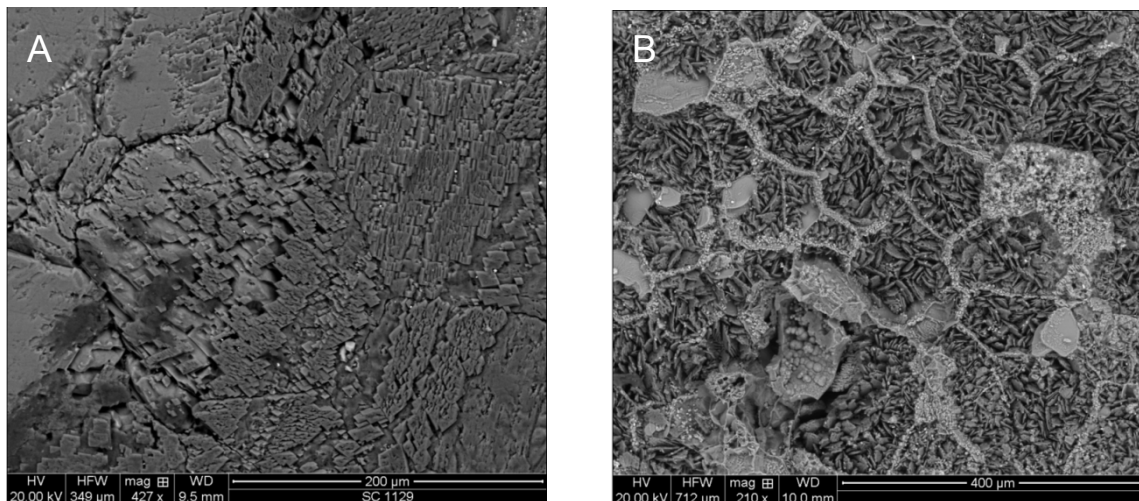
Figure 2: Dolomotisation of marble at A: front face of marble. The image is a backscattered electron image sample (Quanta 450 FEG ESEM, 60 Pa) of the unpolished sample. The lighter grey areas are calcite; the darker grey areas are dolomite B: Looking along the crack. The lighter grey boundaries are proto-dolomite with low amounts of calcium. The interior of the grains is magnesium carbonate. Large crystals of silicate minerals are also visible.

Isolation of variables affecting dolomitisation of limestone

The reactors have also initially been used to isolate the effect of fluid flow rate on the rate of mineral transformation and analyse associated changes in porosity. Dolomitisation of limestone was selected as an appropriate process to study the phenomena. Mineral samples analysed were 4.3mm in diameter by 4mm length, to allow optimal resolution during MCT analysis (5 microns). Sample's were wrapped in Teflon and placed in a vespel plastic sheathing before being placed in the reactor's sample holder to ensure a fluid tight fit.

Reaction fluid was composed of 1 molar magnesium chloride ($MgCl_2 \cdot 6H_2O$) and 1 molar calcium chloride ($CaCl_2 \cdot 2H_2O$) as suggested by Kaczmarek and Sibley (2011). A magnesium/calcium ratio of 1.14:1 was used to minimise time needed for substantial dolomitisation of the limestone to occur (i.e. less than 48 hours for > 50% dolomitisation). Other variable values used in the experiment are shown in table 1. The samples were placed in the reactors for 24 hours.

Table 1: Parameters for variable flow rate experiment and level of dolomitisation achieved and associated porosity.

Flow rate (ml/min)	1	10
Temperature (^{o}C)	200	200
Pressure (Bar)	250	250
Mg:Ca ratio	1.14:1	1.14:1
% proto-dolomitisation	36	19
Porosity %	17	10

Formation of proto-dolomites occurred within 24 hours and was negatively correlated with fluid flow rate (table1). It is likely that faster flow rates inhibited nucleation of the dolomite onto the limestone surface. Porosity increased with dolomitisation due to the smaller volume of the replacement dolomite (because of magnesium's smaller ionic radius) compared to calcite.

Future work

Further work on mineral transformations in hydro-thermal systems will involve analysing the independent effect of fluid composition, pressure, and temperature on transformation rates and porosity generation.

The above methodology is being applied to mineral samples taken from the Otway Basin Geothermal Well (Ladbroke Grove 1). Mineral permeability varies at this site depending on whether the sample is taken from above or below the oil-water contact point. We will use our flow through reactors to simulate these environments and, by subjecting samples to differing pressure/temperature regimes, alter their porosity, thus gaining an understanding of the diagenetic processes responsible for the sample's natural permeability.

The ultra high pressure/temperature reactors under development will also allow us to simulate and study more extreme pressure/temperature regimes. The data gathered may then be used to develop reactive fluid flow models linking pressure, temperature, fluid flow rate and fluid composition to mineral transformation and permeability in hydrothermal systems.

Acknowledgments

References

Putnis, A., 2009. *Mineral Replacement Reactions* Reviews in Mineralogy and Chemistry,70, 87-124

Xia, F., Brugger, J., Ngothai, Y., O'Neill, B., Chen, G., Putnis, A., Pring, A. 2009. Mechanism and kinetics of pseudomorphic mineral replacement reactions: A case study of the replacement of pentlandite by violarite, *Geochimica et Cosmochimica Acta*, 73, 1945-1969.

Berkowitz, B., 2002. Characterising flow and transport in fractured geological media: a review. Advances in Water Resources 25, 861-848.

Is it hot enough down there?
Assessing geothermal potential in the Sydney-Gunnedah-Bowen Basin

Danis, C[1*]., O'Neill, C[1]. and Quenette, S[1].

Macquarie University and SMEC Australia

cara_danis@mq.edu.au

The Earth's upper crust hosts many important economic resources, from minerals to groundwater to energy, but the subsurface structure and associated thermal structure is poorly understood. Internal heat is the driving force behind many of the Earth's processes and is now being considered as a new form of clean renewable energy. High resolution 3D thermal models, incorporating detailed geological structure and real world data, are effective in assessing thermal structure and provide improved temperature estimates for geothermal exploration. Unlike historical 1D models and extrapolated temperature at depth maps, 3D thermal models are appealing to the geothermal exploration industry as they are not limited by the sparse nature of down-hole temperature measurements or heat flow and the uncertainties of such models can be calculated.

In the Sydney-Gunnedah-Bowen Basin (SGBB) system, Australia's energy rich sedimentary basin, the thermal structure is poorly understood resulting in its geothermal potential largely being ignored. Thermal modelling using optimised parameters shows estimated temperatures at 5km below the surface, the economic limit of drilling, to range from 120°C to 240°C, with highest temperatures under thick sediments with multiple insulating coal layers. Using the 150°C temperature contour as in indicator for potential geothermal prospectivity, the most potential basins are in the Bowen and Sydney.

Keywords: geothermal potential, Sydney-Gunnedah-Bowen Basin, thermal structure

Introduction

Multidimensional, scalable geodynamic models are required to combine the knowledge of heat flow and thermal characteristics, with detailed geological structure and real world measurements, to better understand the thermal structure of the Earth's upper crust. Historical approaches, using 1D models (i.e. Chopra and Holgate, 2006) and extrapolated temperature at depth maps (i.e. Gerner and Holgate, 2010) have inherent limitations and are inappropriate for complex systems (Danis et al. 2012a). Around the world, the resources of the upper crust are experience rapid rates of development as demand increases. In Australia the development of multiple resources, i.e. minerals, energy (coal, coal seam gas, natural gas, geothermal), groundwater, in the energy rich sedimentary basin of the Sydney-Gunnedah-Bowen Basin (Figure 1) has highlighted the lack of subsurface information that exists, particularly thermal structure.

The advancement of geothermal energy exploration in the SGBB has been limited by scarce and inaccurate thermal datasets, oversimplified interpretations and under-constrained thermal models (Mussons et al., 2009). Geothermal exploration requires accurate assessments of the temperature at depth. High resolution 3D thermal models provide a new method of accurately assessing the thermal structure of the SGBB with representative estimates of temperature at depth. 3D thermal models in systems such as *Underworld* are advantages as they approach the problem of assessing thermal structure from the upper crustal scale (>500km x 500km), as opposed to the small scale (<25km x 25km) reservoir models used for resource modelling, allowing 3D elements, like heat flow, to fully interact with detailed geological structures and physical rock properties. The big advantage of this model is the uncertainty of parameters used have characterised, optimised for best-fit to match real world observables.

The 3D thermal model of the SGBB shows the importance of subsurface architecture and geology on heat flow, with high temperatures observed in the Bowen and Sydney Basin, under thick sediments with multiple insulating coal layers. The depth of the 150°C temperature contour provides a primary indicator of geothermal potential. Assessing temperatures, at 5km below the surface, shows parts of the Sydney and Bowen basins generally exceed 170°C with some areas in the Bowen Basin reach over 200°C.
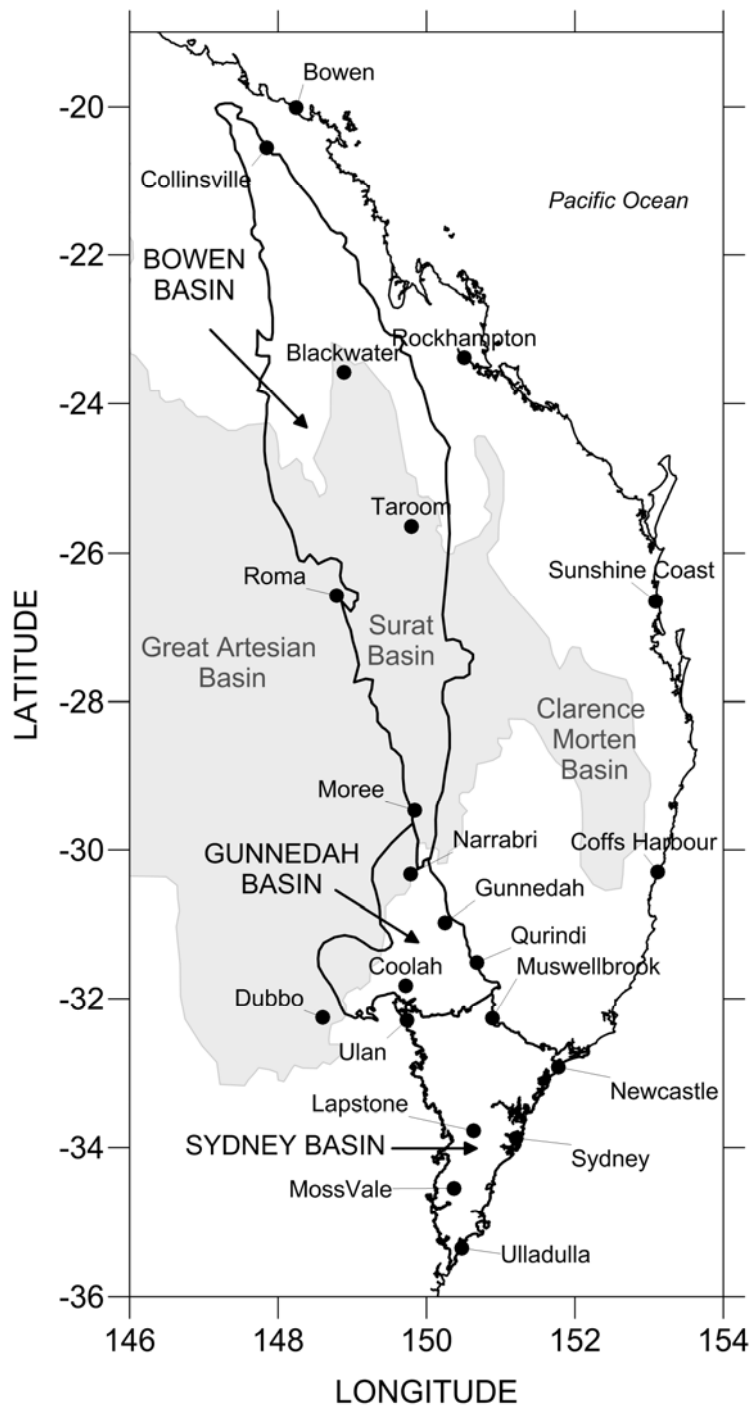
Figure 1: *Location of Sydney-Gunnedah-Bowen Basin, Eastern Australia showing major town names. Grey shaded area is the outline of the overlying Great Artesian Basin and Surat Basin and Clarence Moreton Basin.*

Method

High resolution 3D model of the SGBB is created in the *Underworld* platform, with the detailed geological model used previously in Danis et al. (2010, 2011, 2012b) (Figure 2), and run using the *Underworld-GT* toolbox.
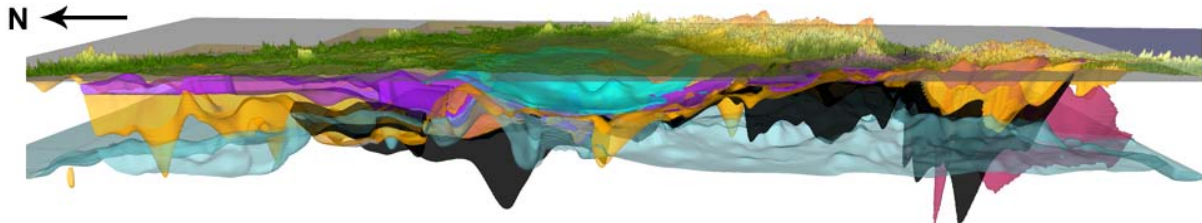
Figure 2: Image of the Sydney-Gunnedah-Bowen Basin 3D Geological model from the gLucifer viewer associated with Underworld. This is a cross-section view looking toward the east through the model. Geological layer surfaces are shown with a level of transparency and surface topography is overlain on top.

This model covers the area between Latitude -36 to -19 and Longitude 147 to 154 at a resolution 3000m by 17m by 3000m. The four major material volumes; basement, basal volcanics, sediment and coal measures, are imported in as ten surfaces, in stratigraphic order, and smooth particle hydrodynamics is used to interpolate between the surface points to create the surface geometry of the chosen resolution.

For each of the material types thermal properties area assigned (Table 1) which have been derived from material and subsurface parameter optimisation work. This work involved undertaking a parameter sensitivity analysis and comparing the resulting modelled geotherms to measured geotherms. In this way the high resolution 3D model was calibrated against real world observables. The 'best-fit' parameters from the sensitivity analysis satisfy the thermal constraints imposed by over 300 temperatures at depth points across the Sydney Basin.

The work of Clauser and Huenges (1995) demonstrate there is a significant decrease in thermal conductivity of rocks when temperature is increased; therefore this model contains temperature dependent conductivity parameters for each material. In Table 1, K_0 represents the conductivity of the material at the surface at T_0, which is 15°C. Thermal conductivity decreases linearly between the surface to a point where it remains at a constant value K_{crit}, at T_{crit} which is 300°C.

Table 1: Thermal Properties of Materials in the Underworld Model

Material	Density (t/m^3)	K_0 (W/m-K)	K_{crit} (W/m-K)	Heat Production (µW/m^3)
Sediment	2.46	2.00	1.50	1.25
Coal Measures (Greta/Maules/Reid Dome/Jurassic)	1.90	3.0	0.20	1.25
Coal Measures (PCM)	1.90	1.20	0.20	1.25
Basal Volcanics	2.95	3.00	2.25	0.50
Basement (under fault)	2.70	3.00	2.25	2.00
Basement	2.70	3.00	1.50	2.00

In the model the temperature boundary condition is 15°C at the surface, the basal temperature at 12km is 345°C and the side boundary conditions are reflective. The model is run from low resolution to high resolution and the temperature at 5km below the ground surface extracted and contoured, as shown in Figure 3.
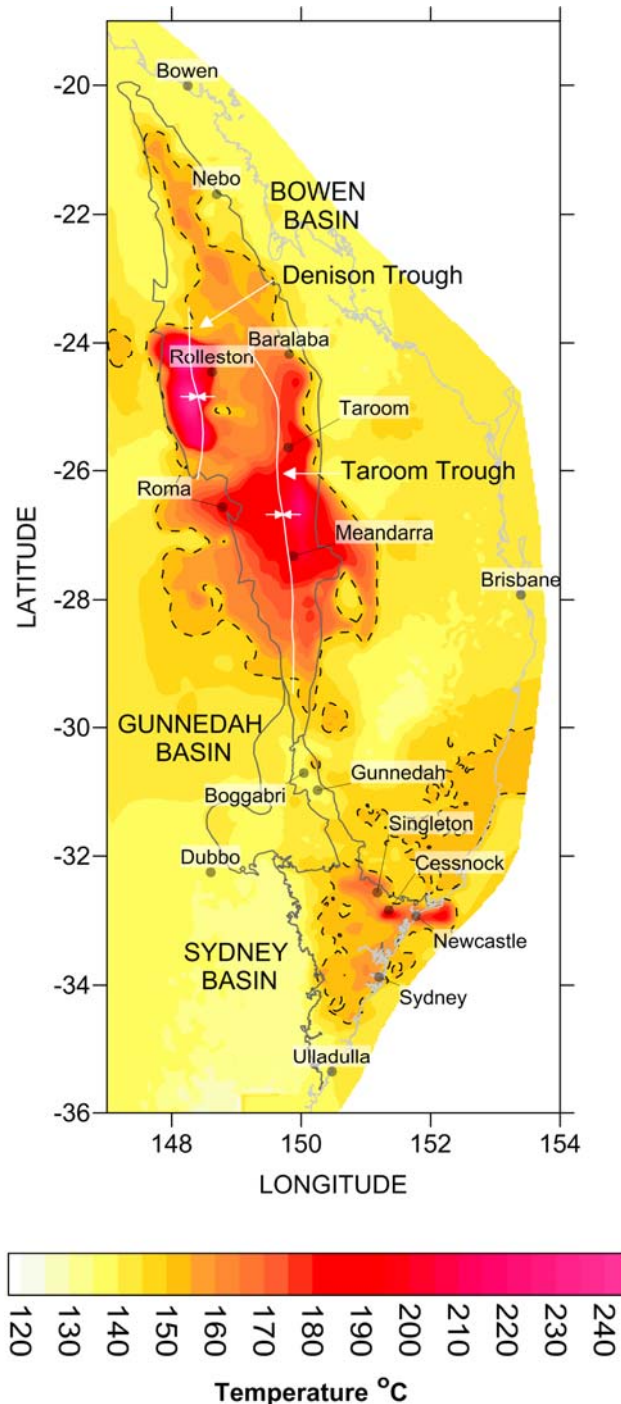
Figure 3: Temperature contour map of the Sydney-Gunnedah-Bowen Basin at 5km below the surface. The temperature colours range from yellow (140°C) through red (190°C) to magenta (240°C). Dashed black line represents the 150°C temperature contour. Basin outline and coastline in grey with key place names. Highest temperatures are modelled in the Bowen Basin near Rolleston (220°C) and in the Taroom Trough (190°C) and in the Sydney Basin near Cessnock and Newcastle (180°C)

Results

Using high resolution and calibrated 3D thermal models to estimate the temperature at depth is a cost effective way of assessing the geothermal potential of the SGBB. The current economic limit of drilling and development has been described by many as approximately 5km below the surface (e.g. Budd et al. 2008) therefore in Figure 3 a contour map of the model estimated temperature is present for this depth. It shows within the basin system temperatures range from 140°C to 240°C. If the 150°C temperature contour is considered an indicator of geothermal potential then a vast majority of the basin system satisfies this condition. In order to achieve higher temperatures there is always the option to drill deeper.

The major contributing factor to high temperature at depth is the coal measures and the more coal measures in an area the higher the temperature. The depositional cycles in the basin system result in two extensive coal events, the Permian and the Jurassic. The Permian is considerably thick in the Bowen Basin and when Jurassic Coal Measures occur in the same location the insulating effect of the coal measures is enhanced thus producing higher temperatures. This is less common in the Sydney Basin as there is no Jurassic Coal Measures and the Early Permian Coal (e.g. Greta and Clyde Coal Measures) Measures are not nearly as extensive.

Temperature in the Sydney Basin ranges from approximately 140°C to 185°C. The offshore part of the Sydney Basin is not considered practical for exploration and is not well constrained in this model. Highest temperatures are modelling near Cessnock and between Singleton and Newcastle temperatures at 170°C to 180°C. This is reflecting the presence of multiple coal measures; the Permian Coal (PCM) and the lower Greta Coal, and thick sediments (3-4km).

The Gunnedah Basin temperature is modelled between 140°C to just above 150°C. This reflects the shallow nature of the basin structure where sediments are generally 1km thick. Temperatures are higher in the Maules Creek sub-basin, west of Boggabri, at 150°C as a result of two sets of coal measures. In essence the Gunnedah Basin is not hot enough for geothermal potential within the current limit of economic drilling.

Temperature in the Bowen Basin range from 140°C to 240°C, with higher temperatures concentrated between Meandarra and Baralaba. In the Denison Trough, near Rolleston, the temperature ranges from 190°C to 240°C, a result of thick overlying sediment (~4km) and the Permian and Reid Dome Beds Coal Measures. In the southern part of the Basin, between Roma, Taroom and south of Meandarra the addition of Jurassic Coal measures, with the sediments and Permian Coal Measures results in temperatures of around180°C to 210°C.

If the insulating effects of the coal measures are not considered in the thermal model, as such the properties are the same as the sediments, then modelling suggests that the temperature at 5km would struggle to reach 150°C anywhere in the basin system. Therefore coal, and its thermal properties, is very important when modelling and considering the geothermal potential of an area. The more coal there is the greater the likelihood that the temperature at depth will be high.

Conclusions

The geothermal potential of the SGBB system has largely remained unexplored, due to a limited understanding of the thermal structure of the system. High resolution 3D thermal modelling, using a detailed geological model and optimised 'best-fit' thermal properties and subsurface parameters, allows for a comprehensive assessment of the thermal structure of the SGBB as well as providing representative estimates of temperature at depth.

For a vast part of the Bowen Basin and in some parts of the Sydney Basin temperatures at 5km exceed 180°C making it indeed hot enough to consider more detailed geothermal exploration. There is potential for significant geothermal resources. Further refinement of temperature at depth can be achieved through sensitivity analysis of each model material and calibration of the model against an ever increasing suite of real world observables (temperature, thermal conductivity and heat flow etc.).

References

Budd, A., Holgate, F., Gerner, E., Ayling, B., 2008. *Pre-competitive geoscience for geothermal exploration and development, Geoscience Australia's Onshore Energy Security Program and Geothermal Energy Project*. GRC Transactions 32, 347-350

Chopra, P., Holgate, F., 2006. *A GIS analysis of temperature in the Australian Crust.* Proceedings of the World Geothermal Congress, Turkey, Abstracts

Clauser, C., Huenge, E., 1995. *Thermal conductivity of rocks and minerals – Rock Physics and Phase Relations, A handbook of physical constraints.* American Geophysical Union

Danis, C., O'Neill, C., Lackie, M., 2010. *Gunnedah Baisn 3D architecture and upper crustal temperatures.* Australian Journal of Earth Sciences 57, 483-505

Danis, C., O'Neill, C., Lackie, M., Twigg, L., Danis, A., 2011. *Deep 3D structure of the Sydney Basin using gravity modelling.* Australian Journal of Earth Sciences 58, 517-542

Danis, C., O'Neill, C., Lee, J., 2012a. *Geothermal state of the Sydney Basin: assessment of constraints and techniques.* Australian Journal Earth Sciences 59, 75-91

Danis, C., O'Neill, C., Lackie, M., 2012b. *Building 3D geological knowledge through regional scale gravity modelling for the Bowen Basin.* Exploration Geophysics 43, 8-25

Gerner, E., Holgate, F., 2010. *OzTemp – Interpreted temperature at 5km depth image.* Geoscience Australia

Mussons A., Harrison, B., Gordon, K., Wright, S., Sandiford, M., 2019. *Thermal thinking: optimal targeting for Australian geothermal explorers.* Proceedings of the Australian Geothermal Energy Conference, Brisbane, Record 2009/35

Review of thermal conductivity correction methods for prediction at reservoir conditions

Dillinger, A., Ricard, L. P., Esteban, L.

CSIRO Earth Science and Resources Engineering, Kensington WA 6151

Ludovic.Ricard@csiro.au

Abstract

Thermal conductivity is a key parameter for temperature measurement interpretation, thermal modelling and also for geothermal reservoir assessments. Thermal conductivity depends mostly on mineralogy, porosity, texture (grain size, grain contact density, pore size and pore aspect ratio), fluid saturation, temperature and pressure. Direct measurement at reservoir depth is still not a common practice. Instead, a large variety of methods exists to predict thermal conductivity knowing the mineralogy, porosity or density for instance; or commonly measured under laboratory conditions on recovered materials from boreholes: cuttings and core samples.

To inform modelling studies with accurate sub-surface thermal conductivity values, the thermal conductivity measurements have to be corrected from laboratory to in-situ conditions. This 'lab to in-situ' correction has been the focus of a significant number of studies that can be classified as empirical, effective theories and numerical approaches. Those methods have investigated rock types ranging from sedimentary to igneous and metamorphic rocks.

The aim of this contribution is to present a comparative analysis of in-situ corrected thermal conductivity based on the different model approaches applied on selected reservoirs from Australia representative of the geothermal resources. In both cases, a large number of correction methods found in the literature have been tested. Each method has been compared while taking into account their associated uncertainties on the thermal conductivity assessment as a function of temperature and pressure.

Keywords

Thermal conductivity; temperature; pressure; 'lab to in-situ' correction

Introduction

Many petroleum and geothermal industrial applications (Prensky, 1992) require the interpretation of temperature measurements, the estimation of heat-flow, the knowledge of thermal properties and the high-temperature behaviour of rock/fluid systems over different scales ranging from the core to the basin scale. One of the key parameter for geothermics analysis is the thermal conductivity of the rock-fluid system. The thermal conductivity is the capacity of a material to conduct and transmit heat. It is primarily controlled by the mineral composition (each mineral has its own conductivity value (Horai, 1971)), the porosity (different conductivities between rock matrix and interstitial fluids (Brigaud and Vasseur, 1989, Beardsmore and Cull, 2001)) and the texture of the rocks (degree of organisation (Midttomme et al., 1998)). Besides that, thermal conductivity shows a great dependence on in-situ conditions: it decreases with temperature, as thermal cracking by differential expansion of minerals creates contact resistances between grains; while it increases with increasing stress (and pressure), as grains contact is enhanced by the reduction of the intergranular space (Birch and Clark, 1940, Roy et al., 1981, Clauser and Huenges, 1995).

In most deep resource studies, the thermal conductivity parameter are measured on core samples or cuttings recovered from boreholes. These measurements are achieved under ambient laboratory conditions, which obviously arises problems of reliability and representativity of the 'in-situ' conditions at the time of modelling the geothermal reservoir. Laboratory room condition measurements would then need to be corrected to 'in-situ' conditions. The accuracy of petrophysics modelling studies is

based on the capability of the model to reproduce the 'in-situ' conditions of the test specimen. The estimation and prediction of thermal conductivity depending on the geological and petrophysics parameters (temperature, stress, petrology, amount of liquid, distribution of porosity, grain size, density, anisotropy...) has been the focus of several studies.

Since high-temperature and high-pressure measurements involve experimental difficulties and since it is not possible to duplicate in the laboratory the conditions of the earth's interior, theoretical and predictions methods can be used to extrapolate laboratory measurements to high temperatures and pressures. This work suggests a review on the different modelling techniques and its application to selected rock type for the temperature interpretation and prediction at great depth. The prediction of thermal conductivity in the 'in-situ' conditions is achieved by following empirical models stemming from the literature. As the mineralogy, porosity and texture are the predominant parameters controlling the rock thermal properties; special care is dedicated to the rock type which actually leads the selection of the proper model.

Thermal conductivity dependencies

Temperature

For a structurally perfect isotropic crystal, lattice conductivity λ_l (W m^{-1} K^{-1}) tends to be theoretically inversely proportional to temperature T (K) (Buntebarth, 1991). In reality, rocks are composed of a mixture of highly disordered crystals of different compositions. Therefore, thermal conductivity of rocks decreases more slowly (λ_l = T-n, where 0 < n < 1), remains independent (poor conductors) or tends to slightly increase with temperature in some instances (feldspar aggregates, glasses and vitreous materials) (Somerton, 1992).

These relationships are valid in the temperature range 0 – 1200 ºC, where phonon conductivity dominates. They are no longer valid at higher temperatures, heat transfer being mainly driven by radiation. The radiative thermal conductivity in contrast tends to be proportional to the cube of the temperature, following a T3 law (Clauser et al., 1988).

Measurements of thermal conductivity as a function of increasing temperature generally show an initial decrease with temperature, until around 1000 – 1200 ºC, then the radiative component balances and sometimes inverts this decreasing trend (Clauser and Huenges, 1995).

During the last two decades, several authors performed empirical models for the prediction of thermal conductivity within the in-situ conditions of temperature. These models are usually based on experimental and literature datasets.

Pressure

The pressure dependence on thermal conductivity consists in two phenomena. For an increasing pressure value up to 100 MPa, rocks are compressed, the pore space is reduced and microcracks gradually disappear, leading to the rapid rise of thermal conductivity to a more stable level (Buntebarth, 1984). This threshold change in thermal conductivity as well as in diffusivity (Seipold, 1995) can reach more than 10% for siltstones, clays and marls. Beyond 100 MPa, thermal conductivity increases linearly with the rising pressure due to the reduction of the intrinsic porosity and the compressibility of the rock-forming minerals. However, the variation of thermal properties with pressure does not seem to be large enough to cause grave errors for the heat flow calculation (Sekiguchi, 1984).

Discussion

After a large literature review, several models of thermal conductivity prediction at in-situ conditions were investigated with regard to the rock type they are developed for. Most of the models found in the literature are yielded through linear regressions fitting the experimental data sets. It becomes obvious that these models, and especially their related parameters, are mainly dependent on the geological

and geothermic context where the samples are stemming. Therefore, the choice of the proper empirical model to correct thermal conductivity measurements from laboratory to depth conditions has to be done by attentively considering the context of sampling.

The predictive models were first computed in function of the temperature and pressure parameters, with regard to different rock types. Special attention is dedicated to the sandstones and shales, their curves being normalized by using thermal conductivity measurements at room temperature stemming from existing core measurements. Those models are used for temperature versus depth predictions where the uncertainty of the temperature at a given depth is linked to the uncertainty on the thermal conductivity variation with temperature and the approach used to model it. Each step enables the comparison of the different models, highlights their discrepancies, and gives a preview on the errors and uncertainties they provide.

References

Beardsmore, G.R. & Cull, J.P., 2001. *Crustal Heat Flow: A Guide to Measurement and Modelling,* edn, Vol., pp. Pages, Cambridge University Press.

Birch, F. & Clark, H., 1940. The thermal conductivity of rocks and its dependence upon temperature and composition, *Am. J. Sci.,* 238**,** 529-558.

Brigaud, F. & Vasseur, G., 1989. Mineralogy, porosity and fluid control on thermal conductivity of sedimentary rocks, *Geophysical Journal International,* 98**,** 525-542.

Buntebarth, G., 1984. *Geothermics; an introduction,* edn, Vol., pp. Pages, Springer-Verlag, Berlin, Berlin, Federal Republic of Germany (DEU).

Buntebarth, G., 1991. Thermal properties of KTB-Oberpfalz VB core samples at elevated temperature and pressure, *Scientific Drilling,* 2**,** 73-80.

Clauser, C. & Huenges, E., 1995. Thermal conductivity of rocks and minerals. *in Rock Physics & Phase Relations: A Handbook of Physical Constants*, pp. 105-126AGU, Washington, DC.

Clauser, C., Rybach, L., Stegena, L. & Haenel, R., 1988. *Opacity; the concept of radiative thermal conductivity,* edn, Vol., pp. Pages, Kluwer Academic Publishers, Dordrecht, Dordrecht, Netherlands (NLD).

Horai, K.I., 1971. Thermal conductivity of rock-forming minerals, *Journal of Geophysical Research,* 76**,** 1278-&.

Midttomme, K., Roaldset, E. & Aagaard, P., 1998. Thermal conductivity of selected claystones and mudstones from England, *Clay Min.,* 33**,** 131-145.

Prensky, S., 1992. Temperature measurements in boreholes: an overview of engineering and scientific applications, *The log analyst,* 33**,** 313-333.

Roy, R.F., Beck, A.E. & Touloukian, Y.S., 1981. Thermophysical Properties of Rocks. *in Physical Properties of Rocks and Minerals*, pp. 409-502, eds. Touloukian, Y. S., Judd, R. R. & Roy, R. F. McGraw Hill, New York.

Seipold, U., 1995. The variation of thermal transport properties in the Earth's crust, *Journal of Geodynamics,* 20**,** 145-154.

Sekiguchi, K., 1984. A method for determining terrestrial heat flow in oil basinal areas, *Tectonophysics,* 103**,** 67-79.

Somerton, W.H., 1992. Thermal properties and temperature-related behavior of rock/fluid systems, *Thermal properties and temperature-related behavior of rock/fluid systems.*

A Realistic Assessment of Recoverable Thermal Energy from Australian Geothermal Reservoirs: A Simulation Study

Nima Gholizadeh Doonechaly[1], Sheik S. Rahman[1] and Andrei Kotousov[2]

[1]School of Petroleum Engineering, University of New South Wales, Sydney, Australia, [2]School of Mechanical Engineering, University of Adelaide, Adelaide, Australia,

sheik.rahman@unsw.edu.au

Keywords: Reservoir stimulation, shear dilation, distributed dislocation, local thermal non-equilibrium, FEM.

Summary

This paper presents an innovative distributed dislocation theory for estimation of change in fracture aperture due fluid induced pressure. The new approach is used to analyze the potential for thermal energy recovery from the Patchawarra geothermal reservoir in Australia. Results of this study show that the time required to stimulate a 500 m2 reservoir rock and sustain commercial flow rate (80 l/s) is much greater (two to three folds) than that previously studied. These results, however, agree well with the experience of existing EGS trials around the world. Thermal stresses induced during the circulation of cold water have a significant bearing on the long term production rate. As thermal drawdown of the rock matrix takes place, tensile thermal stresses are induced which allow residing fractures to dilate and enhance permeability. This gradually increases the fluid velocities between the injector and producer, yielding increasing production rates with time. It was also observed that the maximum thermal energy that can be recovered by use of our current know-how would be as much as 42%.

Introduction

Stimulation of geothermal reservoirs by fluid induced shear displacement has been used to create Enhanced Geothermal Systems (EGS). Models used to predict the change in fracture aperture and the consequent permeability enhancement are based on simple laboratory tests and field observations as well as best-guess estimates. In this study the reservoir, wellbores and the natural fractures (discrete) are coupled in a poro-thermo-elastic environment. The distributed dislocation technique is used to simulate the roughness induced opening of fractures in the presence of compressive and shear stresses as well as fluid pressure inside the fracture. This technique has allowed us for the first time to compute accurately changes of aperture along the fracture length of any number of discrete fractures in all parts of the reservoir due to induced fluid pressure and temperature. We have used local thermal non-equilibrium due to circulation of cold fluid to account for long term response. Also considered are the characteristic properties of rock and fracture to accurately simulate rock deformation.

Model Setup

A square region of the Patchawarra geothermal reservoir is chosen with a side length of 500 m at a depth of 2660 m. The characteristic data for this reservoir is presented in Table 1. Two wells, injection and production are placed at a distance of 700m apart. The reservoir is divided into 140,000 grid blocks. Maximum and minimum horizontal principal stresses are acting along the x and y axis. Stress, rock and reservoir parameters used for this study is shown in Table 2.

Table 1: Characteristic data using STAR resistivity image logs from Well A.

Top	2660
Bottom	2879
Number of fractures	69
Dip	30-60
Azimuth	065°N
Azimuth STD	17°
Vertical Stress (MPa)	54
Max. Horizontal Stress (MPa)	79
Min. Horizontal Stress (MPa)	60

The abovementioned model is meshed using triangular elements. For improving the stability linear triangles are used for pressure and temperature and quadratic triangular element for the displacement degrees of freedom. No flow boundary condition is applied at the boundary of the reservoir and the fluid is injected at the injection well. The production well starts producing with a set pressure at the end of stimulation period.

Overall, four major models are integrated to estimate stress changes due to fluid induced pressure and thermal drawdown by circulation of cold fluid and consequent changes in permeability. They include: generation of subsurface fracture map, simulation of fluid flow and heat transfer and reservoir stimulation in poro-thermo-elastic environment.

Table2: Stress and reservoir data for Patchawarra formation geothermal reservoir.

Rock Properties	
Young's modulus (GPa)	56
Poisson's ratio	0.25
Density (kg/m^3)	2650
Fracture basic friction angle (deg)	40
Shear dilation angle (deg)	2.8
90% closure stress (MPa)	20
In situ mean permeability (m^2)	9.0×10^{-17}
Fracture properties	
Fractal Dimension, D	1.2
Fracture density (m^2/m^3)	0.33
Smallest fracture radius (m)	15
Largest fracture radius (m)	250
Stress data	
Maximum horizontal stress (MPa)	78.9
Minimum horizontal stress (MPa)	53.3

Fluid properties	
Density (kg/m^3)	1000
Viscosity (Pa s)	3×10^{-4}
Hydrostatic fluid pressure (MPa)	27.5
Injector pressure, stimulation (MPa)	51.7
Injector pressure, production (MPa)	32.6
Producer pressure, stimulation (MPa)	N/A
Producer pressure, production (MPa)	22.3
Other reservoir data	
Well radius (m)	0.1
Number of injection wells	1
Number of production wells	1
Reservoir depth (m)	2660

Generation of subsurface fracture map

A hybrid of deterministic and stochastic techniques is used to generate subsurface discrete fracture network (Gholizadeh Doonechaly and Rahman, 2012). In this study, the tectonic history and characteristic data on fracture properties as well as reservoir structure of the Patchawarra formation available in the open literature are used to construct the fracture map (Mildren and Burgess, 2005, see Table1).

For the purpose of modelling tectonic history and in-situ stress (current) a Finite Element Method (FEM) is used. The reservoir structure is reconstructed by unfolding and folding (reverse and forward model) in a single tectonic event. Also a non-linear visco-elastic model is used to consider the effect of deformation on rock viscosity. After reconstructing the original shape of the layer, stress tensor values as well as the stress invariants are calculated for each node based on the deformation history of the model. Mohr-Colomb fracture criterion, which relates the critical strength of the material to its stress state, is used to determine whether the obtained stress exceeds strength (shear) of the rock. If the obtained stress tensor satisfies failure criterion, stress invariants are used to calculate the rate of formation of fractures for each node. Rate of formation of fractures is used as one of the most important input parameters for the next step of the Neural-stochastic simulation. As part of neuro-stochastic simulation, fracture properties (fracture density and fractal dimension) are generated based on their characterized statistical distribution obtained from tectonic simulation and field data (as listed in Table 1). In the next step the reservoir is divided into a number of grid blocks. Fracture density and fractal dimension are estimated for the blocks where the fracture data are available. Then the neural network is used to develop a 3D continuum map of fracture density and fractal dimension. Finally, the sequential Gaussian stochastic simulation combined with simulated annealing technique is used to generate the discrete fracture network. The 2D discrete Fracture map of Patchawarra reservoir at depth of 2660m is presented in Fig.1.
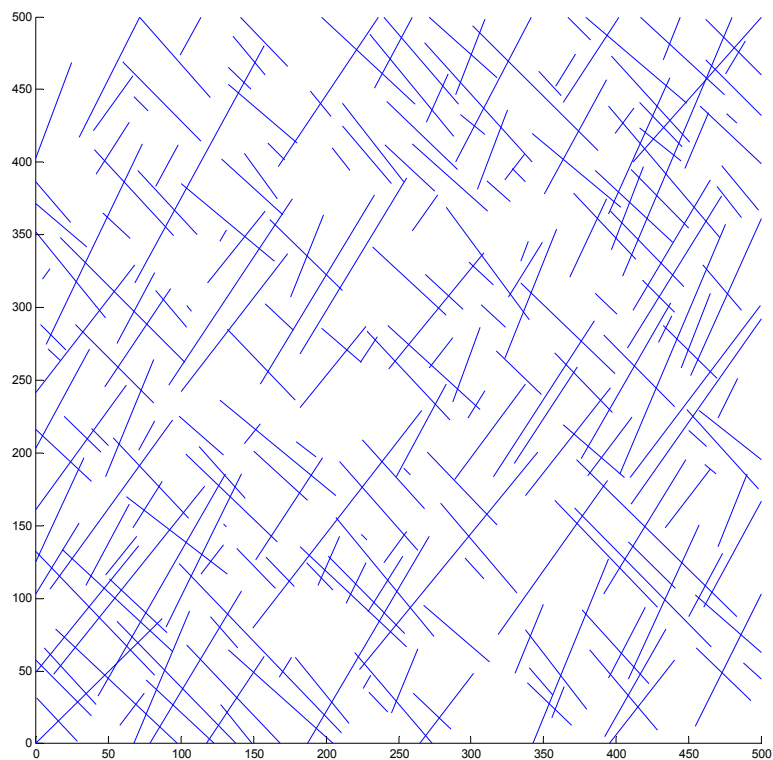
Figure 1: Patchawarra natural fracture network trace at 2660 m.

Fluid Flow Simulation

Fluid flow simulation is carried out using a hybrid of equivalent single continuum and discrete fracture approaches. For the single continuum approach, permeability tensor of each grid block is made known as a priori for the fractures shorter than 120 m. In this study, the effective permeability tensors as proposed by Teimoori and Rahman et al (2003) and later modified by Fahad and Rahman (2011) is estimated for each grid block. In this methodology, short fractures (less than 10m) are considered as part of the matrix pores and the fluid flow through them is simulated using the Darcy's law and Laplace equation. Also the boundaries of the short fractures are subjected to the interface boundary condition. Flow in the medium fractures (less than 120m) is characterized by the Cubic law. Flow region between matrix and fracture is characterized as Poisson's region and fluid flow in this region is simulated after Teimoori and Rahman, et al (2005). The effective permeability tensors are used in the next step as part of the thermo-poroelastic model of the reservoir. A representative schematic of the calculated grid based permeability tensor is shown in Fig. 2a.

In Fig 2b long fractures (longer than 120 m) are superimposed on effective permeability tensors calculated for medium to short fractures (less than 120m). Fluid flow is simulated using both effective permeability tensors and flow through discrete fractures as shown in Fig. 2b. Fractures bigger than 120 m, are discretized in the domain using zero thickness elements as shown in Fig. 3.
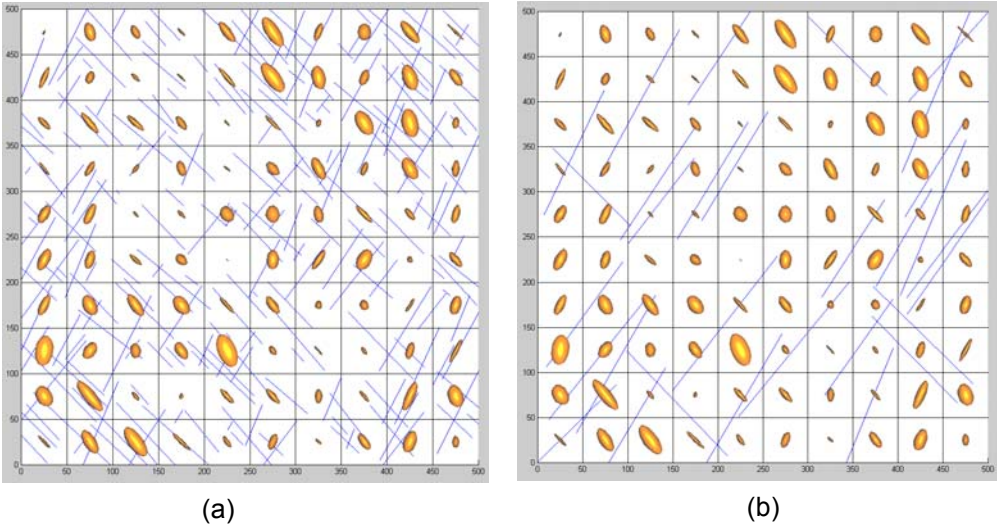
Figure 2: (a) Natural fractures (shorter than 120 m) along with calculated permeability tensors for each grid block of 500 m x 500 m reservoir; (b) long fractures (longer than 120 m) superimposed on effective permeability tensors calculated for medium to short fractures (less than 120m)
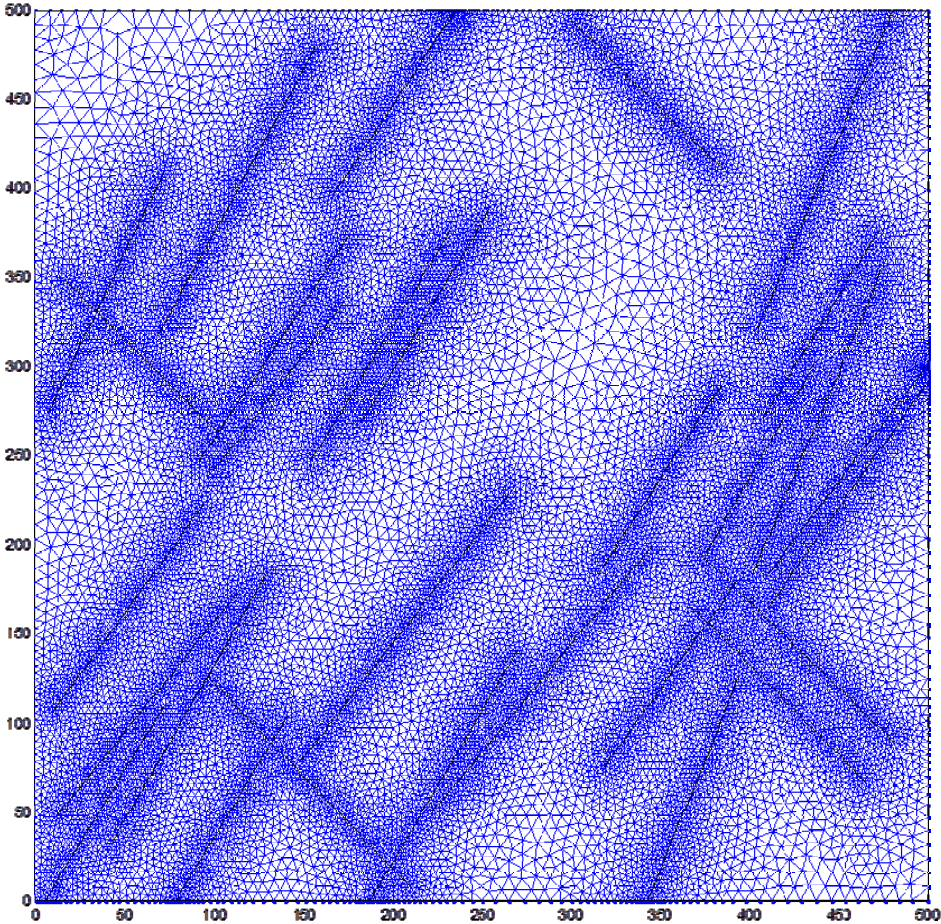
Figure 3: Discretisation of fractures longer than 120m

Heat transfer model

A finite element based thermo-poroelastic model is developed for evaluating fluid flow, pressure and temperature at different sections of the reservoir. The het transfer model consists of three parts: a) deformation of the porous media within the reservoir caused by the in-situ stresses and injection pressure, b) fluid flow within the reservoir, and c) thermal conduction and convection by diffusion and advection respectively. The governing equations used for the fully coupled thermo-poroelasticity are as follows: (Kurashige, 1989; Ghassemi et al., 2002; Shaik and Rahman, 2011):

$$\left(K + \frac{G}{3}\right)\nabla(\nabla \cdot u) + G\nabla^2 u - \alpha\nabla p - \gamma_1\nabla T_R = 0 \quad \frac{\partial \zeta}{\partial t} = \frac{k}{\mu}\nabla^2 p \tag{1}$$

$$\dot{\zeta} = \alpha\dot{\varepsilon}_{ii} + Q'\dot{p} - \gamma_2\dot{T} \tag{2}$$

$$\dot{T}_f + \nabla(J_f T_f) - c_f{}^T\nabla^2 T_f = 0 \tag{3}$$

$$\dot{T}_R - c_R{}^T\nabla^2 T_R = 0 \tag{4}$$

Where, K is the bulk modulus , G is the shear modulus , u is the displacement, α is the Biot's coefficient, γ_1 is the thermal expansion coefficient of solid, γ_2 is the thermal expansion coefficient of fluid (K^{-1}), T_R is the rock temperature, T_f is the fluid temperatures and p is the pore pressure. The above governing equations have allowed us to formulate instantaneous non-equilibrium heat transfer between fluid in fracture and matrix which results in stress perturbation. In instantaneous non-equilibrium, the solid matrix has a different temperature from that of the saturating fluid and the temperature difference between two phases decreases with time until it reaches a state at which it may be considered as instantaneous equilibrium. A schematic of the model setup for instantaneous non-equilibrium is shown in Fig. 4.
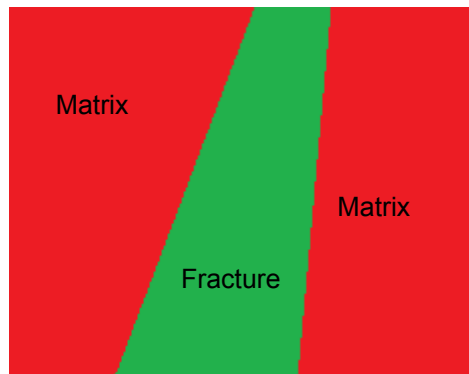
Figure 4: Fracture cutting through the matrix

In instantaneous non-equilibrium heat transfer within the rock is modelled by conduction and heat transfer in fluid by conduction and convection. The system of linear equations is solved by Staggered Partitioning method and the Predictor-corrector steps used to obtain stable temperature results.

Fracture Response to Stimulation model

The analytical model recently developed by Kotousov and Rahman, et al 2011 is used to model the shear slippage of the fracture surfaces with respect to each other which causes a change in the

fracture aperture. Two main assumptions are made for this purpose. Firstly, the sliding of the fracture surfaces with respect to each other which is characterized by the classical Coulomb friction law as:

$$\tau_n = \tau_0 + f\sigma_n$$

(5)

Where, τ_0 is the threshold shear stress at which the fracture surfaces start to slide, f is the friction factor, σ_n is the normal stress and τ_n is the shear stress during the slippage.

Next, the fracture aperture is described based on the surrounding in-situ stress condition. In this model any shear displacement of fracture surfaces causes the fracture to open. The effect of surface roughness is simulated by distributed elastic springs as illustrated in Fig.5.
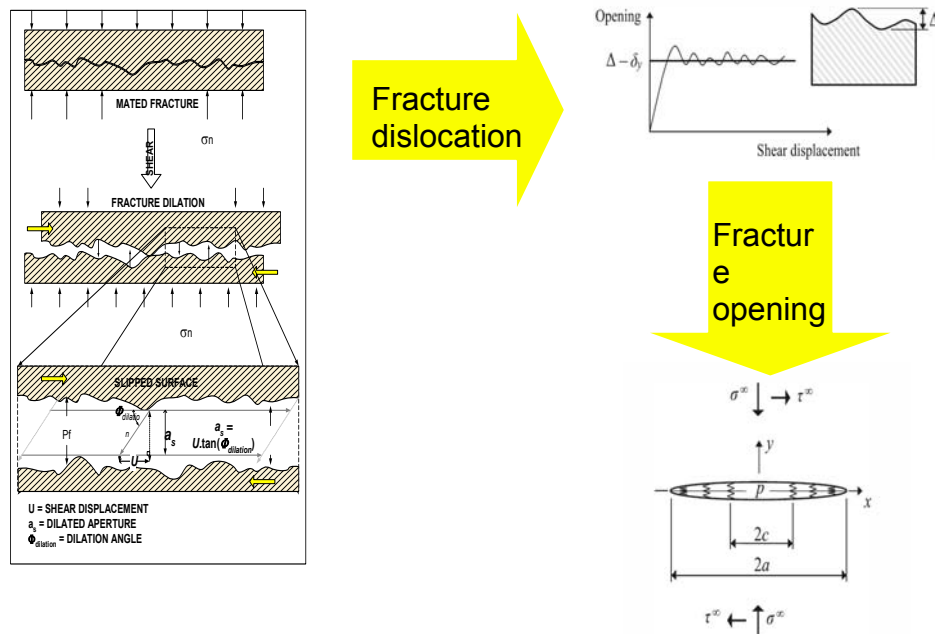
Figure 5: *Roughness induced opening of fractures are modeled using distributed dislocation densities.*

The contact between surfaces diminishes when the opening exceeds the overall the roughness of the fracture surfaces. The constitutive equations for the adopted simplified model are as follow:

$$\sigma_n = k\overline{E}(\Delta - \delta_y) \quad \delta_y < \Delta$$

(6)

$$\sigma_n = 0 \quad \delta_y \geq \Delta$$

(7)

Δ is the characteristic height of the fracture. Also E is the Young modulus of elasticity and k is the spring constant. The above set equations are solved numerically using dislocation density to obtain values for fracture opening due to induced fluid pressure.

Results and Discussion

Initially, field data, such as the reservoir structure, fracture orientation, size and other fracture parameters from Patchawarra geothermal reservoir, which influence reservoir performance, are acquired from the open literature.

This information is used to investigate fracture stimulation by injected fluid pressure and thermal stress and consequent changes in permeability (in terms of Log_{10} RMS fluid velocity) both in short and long term. The reservoir permeability for each block is calculated based on the discrete fracture network data and fluid flow simulation. Then the pore pressure, Log_{10} RMS velocity, temperature and stress tensor across the reservoir for a given induced fluid pressure at each time step are estimated. The residual fracture aperture as a result of change in local effective stress are determined and evaluated.

The reservoir is pressurized by injecting fluid through the injection well. To increase the injectivity, a pair of co-planar fractures of half-length of 50m is placed at both the injection and production wells. The pressurization was carried out over a period of 60 weeks. During the pressurization, the change in fracture width for each individual natural fracture and the resulting permeability tensor were calculated. Following stimulation of the reservoir, a flow test was carried out over a period of 20 years. During the flow test, changes in fracture apertures due to thermo-poro-elastic stresses and the consequent changes in permeability were determined. Also estimated were the thermal drawdown, produced fluid temperature and production rate.

Effect of stimulation time on shear dilation

Results of shear dilation are presented as average percentage increase in fracture aperture and dilation events with time (see Figs.6 and 7a, b and c). From Fig. 6, it can be seen that there exists three distinct aperture histories: 0-40 weeks, 40-50 weeks and 50 weeks and above. Until about 40 weeks, there exists a slow but linear increase in occurrence of dilation events due to induced fluid pressure of 51.7 MPa (bottomhole) and the average increase in aperture reaches a value of about 18%. Following this, the rate of occurrence of dilation events increases sharply until about 50 weeks thus, reaching 60% average increase in fracture aperture. After this time, no significant dilation events can be observed (a plateau of events is reached). This infers that for every set of reservoir and stress parameters as well as injection schedule, an optimum level of shear dilation can be achieved. In Figs. 7 (a, b and c) the dilation events at different stimulation times are presented. From these figures it can be seen that it takes about 50 weeks for shear dilation events to reach the production well. When the results of this study are compared with previous study (Koh and Rahman et al, 2011), in which shear dilation events are estimated based on a simplistic model Willis-Richards et al, 1996) a number of differences can be observed. Firstly the time required to overcome the threshold stress is 40 weeks which is about 12 weeks longer than the previous studies. Secondly, the time required to create maximum effective reservoir volume is almost 20 weeks longer than that the previous studies (40 weeks). Thus results of this study clearly demonstrate that the material properties, such as the surface roughness and Modulus of Elasticity used to estimate residual aperture provide a more conservative prediction of shear displacement events and the resulting residual aperture. These results also show that the reservoir volume (interconnected fracture networks for effective the heat transfer area) estimated by the new stimulation technique (this study) is much smaller (lower retained fracture aperture) which is in consistent with experiences with most EGS trials.

Increase in average fracture aperture vs. Time
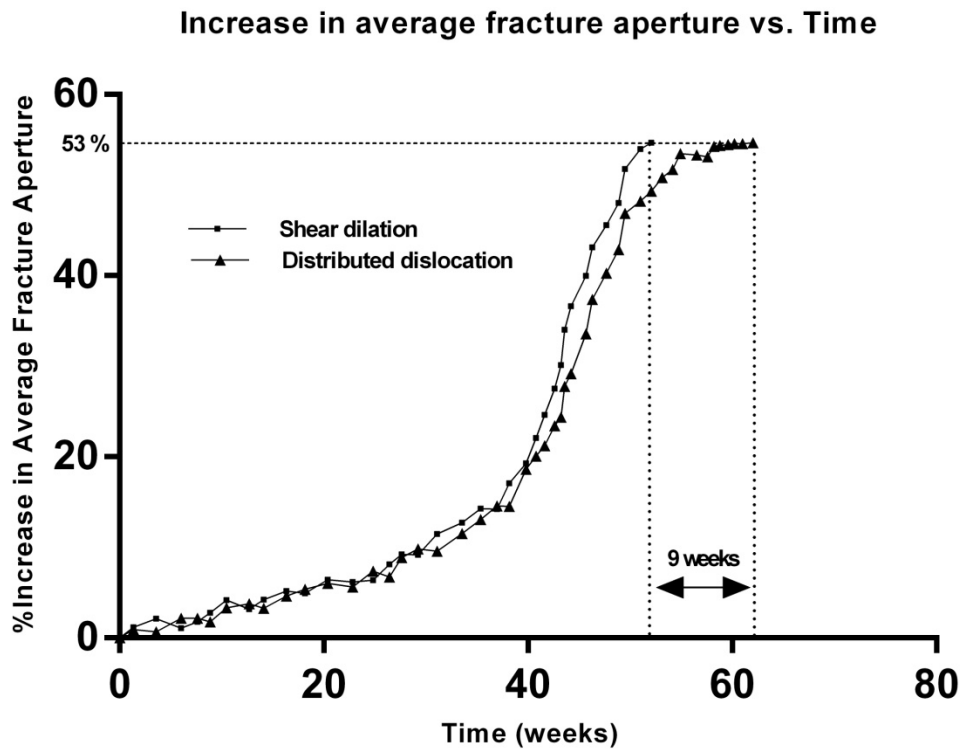
Fig. 5: *Increase in average fracture aperture (retainable) with stimulation time. Strike slip stress regime with σH = 78.9 MPa and σh = 53.3 MPa, P_{inj} = 68.9 MPa,*
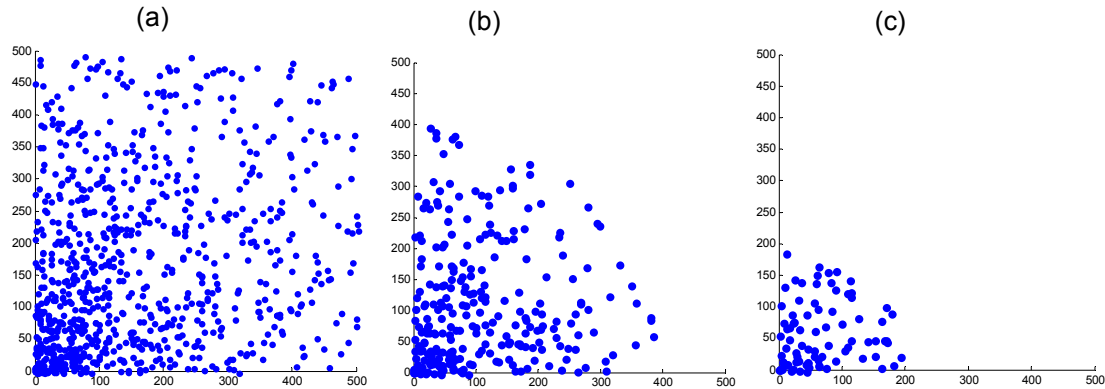
Fig. 6: *Cumulative shear dilation events of the fracture network during different stages of stimulation: after (a) 1 week, (b) after 24 weeks and (c) after 52 weeks for a strike slip stress regime with σH = 78.9 MPa and σh = 44.8 MPa, P_{inj} = 51.7 MPa. The event's locations are in the Cartesian coordinates in meters.*

Numerical flow test

Following the 60 weeks of stimulation, a flow test was carried out with a bottomhole injection pressure of 32.6 MPa and a production pressure of 22.3 MPa (at a reservoir impedance of 10 MPa between the injection and production wells) for period of 20 years. During this production period, pore pressure profile, Log_{10} root means square (RMS) velocity profile (which is directly proportional to the permeability), effective stress and the matrix temperature drawdown are monitored. In Figs 7 (a, b, and c) and 8 (a, b, and c) the Log_{10} RMS fluid velocity profile and the pore pressure after 1 year, 10 years and 20 years are presented respectively. From the results this study it can be observed that during the early production period (one month) high pore pressure is primarily built up around the injection well and the flow of fluid is primarily through major inter-connected flow paths (see Figs 7 a

and 8 a). With the progress of time the injection pressure advances towards the production well and at the about 10 years of production time it reaches half way between the injection and production wells. By this time the fluid sweeps through a significant part of the reservoir. During 20 years of production produced fluid temperature dropped from 200 to 140 °C (see Fig.11). Because of the low fluid contact area at the early stage of production, the heat transfer and the resulting thermal drawdown is very low. With the pass of time the fluid sweeps over a large part of the reservoir which increases thermal drawdown. At the end of the 20 years of production the average matrix temperature drops from 200 to 150°C which is quite low (drop) compared to previous study (Koh and Rahman, 2011). This is due to the fact that previous study is based in thermal equilibrium.

(a)   **(b)**   **(c)**
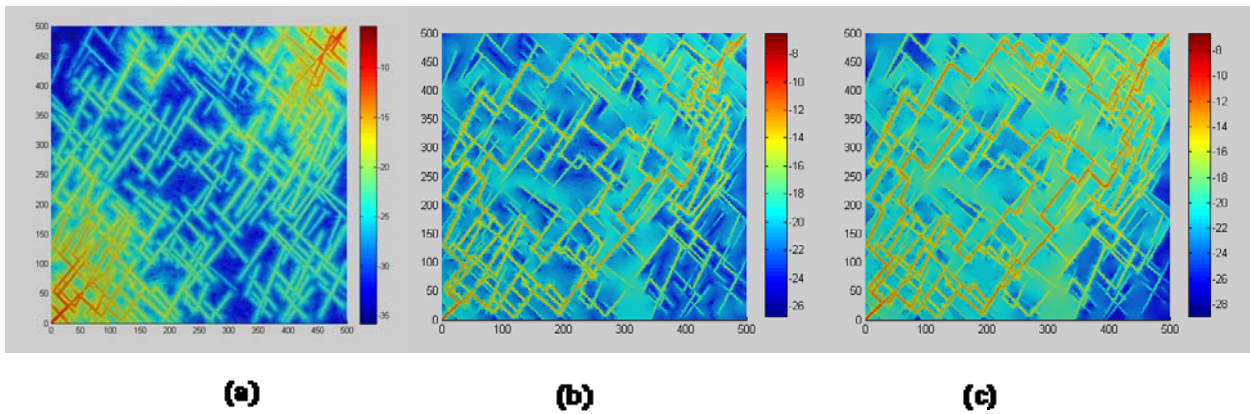
Figure 7: Log10 RMS fluid velocity profile of the Patchawarra reservoir (a) after 1 year, (b)after 10 years and (c) after 20 years of production with σH = 78.9 MPa and σh = 44.8 MPa, P_{inj} = 32.6 MPa.

(a)   **(b)**   **(c)**
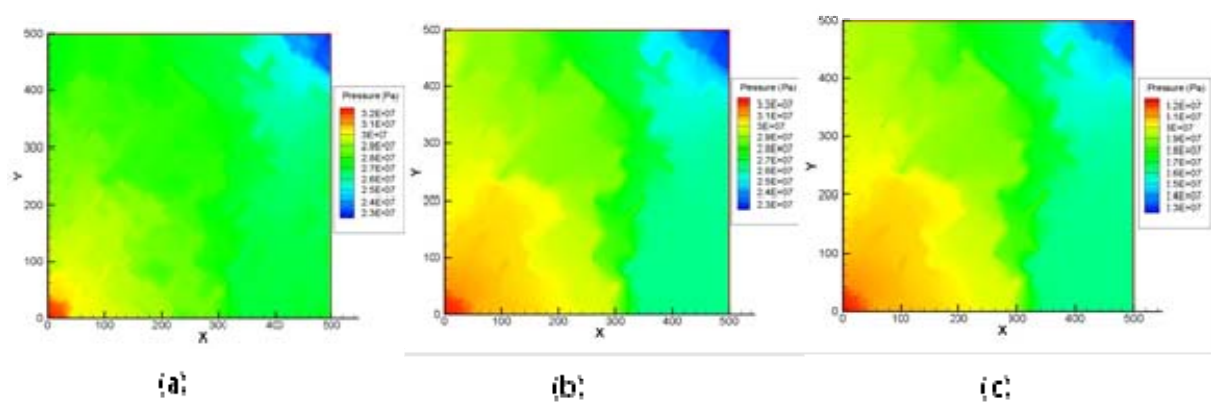
Figure 8: Pore pressure of the Patchawarra reservoir (a) after 1 year, (b) after 10 years and (c) after 20 years of production with σH = 78.9 MPa and σh = 44.8 MPa, P_{inj} = 32.6 MPa.
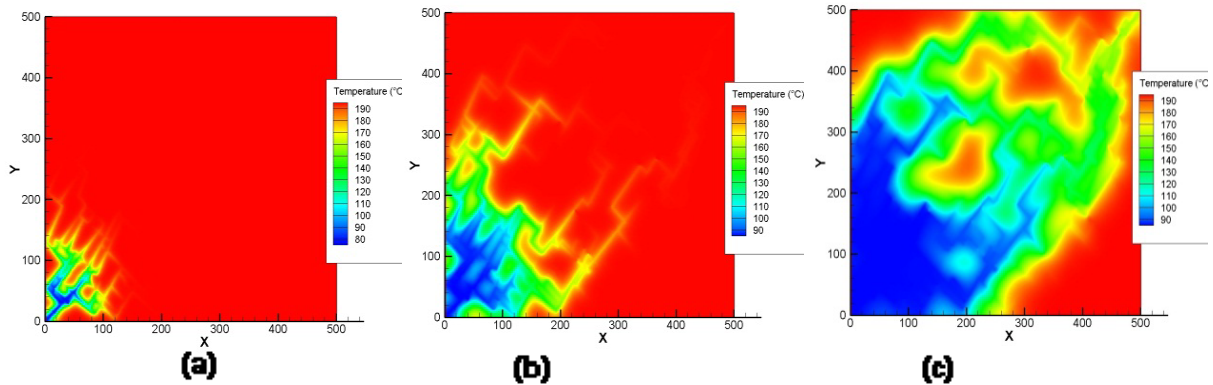
Figure 9: *Matrix temperature of the Patchawarra reservoir after a)1, b)10 and c)20 years of production with σH = 78.9 MPa and σh = 44.8 MPa, Pinj = 32.6 MPa.*

In Fig.10 the x- and y components of effective stress distribution of the Patchawarra geothermal reservoir during different stages of production are presented. These results show that by the end of 20 years of production the effective stresses throughout the reservoir are significantly reduced, thus allowing most fractures to open and conduct fluid. The reduction in the effective stresses is caused by the circulating fluid as well as thermal drawdown. Also the effect of local thermal non-equilibrium is presented in Fig.10 which shows that there is a significant difference in the produced fluid temperature with and without the local thermal equilibrium.
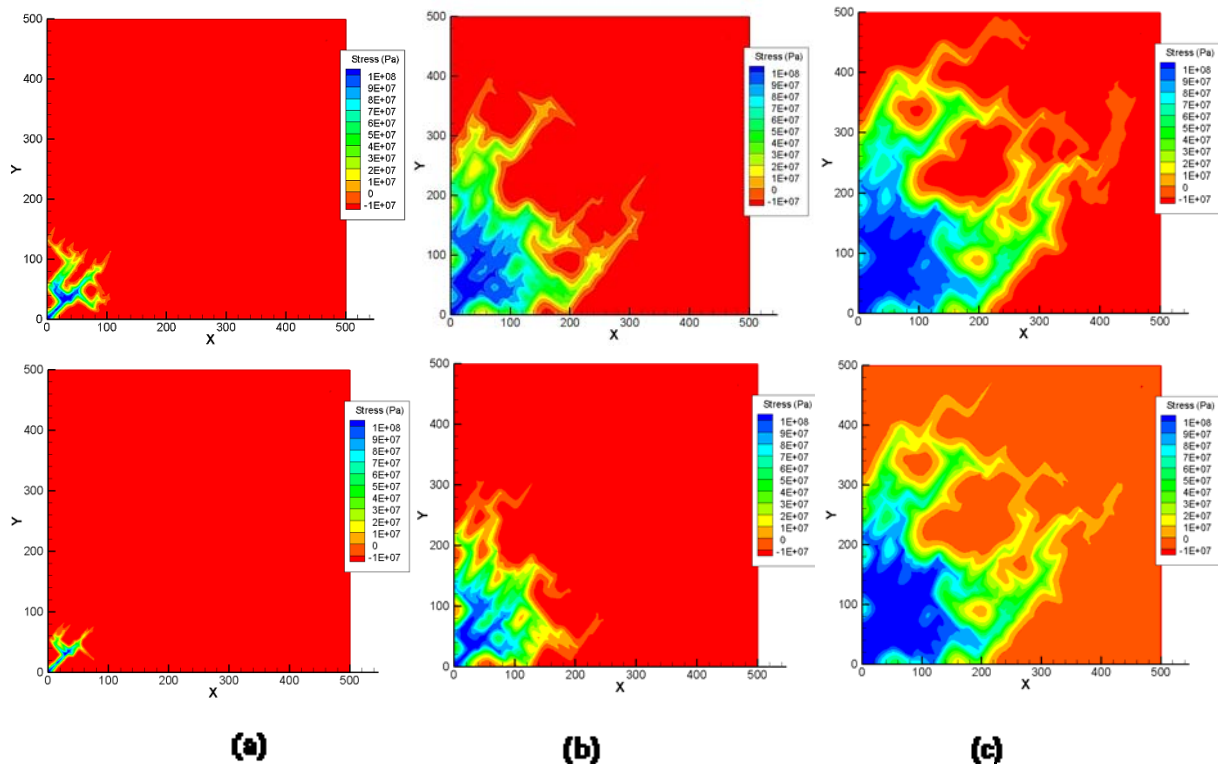
Figure 10: *x (top) and y (bottom) components of effective stress distribution at different production stages: (a) after 1 year, (b) after 10 years and (c) after 20 years for σH = 78.9 MPa and σh = 44.8 MPa, Pinj = 32.6 MPa and Pprod=22.3 MPa, Tinj = 80 °C, Tmatr = 200 °C*
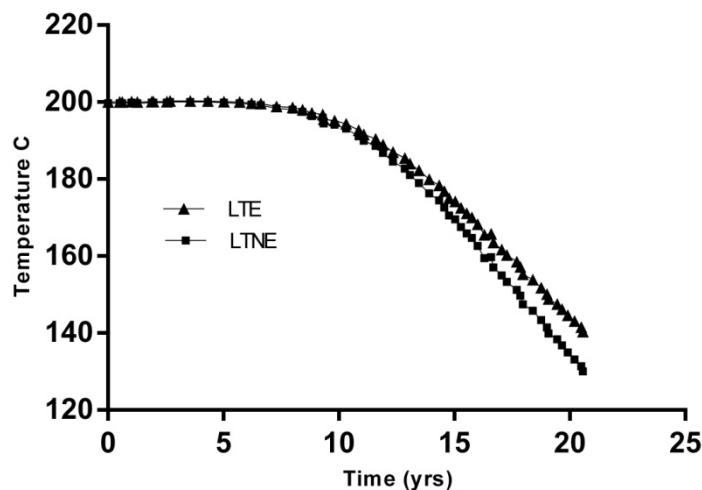
Figure 11: *Matrix temperature drawdown as a function time: a comparison between local thermal equilibrium (LTE) and local thermal non-equilibrium (LTNE).*

Conclusions

1. The hybrid of numerical simulation of tectonic history and stochastic analysis of field data provides a more realistic generation of subsurface discrete fracture map.

2. A fully coupled thermo-poro;elastic reservoi model has allowed us to study changes in stresses and resulting permeability of the reservoir.

3. Formulation of local thermal non-equilibrium has also allowed us to estimate stress gradient between fracture and matrix due to circulating fluid.

4. The new technique of simulating shear dilation using dislocation densities provides a more realistic assessment of reservoir stimulation by induced fluid pressure and temperature drawdown by circulating fluid.

References

Baria, R., Baumg¨artner, J., G´erard, A., Jung, R., Garnish, J., 1999. European HDR research programme at Soultz-sous-Forˆets (France) 1987–1996. Geothermics 28, 655–669.

Beeler, N.M., Simpson, R.W., Hickman, S.H. and Lockner, D.A., 2000. Pore fluid pressure, apparent friction, and Coulomb failure, J. Geophys. Res. 105, 25533– 25542.

Beeler, N. M., Wong, T. F. & Hickman, S. H., 2003. On the expected relationships among apparent stress, static stress drop, effective shear fracture energy, and efficiency. Bull. Seismol. Soc.Am. 93, 1381-1389.

Ghassemi, A. and G. Suresh Kumar (2007). "Changes in fracture aperture and fluid pressure due to thermal stress and silica dissolution/precipitation induced by heat extraction from subsurface rocks." Geothermics 36(2): 115-140.

Ghassemi, A., Nygren, A., Cheng, A., 2008. Effects of heat extraction on fracture aperture:A poro–thermoelastic analysis. Geothermics 37, 525–539.

Gentier, S., Rachez, X., Ngoc, T. D. T., Peter-Borie, M. and Souque, C. (2010). "3D Flow Modelling of the Medium-Term Circulation Test Performed in the Deep Geothermal Site of Soultz-Sous-forets (France). Proceedings Worlf Geothermal Congress 2010 - Bali, Indonesia, 25-29 April 2010.

Jing, Z., J. Willis-Richards, et al. (2000). "A three-dimensional stochastic rock mechanics model of engineered geothermal systems in fractured crystalline rock." J. Geophys. Res. 105.

Koh, J., H. Roshan, et al. (2011). "A numerical study on the long term thermo-poroelastic effects of cold water injection into naturally fractured geothermal reservoirs." Computers and Geotechnics 38(5): 669-682.

Kumar, G.S. and Ghassemi, A., 2005. Numerical modeling of non-isothermal quartz dissolution/precipitation in a coupled fracture–matrix system. Geothermics 34 (2005) 411–439.

McDermott, C.I. and Kolditz, O., 2006. Geomechanical model for fracture deformation under hydraulic, mechanical and thermal loads. Hydrogeol. J. 14, 487–498.

Mildren, S., J. Burgess, et al. (2005). Multiple Application of Image Log Data to EOR Operations in the Cooper Basin, Australia. SPE International Improved Oil Recovery Conference in Asia Pacific. 5-6 December, Kuala Lumpur, Malaysia.

Murphy, P. Negraru and M. Richards 2007 Impact of enhanced geothermal systems on US energy supply in the twenty-first century Journal: Philosophical Transactions of the Royal Society A: Mathematical, Physical and Engineering Sciences Volume: 365 Issue: 1853 Pages: 1057-1094 Date: April 15, 2007

Muskat, M. (1937). The Flow of Homogeneous Fluids Through Porous Media, Edwards Publisher.

Narayan, S. P., Z. Yang, et al. (1998). HDR reservoir development by fluid induced shear dilation: A numerical study of the Soultz and the Cooper Basin granite rock. International Hot Dry Rock - Forum, Strasbourg, France.

O'Sullivan, M.J., Pruess, K., Lippmann, M.J., 2001. Geothermal reservoir simulation. The state of practice and emerging trends. Geothermics 30 (4), 395–429.

Rahman, M. K., M. M. Hossain, et al. (2000). "An analytical method for mixed-mode propagation of pressurized fractures in remotely compressed rocks." International Journal of Fracture 103(3): 243-258.

Rahman, M. K., M. M. Hossain, et al. (2002). "A Shear-Dilation-Based Model for Evaluation of Hydraulically Stimulated Naturally Fractured Reservoirs." Int. J. for Numerical and Analytical Methods in Geomech. 26(5).

Sanyal, S. K., E. E. Granados, et al. (2005). An Alternative and Modular Approach to Enhanced Geothermal Systems. World Geothermal Congress 2005, Antalya, Turkey.

Sausse, J., Desayes, C. and Genter, A. (2007). "From geological interpretation and 3D modelling to the characterization of the deep seated EGS reservoir of Soultz (France)." Proceedings European Geothermal Congress 2007, Unterhaching, Germany, May 30-June 1, 2007.

Shaik, A. R., M. A. Aghighi, et al. (2008). "An Innovative reservoir simulator can Help Evaluate Hot Water Production for Economic Development of Australian Geothermal reservoirs." GRC Transactions 32: 97 102.

Shaik, A.R., Koh, J., Rahman, S. S., Aghighi, M. A. and Tran, N. H., 2009. Design and evaluation of well placement and hydraulic stimulation for economical heat recovery from enhanced geothermal systems. GRC Annual Meeting October 4–7, 2009, conference proceedings.

Shaik, A. R., S. S. Rahman, et al. (2011). "Numerical simulation of Fluid-Rock coupling heat transfer in naturally fractured geothermal system." Applied Thermal Engineering 31(10): 1600-1606.

Shaik, A.R., Koh, J., Rahman, S. S., Aghighi, M. A. and Tran, N. H., 2009. Design and evaluation of well placement and hydraulic stimulation for economical heat recovery from enhanced geothermal systems. systems. GRC Annual Meeting October 4–7, 2009, conference proceedings.

Tran, N., Z. Chen, et al. (2007). "Characterizing and modelling of fractured reservoirs with object-oriented global optimization." Journal of Canadian Petroleum Technology 46(3): 39-45.

J. W. Tester, B. J. Anderson, A. S. Batchelor, D. D. Blackwell, R. DiPippo, E. M. Drake, J. Garnish, B. Livesay, M. C. Moore, K. Nichols, S. Petty, M. Nafi Toksoz, R. W. Veatch, R. Baria, C. Augustine, E.

Willis-Richards, J., K. Watanabe, et al. (1996). "Progress toward a stochastic rock mechanics model of engineered geothermal systems." J. Geophys. Res. 101(B8): 17481-17496.

Zimmermann, G., Moeck, I., Blöcher, G. (2010): Cyclic waterfrac stimulation to develop an enhanced geothermal system (EGS): Conceptual design and experimental results. - Geothermics, 39, 1, 59-69

Zhou, X. X., Ghassemi, A. and Cheng, A. H.-D., 2009. A three-dimensional integral equation model for calculating poro- and thermoelastic stresses induced by cold water injection into a geothermal reservoir. Int. J. Numer. Anal. Meth. Geomech. 2009; 33,1613–1640

Experimental evaluation of the flow properties in the Perth Basin Mesozoic sandstone formations, Western Australia

Esteban, L.[1], Dillinger, A.[1], Ricard, L. P.[1]

[1]CSIRO Earth Science and Resource Engineering, 26 Dick Perry Avenue, Kensington, 6151, Perth, Western Australia

Lionel.Esteban@csiro.au

Abstract

A deep well, Gingin-1 well, from the Perth Basin (Western Australia) was sampled for measurements of its thermal and fluid flow properties through the Cretaceous and Jurassic sandstone units. Thermal conductivity along with porosity and permeability dataset were recently reported and were used to compare them to a new investigation of fluid distribution and pore geometry per facies types.

Laboratory Nuclear Magnetic Resonance (NMR) measurements at 2 MHz frequency were performed under fully water saturated condition on the previously analysed set of samples to infer the pore size distribution and to distinguish between movable water (macro-porosity) and irreducible water (micro-porosity integrating capillary and clay bound water pore sizes). These information helped to compute permeability from two existing models and were compared to helium gas porosity and permeability measurements using capillary pressure curve transform laws. New porosity versus permeability equations with their associated uncertainties were deduced from these results. Direct relationships were recorded in the Perth basin between pore size contributions and the facies type but also with the thermal conductivity response.

Finally, the knowledge of the pore geometry makes possible the estimation of the permeability log from NMR and improves the thermal conductivity estimations that can directly be used from the common standard logs, such as the neutron-density or the gamma-ray. Such new composite logs should improve temperature profile interpretation, temperature prediction and reservoir characterization in the Perth basin; and attempt to be applied on other similar reservoirs.

Keywords

NMR, porosity, permeability, thermal conductivity, flow properties, Perth basin, sandstone

Introduction

Hydraulic and thermal properties are key parameters for groundwater, petroleum and geothermal resources evaluation. Two of the key parameters that control the hydraulic flow properties are porosity and permeability (deMarsily, 1986). For geothermic studies, the rock thermal conductivity is the controlling parameter if we assume that conduction is the main heat transfer mechanism in the upper crust (Bearsdmore and Cull, 2001). These properties are dependent on rock mineralogy, grain size and sedimentology facies. It is crucial as part of a resource estimation workflow to properly assess these parameters with their associated uncertainties in regard to their distribution along target depth.

The pore size distribution, the permeability and the thermal conductivity are challenging parameters to access from the wireline logs. On the other hand, low field Nuclear Magnetic Resonance (NMR) recently became the most promising tool in the petroleum industry to directly measure the porosity and pore size distribution with a fearsome accuracy (Prammer, 1994; Prammer et al., 1996; Coates et al., 1999). Such information are then used to compute the permeability (Coates et al., 1998) and should help to better yield the classical empirical law for the thermal conductivity (Woodside and Messner, 1961), knowing the lithology. The end point of such approaches are the need of calibration of NMR

logs and porosity logs to properly establish the equations of transformation to estimate the permeability (Coates et al., 1999) and thermal conductivity (Brigaud and Vasseur, 1989).

The Jurassic formations of the Perth basin, Western Australia, own a hot sandstone aquifer and are targeted for geothermal investigations. The aim of this work is to define the most appropriate and laboratory-calibrated equations to predict flow properties in the Perth Basin through a study case: the Gingin-1 well. It thus demonstrates the excellent implication and utility of NMR method by using recently published data on thermal conductivity, mineralogy and helium gas porosity-permeability in the Perth basin (Delle Piane et al., 2012). These new defined equations to predict permeability and thermal conductivity will be directly applicable on the Perth Basin when NMR logs and basic triple combo logs (gamma-ray, neutron-density, sonic) will be available.

Material and methodology

The Gingin-1 well is located in the Perth basin at 200 km up North of Perth city, Western Australia (Fig. 1). A collection of 57 plugs of 1.5 inch diameter and ± 5 cm long were extracted regularly along its depth trough three formations: Yarragadee, Cadda and Cattamarra Coal Measures. Each of these samples were subjected to a laboratory workflow of measurements during the recent works of Delle Piane et al., 2012 and Timms et al., 2012 on mineralogy and facies characterizations, Helium gas porosity-permeability and water saturated thermal conductivity.
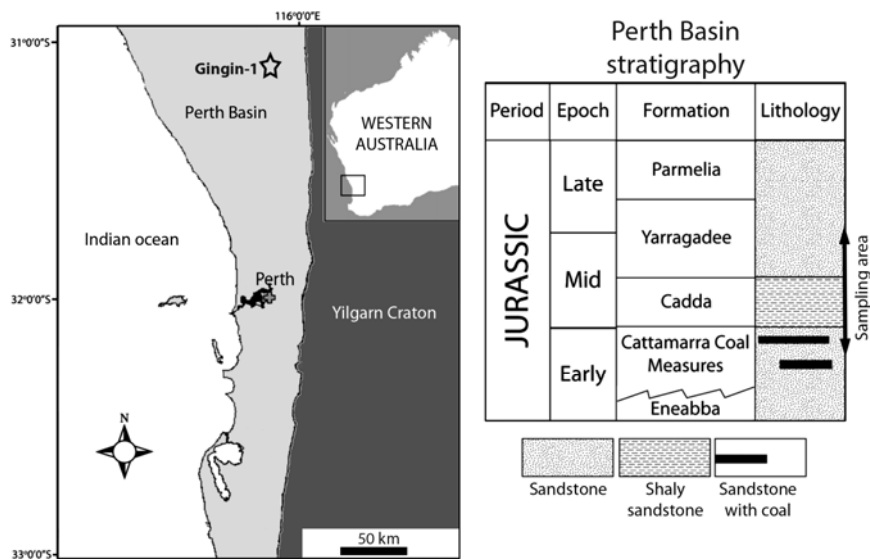
Figure 1: *Location of the Gingin-1 well in the Perth basin (Western Australia) along with the general stratigraphy of the formations encountered.*

The same sample collection under water saturation was recently used again to determine its porosity and pore size distribution in laboratory with a low field NMR using a Maran Ultraspectrometer from Oxford instruments Ltd. running at 2 MHz. Low field NMR acquires the relaxation time decay of the proton H+ (i.e. aqueous water in our case) which indirectly corresponds to the water content in the pore network. The transversal relaxation time (T_2) decay can then be inversed to generate the pore distribution of the water in the pore network (Straley et al., 1997).

Based on the NMR results, several equations of permeability from the literature were applied on the NMR dataset with facies types discriminations, such as Timur-Coates (Timur, 1967; Coates et al., 1998), Swanson (Swanson, 1981) and Schlumberger-Doll-Research (Seevers, 1966) from which we used a T_2 cut-off that separates the movable water (FFI) from the non-movable water (BVI), based on the literature and based on the best T_2 cut-off that fit the helium gas permeability.

The laboratory thermal conductivity presented in Delle Piane et al., 2012 has been compared to the thermal conductivity computation using the so-called empirical geometric mean equation (Woodside & Messmer 1961). Similar approach has been done with the matrix thermal conductivity extracted from the mineralogy content of each sample.

Results and discussion

Porosity and permeability

The porosity results from NMR match satisfactory the porosity obtained from water mass intake. The highest porosities are recorded for coarse grains facies (facies A and B), the porosity decreasing while the facies become more and more shaly (facies C to G). Such porosity tendency was revealed in Delle Piane et al., 2012, who highlighted the control of the energy of a depositional environment on the sediments' porosity.

The permeability variation along the depth of the well computed from NMR using the Coates, SDR and Swanson equations are similar to the helium gas permeability. The Coates and Swanson Max equations seem to be more appropriate for the high energy facies (i.e. high porosity) with values of permeability close to the helium gas, while the SDR and Swanson Min approaches are more suitable for the low energy facies.

The best T_2 cut-off stemming from the Coates equation, which fits the helium permeability (Fig. 2), falls in around 30 ms (classically found in the literature sandstones), except for the facies Ai, which is twofold higher (64 ms), and the Aiii, B and F/G facies with 6, 13 and 2 ms respectively. Facies B corresponds to the transitional facies between high and low energy depositional environment. This facies type could be the optimum energy where clay minerals influence is negligible, therefore favouring the permeability and hydraulic flow property. In other words, if the facies type and porosity log are known, the permeability log can be directly computed using these T_2 cut-off on the equation of Coates.

The Swanson permeability equation based on MICP principle has been computed, as well as its upper and lower boundaries considering the probable variations of the surface relaxivity parameter. The results thus obtained tend to fit the helium gas permeability. These new equations can be applied to constrain the permeability log if no information is available on the facies type. However, such equation will induce some "smoothing" in the variability induced by the facies signature and effort should be focused on facies discrimination for a better permeability prediction.

Facies	Best T2 (ms)
Ai	62.428
Aii	32.392
Aiii	5.572
B	12.964
C	29.254
D	27.376
E	35.741
F/G	2.299
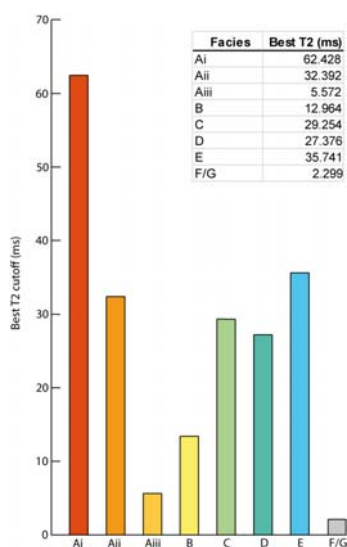
Figure 2: Computed T_2 cut-offs when fitting the NMR permeability from Coates equation with the Helium gas permeability.

Thermal conductivity

The geometrical mean is used to predict thermal conductivity under water saturation, using the total porosity and the matrix thermal conductivity from laboratory dataset and mineralogical mapping. It results in a satisfactory matching between computed thermal conductivity and laboratory results, even though some discrepancies persist. The irreducible porosity, corresponding to the small pores from the bi-modal pore size T_2 distribution, is used instead of the total porosity in the geometrical mean. As intuitively expected, the porosity involving short distances between grains (i.e. small pores) is much more efficient towards thermal conductivity than the big ones filled with low-conductivity water. In classical bi-modal pore distribution of sandstone, it is then not surprising to find such dominance of thermal conductivity of small pores over the big pores.

Conclusion

The petroleum NMR approach is opening a new window for geothermal reservoir characterization. Low field NMR logging tools are the future and become less and less expensive to apply for a better accuracy with time. NMR offers the ability to directly assess the porosity and pore size distribution as well as it drastically improves the permeability and thermal conductivity predictions. Combined to a well defined facies stratigraphy from gamma-ray/resistivity logs or image analysis, the errors systematically found on permeability and thermal conductivity estimations will be history to finally properly assess the temperature and heat flow properties along a reservoir.

References

Bearsdmore, G. R., Cull, J. P. (2001). *Crustal Heat Flow, A Guide to Measurement and Modelling*. Cambridge: Cambridge University Press, 324 pp.

Brigaud, F. and Vasseur, G., 1989. *Mineralogy, porosity and fluid control on thermal conductivity of sedimentary rocks*. Geophys. J., 98, 525-542.

Coates, G. R., Marschall, D., Mardon, D., Galford, J., 1998. "*A new characterization of bulk-volume irreducible using magnetic resonance*" The Log Analysts, 39, pp. 51-63.

Coates, G.R., Xiao, L. and Prammer, M.G., 1999. *NMR logging, principles and applications*. Ed: R.F. Sigal and S.J. Bollich, Halliburton Energy Services Publication H02308., 252pp.

Delle Piane, C., Esteban, L., Timms, N. and Israni, S.R. (2012). *Physical properties of Cretaceous and Jurassic units of the Perth Basin, Western Australia. Implications for geothermal exploration*. Submitted.

de Marsily, G. 1986. *Quantitative hydrogeology, Groundwater hydrology for engineers*. Academic Press, San Diego, USA, 440 pp.

Timms N., Olierook H., Delle Piane C., Esteban L., Israni S., Wilson M., Stütenbecker L., Hamilton J., Cope P., Evans C., Pimienta L., McLaren S., 2012. Section 5 – *Mineralogy, diagenesis and petrophysical properties of potential geothermal target rocks in the central Perth Basin*. WAGCOE Perth Basin Geomodel Report.

Prammer, M.G., 1994, *NMR pore size distributions and permeability at the well site,* SPE 28368, 1994 SPE Annual Technical Conference and Exhibition Proceedings, v. Ω (Formation evaluation and reservoir geology), p. 55–64.

Prammer, M.G., et al., 1996, *Measurements of clay-bound water and total porosity by magnetic resonance logging*, SPE 36522, 1996 SPE Annual Technical Conference and Exhibition Proceedings, v. Ω (Formation evaluation and reservoir geology), p. 111–118. Also published in 1996 in The Log Analyst, v. 37, no. 5, p. 61–69.

Seevers, D. O., 1966, *A nuclear magnetic method for determining the permeability of sandstones,* paper L, *in* 7th Annual Logging Symposium Transactions: Society of Professional Well Log Analysts.

Straley, C., Rossini, D., Vinegar, H.J., Tutunjian, P.N. and Morriss, C.E., 1997. *Core analysis by low-field NMR*. The log Analyst, 38, 84-94.

Swanson, B. F., 1981, *A simple correlation between permeabilities and mercury capillary pressures.* Journal of PetroleumTechnology, 33, 2498–2504.

Timur, A., 1967, *Pulsed nuclear magnetic resonance studies of porosity, movable fluid and permeability of sandstones*, SPE 2045, 42nd Annual Meeting preprint, SPE. Later published in 1969 in Journal of Petroleum Technology, v. 21, no. 6, p. 775–786

Woodside, W. and Messmer, J. 1961. *Thermal conductivity of porous media. II. Consolidated rocks*. Journal Of Applied Physics 32, 1688-999.

Application of Connectivity Measures in Enhanced Geothermal Systems

Younes Fadakar-Alghalandis [1], Peter A. Dowd [1], Chaoshui Xu [1]

[1] School of Civil, Environmental and Mining Engineering, The University of Adelaide, Adelaide, Australia

younes.fadakar@adelaide.edu.au

Abstract

The three major determinant factors for the productivity of hot dry rock geothermal reservoirs are fractures, fluid and heat. Fractures create an interconnected network that provides the pathways for fluid flow, which in turn facilitates heat exchange from the rock masses. The connection between fractures is therefore a critical characteristic of a successful heat producing geothermal system. Connectivity analysis is also an important component in the design, assessment and development of fracture-based reservoirs particularly enhanced geothermal systems. In this paper, we evaluate the application of two connectivity measures: the connectivity field and the connectivity index, of a fracture network. Both measures are well suited to stochastic modelling, which provides a means of incorporating the uncertainty due to lack of data. We demonstrate the effectiveness of both measures in the determination of preferential pathways through the fracture network. We also demonstrate the use of the connectivity field in determining the optimal location of an injection or production well so as to maximise the reservoir performance. The two measures show good correlation with other established connectivity measures such as X_f and P21 (P32). They are also shown to be useful in the evaluation of percolation state of a fractured rock mass.

Keywords Connectivity Index, Connectivity Field, Ranked Flow Pathways, Optimal Drilling Locations

Introduction

The productivity of hot dry rock geothermal reservoirs is mainly dependent on three factors: heat, fluid and fractures. In an enhanced geothermal system (EGS) reservoir, the heat transfer is facilitated by fluid passing through the channels established by interconnected fractures, termed the heat exchange chamber of the geothermal reservoir. The injection and production wells are connected directly through the chamber, completing the geothermal energy extraction circle.

Connections between fractures in fracture networks create basic pathways for the geothermal flow. The characterisation of the geothermal reservoir connectivity as a fundamental step of fracture network modelling is therefore vitally important in all stages of the reservoir's life cycle, including the design, the assessment and the development. The methods introduced in this paper are helpful to increasing our understanding of connectivity of fracture-based reservoirs.

We demonstrate applications of two important connectivity measures i.e., Connectivity Index (CI, Xu et al. 2006) and Connectivity Field (CF, Fadakar-A et al. 2012) for the effective connectivity characterisation of fracture networks. The methods are well-suited to stochastic modelling where the uncertainty associated with the evaluations is addressed in a probabilistic form. We demonstrate some particular applications of the two measures including the determination of main directions of geothermal flow using CI, preferential flow pathways using CF and optimal locations of injection and production wells using CF.

Connectivity in Fracture Networks

The Connectivity Measures

The connection between two fractures in a fracture network can be defined based on the connectivity measure between two points in space introduced in Allard (1993) and later developed in Pardo-

Iguzquiza and Dowd (2003), which is basically an indicator variable of 1 if the two points are connected and 0 otherwise. Accordingly, if two fractures are directly connected to each other (i.e., they intersect) or are indirectly connected (i.e., there is a pathway via other connected fractures) then they have a connectivity indicator of 1 (see Fadakar-A et al. 2011 for intersection types). The measure can be extended for different scenarios as follows:

$$
\begin{array}{l|ll}
C_p & \mathbf{1}(x \leftrightarrow y) & & \text{between two points} \\
C_v & \mathbf{1}(x_v \leftrightarrow y_v) & v \in S = R^n & \text{between two supports} \\
C_f & \mathbf{1}(f_i \leftrightarrow f_j) & f = \{v\} & \text{between two fractures : set of supports} \\
C_c & \mathbf{1}(c_m \leftrightarrow c_n) & c = \{f\} & \text{between two fracture clusters} \\
C_w & \mathbf{1}(w_p \leftrightarrow w_q) & w = \{c\} & \text{between two wells}
\end{array}
$$

where supports are representative subspaces in the region of study and fracture clusters are generated by explicitly interconnected fractures.

The Connectivity Index (CI)

The Connectivity Index is a probabilistic measure which results in the likelihood of connectivity between two support cells in a fracture network. A successful application of CI in determining the main direction of flow in a fracture network is reported in Xu et al. (2006). Although the CI does not deal with flow through fractures, the resulting preferential flow direction is noticeably consistent with the output from finite element method. The CI is defined as follows (Xu et al. 2006):

$$
\mathbf{CI} = \tau(v) = \mathbf{Pr}(x_v \leftrightarrow y_v), \qquad \forall x_v, y_v \in R^n
$$

The Connectivity Field (CF)

The Connectivity Field as proposed in Fadakar-A et al. (2012) is a new measure which quantifies the connectivity relationship between fractures in a fracture network. The CF is defined as follows:

$$
\mathbf{CF} = \int_v^\xi C_\xi dv, \qquad C_\xi = \mathbf{1}(x_{v\xi} \leftrightarrow y_v)
$$

where for a two-dimensional grid of size $m \times n$, the connection measure $C_\xi(\xi = \{(i, j) | i = 1..m, j = 1..n\})$ is computed as the indicator value between the ξth cell and all other cells. This generates a total number of $m \times n$ sets of connectivity matrices. The CF is then evaluated by summing up indicators in these matrices (Fadakar-A et al. 2012).

Relationships between CI and CF

One extension of CF is the Probabilistic Connectivity Field (PCF, Fadakar-A et al. 2012) that provides a means of CF assessment in a stochastic fracture modelling framework. PCF basically uses fracture network realizations generated by Monte Carlo simulations from the fracture network model. PCF shows close relationships with CI and the extension of CI termed Connectivity Index Field (CIF, Fadakar-A et al. 2013) as follows:

$$\mathbf{PCF} = \frac{1}{k}\sum(\mathbf{CF})_{r=1}^{k} = \frac{1}{k}\sum\left(\frac{1}{\eta}\sum\left(\mathbf{1}\left(v_{i,j}\leftrightarrow v_{p,q}\right)_{\substack{q=1\\p=1}}^{\substack{p=m\\q=n}}\right)_{\substack{i=1\\j=1}}^{\substack{i=m\\j=n}}\right)_{r=1}^{k} = \frac{1}{k}\sum\left(\frac{1}{\eta}\sum\left(\mathbf{1}\left(v_{i,j}\leftrightarrow v_{p,q}\right)^{p,q\in A}\right)^{i,j\in A}\right)_{r=1}^{k} = \frac{1}{k}\sum\left(\frac{1}{\eta}\sum\left((\mathbf{C}_A)^{i,j\in A}\right)\right)_{r=1}^{k}$$

$$\mathbf{CI} = \frac{1}{k}\sum\left(\mathbf{1}\left(v_{i,j}\leftrightarrow v_{p,q}\right)_{\substack{q=1\\p=1}}^{\substack{p=m\\q=n}}\right)_{r=1}^{k} = \frac{1}{k}\sum\left(\mathbf{1}\left(v_{i,j}\leftrightarrow v_{p,q}\right)^{p,q\in A}\right)_{r=1}^{k} = \frac{1}{k}\sum(\mathbf{C}_A)_{r=1}^{k}$$

$$\mathbf{CIF} = \frac{1}{\eta}\sum\left(\frac{1}{k}\sum(\mathbf{C}_A)_{r=1}^{k}\right)^{i,j\in A}$$

where k is the number of realizations per simulation, η is the standardization factor, A is the region of study, v is support cell, and m, n are dimensions of the grid covering A.

Applications of CI and CF in characterising fracture networks

The stationary CI (SCI, Xu et al. 2006) is an extension of CI for stationary cases which considers distances between supports rather than their actual coordinates. SCI can effectively be used to determine preferential flow directions in a connected fracture network by comparing the SCI computed for different directions. The preferential flow directions can be visualised clearly as demonstrated in a 2D example shown in Figure 1. Note that the choice of distance h here can be guided by the available information of the region of study otherwise a series of simulations for varying h sizes can be conducted (see Fadakar-A et al. 2012 and 2013 for details). Preferential flow direction of the fracture network is closely related to the overall major direction of flow passing through the fracture network. As shown in Figure 1, the resulting preferential flow direction (solid lines) is noticeably consistent with the one computed using finite element method (dashed lines).
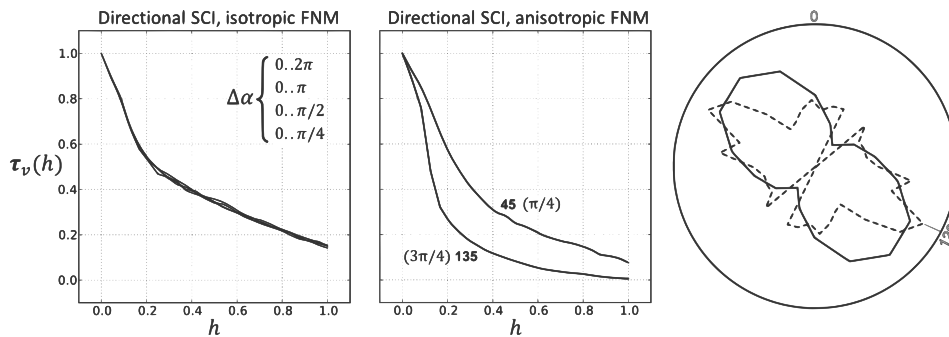
Figure 1: SCI is able to distinguish effectively between isotropic and anisotropic fracture networks. As a result, SCI determines the major flow direction that is comparably accurate with regard to the one derived from conventional finite element methods.

The procedure of the application of CF for the assessment of potential flow pathways in a fracture network is shown in Figure 2(A). The CF is also useful to help determine ranked pathways. Ranked pathways are those that can be of interest in fracture stimulation process for the expansion of the reservoir. An example of a ranked pathway is marked in Figure 2(A, "Pathways") where pathways with higher rank are shown as bold dashed line. In the example given two lower rank pathways are shown as dotted line. PCF, on the other hand, is also helpful to the characterisation of flow pathways in a fracture network model as demonstrated in Figure 2(B). The figure clearly demonstrates that there is a preferred orientation towards NE-SW (i.e., ~45 degree) in the connectivity through fracture network model which is consistent with the model parameters given in Figure 2(B).
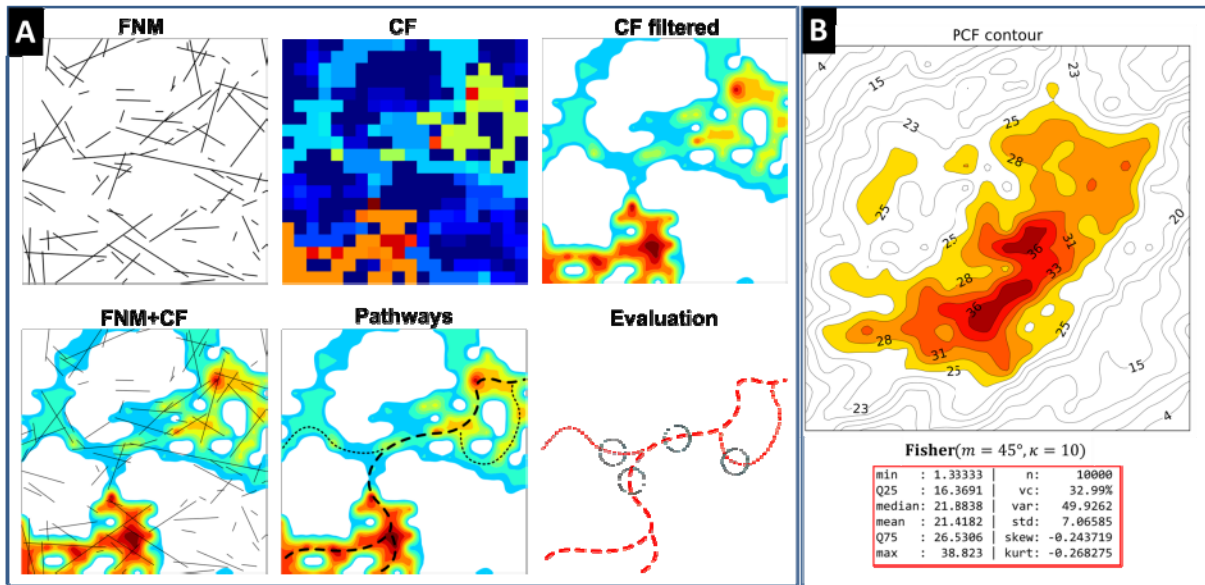
Figure 2: *(A) The procedure of determining ranked flow pathways using the CF measure. (B) PCF is used to characterise the connectivity of a fracture network model.*

The map of CF (filtered) shown in Figure 2(A) suggests potential further interesting applications. One is to locate the optimal drilling locations considering that the higher the value of CF the larger the fracture cluster connected to that location. In the example shown in Figure 2(A), the red region in the "Pathways" map is the most suitable area in terms of high connectivity within the region. In addition, in the case of using the fracture network model to evaluate the uncertainty associated with the CF map, PCF can be used to determine the optimum locations for drilling to maximise connectivity between the well and the reservoir (Figure 2(B)). PCF is also useful in the determination of the reservoir extent (connected area) as shown in Figure 2(B) with filled contours.

Our studies also show that both CI and CF are highly correlated with the traditional connectivity measures such as Xf, P21 (P32) and the percolation state. The detailed comparisons and discussion are reported in Xu et al. (2006), Fadakar-A et al. (2012) and Fadakar-A et al. (2013) and therefore are not to be repeated here.

Concluding Remarks

Connectivity Index (CI) and Connectivity Field (CF) are two new connectivity measures which can help characterise connectivity of fracture networks and provide practical applications especially for fracture-based geothermal reservoirs such as EGS. While CI is shown to be able to provide comparable results in the determination of the main flow direction in the fracture system with conventional deterministic methods (such as FEM), CF gives new insights into the evaluation of flow pathways in the network. CF is also helpful in locating optimal drilling locations. Full coverage of applications of the two measures can be found in Fadakar-A et al. (2012) and Fadakar-A et al. (2013).

Acknowledgements

References

Allard D, HERESIM Group, 1993, On the connectivity of two random set models: the truncated Gaussian and the Boolean, in Soares A, Ed., Geostatistics Troia'92, Kluwer Academic Publishers, 467-478.

Fadakar-A Y, Dowd P.A, Xu C, 2012 (in review), Connectivity Field: A new measure for characterising fracture networks, Journal of Mathematical Geosciences.

Fadakar-A Y, Dowd P.A, Xu C, 2013*, Connectivity Index: developments and applications, work in progress.

Fadakar-A Y, Xu C, Dowd P.A, 2011, A general framework for fracture intersection analysis: algorithms and practical applications, Proceedings of the 2011 Australian Geothermal Energy conference, 15-20.

Pardo-Iguzquiza E, Dowd P.A, 2003, CONNEC3D: a computer program for connectivity analysis of 3D random set models, Computers & Geosciences, 29(6):775-785.

Xu C, Dowd P.A, Mardia K.V, Fowell R.J, 2006, A Connectivity Index for Discrete Fracture Networks, Mathematical Geology, 38(5):611-634.

Conformal mapping and remote sensing

Farrar, L.J.D. and Holland M.A.

farrar3@hotmail.com

Mapping by elementary functions of complex variables, maintains the retention of a perceptive approach to the analysis of geophysical information.

Perception may be considered in terms of symmetry, sequence, scale, and subdivision. It may be measured by the extent to which it is familiar, functional, factual and flawed. Modern computer graphics retains the capacity to blur these criteria.

The development and application of this approach took place at Tennant Creek (N.T. Australia) from 1985 to 1994, as a major part of a strategy to locate gold-bearing magnetite pods, utilising a geophysical drillhole probe. Broader mathematical implication was realised in 2005, and has since received ongoing attention.

It is difficult to reveal an analytic function whose real or imaginary component satisfies the boundary conditions that constrain genuine granitic form. However, conformal transformations may be used to obtain a region and problem simple enough that such a function is evident.

The development and application of a useful analytic function, relevant to gravity and thermodynamic analysis, is to be presented.

Geometric Algebra (GA) and closely related Clifford Algebra (CA) is employed as a unifying and conceptually interpretable framework for combining models of complex phenomena in Geothermal Energy. One distinguishing feature of GA is that "twist" is incorporated axiomatically as a natural feature of geometry and physical models as a combined medium. Other features including complex analysis, analytic functions and partial differential equations can be considered together within the context of GA/CA.

In a 2-dimension space (i.e. a plane), an algebra G^2 is produced by the addition of a scalar (1), two orthoganal vectors (e_1, e_2) and a new type of element is introduced for GA called a bivector $e_1 \wedge e_2$ (where "∧" is called wedge). Elements of this kind are called multivectors.

Two multivectors are multiplied together as follows:

Let $A = a_0 + a_1 e_1 + a_2 e_2 + a_3 e_1 \wedge e_2$, where a_0, a_1, a_2 are scalars and e_1, e_2 are othogonal vectors in 2-d space,

and $B = b_0 + b_1 e_1 + b_2 e_2 + b_3 e_1 \wedge e_2$, where b_0, b_1, b_2 are scalars and e_1, e_2 are othogonal vectors in 2-d space.

The AB (i.e. multivector A "multiplied" by multivector B) is defined as

$P = p_0 + p_1 e_1 + p_2 e_2 + p_3 e_1 \wedge e_2$ where

$p_0 = a_0 b_0 + a_1 b_1 + a_2 b_2 - a_3 b_3$

$p_1 = a_0 b_1 + a_1 b_0 + a_3 b_2 - a_2 b_3$

$p_2 = a_0 b_2 + a_2 b_0 + a_1 b_3 - a_3 b_1$

$p_3 = a_0 b_3 + a_3 b_0 + a_1 b_2 - a_2 b_1$

In general $AB \neq BA$ in GA.

Complex Numbers,

A multivector which is the combination of a scalar and a bivector, can be interchanged to a complex number by premultiplying by vector e_1.

Geothermal potential of Rottnest Island, Western Australia

Christina Gehrke[1,2], Ludovic P. Ricard[1] and Heather A. Sheldon[1]

[1]CSIRO Earth Science and Resource Engineering, 26 Dick Perry Avenue, Kensington, 6151, Perth, Western-Australia. [2]University of Hamburg, Department Geosciences, Geological-paleontological Institute and Museum, Bundesstrasse 55, 20146 Hamburg, Germany

Ludovic.Ricard@csiro.au

Abstract

Rottnest Island is located *18 kilometres* offshore west of Perth, in the Perth Basin, Western Australia. In a recent review, Rottnest Island Authority committed itself to make Rottnest Island sustainable. Existing evaluations of geothermal potential in the Perth Basin have been mainly onshore, especially in the Perth Metropolitan Area and the North Perth Basin. The present study focuses on the evaluation of the local geothermal resources of Rottnest Island for electricity generation and direct use applications as part of a solution for the energy sustainability of the island.

A collection of 13 petroleum wells around the island and a significant number of 2D seismic lines provide constraints on the geology and geothermal resources. The geothermal resource evaluation is based on an integrated study combining structural geology, hydrogeology and petrophysics of the confined aquifers beneath Rottnest Island. Temperature at top and bottom of those aquifers, average permeabilities and porosities are used for the assessment of possible geothermal applications such as electricity generation and direct heat use applications.

Keywords

Rottnest Island, geothermal resource, temperature, permeability, porosity, Badaminna Fault System

Introduction

Attracting over half a million visitors every year, Rottnest Island is a popular destination for holidaymakers and tourists in Western Australia. The Island meets or exceeds the expectations of 94% of its visitors (Rottnest Island Authority, 2011). However, the Island carries the reputation of being an expensive place for holidays due to the high cost of doing business on Rottnest. Part of the high costs can be assigned to the energy cost to power a remote island. All power requirements for the Island are generated locally using a combination of diesel generators and a wind turbine. The fuel has to be transported to the Island for an extra-cost of $539,000 for the 2010-2011 period compared to mainland prices.

Geothermal energy can be used for electricity generation but also for direct heat use applications (Gudmundsson, 1988), such as heating swimming pools and thermal regulation of buildings. For example, at least 7 geothermal projects in the Perth Metropolitan Area provide direct heating applications for leisure centres (Pujol, 2011). These direct-use applications exploit the high porosity and permeability of the sedimentary aquifers in the Perth Basin, which allow hot water to be extracted economically without requiring any artificial enhancement of the permeability. This type of geothermal resource is described as a Hot Sedimentary Aquifer (HSA) system. Recent work by the Western Australian Geothermal Centre of Excellence has confirmed the existence of HSA resources in the onshore Perth Basin, but the offshore resources have yet to be evaluated.

In this study, we collate existing petroleum exploration data from around Rottnest Island and assess it in the context of geothermal resource exploration. The data will be utilized to define the possible geothermal systems underlying Rottnest Island and finally put in perspective with possible geothermal applications.

Rottnest Island geology

Rottnest Island (Fig. 1) is about 10.5 kilometres long (east-west), up to 4.5 kilometres wide and covers about 1900 hectares (Playford, 1976). Located 18 kilometres west of Perth, Western Australia, it is part of the Perth Basin, a north to north-northwest trending, onshore and offshore sedimentary basin, extending about 1300 km along the south-western margin of the Australian continent. The offshore part of the southern Perth Basin is known as the Vlaming Sub-basin, an elongate, north-south trending depocentre on the continental shelf and upper continental slope (20–1000 m water depth), which contains more than 12 km of sedimentary section (Jurassic to Early Cainozoic; Fig. 2). Structurally, it belongs to an extensional system on Australia's southwestern margin, formed during the Palaeozoic to Mesozoic rifting of eastern Gondwana. The Vlaming Sub-basin is separated from the onshore part of the basin by the Badaminna Fault Zone, which comprises up to three west dipping, north-south striking faults (Crostella and Backhouse, 2000; Fig. 2).
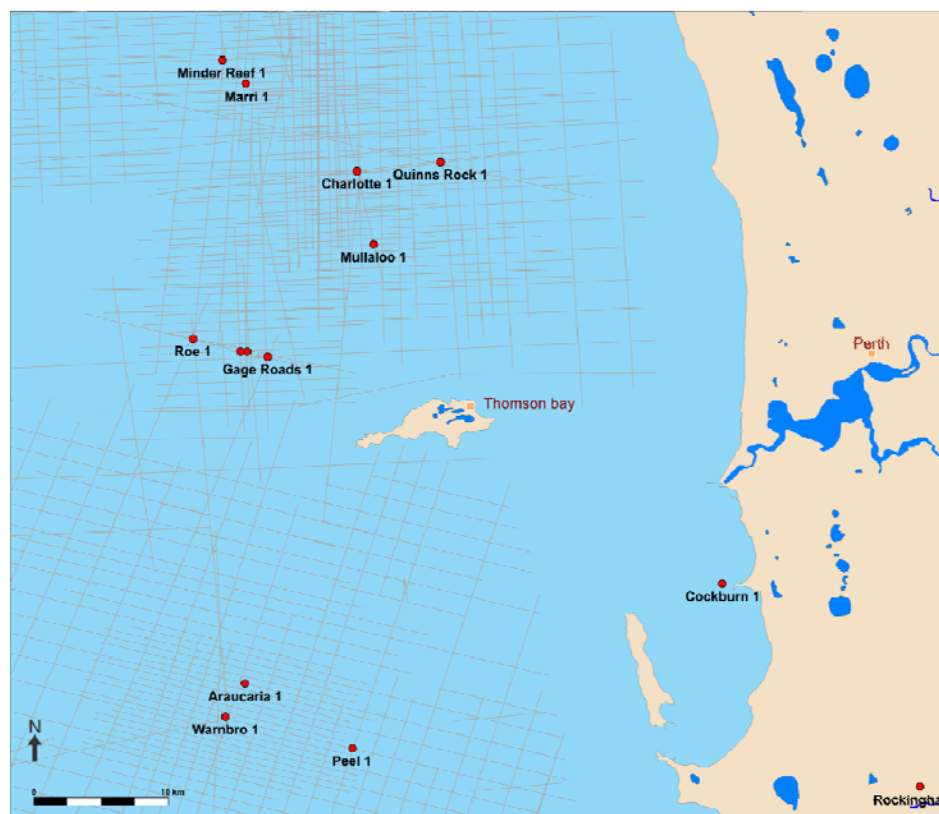
Figure 3: Location of Rottnest Island with surrounding petroleum wells and 2D seismic lines.
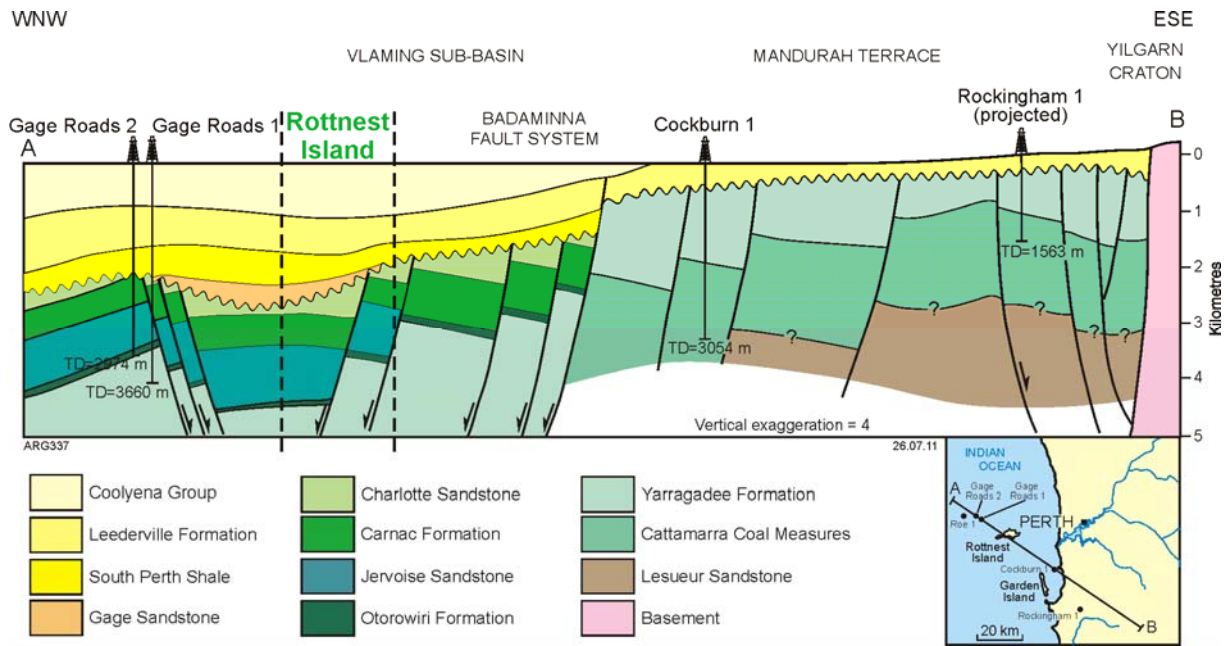
Figure 4: *WNW-ESE structural section through Rottnest Island (from Crostella and Backhouse, 2000).*

Results

Direct-use geothermal applications typically require temperatures between 60 and 100 °C (Gudmundsson, 1988). Bottom-hole temperatures (BHTs) and temperatures from drill stem tests (DSTs) from 13 petroleum wells in the vicinity of Rottnest Island were assessed to determine the depth interval over which this temperature range might occur. In these wells, temperatures of 60 to 100 °C were encountered between 1300 and 3000 m below sea level (Fig. 3). Temperatures above 100 °C are reported at depths greater than 3500 m. The depth interval 1300-3000 m corresponds to the Parmelia Group (Early Cretaceous). More precisely, in the Gage Roads 1 well, which is the closest well to Rottnest Island (15 km to the West), the Jervoise Sandstone and the Otorowiri Formation represent most of the interval. The Jervoise Sandstone is reported to be predominantly sandstone with minor siltstone and shale beds particularly in the upper part. The Otorowiri Formation is reported to be a silty shale unit, and is therefore unlikely to be sufficiently permeable to host a HSA geothermal system. Porosity and permeability measurements obtained on core samples for the Jervoise Sandstone are available from several wells in the area (Fig. 3). The permeability measurements vary from 20 to more than 5000 mD while the porosity ranges from 18 to 30% with an average of 23%. The Jervoise Sandstone therefore appears to be a possible target for a HSA system with potential for direct use geothermal applications. More details will be presented and discussed at the conference.
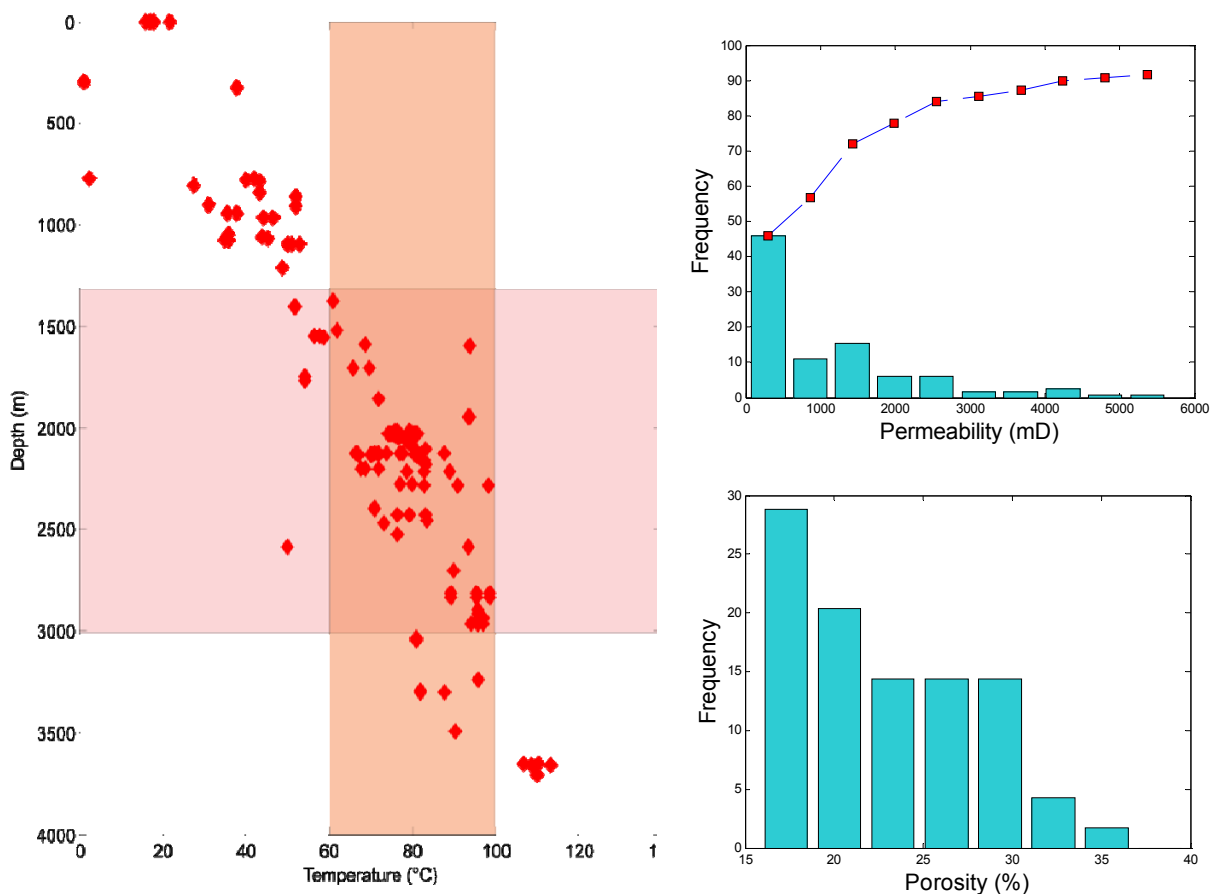
Figure 5. *Left, temperature (from BHTs and DSTs) versus depth, highlighting the 60-100 °C range for direct-use geothermal applications and the associated depth interval. Right, normalized frequency of permeability (with cumulative frequency curve) and porosity measurements from the Jervoise sandstone.*

References

Crostella, A. and Backhouse, J., 2000. Geology and petroleum exploration of the Central and Southern Perth Basin, Western Australia. Geological Survey of Western Australia Report 57, Perth.

Gudmundsson, J.-S. 1988. The elements of direct uses. Geothermics (17), 119-136.

Hot Dry Rocks Pty Ltd, 2008. Geothermal energy potential in selected areas of Western Australia (Perth Basin).

Playford, P.E., 1976. Rottnest Island: geology and groundwater potential.

Pujol, M. 2011. Examples of successful hot Sedimentary Aquifer direct-use projects in Perth, Western Australia. In: Middleton, M. & Gessner, K. (eds.) *Western Australian Geothermal Energy Symposium*. Perth, Western Australia, 23.

Rottnest Island Authority, Annual Report 2010-2011.

Transmission Challenges and Potential of Integrating Geothermal Resources of Cooper Basin to the Australian Electricity Grid

Kazi Hasan[1,2] and Tapan Saha[1,2]

[1]Queensland Geothermal Energy Centre of Excellence (QGECE). [2]School of Information Technology and Electrical Engineering, The University of Queensland, St Lucia, QLD 4072, Brisbane, Australia

k.hasan@uq.edu.au; saha@itee.uq.edu.au

Large scale geothermal resource interconnection to the existing Australian electricity grid requires a long transmission line and high capital investment. This connection will also considerably change the power flow pattern, network security planning and market operation aspects. While looking at these issues, this study comprehensively identifies the regulatory, economic and technical challenges of transmission in the context of Cooper Basin geothermal connection. A brief overview of the connection cost allocation policies is presented and implemented in the Cooper Basin geothermal power transmission. The optimal power flow analysis of the Queensland electricity network is performed considering the Cooper Basin connection, which shows the potential of the project considering emission cut and increased net market benefit. This study also simulates Queensland electricity network with three other large scale renewable generation projects, namely Copper String, Kennedy Wind Farm and PNG hydro. Simulation study confirms that the commencement of Cooper Basin project attains higher power injection and expected benefit with lower amount of estimated costs. This is because of the large amount of cheap geothermal power penetration to the area near South East Queensland, where load (61%) is significantly higher than the generation (9%).

Keywords: geothermal power, transmission challenges, connection cost allocation, net market benefit, cost recovery, Queensland electricity network

Introduction

Modern power system planning approaches are notably prejudiced by renewable portfolio development and emission pricing employment. Conventional generation resources inherently cause emission, and intermittent renewable resources suffer from the uncertainty of supply, higher footprint and price competitiveness. Bridging the gap of conventional and intermittent generation technologies, geothermal resources can maintain secure, sustainable, reliable and economic power supply. Geothermal energy has a considerable potential to penetrate to the Australian National Electricity Market (NEM) as an emission free, price competitive and base load electricity. Apparently the largest 'geothermal power zone' is located in the Cooper Basin area, which is around 1000 km away from major load centers. A long distance high capacity transmission line is required to connect this geothermal power to the existing electricity grid.

In this perspective, in the Queensland Geothermal Energy Centre of Excellence at the University of Queensland, Brisbane, the power transmission program addresses the issues of transmission planning to connect geothermal power plants to the national electricity grid. Based on this research, one journal paper has been published and two other journals are under review [*Hasan et al.*, 2012b; *Hasan et al.*, 2012c; *Radzi et al.*, 2012]. Five national and international conference papers have also been published in this topic [*Eghbal et al.*, 2011; *Hasan et al.*, 2011a; b; c; 2012a]. Selected summary of those works is presented here for the Australian Geothermal Energy Conference 2012 audiences.

This research particularly investigates the Cooper Basin geothermal connection to the Queensland electricity grid, specifically looking at the transmission cost borne by generation developers and net market benefit obtained by geothermal power connection. A case study of the Queensland electricity network is simulated with 'Powerlink Queensland' power system (PSS/E) data considering Cooper Basin and few other connections to the Queensland network.

Challenges of Long Distance Bulk Power Transmission

One disputable aspect of the transmission planning is that which comes first. Is it generation or transmission? Also, a long distance transmission faces the problem of first mover disadvantage. [*Chattopadhyay*, 2011; *Swider et al.*, 2008]. Another fundamental challenge in the Australian NEM jurisdiction is to endure the Regulatory Investment Test for Transmission (RIT-T). Achieving the economies of scale is also challenging in different market scenarios. Further, a remote generation project has to compete with grid-nearby conventional generation sources. Investment cost allocation and cost recovery also jeopardize the long distance transmission planning domain. [*Chattopadhyay*, 2011].

In case of the Cooper Basin geothermal project, a number of 50MW and/or 100MW generators will be dispersed in few hundred kilometers area. Fig.1 depicts the connection arrangements for such transmission facilities [*Hasan et al.*, 2011a; *Hasan et al.*, 2012b; *Radzi et al.*, 2012]. The technology (HVDC or HVAC), voltage level and network configuration will depend on the amount of generation, possibility of staged development and/or tapping in the transmission corridor.
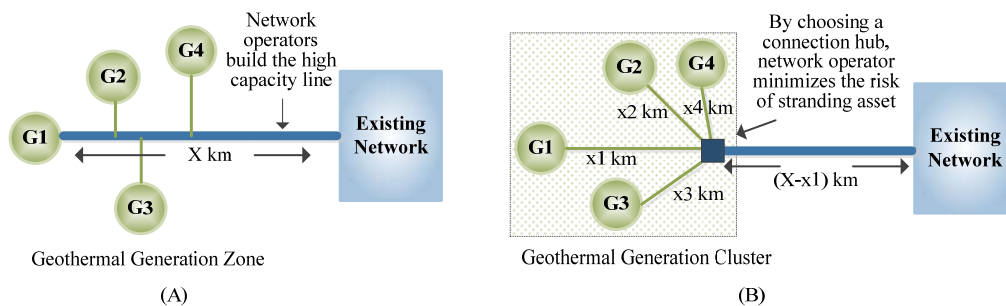
Fig.1: Dispersed geothermal generators will be connected to a collection system and then transfer the power over a high voltage line to be connected to the main grid. (A) A connection scheme when the network operators build high capacity transmission line. (B) The hub approach of network connection, where the network operators significantly share the cost burden and the risk of stranding assets with generation developers [Hasan et al., 2012c].

Transmission cost allocation for Long Distance Bulk Power Transmission

Transmission connection cost allocations are generally classified as super-shallow, semi-shallow, shallow and deep connection pricing. The connection cost allocation policy are adopted from the European RES-E (Renewable Energy Resources for Electricity), as shown in Fig.2 [*Swider et al.*, 2008].
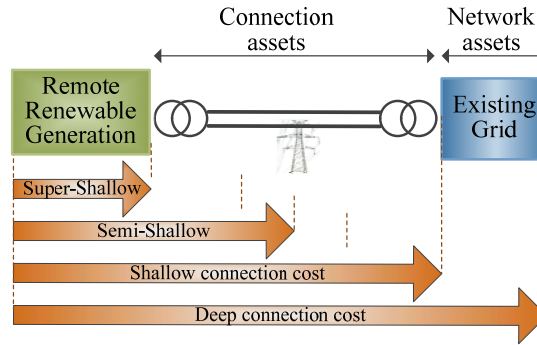
Fig.2: Connection cost allocation for long distance bulk power transmission. In the super-shallow scheme, renewable generators are responsible only for the generation development. The market operator builds the transmission line up to their premises. In the semi-shallow policy, there is a provision to divide the grid-integration cost among generators and consumers. The proportion of connection cost for generation developers and/or consumers depends on their negotiation with the market operators. Further, in shallow connection scheme, the connection charge has to pay fully by the connecting generators. In the deep charging policy, generators are responsible to pay for grid connection costs as well as grid reinforcement costs. [Swider et al., 2008].

Net Market Benefit

The net market benefits have been calculated for transmission upgrades to compare against the expected costs. Firstly, an hourly optimal power flow (OPF), in MATLAB-based MATPOWER simulation, calculates the power flow and market dispatch. Then by aggregating the benefits underlying this flows/dispatch– the net market benefit has been obtained. The detail of the net market benefit framework is found in [*Hasan et al.*, 2011b]. The net market benefit consists of the surpluses obtained by producers, consumers, and merchandisers. Net market benefit also accumulates the carbon emission tax and Large-scale Renewable Energy Target (LRET) payment, as defined in the Australian NEM. The objective function of a yearly net market benefit is formulated as below,

$$Max \sum_{t=0}^{8760} \left[\sum_{i \in n_g} \left(p_g^i \cdot \lambda_g^i - p_g^i \cdot \phi_g^i \right) + \sum_{i \in n_d} \left(CS_d^{i'} - CS_d^i \right) + \left(\sum_{i \in n_d} p_d^i \cdot \lambda_d^i - \sum_{i \in n_g} p_g^i \cdot \lambda_g^i \right) - \sum_{i \in n_g} \left(E_i \cdot \pi_{CO_2} \right) + \Sigma \left(\psi_i \cdot \sigma \right) \right]$$

(1)

Where, t is the time span (hour), n_g is number of generator set, n_d is number of load set, p_g^i is power produced by generator i (MW), λ_g^i is Locational Marginal Price (LMP) at generator bus i ($/MWh), ϕ_g^i is generation cost of generator i ($/MWh), CS_d^i is consumer surplus earned by consumer i ($), $CS_d^{i'}$ is consumer surplus before augmentation ($), p_d^i is the power consumed by load i (MW), λ_d^i is LMP at load bus i ($/MWh), E_i is the amount of CO_2 produced by generator i (ton), π_{CO_2} is emission cost ($/ton CO_2), ψ_i is renewable generation from generator i (MW), σ is LRET payment ($/MWh).

Queensland Case Study – Long Distance Bulk Power Transmission

Network data

Queensland network of the Australian NEM is simulated in this study. This network is 1700km long, having a generation capacity of 12,788 MW in 2010, which is forecasted to be 15,500MW in 2015 [*PowerLink*, 2011]. Queensland network area with different zones is shown in Fig.3.a and b.
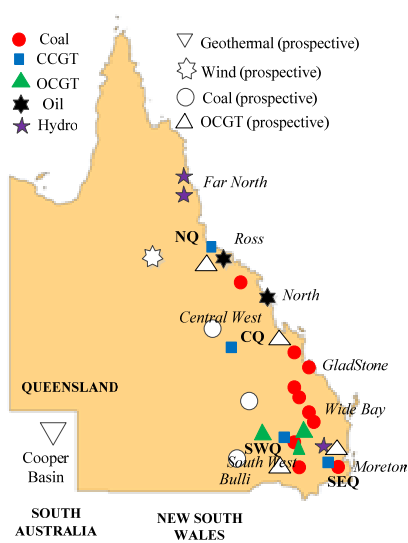
Fig.3.a: *Queensland network of the Australian NEM [PowerLink, 2011]. Location and type of existing and prospective generation resources are shown here. Prospective generation resources are located far away from the grid. Consequently, transmission system development for prospective generation will be challenging due to the long distance line and high capital investment.*
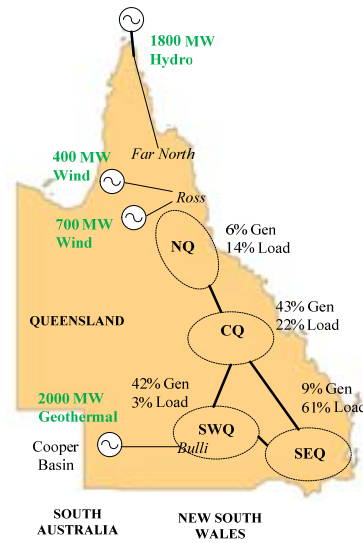
Fig.3.b: *Different zones of the Queensland network – North (NQ), Central (CQ), South-East (SEQ), and South-West (SWQ) [PowerLink, 2011]. The CQ zone has the highest (43%) percentages of generation, followed by SWQ (42%), SEQ (9%), and NQ (6%). In contrast, SEQ zone has the highest (61%) ratio of load. The share of load for CQ, NQ, and SWQ are 22%, 14% and 3%, respectively.*

Projects to be connected

Four long distance transmission projects are evaluated in this study. Table 1 presents the amount of generation, distance and zone of projects. A brief overview of the projects is given below.

Table 1 Overview of the large scale renewable projects to be connected to the Queensland network

Project	Generation (MW)	Transmission line (km)	Area	Zone
Copper String	400	720km overhead line	Ross	NQ
Cooper Basin	2000	1000km overhead line	Bulli	SWQ
Kennedy Wind Farm	700	300km overhead line	Ross	NQ
PNG Hydro	1800	250km cable +1200km OH	Far North	NQ

Copper String project [*CopperString*, 2012]: It will be connected from Mount Isa of North West Queensland to the Townsville of the existing network. It is designed for 400MW with a length of 720 km. Construction work is scheduled to start in late 2012, and the project completion date is early 2015.

Cooper Basin Geothermal [*QGECE*, 2010.]: The potential connection point from Cooper Basin is the Western Downs in the existing grid. In this case study, transmission capacity is considered as 2000MW. As reported by the Geodynamics, construction and commissioning of a 25MW commercial demonstration plant is scheduled for 2015.

Kennedy Wind Farm [*Windlab*, 2012]: The Kennedy Wind Farm Project is located in Hughenden, approximately 290 km South-West of Townsville. The transmission capacity is estimated at around 700 MW through a 290 km transmission line. Approval was sought for this project in late 2011, construction is scheduled from 2012 and commercial operation is expected from 2014.

PNG Hydro: The PNG Hydro project is expected to generate 1,800MW hydro power in Papua New Guinea (PNG). This power will be transmitted to the existing Australian NEM grid. 250 km subsea cable and 1200 km overhead transmission line is designed to transfer this power to the far north Queensland.

Results and analysis

Optimal power flow results and economic analysis are presented in this section. Connection cost allocations, net market benefits and impacts on the existing network have been discussed below.

Connection costs

Table 2 presents the connection costs for different projects according to different cost allocation schemes. There is no cost burden on renewable generators according to the super-shallow policy. The transmission infrastructure is built by the Transmission Network Service Provider (TNSP) and further the cost is socialized among consumers. The semi-shallow policy divides the transmission connection cost between producers and consumers. This methodology offers a platform for negotiation between the generation developers and TNSPs. A 50-50 cost sharing scheme is implemented in this study. However, in a real life scenario, this proportion can be any percentage based on the agreement among market participants. Further, according to the shallow cost allocation policy, the connection cost is borne by the generators. This is the usual generation connection policy in the Australian NEM. Under the current Australian scheme, remote renewable generation developers of the CS, CB, KWF and PNG are responsible for paying few billion dollars for network integration. This arrangement of high connection cost eventually can delay or defer the long distance renewable power integration to the grid [*Hasan et al.*, 2012b].

Table 2 Connection cost allocation for different projects through different schemes

	Transmission investment (m$)			
	Super-shallow / SENE	Semi-shallow / SENE HUB	Shallow / current NEM policy	Deep
Copper String (CS)	0	550	1100	1200
Cooper Basin (CB)	0	1350	2700	3000
Kennedy Wind Farm (KWF)	0	400	800	900
PNG Hydro (PNG)	0	1600	3200	3600

Net market benefit

The net market benefit is obtained from the optimal power flow of the Queensland network and by equation (1). The main contribution of the net market benefit comes from the consumer benefit, emission tax and LRET payment. The net market benefit also depends on the power dispatch, power flow and power demand in different areas of the network. Fig. 4 shows the net market benefit and annual required revenue (ARR) of the considered projects [*Hasan et al.*, 2012c].
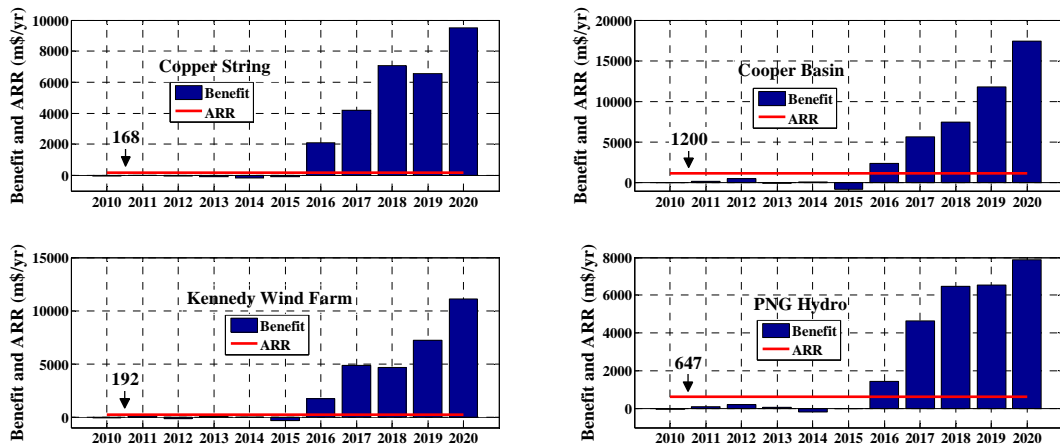
Fig.4 Net market benefit and ARR of the four long distance power transmission projects. The market benefit of Copper String, Cooper Basin, Kennedy Wind Farm and PNG hydro project overcomes the annual required return on capital from the year 2016 and thereafter. Overall the Cooper Basin project offers maximum net benefit, followed by the Kennedy Wind Farm project.

Impacts on the existing network

The impact of four projects on the network in terms of power injections, expected benefits and estimated cost burdens are shown in Table 3. The injected power and expected benefits are obtained from the optimal power flow solution of the Queensland network. The benefits are calculated based on Eq.1. The benefit-to-cost ratio shows the potential of Cooper Basin project compared to others. Combinations of all projects which have higher than 0.5 benefit-to-cost ratios are contained by the CB project. A notable intimation of Table 3 is that the benefit is calculated in m$/yr where the cost is in m$. Also the OPF considers pick loading conditions that may exaggerate the market benefit [*Hasan et al.*, 2012b].

Table 3 Combination of projects and corresponding power injection, expected benefits and costs

Coalition of projects	Injected Power (MW)	Expected Additional Benefits (m$/yr)	Estimated Transmission Investment (m$)	Benefit-to cost ratio
Copper String - CS	85	-1823	1100	-1.65
Cooper Basin - CB	1276	2140	2700	0.80
Kennedy Wind Farm - KWF	0	351	800	0.40
Papua New Guinea - PNG	708	1568	3200	0.50
{CS, CB}	1365	1671	2800	0.60
{CS, KWF}	169	523	1900	0.28
{CS, PNG}	793	1390	4300	0.32
{CB, KWF}	1364	2005	3500	0.57
{CB, PNG}	1984	2717	5900	0.46
{KWF, PNG}	793	1306	4000	0.33
{CS, CB, KWF}	1451	2102	3600	0.58
{CS, CB, PNG}	2064	2836	6600	0.42
{CS, KWF, PNG}	793	1380	5100	0.27
{CB, KWF, PNG}	2064	2693	6700	0.40
{CS, CB, KWF, PNG}	2142	2766	7800	0.36

Conclusions

There are potential geothermal resources in the Cooper Basin area to supply cheap, reliable and baseload power. The ultimate dispute is the remoteness of generation zone, which requires a long distance transmission corridor to transfer large amount of power. This research highlights the potential challenges of transferring geothermal power from Cooper Basin area to the existing Australian NEM network. Some of the regulatory and economic challenges have to be resolved by proactive regulatory decisions. Hub connection approach has been proposed in this research, which could be a way to connect remote generators efficiently. It has been noted that connection cost policy in the NEM is needed to be revised to enhance large scale geothermal generation development.

The net market benefit framework has been implemented for the Queensland electricity network. It is observed that the investment in large scale renewable power projects will be highly rewarded in coming years. As the power demand increases and pollutant coal generators retire, market policy requires clean energy. Consequently, renewable generators are expected to obtain increasing market benefit. The location of the Cooper Basin geothermal is relatively closer to the load centre of South East Queensland, which facilitates higher power dispatch and more benefit-to-cost ratio. Also, the estimated investment in geothermal power will be well satisfied by the expected benefits.

References

Chattopadhyay, D. (2011), Scale Efficient Network Development to Support Renewable Generation Development, *IEEE Transactions on Sustainable Energy*, *2*(3), 329-339.

CopperString (2012), Project Update, edited.

Eghbal, M., T. K. Saha, and K. N. Hasan (2011), Transmission expansion planning by meta-heuristic techniques: A comparison of Shuffled Frog Leaping Algorithm, PSO and GA, paper presented at 2011 IEEE Power and Energy Society General Meeting, 24-29 July 2011.

Hasan, K. N., T. K. Saha, and M. Eghbal (2011a), Renewable power penetration to remote grid - transmission configuration and net benefit analyses, paper presented at 2011 IEEE PES Innovative Smart Grid Technologies Asia (ISGT), 13-16 Nov. 2011.

Hasan, K. N., T. K. Saha, and M. Eghbal (2011b), Tradeoffs in planning renewable power generation entry to the electricity market, paper presented at 2011 IEEE Power and Energy Society General Meeting, 24-29 July 2011.

Hasan, K. N., T. K. Saha, and M. Eghbal (2011c), Modelling uncertainty in renewable generation entry to deregulated electricity market, paper presented at 2011 21st Australasian Universities Power Engineering Conference (AUPEC), 25-28 Sept. 2011.

Hasan, K. N., T. K. Saha, and M. Eghbal (2012a), Emission Pricing and Locational Signal Impact on Generation Portfolio in Large Scale Queensland Network paper presented at 2012 IEEE Power & Energy Society General Meeting, San Diego, California, USA.

Hasan, K. N., T. K. Saha, D. Chattopadhyay, and M. Eghbal (2012b), Benefit-Based Expansion Cost Allocation for Large Scale Remote Renewable Power Integration into the Australian Grid *submitted to Energy Policy*.

Hasan, K. N., T. K. Saha, M. Eghbal, and D. Chattopadhyay (2012c), Review of Transmission Schemes and Case Studies for Renewable Power Integration into the Remote Grid, *submitted to Elsevier Renewable & Sustainable Energy Reviews*.

PowerLink (2011), Annual Planning Report, 2011. Available: http:// www.powerlink.com.au /asp/index.asp? sid=5056& page=Corporate/ Documents&cid=5250 &gid=623.

QGECE (2010.), Queensland Geothermal Energy Centre of Excellence. Available: http: //www.uq.edu.au /geothermal /index.html*Rep.*, The University of Queensland, .

Radzi, N. H., R. C. Bansal, Z. Y. Dong, K. N. Hasan, and Z. Lu (2012), Overview of the Australian national electricity market transmission use of system charges for integrating renewable generation to existing grid, *IET Generation, Transmission & Distribution*, *6*(9), 863-873.

Swider, D. J., L. Beurskens, S. Davidson, J. Twidell, J. Pyrko, W. Prüggler, H. Auer, K. Vertin, and R. Skema (2008), Conditions and costs for renewables electricity grid connection: Examples in Europe, *Renewable Energy*, *33*(8), 1832-1842.

Windlab (2012), Kennedy Wind Farm, edited.

Investigation of Pre-Cooling with Munters Media for Air-Cooled Geothermal Power Plants Performance Enhancement

He S.Y[1,2], Gurgenci H[1,2], Guan Z.Q[1,2], Lu Y.S[1,2]

[1] Queensland Geothermal Energy Centre of Excellence. [2] School of Mechanical and Mining Engineering, The University of Queensland

uqshe1@uq.edu.au

Abstract: Many binary-cycle geothermal power plants are air cooled due to the lack of water source. The performance of air-cooled geothermal power plant will experience a loss in production during hot seasons, at which a high demand for electricity happens. This paper describes an investigation of pre-cooling with Munters CELdek7060 to enhance summer performance. A case study of a proposed 29MWe binary-cycle geothermal power plant located in southwest Queensland was conducted. The plant was cooled by a 100m height Natural Draft Dry Cooling Tower (NDDCT). Two thicknesses of Munters CELdek7060 were employed to pre-cool the tower, i.e., 0.1m and 0.15m. The hourly performance of the proposed plant incorporated with pre-cooled NDDCT was compared with that of un-cooled tower in a typical hot and dry day. Results show that geothermal power plants cooled by NDDCTs can benefit from pre-cooling with Munters CELdek7060 during hot and dry days. The 0.15m-thick CELdek7060 offers slightly better improvement than the 0.1m-thick counterpart. The largest increment of power output happens at around 3p.m. at which the increment can be up to 80%. Moreover, the two pre-cooled towers consume approximately half of wet cooling tower water consumption.

Keywords: Geothermal power plant, natural draft dry cooling tower, Munters CELdek7060, pre-cooling

Geothermal Power Plant Specifications

A proposed binary-cycle geothermal power plant is employed to do this case study. The design details of the plant are given in Table 1.

Table 1: Design conditions of the proposed tower

Items	Values and units
Brine temperature: T_H	523K (250°C)
Normal power output: w	29MWe
Heat dump: Q_c	158MW
Cycle efficiency: η_{th}	15.6%
The atmospheric pressure: P	101.325kPa
Ambient air temperature: T_a	293K (20°C)
Ambient air relative humidity: ϕ	30%
Air mass flow rate: m_a	5955kg/s
Hot water flow rate: m_w	4200kg/s
Hot water inlet temperature: T_{wi}	328K (55°C)
Hot water outlet temperature: T_C	319K (46°C)

The plant is proposed in Charleville, a town in southwest Queensland, Australia. Southwest Queensland has hot and dry summer climate, which is more suitable for evaporative cooling. The case study is conducted based on hourly weather conditions in a typical hot day (i.e., 04th Feb. 2006) in Charleville. The weather data is from Australian Bureau of Meteorology (2009). The hourly air dry-bulb temperature and relative humidity are given in Figure 1.

The cycle performance of a binary-cycle geothermal power plant can be assessed by the First Law using thermal efficiency, i.e.,

$$\eta_{th} = \frac{w}{Q_c + w}$$

(1)

The thermal efficiency of the proposed plant is assumed to be 40% of Carnot Cycle efficiency. The Carnot Cycle, a theoretical thermodynamic cycle, has the same hot and cold reservoir as the proposed plant. Then the thermal efficiency can also be assessed by,

$$\eta_{th} = 40\% \times (1 - \frac{T_C}{T_H})$$

(2)
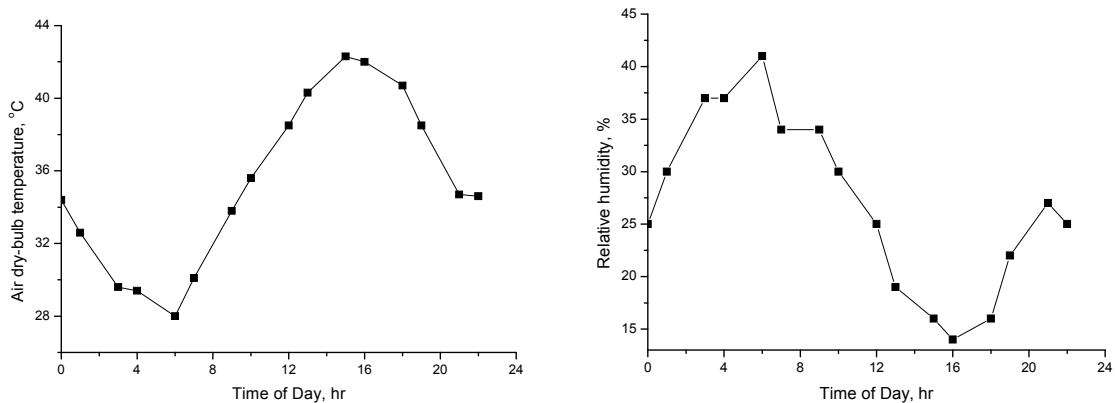
Figure 6: *Hourly weather conditions on 04th Feb. 2006, Charleville, Queensland*

Natural Draft Dry Cooling Tower Specifications

The hyperbolic, natural-draft, dry-cooling tower has a height of 100m. The heat exchanger uses extruded bimetallic finned tubes. The heat exchanger bundles are laid out horizontally at the inlet cross section of the tower and are arranged in the form of A-frames placed in a radial pattern. The specifications of the tower and heat exchanger are summarised in Table 2.

Table 2: Specifications of the cooling tower and heat exchanger

Heat exchanger specifications	Cooling tower specifications
Hydraulic diameter of tube, d_e=0.0216m	Tower height, H_5=100m
Fin diameter, d_f=0.0572m	Tower inlet height, H_3=12.5m
Length of finned tube, L_t=14.4m	Heat exchanger exit height, H_4=14.5m
Number of tube rows, n_r=4	Tower inlet diameter, d_3=65m
Number of tubes per bundle, n_{tb}=165	Tower outlet diameter, d_5=48.5m
Number of water passes, n_{wp}=2	Number of tower supports, n_{ts}=50
Number of bundles, n_b=80	Length of tower support, L_{ts}=12.5m
Apex angle of A-frame, θ=61.5/2	Diameter of tower support, d_{ts}=0.5m
Inside area of tube per unit length, A_{ti}=0.0679m^2/m	Drag coefficient of tower support, C_{Dts}=2.0
Inside cross-sectional flow area, A_{ts}=3.664x10^{-4}m^2	Thickness of the square-edged shell at the
Total effective frontal area of bundles, A_{fr}=2701.7m^2	inlet to the tower, t_s=0.8m
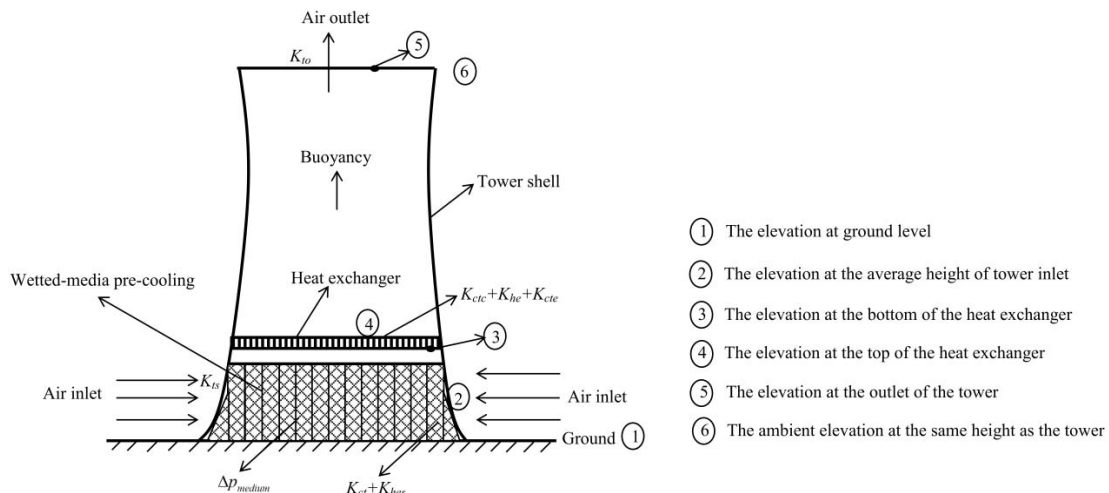
Figure 7: NDDCT pre-cooled with Munters media

The pre-cooled tower is shown in Figure 2. Two thicknesses of Munters CELdek7060 are applied to pre-cool the tower, i.e., 0.1m and 0.15m. The entire tower inlet area is expected to be covered with Munters media. To this end, the frontal area of CELdek7060 is calculated to be 2240m^2. If the pads with dimensions of 2.0mx0.6mx0.15m are employed, the total cost of media is around $121,423 (AAS, 2012; Munters, 2012).

The pre-cooling system follows the nature of evaporative cooling. Water is distributed over the top of the media and drips down by gravity to wet the media uniformly. Air passes through Munters media to form a cross-flow heat and mass exchange process. The water deposited on the media evaporates by extracting its evaporation heat from the air stream and thus cools the air. The pre-cooled air then flows through the heat exchanger to cool the tube-side fluid coming from the power plant.

According to Kroger (2004), a value of air mass flow rate can be found that will satisfy both the energy and draft equations of the NDDCT. A MATLAB code is developed to find this value by a period of iteration. When the equilibrium is reached, the heat rejection rate of the NDDCT would be found.

Munters Medium Performance

The cooling efficiency and pressure drop of 0.1m and 0.15m-thick CELdek7060 are fitted using the data from Munters handbook (2012). When the two thicknesses of CELdek7060 are incorporated into the tower, the hourly air temperature and pressure drop across CELdek7060 are given in Figure 3.
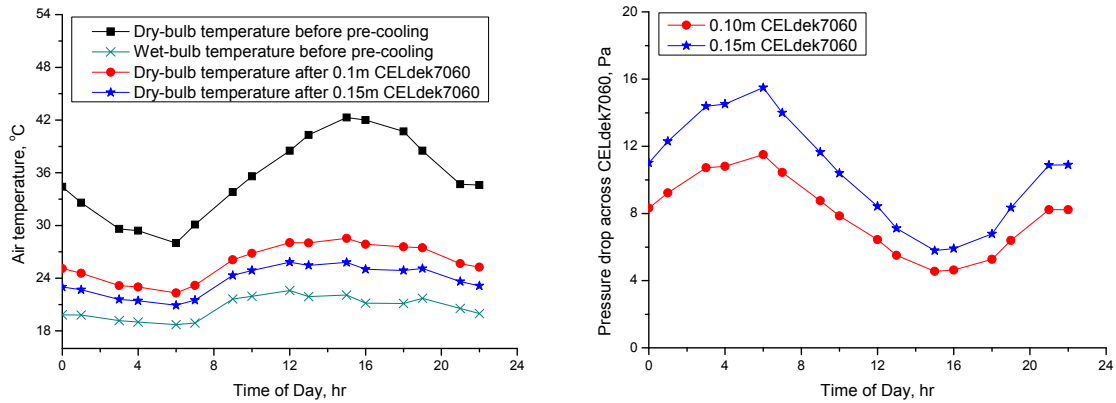
Figure 8: *Hourly air temperature and pressure drop across CELdek7060 (04th Feb. 2006, Charleville)*

Enhancement with Pre-Cooling vs No Enhancement

The hourly air mass flow rate and power output of the proposed power plant with pre-cooling, without any enhancement, are shown in Figure 4. Figure 4 demonstrates that the air mass flow rate of the pre-cooled tower is always lower than that of un-cooled tower, which is due to the additional pressure drop associated with the media. Figure 4 also shows that geothermal power plants cooled by NDDCTs can benefit from the pre-cooling with Munters CELdek7060 during hot and dry days. The 0.15m-thick CELdek7060 offers slightly better improvement than the 0.1m-thick counterpart. The largest increment of power output happens at around 3p.m. at which the increment can be up to 80%.
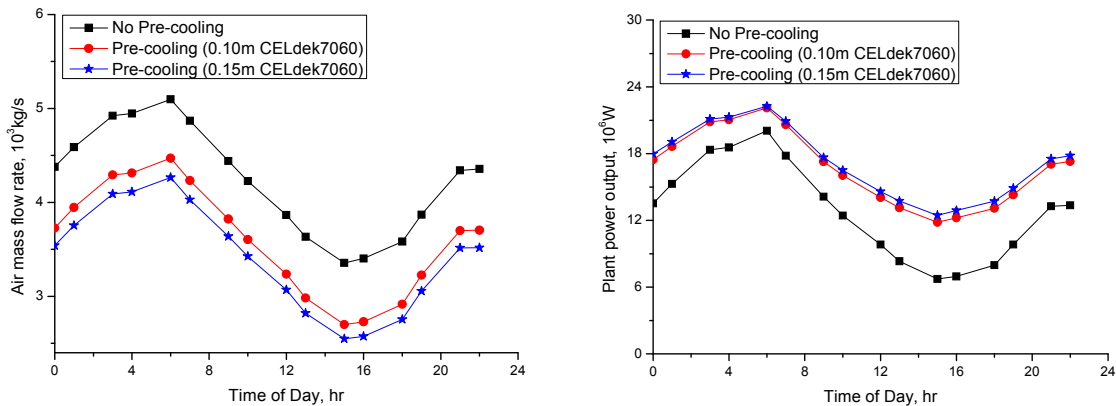
Figure 9: *Hourly air mass flow rate and power output (04th Feb. 2006, Charleville)*

Water Consumption

The hourly water consumption rate and heat rejection rate are given in Figure 5. The average water consumption rates on the day of 04th Feb. 2006 are 14 and 16kg/s for 0.10 and 0.15m CELdek7060, respectively. The average heat rejection rates of the un-cooled tower, pre-cooled tower with 0.10m CELdek7060, pre-cooled tower with 0.15m CELdek7060 are 72, 92 and 95 MW, respectively.
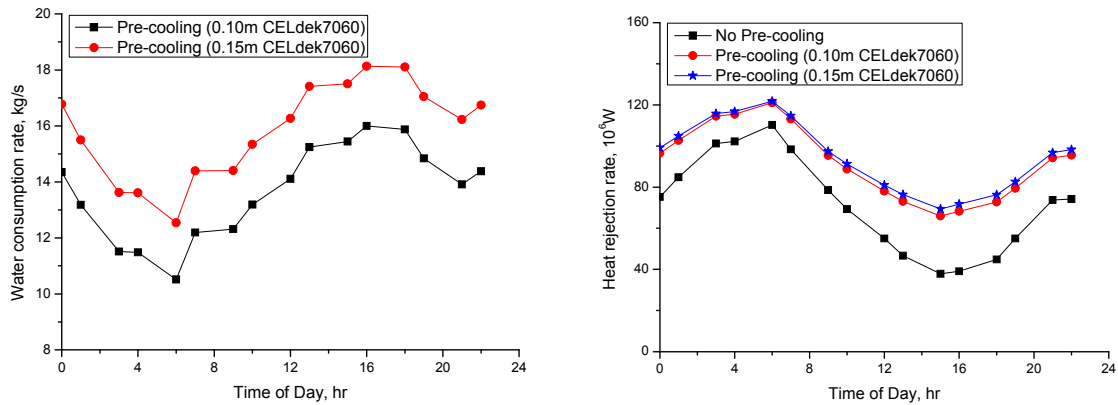
Figure 10: *Hourly water consumption rate and heat rejection rate (04th Feb. 2006, Charleville)*

For wet cooling towers, the total heat rejection results from evaporative cooling (latent heat transfer due to water vaporization) and sensible cooling (sensible heat transfer due to the difference in temperature) (Kroger, 2004; PDHengineer, 2012). The evaporative cooling may account for 80% of the cooling according to the literature (PDHengineer, 2012). If we assume that the latent heat of water vaporization is constant at $h_{vaporization}$=2500kJ/kg. Then, the water consumption of wet cooling tower m_e, can be calculated by the following equation, i.e.,

$$80\% Q_c = m_e \times h_{vaporization} \tag{3}$$

The comparisons of water consumption of dry or water-assisted towers, wet cooling towers are given in Table 3. As can be seen from Table 3, the two pre-cooled towers consume approximately half of wet cooling tower water consumption.

Table 3: The comparisons of water consumption of dry or water-assisted towers, wet cooling towers

Tower type	Average water consumption rate per MW heat rejection, (kg/s)/MW
Dry cooling tower	0
Pre-cooled tower (0.10m-CELdek7060)	0.15
Pre-cooled tower (0.15m-CELdek7060)	0.17
Wet cooling tower	0.32

References

AAS, 2012. Australasian Agricultural Services Pty Ltd. Available from: http://www.ausagservices.com.au/deals/aug12.html.

BoM, 2009. Australian Hourly Temperature, Humidity and Pressure Data. Australian Bureau of Meteorology.

Kroger, D.G., 2004. Air-Cooled Heat Exchangers and Cooling Towers: Thermal-flow performance evaluation and design. Tulsa, Oklahoma, PennWell Corp.

Kroger, D.G., 2004. Air-Cooled Heat Exchangers and Cooling Towers: Thermal-flow performance evaluation and design. Tulsa, Oklahoma, PennWell Corp.

Munters, 2012. Munters products handbook. Available from: http://www.munters.com/en/Global/.

PDHengineer, 2012. Cooling Towers PDHengineer Course No. M-7002. Available from: http://www.pdhengineer.com/courses/m/M-7002.pdf.

Geothermal Resources of Java – Indonesia

Herdianita, N.R.[1,2,3], Situmorang, J.[2], Mussofan, W., Hamzah, I.[2]

[1] Study Program of Geological Engineering, Faculty of Earth Sciences and Technology, ITB, [2] Master Study Program of Geothermal Engineering, Faculty of Mining and Petroleum Technology, ITB, [3] Applied Geology Research Group, Faculty of Earth Sciences and Technology, ITB

herdianita@gc.itb.ac.id

Introduction

Java island of Indonesia is part of the micro-continental Sunda Land formed by the convergent interaction between Indo-Australian and Eurasian plate. Subduction of oceanic crust under the microcontinent Sunda Land formed the volcanic arc along the southern part of Java. These volcanic activities indicated by the occurrence of andesitic strato volcano are the potential heat source for hydrothermal systems in Java.

The occurrence of geothermal surface manifestations, e.g. fumaroles, hot springs, etc, indicates that Java has at least 71 geothermal prospect areas (Figure 1 and Table 1). The resources occur from east to west parallel to the subduction zone in the south of Java. Recognisance survey and geochemistry study show that the geothermal prospects of Java can be divided at least into 5 hydrothermal-system types, i.e. (1) Hydrothermal system associated with Quaternary andesitic volcano, (2) Hydrothermal system associated with Plio-Pleistocene volcanic system, (3) Hydrothermal system associated with structural geology, (4) Hydrothermal system in sedimentary rock basin, and (5) Isolated warm spring with unknown origin hydrothermal system (Table 1).

Most hydrothermal resources are associated with young andesitic volcanoes; the heat transfer to the surface is then influenced by several geological conditions that make the hydrothermal system slightly modified from the hydrothermal volcanic system.

Hydrothermal System Associated with Quaternary Andesitic Volcano

Most of geothermal prospects of Java are belong to this type. The hydrothermal system lie along the range of high-standing Quaternary andesitic volcanoes of Java, e.g. Gunung Salak, Tangkuban Parahu, Papandayan, Slamet, Lawu. The heat source of young volcano causes the hydrothermal systems to become high enthalpy systems having reservoir temperatures of more than $225^{o}C$.

Surface manifestations occur as fumaroles, steaming ground and acid-sulfate hot springs in the upflow zone, i.e. around peak of volcano, and warm bicarbonate or mixed bicarbonate chloride springs in the lateral outflow zone, i.e. in much lower elevation of volcano. Indeed, some geothermal prospects still discharge magmatic fluid as acid sulfate-chloride hot springs, e.g. occurring in active volcano of Arjuno-Welirang. Several volcanic geothermal prospects are also associated with caldera structure, e.g. Rawa Dano and Blawan-Ijen.

Hydrothermal System Associated with Plio-Pleistocene Volcanic System

Plio-Pleistocene volcanic hydrothermal system associated with the intrusion body beneath the surface. This system is found on Gunung Endut, Umbul Telomoyo, and Songgoriti. Surface geothermal manifestation is rare, but can be found as neutral pH, slightly warm, chloride to chloride-bicarbonate springs. The presence of hydrothermal alteration is common, but fumarole and steaming ground are absent.

Hydrothermal System Associated with Structural Geology

Java has several big geological structures, e.g. Cimandiri and Baribis faults, that can be permeable zones for hydrothermal fluids to discharge to the surface. Surface manifestation occurs in this system as bicarbonate warm spring, perhaps seepage, but boiling spring, fumarole and steaming ground are absent. However, the volcanic system sometimes still influences the system, so the reservoir temperatures can still be promising.

Hydrothermal System in Sedimentary Rock Basin

Geothermal prospects associated with high geopressure condition form due to the anomaly pressure in sedimentary basin. Good examples of hydrothermal systems occurring in this sedimentary rock are Gunung Kromong and Cipari, where are characterized by the occurrence of surface manifestations of warm spring having high chloride and TDS contents.

Isolated Warm Spring with Unknown Origin Hydrothermal System

The other geothermal prospects, e.g. Parangtritis, Krakal, Melati, appear in the surface as isolated warm spring within non-volcanic area. The study shows that the origin of these prospects is unknown.
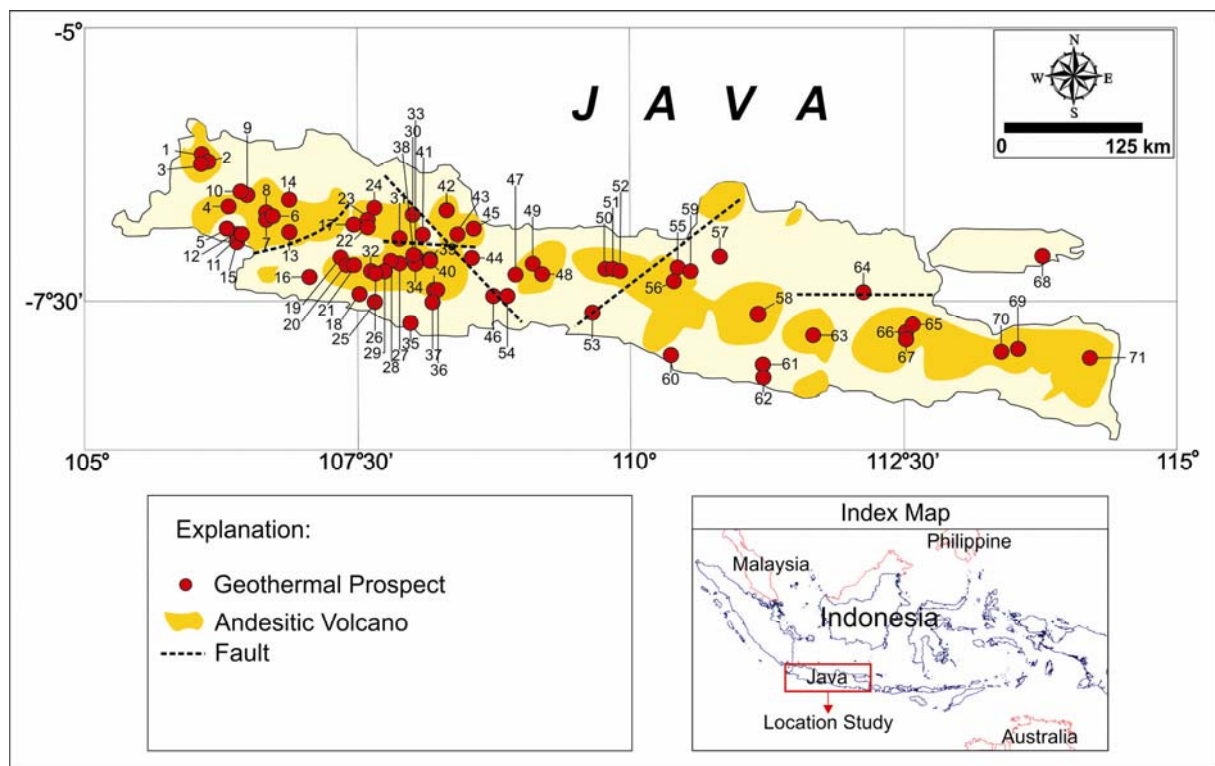
Figure 1. *Hydrothermal system of Java – Indonesia. The resources are 71 geothermal prospect with the total potency of about 10 Giga Watt electricity. Number given on figure is the prospect area referred in Table 1.*

Table 1. Seventy one hydrothermal system of Java – Indonesia indicated by the occurrence of geothermal surface manifestations. Manifestation*: F=fumarole, S=solfatara, SG=steaming ground, HS=hot spring, HP=hot pool, WS=warm spring. Hydrothermal system**: (1) associated with Quaternary andesitic volcano, (2) associated with Plio-Pleistocene volcanic system, (3) associated with structural geology, (4) associated with sedimentary rock basin, and (5) isolated warm spring with unknown origin hydrothermal system.

No.				
1	Rawa Dano	HS, HP	Type B (Karang-Pulosari)	(1), (3)
2	Gunung Karang	F, SG, HS, WS	Type B (Karang-Pulosari)	(1)
3	Gunung Pulosari	F, SG, HS	Type B (Karang-Pulosari)	(1)
4	Gunung Endut	HS, WS	Type B (Endut)	(2)
5	Pamancalan	WS	-	(3)
6	Kawah Ratu	F, SG, HS, HP	Type A (Salak)	(1)
7	Kiaraberes	F, S, HS	-	(1)
8	Awibengkok	F, SG, HS	Type A (Salak)	(1)
9	Ciseeng	WS	-	(1), outflow
10	Bujal Jasinga	WS	-	(4)
11	Cisukarame	HS	Type B	(3)
12	Cisolok	HS	Type B (Halimun)	(3)
13	Selabintana	WS	-	(3)
14	Gede – Pangrango - Pancar	F?, WS	Type A (Gede)	(1)
15	Jampang	WS	-	(3)
16	Tanggeung - Cibuni	HS, WS	-	(2), (3)
17	Saguling	WS	-	(5)
18	Cilayu	HS, WS	Type A (Papandayan)	(1), outflow
19	Kawah Cibuni	SG, HS	Type B (Patuha)	(1)
20	Gunung Patuha	F, HS, HP	Type B (Patuha)	(1)
21	Kawah Ciwidey	SG, HS, HP	Type B (Patuha)	(1)
22	Maribaya	WS	Type A (Tangkuban Parahu)	(1),outflow, (3)
23	Tangkuban Perahu	F, SG, HS, HP	Type A (Tangkuban Parahu)	(1)
24	Sagalaherang	WS	-	(1), outflow
25	Ciarinem	WS	Type A (Papandayan)	(1), outflow
26	Gunung Papandayan	F, SG, HS, HP	Type A (Papandayan).	(1)
27	Gunung Masigit-Guntur	HS	-	(1)
28	Kamojang	F, SG, HS, HP	-	(1)
29	Darajat	F, SG, HS, HP	-	(1)
30	Gunung Tampomas	HS, SP	Type B (Tampomas)	(2)
31	Ciipacing	WS	-	(3)
32	Wayang - Windu	F, SG, HS	Type B (Wayang Windu)	(1), (2)
33	Gunung Telaga Bodas	F, SG, HS, HP	Type B (Telaga Bodas)	(1)
34	Gunung Galunggung	WS	-	(1)
35	Ciheras	WS	-	(1), outflow
36	Cigunung	WS	-	(1), outflow
37	Cibalong	WS	-	(1), outflow

No.	Prospect	Manifestation*	Volcano Activity Type	Hydrothermal System**
38	Gunung Karaha	F, SG, HS, HP	-	(1)
39	Gunung Sawal	WS	-	(2)
40	Cipanas - Ciawi	WS	-	(4)
41	Gunung Cakrabuana	WS	-	(2)
42	Gunung Kromong	HS, WS	Type A (Ciremai)	(4)
43	Sangkanhurip	WS	Type A (Ciremai)	(1), outflow
44	Subang	WS	-	(3)
45	Cibimbin	WS	-	(3)
46	Banyugaram	WS	-	(4)
47	Bumiayu	WS	Type A (Slamet)	(1), outflow
48	Baturaden	F, HS	Type A (Slamet)	(1)
49	Guci	F, WS	Type A (Slamet)	(1)
50	Mangunan - Wanayasa	WS	Type A (Dieng)	(1), (3)
51	Candradimuka	F, SG, HS, HP	Type A (Dieng)	(1)
52	Dieng	F, SG, HS, HP	Type A (Dieng)	(1)
53	Krakal	WS	-	(5)
54	Panulisan	WS	-	(5)
55	Gunung Ungaran	F, SG, HS, HP	Type B (Ungaran)	(1)
56	Gunung Umbul - Telomoyo	WS	-	(2)
57	Kuwuk	WS	-	(5)
58	Gunung Lawu	F, SG, HS, WS	Type B (Lawu)	(1)
59	Klepu	WS	Type B (Ungaran)	(5)
60	Parangtritis	WS	-	(5)
61	Melati	WS	-	(5)
62	Rejosari	WS	-	(5)
63	Telaga Ngebel	HS, WS	Type B (Wilis)	(2)
64	Gunung Pandan	WS	Type B (Pandan)	(2)
65	Gunung Arjuno - Welirang	F, S, SG, HS, HP	Type A (Arjuno Welirang)	(1)
66	Cangar	WS	Type A (Arjuno Welirang)	(2)
67	Songgoriti	WS	Type A (Arjuno Welirang)	(2)
68	Tirtosari	WS	-	(3), (4)
69	Argopuro	WS	Type B (Iyang Argopuro)	(1)
70	Tiris - Gunung Lamongan	WS	Type A (G.Lamongan)	(1)
71	Blawan - Ijen	F, SG, HS, HP	Type A (Ijen)	(1)

Naturally Fractured Hot Rock: Exploring for Deep Permeable EGS Resources in Tasmania

Holgate, F.L.

KUTh Energy Limited

Fiona.Holgate@kuthenergy.com

KUTh Energy Limited (KEN) has actively explored for deep granite-related Enhanced Geothermal System (EGS) resources across its eastern Tasmanian licence areas for over five years (Figure 1). During this time the company has undertaken an extensive work program that has culminated in the recognition of the Lemont and Fingal inferred geothermal resource areas and identified the potential for naturally permeable hot rock plays.

Keywords: Tasmania, EGS, fracture permeability, magnetotelluric, hot rock

Background

A key aspect of KUTh's exploration philosophy in eastern Tasmania is the potential for improvement of the EGS resource-base by acessing natural permeability associated with large crustal fracture zones. Early recognition that a known electromagnetic feature, the *Tamar Conductivity Zone (TCZ)*, may be the geophysical signature of a regional-scale permeable fracture system led to the inclusion of magnetotelluric (MT) survey techniques into the surface exploration program. Described previously in Holgate et al. (2009) and Holgate et al. (2010), this program was also designed to address issues of green-fields exploration for deep EGS resources. Along with MT surveys, work completed by KUTh in Tasmania now includes an extensive regional shallow heat-flow drill program, gravity and aeromagnetic data acquisition, ambient seismic surveys, earthquake focal mechanism determination, seismic hazard assessment, rock property determination and 2- and 3-D thermal and stress state modelling.

Geological Setting

Widespread Jurassic dolerite sills within flat-lying Permo-Triassic sediment of the Tasmania basin obscure basement formations across much of eastern Tasmania. Estimated cover thicknesses of up to 1 km have resulted in much of this area being under-explored with relatively few legacy drill holes and little available deep stratigraphic data. In the far north-east, outcropping basement comprises extensive Devonian granite bodies within Palaeozoic flysch sediments of the Mathinna Supergroup. Modelling of regional gravity data, now supplemented by infill surveys performed by KUTh in 2007 and 2010, indicates the presence of large granite bodies beneath much of eastern Tasmania and provides some indication of both the extent and geometry of the batholith (Figure 1).

The Tamar Conductivity Zone

The Palaeozoic basement terrane outcropping in far north-eastern Tasmania is temporally, lithologically and structurally distinct from the largely Precambrian basement terranes observed in the west of the state (Figure 1). However, the boundary of east and west Tasmanian terranes is obscured beneath Mesozoic cover and the exact nature of this contact is unknown. Coinciding with the area of likely terrane juncture is the Tamar Rift Valley, a Tertiary feature interpreted to represent extensional reactivation of older basement structure (Stacey, 2007). Also observed in this area is the Tamar Conductivity Zone (TCZ) a strong, electrically conductive anomaly in the crust that has previously been interpreted as the geophysical signature of fluid in a regional-scale fracture-permeable zone (Figure 1; Hermanto, 1992).
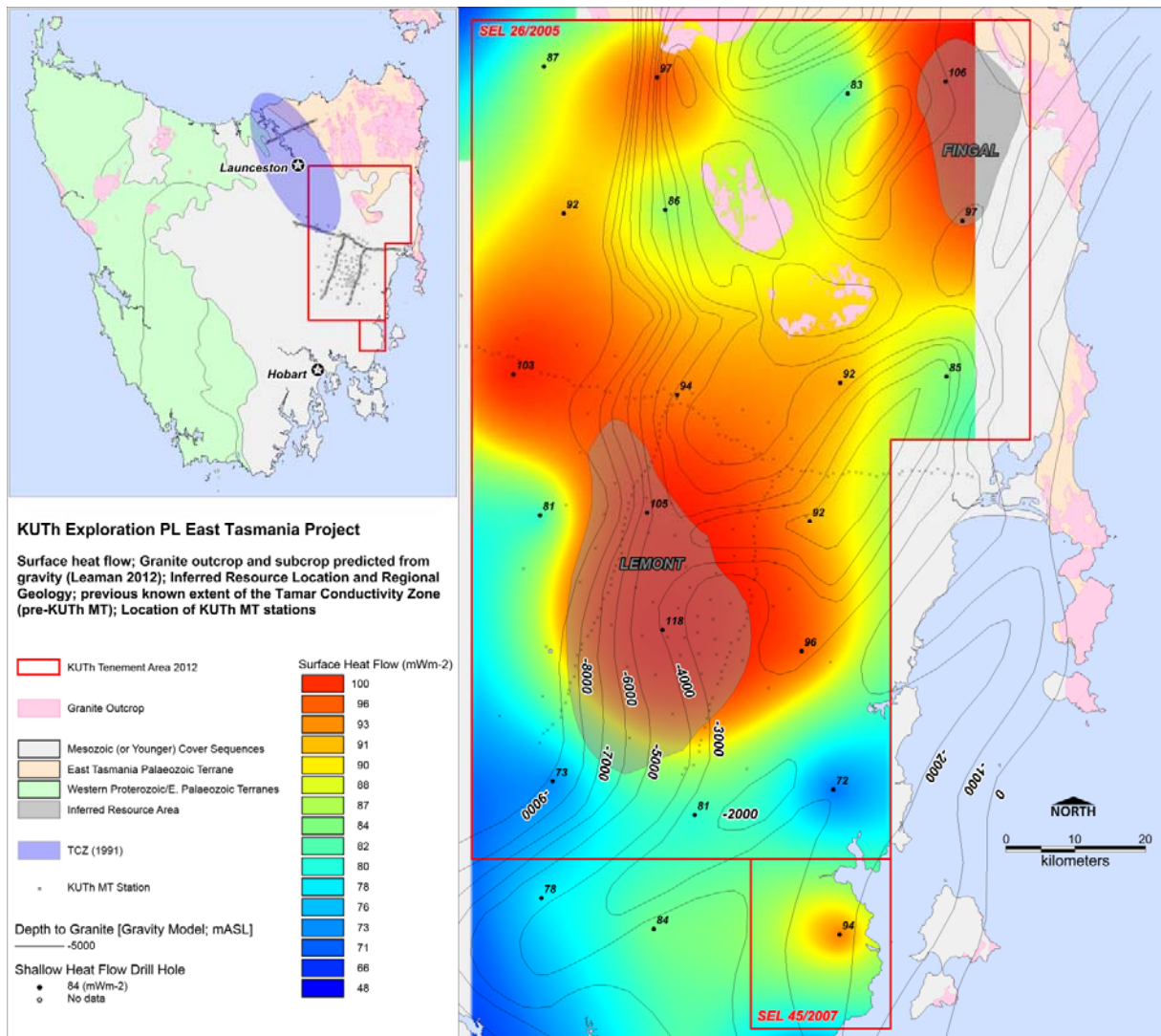
Figure 1: KUTh's Eastern Tasmanian project

Resource Identification

Granites of composition compatible with high heat production (HHP) are observed in outcrop in eastern Tasmania (Goh, 2008) and may also be inferred to continue west as part of the buried batholith. Data derived from KUTh's purpose-drilled 20 x 20 km grid of 36 shallow (ca. 250m) drill holes supports this, indicating the presence of a strong (>90mWm^{-2}) thermal anomaly in central eastern Tasmania that is spatially associated with buried granite (Figure 1). Results of particular note from the heat flow drilling program are the Lemont (118mWm^{-2}), Charlton (105mWm^{-2}) and Mt Nicholas (106mWm^{-2}) holes. Subsequent three-dimensional conductive heat-flow modelling undertaken across these areas has resulted in the estimation of significant inferred geothermal resources at Lemont (KUTh, 2009) and Fingal (KUTh, 2010). In both cases the resource play is inferred to be an EGS associated with HHP granite ('hot rock') buried beneath insulating cover sequences. At Lemont, however, this picture is further complicated by the addition of a potentially permeable fracture zone detected by MT survey directly along strike from the known TCZ.

Magnetotelluric Survey

Recognition of the potential of the TCZ to enhance the prospectivity of hot rock resource plays in eastern Tasmania led to the early incorporation of MT survey techniques into KUTh's surface program. The unique ability of MT to detect deep electrical conductivity implies that it has the potential to map fluid permeability within the crust and continued technological improvements in recent years have facilitated its development as a cost-effective surface geophysical exploration tool. Three successful, consecutive MT surveys were completed by KUTh in 2008, 2009 and 2010 for a total of 297 stations (Figure 1). Combined, these form one of the largest MT surveys conducted in Australia. Initial 2D survey lines were designed to target the known TCZ and determine its southern extent. Subsequent 2- and 3D survey lines and infill arrays targeted areas in and around the Lemont resource. Final results of this work, complied in 2010, reveal a complex pattern of large, very electrically conductive zones at Lemont with the NNW trending TCZ now apparently intersected by an EW-trending feature at the point of highest recorded heat flow (Figure 2).
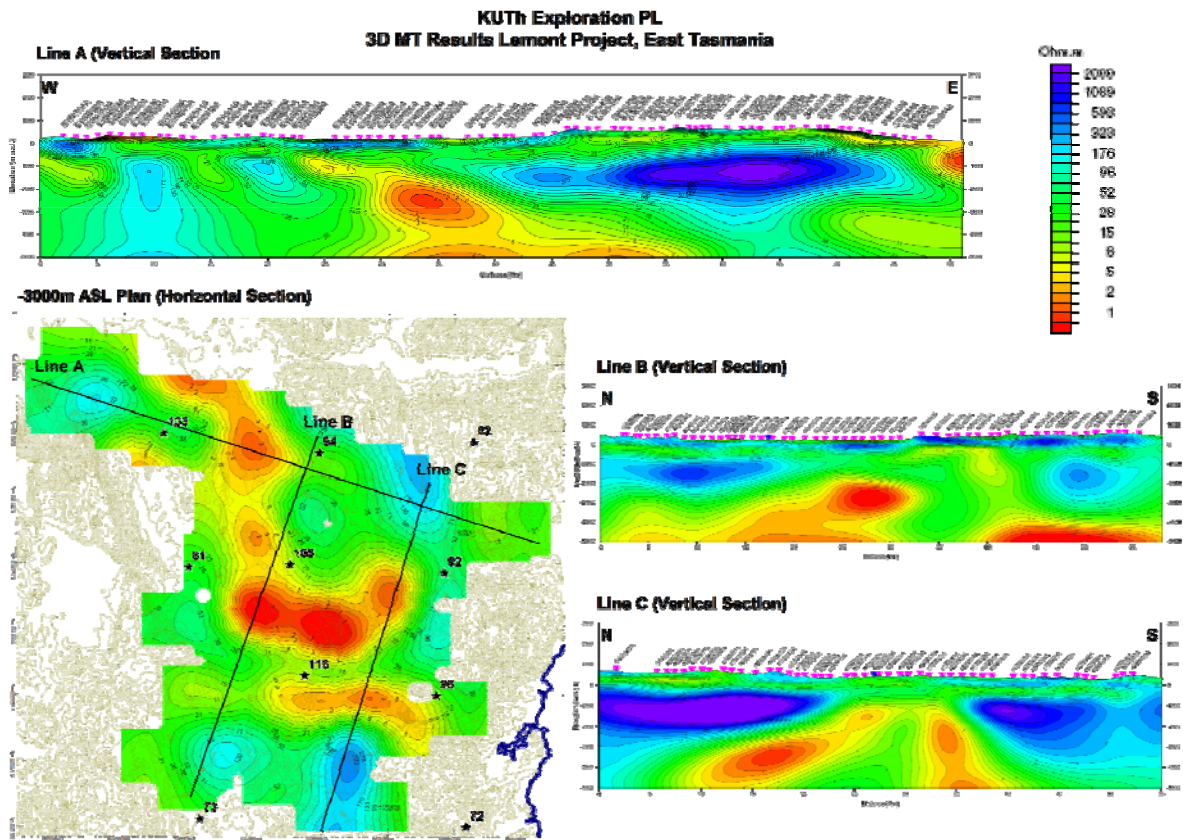
Figure 2: Selected results from the Lemont 3D magnetotelluric survey presented as resistivity images. All images share the same scale (shown); warmer colours indicate increased electrical conductivity. Vertical section lines are as located on the -3000m ASL Plan. Vertical exaggeration of these sections is 2:1. The location of surface heat flow values (mWm-2) from KUTh's shallow heat flow program are shown on the plan as black stars.

Naturally Fractured Hot Rock

The orientation and distribution of the large electrically conductive zones observed within the vicinity of the Lemont resource are consistent with fracture zones interpreted from limited available legacy seismic reflection data and with structural trends observed in both gravity and aeromagnetics. Whilst the interpretation of these features is currently non-unique their apparent spatial association with high heat flow anomalies is suggestive of an influence on the thermal field. Based on these observations KUTh has recognised the possibility of a Naturally Fractured Hot Rock (NFHR) play at Lemont. In essence NFHR is envisioned as a fracture permeable geothermal play with a HHP granitic heat source. In many ways NFHR is akin to a conventional play although with a non-volcanic heat source it is necessarily deeper and cooler than a typical geothermal field.

Forward project planning at Lemont aims to further reduce exploration risk at this site by proving or disproving the NFHR model using deep exploratory drilling to depths of between 2 – 3 km. In undertaking this project, KUTh aims not only to prove the geothermal resource at Lemont but also to investigate the concept of NFHR as a viable EGS play, to improve methods of targeting deep EGS resources by demonstrating the efficacy of surface MT as a tool for detection of crustal permeability and to investigate technologies for reducing the cost of deep exploratory drilling.

References

Goh, H.K.H., 2008. *Properties of North-Eastern Tasmanian Rocks for Geothermal Exploration, University of Tasmania.* University of Tasmania, Honours Thesis, unpublished

Hermanto, M.R., 1990. Magnetotelluric Investigations of the Tamar Lineament. University of Tasmania, PhD Thesis, unpublished

Holgate, F., Goh, H.K.H., Wheller, G., Lewis, R.G.J., 2009. *Exploring Eastern Tasmania: A Novel Geothermal Province*. Proceedings of the Australian Geothermal Energy Conference, GA Record 2009/35

Holgate, F., Goh, H.K.H., Wheller, G., Lewis, R.G.J., 2010. *The Central Tasmanian Geothermal Anomaly: A Prospective New EGS Province in Australia*. Proceedings of the World Geothermal Congress, Bali, Indonesia, 25-29 April

KUTh Energy Limited, 2009. *Statement of Estimated Geothermal Resources Charlton Lemont Geothermal Play*. ASX Release 14 July, http://www.kuthenergy.com/index.php?item=file&target=KUTh_CL_inferred_res_stmnt_14jul09

KUTh Energy Limited, 2010. *Statement of Estimated Geothermal Resources Nicholas Fingal Geothermal Play*. ASX Release 9 March, http://www.kuthenergy.com/index.php?item=file&target=asx_nf_inferred_resource

Leaman, D. E., 2012. *An interpretation of the granitoid rocks of Eastern Tasmania*. Mineral Resources Tasmania, Geophysics Contractor Report 2012/01

Stacey, A., 2007. *The Structural History of Tasmania from the Devonian to the Recent*. University of Tasmania, PhD Thesis, unpublished

Latest QGECE Research on Heat Exchangers

K. Hooman[1]

[1]Queensland Geothermal Energy Centre of Excellence, The University of Queensland

k.hooman@uq.edu.au

Abstract

This paper presents the latest results from our research on heat exchangers for future geothermal power plants. The application of metal foam heat exchangers in natural draft dry cooling towers has been studied in detail. Furthermore, the design of a steel cooling tower is proposed and analysed. Solar-enhanced dry cooling tower, a concept put forward by QGECE, is also examined here. This paper also provides an update on our research on the issue of fouling and dust deposition on air-cooled heat exchangers. Finally, our latest research activities in the field of hybrid cooling for potential application in solar thermal power plants as well as water management in coal seam gas projects are discussed. Some of our technical findings are then related to cost and economical analysis of a sample power plant.

Keywords: heat exchangers, dry cooling, experiment, CFD, theoretical.

Introduction

Research for the sake of improving an already existing engineering system can lead to invaluable results. As such, Queensland Geothermal Energy Centre of Excellence has been trying to get the most out of existing technology with the main goal of compensating for low efficiency of power plants for Enhanced Geothermal Systems. Having said that, a relatively significant part of our research has been focused on conducting research on developing technologies which will enable new arrangements and possibilities without which even the predicted low efficiency of the low enthalpy power plant will be only a shaky assumption [1-6]. Hybrid cooling systems, advanced heat exchangers and efficient power conversion techniques can be mentioned in this category.

As one would expect, answering questions of this nature asks for advanced facilities to deal with fundamental questions to push the boundaries of science and technology. This has been exactly what the Heat Exchanger Program of QGECE has been pursuing over the past twelve months. Thus far, and by a great margin, last year has been the most exciting one in the program' life. Significant investment was made in the facilities to equip our labs to a highly standard level. This includes the purchase of facilities like PIV, LIF, and PDPA. Such facilities allow for rigorous and experimental analysis of complex engineering problems which have to be addressed for designing and finally commercializing advanced heat exchangers and highly efficient power stations.

Again, not unexpectedly, our results lead to advances in the field and more interestingly a synergy with other energy systems including fuel cells, solar-thermal power plants, coal seam gas and coal-fired power plants. This alignment in the goals and objectives attracted more attention from others including prestigious international collaborators and, more importantly, industries and policy-makers to invest in our research and development activities, e.g. through research grants and patents.

In what follows, more technical but high-level information about our current and future research activities will be provided.

Research Activities

Our research activities conducted at QGECE on different projects are as follows.

Dust monitoring in Innamincka

To increase the air-side heat transfer coefficient, and thus minimize the overall resistance of the air-cooled system, is to maximize the surface area density by applying fins. This brings in problems like

the tendency of airborne foreign material to foul the external surface and thus to spoil the expected heat transfer augmentation. Fouling affects the heat transfer coefficient, reduces air flow rate, and increases energy consumption and the cost of maintenance services.

Conducting experiments on a compact microchannel heat exchanger, Bell and Groll [3] reported an increase in the air-side pressure drop of up to 200% where the heat transfer rate could decrease by over 10% due to the fouling caused by ASHRAE dust buildup on the heat exchanger surfaces. Air-side fouling on such surfaces can be classified into air dust deposition fouling, and the microorganism growth fouling (biofouling). Our research at QGECE focuses on the air dust deposition fouling only by monitoring the dust concentration and its particle distribution in Innamincka, one of the potential Australian geothermal power plant sites. The particle size study will also distinguish the particles which rise from soil dust from those which rise from plant pollen.
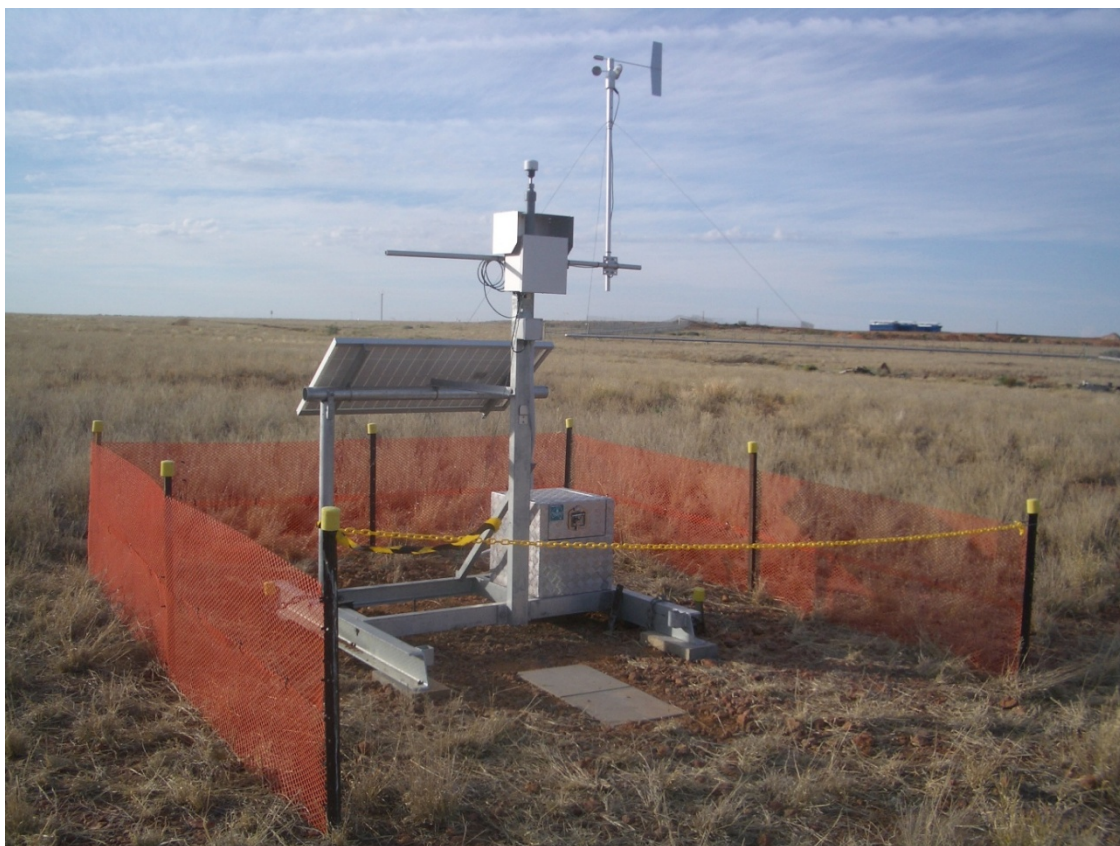
Fig.1 *Dust monitoring system installed in Innamincka (Photo provided by Geodynamic)*

The first stage of the study is to install a dust monitoring device, E-Sampler; a product of Met One Instruments Inc. sold in Australia by Ecotech, onsite to collect real time data of dust concentration, dust sample (for size analysis), wind speed, wind direction and ambient temperature. The whole system includes E-Sampler, solar panels to power the system, wind speed and direction sensor, and mounting frame, as shown in Figure 1.

Figure 2 shows dust concentration, temperature, wind speed and wind direction collected on 22nd May 2011 from about 11:30 am to 14:30 pm. It should be noted that the Innamincka was still in a clear season and the spike shown in the figure were caused by the road dust when trucks drive cross. The north-west wind (300 deg) was blowing with speed of about 6 m/s.

Once the effect of dust on the performance of metal foam heat exchanger has been identified, what remains will be to find methods of mitigation of the effects of dust on the heat exchanger including regular cleaning.
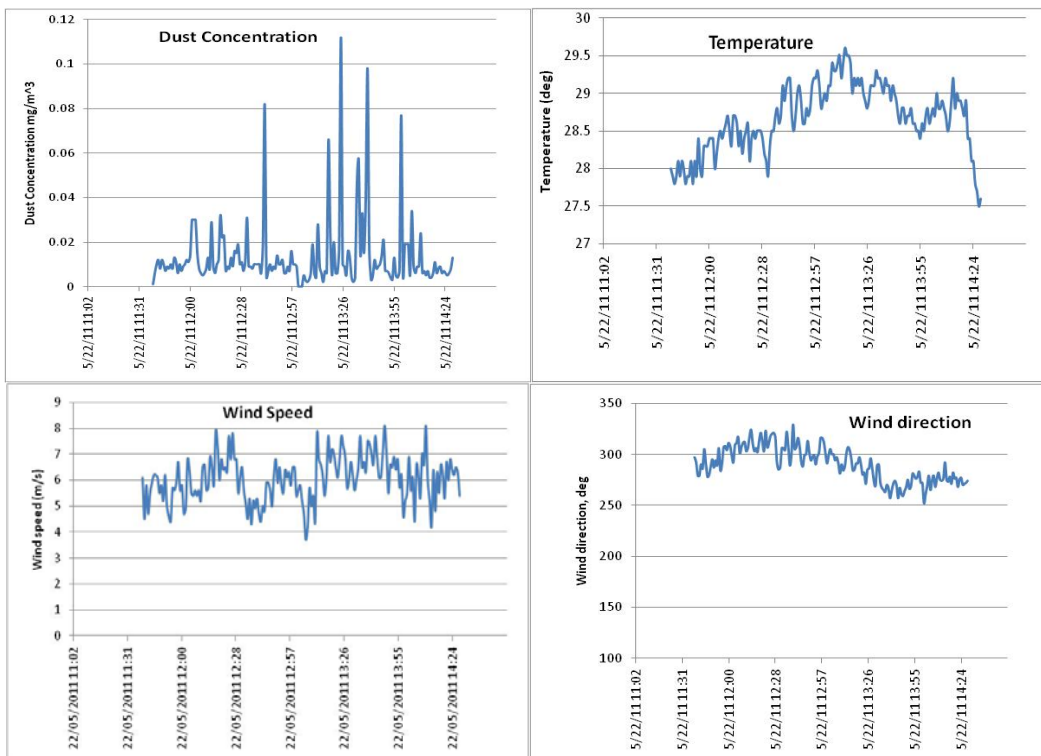
Fig.2 *Data collected on 22nd May*

Solar-enhanced cooling towers

A solar enhanced natural draft dry cooling tower (SENDDCT) would enhance the performance of a natural draft dry cooling tower (NDDCT) by adding solar heat after the heat exchangers and thus increases the buoyancy of the rising air inside the tower. The improved heat transfer rates caused by the higher air flow rates can be exploited to build a cooling system with either less heat exchanger areas or smaller tower sizes resulting in a reduced capital cost.

Three major components for a solar enhanced natural draft dry cooling tower are the heat exchangers, the solar collector (sunroof and ground), and the tower as shown in figure 6. The sunroof is a transparent circular roof which is placed around the foot of the tower at the tower inlet height. Heat exchangers are placed vertically along the outer edge of the solar collector. As sun heats the sun roof, the air under the roof is heated. Warm air naturally rises through the tower and fresh air is sucked in thus providing a cooling air flow through the heat exchanger bundles. The total heat exchange area may be less than the area offered at the perimeter of the solar collector. If this is the case, the rest of the perimeter of the solar collector needs to be blocked.

The performance of this new design concept has been compared with the one of conventional natural draft cooling tower through the tower height needed for certain heat dumped as shown in figure 3. It clearly shows that the tower height for solar enhanced cooling tower is smaller than the height required for the conventional natural draft cooling tower. It has also been observed that the SENDDCT is very beneficial to the power plant owners by increasing their revenue at the peak demand hours during the hottest periods of the year, during which the extra electricity enabled by the solar enhancement is normally also sold at the highest price [7].
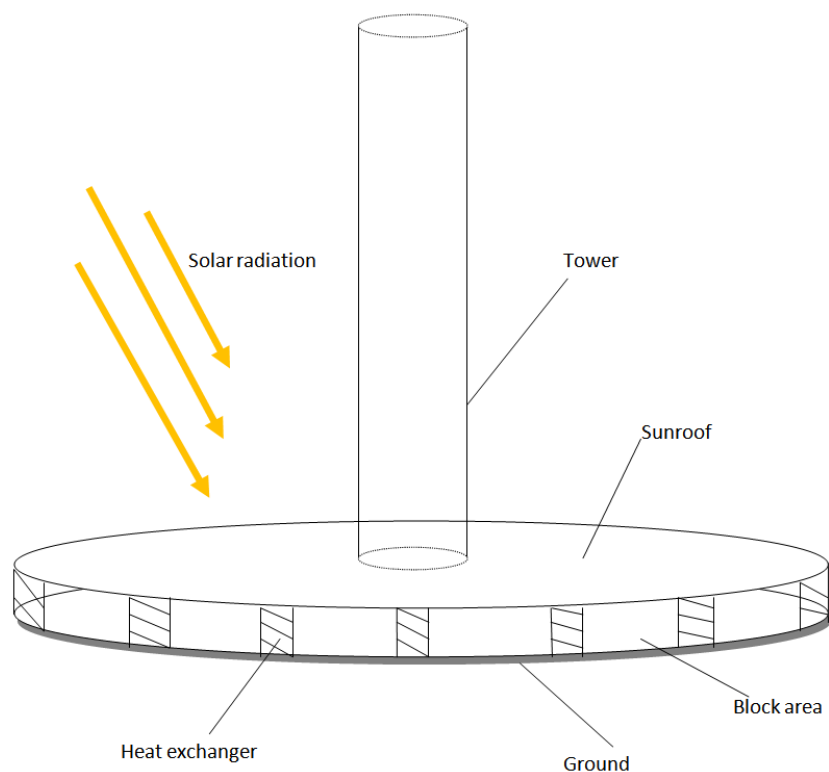
Fig.3 Configuration of solar enhanced natural draft dry cooling tower

Scaling of cooling towers

QGECE is investigating efficient heat exchangers to reduce the cost of towers. This would have been impossible unless a proper test bed is provided. In doing so, a 2m height cooling tower is built and is operational at our QGECE lab, see figure 4. The tower has a square cross-section with a base-throat area ratio of 2. Initial experiments are conducted to evaluate the tower frictional (shape) resistance, i.e. by excluding the heat exchanger resistances. At the same time, a 3D numerical model is built so that parametric study of the problem is possible [5]. Parallel to these tests and simulations a theoretical model is developed to shed some light on the scaling of such NDDCTs [6] and optimizing such systems by balancing the pressure drop and heat transfer offered by different heat exchangers and their arrangements, say flat versus A-frames. Detailed numerical and experimental investigation of this problem is currently being carried out. Furthermore, effects of wind on the tower performance is also analysed theoretically, on top of detailed numerical simulations [8], leading to an extension to the already-existing scaling law developed for no-wind performance of NDDCTs developed by QGECE [6].
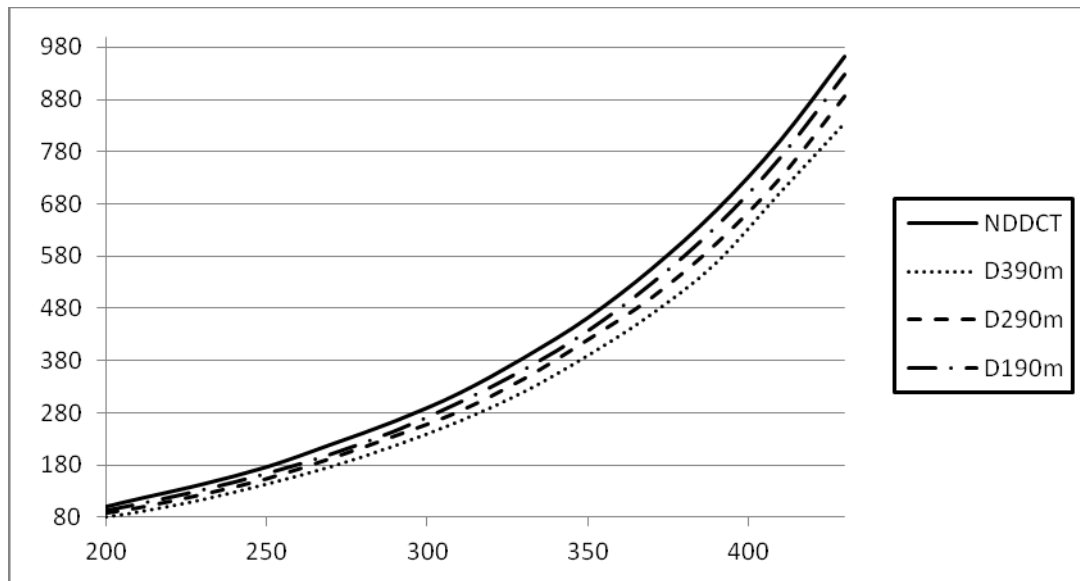
Fig.4 *Tower height comparison required for both towers*

Metal foam heat exchangers

A new design for the heat exchanger bundles in air-cooled condensers is currently being examined at QGECE. The idea is to replace the fins by a thin layer of metal foams, see figure 5, to increase the heat transfer area and, hence, reduce the total tube numbers and heat exchanger size/cost [2]. This can significantly reduce the cost as an efficient heat exchanger will lead to a less expensive (and shorter) cooling tower. A photo of our test section is presented in figure 5 where table 1 presents a comparison between a finned and a foamed NDDCT.

Table 1. A sample design of a natural draft cooling tower for a 25MW geothermal power plant

	Finned Tube	**Metal Foam**
T $_{air}$ @ inlet	20°C	20°C
Air velocity @ inlet	1.87 m/s	1.87 m/s
T $_{water}$ @ inlet	45°C	45°C
Removed heat	142 MW	142 MW
Water mass flow rate	4700 kg/s	4700 kg/s
Air mass flow rate	8050 kg/s	8050 kg/s
Bundle size	2.52 ×15 m	1.9 × 15 m
No. of tubes	16100	9739
No. of rows	4	2
No. of tube bundles	96	116
Tower height	110 m	110 m
Tower inlet diameter	70 m	63 m
Tower outlet diameter	60 m	54 m

Fig. 5 The lab scale model for a NDDCT

Hybrid cooling towers

Inspired by gas turbine power plants [9], using small amount of water to pre-cool the air before it removes the heat from the air-cooled heat exchanger; one can significantly enhance the cooling performance of NDDCTs during periods of high ambient temperatures. The water evaporation can reduce the entering air dry bulb temperature (theoretically) to that of the wet bulb. The cooler air then cools the dry system more efficiently as the approach is now increased by a good margin. QGECE is conducting research on the use of nozzle sprays and wet media to add the water droplets to the air stream. Detailed numerical and experimental analysis is currently being conducted to get a better understanding of the problem and also to be able to tailor the design to the specific needs of the power plant.

Figure 6 The low speed wind tunnel test facility; the test section

Conclusion

A summary of our current research activities on air-cooled heat exchangers at QGECE is presented. Numerical, theoretical, and experimental approaches have been undertaken to tackle the problems addressed here. Some new concepts proposed by QGECE are examined and analysed. Quantitative results will be presented in detail during the oral presentation.

References

[1] Kroger, D.G., 2004. Air-cooled heat exchangers and cooling towers Tulsa, Okl.: Pennwell Corp.

[2] Hooman, K., Gurgenci, H., 2010, Different heat exchanger options for natural draft cooling towers. World Geothermal Congress Nusa Dua, Bali, Indonesia: Paper # 2633.

[3] Bell, I.H., Eckhard, A.G., 2011, Experimental comparison of the impact of air-side particulate fouling on the thermo-hydraulic performance of microchannel and plate-fin heat exchangers, Purdue e-Pubs.

[4] Gurgenci, H., 2010. www.uq.edu.au/geothermal/latest-news-and-highlights/Hal Gurgenci's geothermal blog.

[5] Hooman, K., Gurgenci, H., 2010. Porous Medium Modeling of Air-Cooled Condensers. Transport in Porous Media. (84) 257-273.

[6] Hooman, K. 2010. Dry cooling towers as condensers for geothermal power plants. International Communications in Heat and Mass Transfer. (37) 1215-1220.

[7] Zheng, Z., Guan, Z., Gurgenci, H., Yuanshen L., 2012. Solar enhanced natural draft dry cooling tower for geothermal power applications. Solar Energy, (86) 2686–2694.

[8] Yuanshen, L., Guan, Z., Gurgenci, H., Zheng, Z. (2011). Development of small natural draft dry cooling towers for geothermal power plants. In: Zhao Shun'an and Li Wuquan, Proceedings: The 15th IAHR Cooling Tower and Air-Cooled Heat Exchanger Conference & 2011 Annual Symposium of Industrial Cooling Tower Study Committee of CSEE Thermal Power Chapter, Beijing, China, (308-316). 23 - 26 October 2011.

[9] Guan, Z., Zheng, Z., Gurgenci, H. (2012). Hybrid natural draft steel cooling tower for geothermal power plant applications. In: Reinhard Harte and Rudiger Meiswinkel, Proceedings ISCT 2012 6th International Symposium on Cooling Towers. ISCT 2012 6th International Symposium on Cooling Towers, Cologne, Germany, (607-616). 20-23 June 2012.

Evaluating the potential contribution of Geothermal Energy to the National Electricity Market

Huddlestone-Holmes, C. R.[1,2,3], and Beardsmore, G. R.[4]

[1]CSIRO Earth Sciences and Resource Engineering, [2]CSIRO Energy Transformed Flagship, [3]CSIRO Petroleum and Geothermal Research, [4]Hot Dry Rocks Pty. Ltd.

cameron.hh@csiro.au

Abstract

We have assessed the distribution of Australia's geothermal energy potential and the contribution it could make to the National Electricity Market. Understanding the potential contribution of available energy resources to future generation needs is an important tool for planning. While there have been several assessments of the size of Australia's geothermal potential, there have been few attempts to see how much of the heat could reasonably be used, and what the distribution of the heat is. We have used the global protocol for estimating and mapping global enhanced geothermal system (EGS) potential (Beardsmore et al., 2011.) as the basis for our estimation of the contribution geothermal energy can make to the National Electricity Market.

Any broad estimate of geothermal potential at continent scale will be based on a set of assumptions. These assumptions include minimum resource temperature, maximum depth, recovery factors and the conversion efficiencies of power plants. In the Australian context most of these parameters are unknown. We report on the sensitivity of the energy and power production estimates to these assumptions. This analysis also provides some insights in to the gaps we have in our understanding of Australia's geothermal potential and the interdependency between reservoir depth, temperature, flow and drilling costs required to make geothermal viable in Australia.

Introduction

In July 2012, CSIRO was contracted by Australian Energy Market Operator (AEMO) to provide information on the geothermal potential of eastern Australia and its capacity to supply electricity to the National Electricity Market, amongst a range of other technologies. This analysis was completed for Hot Sedimentary Aquifer (HSA) and Enhanced Geothermal Systems (EGS) and the results are presented in Huddlestone-Holmes and Russell (2012) with a summary in Table 1. These data are being used as input data for the AEMO 100% Renewables Study that is being completed for the Department of Climate Change and Energy Efficiency (DCCEE, 2012). CSIRO subcontracted Hot Dry Rocks Pty Ltd to assist with this project.

Table 1: A summary of the geothermal energy potential of the five states and territories covered by the NEM. The maximum installable capacities exclude areas that have land use incompatible with geothermal energy generation (e.g. national parks, built up areas, waterways, football fields). South Australia and Queensland were only partially covered by this study. Total installed generating capacity in Australia is approximately 55,000 MWe.

State	HSA Potential (EJ)	HSA maximum installable capacity (MWe)	EGS Potential (EJ)	EGS maximum installable capacity (MWe)
NSW and ACT	2,803	15,289	209,168	1,109,741
VIC	450	2,593	30,673	144,215
Total	**55,245**	**361,058**	**942,034**	**5,142,199**

Geothermal energy use for electricity generation in Australia is still undemonstrated and there is a great deal of uncertainty about how geothermal energy will be exploited, the cost of developing a geothermal resource, and what constitutes a viable resource. The assessment of the geothermal potential will necessarily be based on a large number of assumptions. In this paper we briefly discuss the assumptions and make some recommendations for further work.

Method

The first step in the process was to quantify the potential heat available for HSA and EGS. We followed the approach described in Beardsmore et al (2011) with some modification. The geology and thermal model developed by Hot Dry Rocks (2011) was used as the primary input data. The geothermal energy potential was determined as heat in place. Heat in place is a commonly used parameter to quantify geothermal potential, as it is independent of the method or rate of heat extraction. The parameters used for estimating the HSA and EGS potential are presented in Table 1. The lower maximum depth for HSA reflects the likelihood that permeability in sedimentary rocks will be too low at depths greater than 4,500 m. The density of sedimentary rocks that make up HSA resources will typically be lower than the crystalline basement rocks targeted for Hot Dry Rock/EGS resources. The maximum depth of HSA potential was further constrained by the depth to basement where the basement was less than 4,500 m deep. Similarly, EGS potential was limited to basement rocks where the temperature is estimated to be over 130°C.

Table 1: This table shows the parameters used to calculate the heat in place for HSA and EGS. The lifespan and recoverability factors are used for estimating potential electricity generation.

Parameter	HSA	EGS
Minimum Temperature	130°C	130°C
Maximum Depth	4,500 m	6,000 m
Rock Density	2,400 kg/m^3	2,550 kg/m^3
Rock Specific Heat	1,000 J/kgK	1,000 J/kgK
Base Temperature	Average ambient + 80°C	Average ambient + 80°C
Lifespan	100 years	100 years
Recoverability Factor	0.175	0.14

The heat in place (H) in Exajoules was calculated using:

$$H = \rho \times C_p \times V \times (T_x - T_b) \times 10^{-19}$$

where ρ is the density, C_p is the rock specific heat, V is the volume of rock, T_x is the rock temperature and T_b is the base temperature.

AEMO also required an estimate of the electrical power that could potentially be generated from the stored heat. This was calculated using:

$$P = H \times 10^{12} \times R \times \eta_{th} / 3.1563 \times 10^9$$

where R is the recoverability factor, η_{th} is the conversion efficiency and 3.1563 x 10^9 is the number of seconds in 100 years. The conversion efficiency is as provided by DiPippo (2007) for binary power stations:

$$\eta_{th} = 0.65 \times \frac{(T_r - T_0)}{(T_r + T_0)}$$

where T_r is the temperature of the geothermal fluid and T_0 is the average ambient temperature, both in degrees Kelvin. In this study the effect of temperature draw down in the reservoir has not been considered.

AEMO also required an estimate of generating capacity on an hourly basis to enable a comparison with other renewable generating technologies such as wave, solar and wind. The output of a geothermal power plant is affected by the ambient temperature, particularly for air-cooled power plants. To do this we used modelled ambient air temperatures (2m above ground level) and the approach outlined by DiPippo (2007) to provide an output factor as a function of geothermal fluid temperature (T_r), average ambient temperature (T_0) and hourly ambient temperature (T_{0i}):

$$P_i = \frac{(T_r - T_{0i})}{(T_r + T_{0i})} \bigg/ \frac{(T_r - T_0)}{(T_r + T_0)}$$

All temperatures are in degrees Kelvin. Ambient temperature data are derived from the NCEP Final (FNL) Operational Model Global Troposphere Analyses (Caplan et al., 1995 and NCEP 2012).

Figure 1 shows the variation in output for a nominal one megawatt, air-cooled power plant located in north east South Australia as a function of time (a proxy for air temperature).
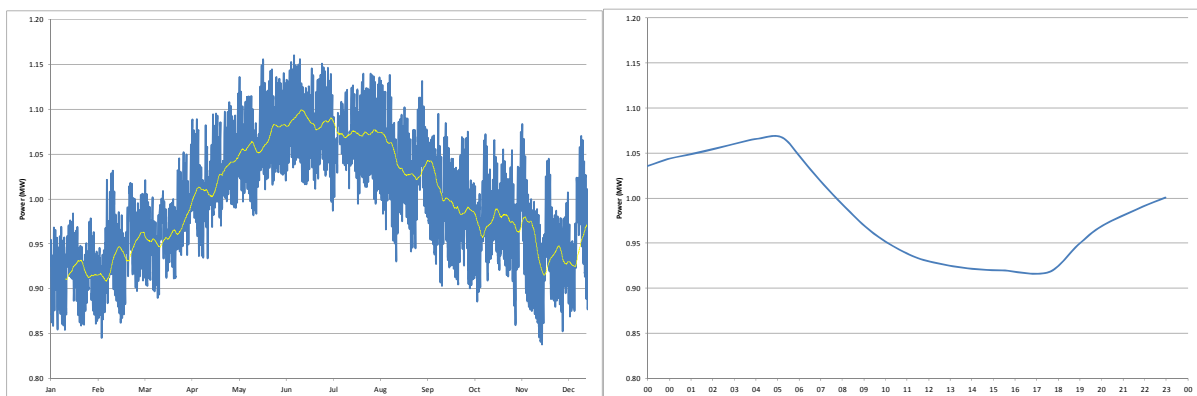
Figure 1: Power output from a nominal 1 MW power station over the 2006 calendar year (left) and over 24 hours (18 November, 2006). The annual performance has a notable increase in output over winter and decline in the summer months. The daily pattern shows a similar decline in output throughout the day and a peak output in the early hours of the morning, where temperatures are lowest.

Discussion

The analysis of the potential contribution that geothermal energy could make to the National Electricity Market described above is based on some key assumptions and constraints. A key constraint of the analysis was that we could only look at the geothermal potential as either HSA or EGS, we could not categorise them in any other way (e.g. high grade versus low grade heat, however they may be defined). These estimates are forecasts as to what resources may be accessed in 2030 and 2050. Predicting the constraints, which will be controlled by technology and costs, on resources well in to the future using technology that has yet to be demonstrated is a difficult task.

One of the constraints placed on the analysis was that the assessment of geothermal potential had to be consistent with the Australian Energy Technology Assessment (AETA, BREE, 2012). The estimates for geothermal energy costs in the AETA are significantly higher than previous estimates (see Huddlestone-Holmes and Hayward, 2011), due in part to "a better understanding of drilling costs". However, neither these drilling costs nor the parameters that would influence them (e.g. maximum depth, cost per well, number of wells per MW of generating capacity) were provided. Similarly, the O&M costs estimated for geothermal in the AETA are higher than previous estimates, contribute significantly to the high levelised cost, and are not explained. The opacity around drilling

costs in particular made the choice of parameters to define the limits of possible future geothermal resources difficult as they may or may not be entirely consistent with the assumed costs.

The key assumptions we used are discussed briefly below.

Minimum Resource temperature

The minimum temperature for a possible geothermal resource was chosen as 130°C. This temperature was chosen as the lowest likely temperature from which geothermal energy would be commercially produced by 2050. This cut off temperature depend strongly on the costs of drilling and the efficiency of the conversion of heat to electricity.

Base Temperature

The base temperature is a key assumption in these estimates and represents the temperature to which the crust can theoretically be reduced through utilization of geothermal heat (Beardsmore et al 2011). The constraint of ambient temperature plus 80°C was chosen to be consistent with Beardsmore et al (2011). The effects of temperature drawdown were not included in this assessment. This was because we considered it to be an economic rather than technical limiting factor.

Maximum Depth

The maximum depth for EGS was chosen as 6,000 m based on the assumption that drilling to these depths will be technically and economically viable by 2030. The maximum depth for HSA was chosen as 4,500 m as a depth below which compaction and diagenetic processes have typically destroyed permeability (e.g. Ajdukiewicz and Lander, 2010, Cooper and Beardsmore, 2008).

Recoverability Factor

The default recovery factors for HSA and EGS were taken as listed in the 2nd edition of the Geothermal Lexicon (Lawless, 2010), which were in turn based on values assumed by the USGS.

Lifespan

The AEMO 100% renewables study was conducted to consider fully renewable energy resources. Geothermal energy projects in Australia will most likely 'mine' heat, as the rate at which heat is extracted from a geothermal reservoir will likely be higher than the rate at which heat is replenished in the reservoir due to geological processes. This imbalance will result in the temperature decreasing over time in the part of the reservoir that is being accessed (heat energy is most rapidly removed from parts of the reservoir accessed by wells, with slow replenishment by conductive loss of heat from the surrounding rocks into the reservoir). If the total geothermal heat beneath Australia is considered, as long as not more than 10% of that heat is being accessed at any one point in time, geothermal can be effectively considered to be renewable (Massachusetts Institute of Technology, 2006). For that reason, the estimates of geothermal potential reported on here are based on a 100-year reservoir lifespan.

Conversion Efficiency

Conversion efficiency uses the trilateral limit proposed by DiPippo (2007), with an efficiency factor of 0.65. This efficiency factor is at the upper end of the range considered by DiPippo and was chosen to reflect technology advances expected by 2030-2050.

Conclusions

The assessment showed that within eastern Australia geothermal energy could support up to 100 times Australia's current generating capacity (see Huddlestone-Holmes and Russell, 2012). While using more conservative assumptions than those outlined above may reduce this capacity, it is clear that the potential contribution of geothermal energy to Australia's future energy needs is significant.

The next step is to produce more detailed analysis of costs and constraints on Australia's geothermal energy potential that would enable more realistic modelling of the possible contribution of geothermal energy. The AETA (BREE, 2012) assumes a single cost for all HSA resources and a single cost for all Hot Dry Rock/EGS resources. The reality is likely to have significantly greater variability based on resource temperatures and depths. Resources with high temperatures at shallow depths are likely to be cheaper to develop for the same amount of electricity production than deeper and/or cooler resources. The exploitation of geothermal resources is likely to start with resources with the best combination of temperature, accessibility (depth and permeability) and access to market. As the industry grows, it is also reasonable to expect that costs will fall and that less favourable resources will become commercially attractive.

Acknowledgements

References

Ajdukiewicz, J. M., and Lander, R. H. 2010. Sandstone reservoir quality prediction: The state of the art. AAPG Bulletin, 94(8), 1083–1091. doi:10.1306/intro060110

Beardsmore, G.R., Rybach, L., Blackwell, D. and Baron, C. 2011. A protocol forestimating and mapping global EGS potential. Version 1.1. Unpublished, May 2011.

BREE - Bureau of Resources and Energy Economics (2012). Australian Energy Technology Assessment 2012.

Caplan, P., Derber, J., Gemmill, W., Hong, S.-Y., Pan, H.-L. and Parrish, D. 1999. Changes to the 1995 NCEP operational medium-range forecast model analysis-forecast system. Weather Forecast., 12(3), 581–594.

Cooper, G. T., and Beardsmore, G. R. 2008. Geothermal systems assessment : understanding risks in geothermal exploration in Australia. PESA Eastern Australasian Basins Symposium III (pp. 411–420). Sydney.

DCCEE. 2012. http://www.climatechange.gov.au/government/initiatives/aemo-100-per-cent-renewables/aemo-scoping-document.aspx. Accessed 15 Ocober 2012.

DiPippo, R. (2007). Ideal thermal efficiency for geothermal binary plants. Geothermics, 36, 276–285.

Hot Dry Rocks (2011). Summary of Process and Data Sources Used in the Development of the EGS Potential Maps and Tables of Australia. Unpublished report prepared for Google.org. 20pp.

Huddlestone-Holmes, C.R. and Russell, C. 2012. AEMO 100% Renewable Energy Study: Geothermal Energy. CSIRO, Newcastle, Australia.

Huddlestone-Holmes, C.R. and Hayward, J. (2011). The potential of geothermal energy. CSIRO report for the prepared as input to the Garnaut Review Update. Available at http://www.csiro.au/en/Outcomes/Energy/Renewables-and-Smart-Systems/Garnaut2011-geothermal-energy.aspx

Lawless, J.V. 2010. Geothermal Lexicon for Resources and Reserves Definition and Reporting, 2nd Edition. Geothermal Code Committee, Australian Geothermal Energy Group. Downloaded from http://www.agea.org.au/geothermal-energy/fact-sheets-resources/.

Numerical simulation as a tool for understanding geothermal resources

Kirkby, A.L. [1], Meixner, A.J. [1], Lescinsky, D.T. [1], and Budd, A.R. [1]

[1] Geoscience Australia, GPO Box 378, Canberra ACT 2601

Alison.Kirkby@ga.gov.au

Introduction

In recent years Geoscience Australia (GA) has used 3D thermal modelling techniques to prepare regional scale geothermal assessments in several regions of Australia. These 3D thermal models have incorporated direct temperature measurements, heat flow determinations, thermal conductivity measurements and heat production estimates based on the national geochemical database (OZCHEM). They have also incorporated other geoscience datasets such as outcrop geology, drill hole, seismic, gravity and magnetic data. On a smaller scale, GA, together with the Council of Scientific and Industrial Research - National Geophysical Research Institute (CSIR - NGRI) of India, is developing a 2D coupled fluid and heat flow model of the Tattapani hot spring region, located in Chhattisgarh State, India. This model incorporates available geological, geophysical, water chemistry and temperature data, together with thermal conductivity and heat production measurements.

The techniques used to perform GA's regional geothermal assessments have evolved over time. The initial assessment of North Queensland (Ayling and Lewis, 2010) was based on a 2D GIS approach. Subsequent assessments of the east-central South Australia (Meixner et al., 2011) and the southern Northern Territory (Meixner et al., 2012a) were based on thermal modelling from 3D geological maps constructed over the assessment regions. The thermal modelling for the latter two assessments used the Geomodeller software (Gibson et al., 2008) to predict the 3D temperature distribution as well as the vertical heat flow at the surface. The resulting assessments were quantitative, however, due to computational restrictions, uncertainty in the temperature and heat flow modelling was assessed only qualitatively. More recently a 3D geological map has been produced in the Cooper Basin region of South Australia and Queensland (Meixner et al., 2012b). This 3D map builds on an earlier 3D map (Meixner and Holgate, 2009) by encompassing a larger area as well as incorporating more detailed stratigraphy and updated gravity inversions. Thermal modelling on this 3D map, which included uncertainty estimations of the predicted temperatures based on thermal property uncertainty, was conducted using the Simulator for HEat and MAss Transport (SHEMAT) software package (Clauser, 2003).

This paper focuses on the thermal modelling conducted in the Cooper Basin and Tattapani hot spring regions in order to highlight the latest work being done by Geoscience Australia to improve our understanding of the temperature and fluid flow fields in areas away from direct measurements.

Cooper Basin

The Cooper Basin region (Figure 1) is coincident with a prominent geothermal anomaly (Cull and Denham, 1979; Cull and Conley, 1983; Somerville et al., 1994) and forms part of a broad area of anomalously high heat flow (Sass and Lachenbruch, 1979). High-heat-producing granites, including granodiorite of the Big Lake Suite (BLS) at the base of the Cooper and Eromanga basin sequences, combined with thick Cooper and Eromanga sedimentary sequences of low thermal conductivity, result in temperatures as high as 270 °C at depths of 4.5 – 5 km (Holgate, 2005). The location and characteristics of other granitic bodies are poorly understood and accurately identifying them is an important first step towards future geothermal exploration in this region.
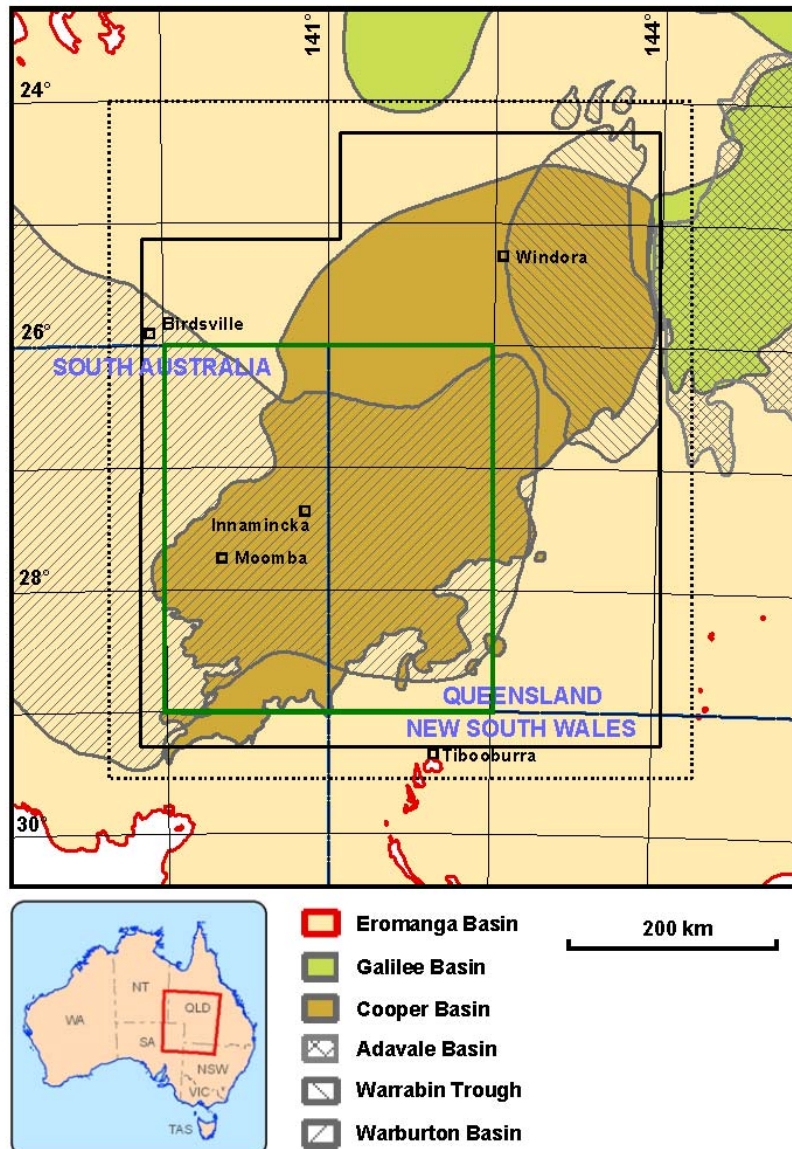
Figure 1: Location of the Cooper Basin region, showing the spatial extents of the stacked Warburton, Cooper and Eromanga basins. The outer black solid line indicates the extents of the Version 2 Cooper Basin 3D Map (Meixner et al, 2012b), while the dashed black line shows the buffered extents used for the gravity inversions. The solid green box shows the extents of the Version 1 Cooper Basin 3D map (Meixner and Holgate, 2009).

A regional 3D geological map of the Cooper Basin region has been produced from 3D inversions of Bouguer gravity data, using geological data to constrain the inversions (Meixner et al., 2012b). The map covers the entire Cooper Basin area and extends to 13 km depth. The map was attributed with boundary conditions consisting of a constant temperature at the surface, constant heat flow into the base of the model, was well as an estimate of the thermal conductivity and heat production for each cell in the model. These values were assigned based on a combination of direct measurements, estimates from lithological descriptions and geochemical data, and published values for some formations.

Forward predictions of temperatures were carried out using SHEMAT (Clauser, 2003) on the National Computing Infrastructure supercomputing facility at the Australian National University (NCI). Use of

this software on the NCI has resulted in considerable improvements in computational efficiency over the Geomodeller software, and has allowed multiple runs to be performed simultaneously to help refine the input properties. The initial thermal model produced temperature predictions that were too low compared with the available down-hole temperature measurements. It was necessary to substantially increase the heat production of the basement and granite units as well as the basal heat flow in order to match the measured temperature and heat flow data. In the final model, the basement was split up into three blocks with different heat production values. Final values for basement heat production range from 3.8 - 5.3 µW/m^3, while final values for granite range from 3.8 – 8.7 µW/m^3. The final value for basal heat flow was 48 mW/m^2. It was also necessary to reduce the thermal conductivity of the basin sediments in order to match the temperature data.

The final, optimised thermal model (Figure 2a) shows strongly elevated temperatures (up to 235 °C) at 4 km depth in the vicinity of the BLS (central-southern Cooper Basin), as well as broader regions of elevated temperature (190 – 200 °C) in the northwest of the study area toward Mt Isa, beneath the Warrabin Trough in the northeast of the study area, and southeast of the BLS. Cooler temperatures (~160 °C) were predicted at 4 km depth in the southwestern corner of the study area.
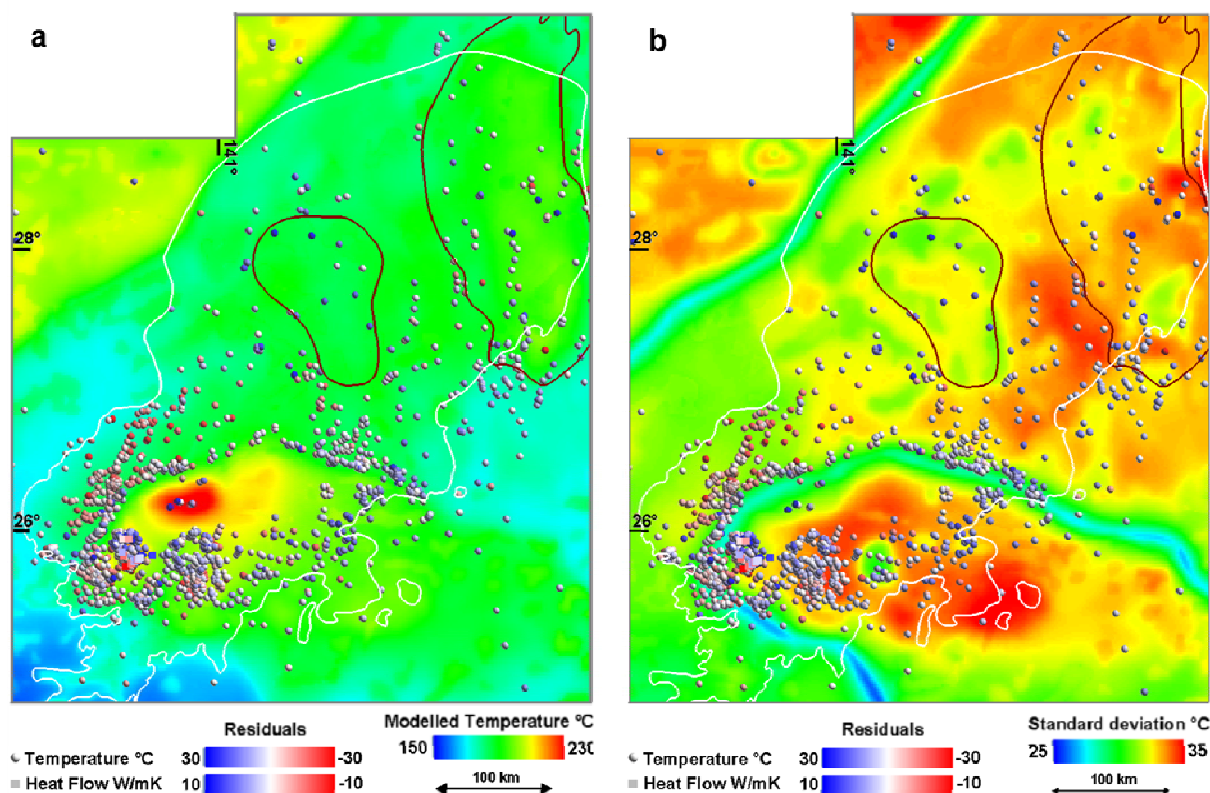
Figure 2: (a) Predicted temperature at 4 km depth, and (b) standard deviation on the temperature predictions resulting from uncertainty in the input parameters. In both figures, coloured symbols show the calculated residuals (measured minus modelled) at the measurement locations; temperature residuals are represented as circles and surface heat flow residuals as squares. Outline of the Cooper Basin shown in white; outline of the Warrabin Trough and the Barrolka Gravity Low are shown in maroon.

Stochastic modelling was carried out on the final thermal model in order to characterise the uncertainty of the predicted temperatures and heat flow values due to the uncertainty in the input thermal properties. The thermal property uncertainty values were defined by specifying a mean value and a standard deviation based on a normalised property distribution. Statistical analysis of the multiple computed thermal models resulted in a mean value and standard deviation of the temperature

and vertical heat flow at each point in the model (Figure 2b). The stochastic modelling technique was implemented using SHEMAT, combined with the Python scripting library PySHEMAT (Wellmann et al., 2012), and other scripting libraries developed internally. The stochastic runs were performed using the NCI. The resulting uncertainty map shows that the highest absolute uncertainty values (~35 °C) occur in the southern Cooper Basin, in and around the Warrabin Trough, and in the northwest corner of the study area. These high temperature uncertainties were the combined result of relatively large heat production uncertainties assigned to the basement units and the high thermal conductivity uncertainty estimates applied to the thick sequences of Cooper and Eromanga basin sediments.

Tattapani

The Tattapani hot spring area is located in north-eastern Chhattisgarh State, India. The hot springs are located near the intersection of the mapped east-northeast trending Tattapani Fault and a northeast trending cross fault (Figure 3). The Tattapani Fault forms part of a larger east-northeast trending tectonic zone, the Son-Narmada-Tapti lineament which extends approximately 500 km across central India (Shanker et al., 1987). The Tattapani Fault dips at approximately 78° to the north-northwest and truncates the southern extent of Permo-Carboniferous rocks of the Gondwana Supergroup against Proterozoic crystalline basement rocks (Thussu et al., 1987). The fault is defined by a well-developed, 20 m thick, fault gouge which has been mapped across the hot spring area.
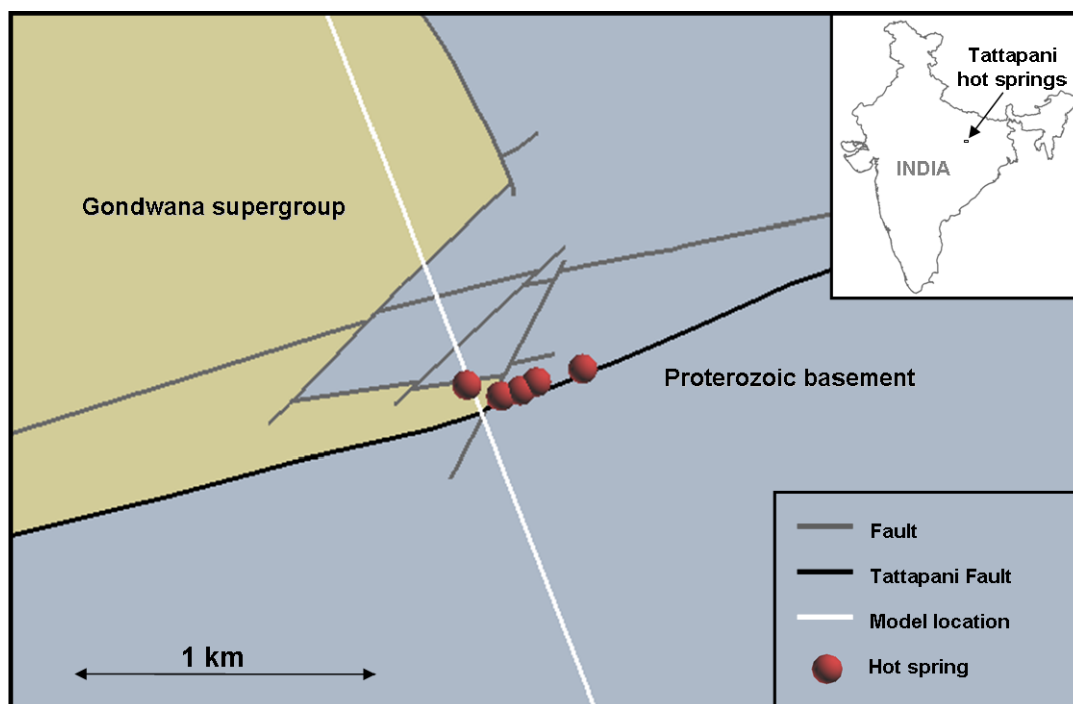
Figure 3: *Location map showing the Tattapani hot springs, Tattapani Fault, and other faults in the Tattapani area. The central part of the model profile is shown in white. Modified after Shanker et al. (1987).*

The Tattapani hot springs discharge water at 50 – 98 °C (Thussu et al., 1987), with water chemistry data indicating that the waters are primarily meteoric in origin. Given that the ground surface elevation increases from north to south in the Tattapani area, it can be expected that the source for the fluids would be located to the south of the hot spring area. Shallow drilling and temperature logging has shown that in the hot springs area temperatures of ~100 – 110 °C occur at approximately 80 m depth (Thussu et al., 1987; GSI, 1991). These temperatures remain fairly constant down to the maximum logged depth of ~500 m. The nearest conductive heat flow measurement is located ~100 km away from the anomalous zone and has a value of 107 mW/m^2 (Rao and Rao, 1983). However, the

geological setting in which this heat flow value is located is different to that of the Tattapani hot spring area and so this measurement may not be representative of the Tattapani hot spring area.

A number of geophysical surveys have been carried out in the Tattapani area. These include historical gravity and electrical geophysical methods (Joga Rao et al., 1987). The gravity survey revealed a ~2 mGal gravity anomaly over the Gondwana Supergroup, consistent with a sediment depth of ~200 m (Joga Rao et al., 1987). Gradient array resistivity surveys and Audio-Magnetotelluric (AMT) surveys revealed a conductivity anomaly close to the Tattapani Fault (Joga Rao et al., 1987). More recently, deep magnetotelluric data were collected (Veeraswamy and Harinaryana, 2006). These delineate a strong electrical conductivity anomaly directly beneath the fault extending to depths of up to 10 km. These electrical anomalies are interpreted to be the results of fluid filled fractures.

A 2D coupled fluid and heat flow model has been generated for the Tattapani region (Figure 4a). The model extends to 16 km depth and is 40 km in horizontal extent. The large horizontal and vertical extent was required in order to avoid edge effects in the model. The model incorporates the Gondwana Supergroup, approximated as a 200 m thick layer of sediments. The model also incorporates Proterozoic basement that has been divided into five blocks. The first two blocks form the northern and southern walls of the Tattapani Fault and extend to 4 km depth. The second two blocks extend from 4 to 8 km depth. The fifth block encompasses basement rocks at depths > 8 km. The model also includes the Tattapani Fault as a separate element. The Gondwana Supergroup was assigned a thermal conductivity of 1.8 W/mK and a heat production of 1.3 $\mu W/m^3$. These values are taken from estimates for these parameters for sediments of the Permo-Carboniferous Arckaringa Basin, South Australia (Meixner et al., 2012a), a similar age to the Gondwana Supergroup. The two shallow basement blocks and the fault were assigned a thermal conductivity of 3.1 W/mK and a heat production of 6.0 $\mu W/m^3$ based on measured values (Sukanta Roy, Pers. Comm.; GA unpublished data). The second two blocks (4 – 8 km depth) were assigned slightly lower heat production values of 3.0 $\mu W/m^3$. The deeper basement block was assigned a thermal conductivity of 3.1 W/mK and a heat production of 1.5 $\mu W/m^3$. As there are no measured values for porosity and permeability, these parameters were estimated. Initial values of 1% (porosity) and 10^{-17} m^2 (permeability) for basement shallower than 8 km, 1% and 10^{-18} m^2 for basement deeper than 8 km, and 20% and 10^{-14} m^2 for both the Tattapani Fault and the Gondwana Supergroup, were assigned based on suggested ranges from Clauser (2003) for crystalline, fractured, and sedimentary rocks.

The boundary conditions were assigned as follows. The top of the model was assigned a constant temperature of 25 °C, and a constant hydraulic head. The top of the model was set to a constant elevation, however in order to simulate the effects of variable elevation on hydraulic head, hydraulic head values in the top layer of cells in the model were set as a function of the ground surface elevation. These elevation values were obtained from the global ETOPO1 dataset (NOAA, 2012). The base of the model was assigned a constant heat flow of 59 mW/m^2. This value was obtained by subtracting the heat flow contribution of the basement rocks (48 mW/m^2) from the nearest measured heat flow value (107 mW/m^2). The base of the model was assigned an impermeable boundary to simulate the meteoric origin for the fluids. The sides of the model were set as no-flow boundaries for both heat and fluids.

A preliminary result is presented in Figure 4. The temperature, conductive heat flow and flow velocity was calculated using the SHEMAT software. The total vertical heat flow was calculated by summing the conductive and advective heat flow components. It was necessary to increase the permeability of the basement blocks south of the Tattapani Fault to 10^{-16} m^2 in order to allow fluid to penetrate through the basement down to the depth of the base of the fault. With lower permeability values, fluid circulation did not occur, and no flow was observed up the fault. It was also necessary to increase the basal heat flow to 67 mW/m^2. The modelling has shown that it is possible to obtain localised strongly elevated temperatures without the requirement for a localised heat source. The model predicts temperatures at 500 m depth that are about 20 °C lower than the measured values. The heat flow, however, away from the disturbed region in the model is predicted to be 6 mW/m^2 higher than the nearest measured value, suggesting that a localised source of heat may be required to match the data.
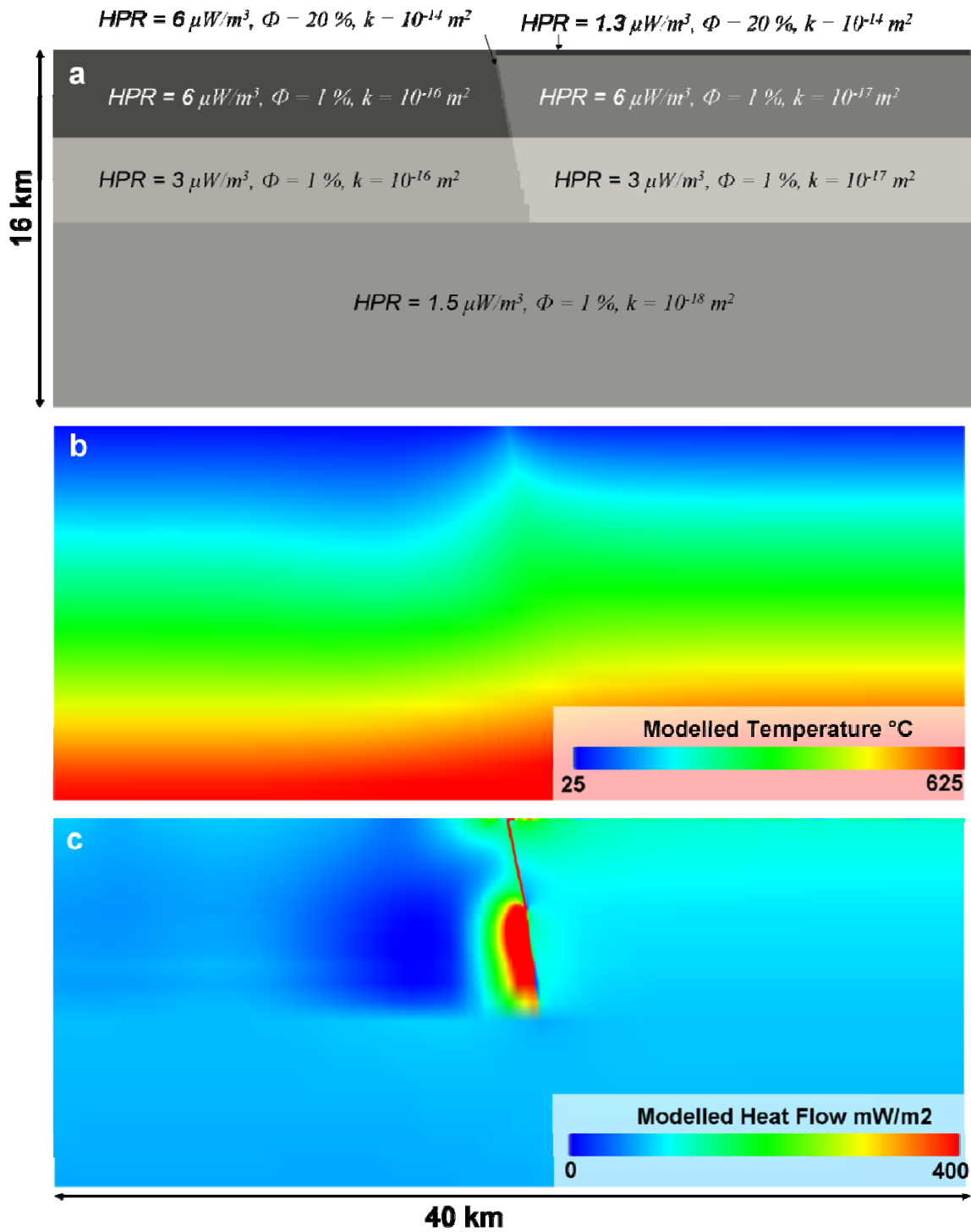
**Figure 4:** *A preliminary 2D model of the Tattapani hot spring region, Chhattisgarh, India. (a) the model, showing the five basement blocks and physical properties referred to in the text, (b) modelled temperature showing temperatures ranging from 25 to 590 °C which are elevated at shallow depths beneath the fault, (c) modelled heat flow showing that the heat flow is considerably elevated within and around the Tattapani Fault.*

Conclusions

Numerical simulation of the temperature field in the crust can be used on a variety of scales to improve our understanding of a resource and to guide future data collection. GA is applying numerical simulation techniques to areas both within Australia and internationally to improve the understanding of both the character and distribution of geothermal resources.

The thermal modelling and subsequent stochastic modelling conducted in the Cooper Basin region has not only improved our understanding of the geothermal resource and its uncertainty in this region, but also increases our understanding of the thermal properties such as the basal heat flow, basement heat production and thermal conductivity of the sediments. The initial thermal model based on measured and estimated values of basal heat flow, basement heat production and sediment thermal conductivities was too 'cool' resulting in large mismatch between the measured and the modelled temperature and heat flows. The optimised model, which produced the best match with measured data, required an increase in basal heat flow, basement heat production and a decrease in sediment thermal conductivities. The production of a thermal model which matches the measured data increases our confidence in locating areas that have high geothermal potential in the absence temperature or heat flow data. The production of a thermal model where there is temperature data as well as a comprehensive understanding of the basin shape and stratigraphy has allowed us to develop methods that can then be applied to produce assessments in regions with less prior geological and thermal knowledge.

A 2D model of the Tattapani hot spring area has been developed, providing a better understanding of the fluid and heat sources in the region. The model has shown that it is possible to obtain elevated temperatures at shallow depths without the requirement for a localised heat source. However, to reproduce temperatures as high as those that have been observed in boreholes, a localised heat source may be required. The model has highlighted priority areas for future data collection. In particular, the model could be better constrained by additional heat flow data in the area, and better constraint on flow parameters, in particular, the permeability structure of the basement and in particular, the Tattapani Fault. Further modelling will be performed to improve the match between the model and the measured data and provide a range of viable models. This will allow an improved understanding of the temperature and fluid flow fields at depth, and will allow various hypotheses regarding fluid and heat sources to be tested.

Acknowledgements

References

Ayling, B.F., and Lewis, B., 2010. Geothermal Systems, in: Huston, D.L. (ed). An assessment of the uranium and geothermal potential of north Queensland. Record 2010/14. Geoscience Australia: Canberra.

Clauser, C. (ed.), 2003. Numerical Simulation of Reactive Flow in Hot Aquifers: SHEMAT and Processing SHEMAT. Springer-Verlag: Berlin Heidelberg, 332pp.

Cull, J.P. and Denham, D., 1979. Regional variations in Australian heat flow. Bureau of Mineral Resources, Journal of Australian Geology and Geophysics, 4: 1-13.

Cull, J.P. and Conley, D., 1983. Geothermal gradients and heat flow in Australian sedimentary basins. Bureau of Mineral Resources, Journal of Australian Geology and Geophysics, 8: 329-337.

Gibson, H., Stüwe, K., Seikel, R., FitzGerald, D., Calcagno, P., Argast, S., McInerney, P., and Budd, A., 2008. Forward prediction of spatial temperature variation from 3D geology models. Eastern Australian Basins Symposium III. Sydney 14-17 September 2008.

Geological Survey of India, 1991. Geothermal Atlas of India. Geological Survey of India, Special Publication 19, 144 pp.

Holgate, F., 2005. Exploration and Evaluation of the Australian Geothermal Resource. PhD thesis, Australian National University.

Joga Rao, M.V., Rao, A.P., Midha, R.K., Padmanabhan, K., and Kesavamani, M., 1987. Results of geophysical surveys in the Tattapani hot spring area, Surguja District, Madhya Pradesh. Geological Survey of India Record, Vol 115, Pt. 6, pp 66-83.

Meixner, A.J., Gerner, E., Weber, R., Brennan, T., Lewis, B., and Gallagher, R., 2012a. Geothermal Systems, in: Schofield (ed). An assessment of the uranium and geothermal prospectivity of the southern Northern Territory. Record 2012/51. Geoscience Australia: Canberra.

Meixner, A.J., Kirkby, A.L., Lescinsky, D.T., and Horspool, N., 2012b. The Cooper Basin 3D Map Version 2: Thermal modelling and temperature uncertainty. Record 2012/60. Geoscience Australia: Canberra.

Meixner, A.J., Kirkby, A., Champion, D.C., Weber, R., Connolly, D., and Gerner, E., 2011. Geothermal Systems, in: Huston, D. L. and van der Wielan, S. E. (eds). An assessment of the uranium and geothermal prospectivity of east-central South Australia. Record 2011/34. Geoscience Australia: Canberra.

Meixner, A.J., Holgate, F.L 2009, The Cooper Basin Region 3D Map Version 1: A Search For Hot Buried Granites. Record 2009/15. Geoscience Australia: Canberra.

National Oceanic and Atmospheric Administration (NOAA), 2012. Online dataset, National Geophysical Data Center. Downloaded from http://www.ngdc.noaa.gov/mgg/gdas/gd_designagrid.html, August 2012.

Rao, G.V., and Rao, R.U.M., 1983. Heat flow in the Indian Gondwana basins and heat production of their basement rocks, Tectonophysics, Vol. 91, pp 105-117.

Sass, J.H. and Lachenbruch, A.H., 1979. Thermal regime of the Australian Continental Crust, in: M. W. McElhinny (ed.) The Earth: its origin, structure and evolution. Academic Press: London, pp 301-351.

Shanker, Ravi; Thussu, J.L., Prasad, J.M., 1987. Geothermal studies at Tattapani hot spring area, Surguja district, central India. Geothermics, Vol. 16, No. 1, pp 61-76.

Somerville, M., Wyborn, D., Chopra, P., Rahman, S., Estrella, D. and van der Meulen, T., 1994. Hot dry rock feasibility study. Report 94/243. Energy Research and Development Corporation. 133pp.

Thussu, J.L., Prasad, J.M., Saxena, R.K., Prakash, Gyan, and Muthuraman, K. 1987. Geothermal energy resource potential of Tattapani hot spring belt, District Surguja, Madhya Pradesh. Geological Survey of India Record, Vol. 115, Pt. 6, pp 30-55.

Veeraswamy and Harinarayana, 2006. Electrical signatures due to thermal anomalies along mobile belts reactivated by the trail and outburst of mantle plume: Evidences from the Indian subcontinent. Journal of Applied Geophysics, Vol. 58, pp 313 – 320.

Wellmann, J.F., Croucher, A. and Regenauer-Lieb, K., 2012. Python scripting libraries for subsurface fluid and heat flow simulations with TOUGH2 and SHEMAT. Computers and Geosciences, Vol. 43, pp 197-206.

Geology and Geochemistry of Hydrothermal System of West Toba (Indonesia): A Preliminary Study

Kusumasari, B.A.[1], Situmorang, J.[2], Mussofan, W., Herdianita, N.R.[2,3,4]

[1]Economic Geology Laboratory, Department of Earth Resource Engineering, Graduate School of Engineering, Kyushu University, [2]Master Study Program of Geothermal Engineering, Faculty of Mining and Petroleum Technology, Institute of Technology Bandung (ITB), [3]Study Program of Geological Engineering, Faculty of Earth Sciences and Technology, ITB, [4]Applied Geology Research Group, Faculty of Earth Sciences and Technology, ITB.

brenda@mine.kyushu-u.ac.jp, herdianita@gc.itb.ac.id

Project Description

The aim object of this research is to understand the geological condition, history of formation and estimate geothermal potency in Lake Toba. Simbolon and Samosir area, on the western part of Lake Toba, become the main interest for this research. Preliminary study shows that hydrothermal system of West Toba area has 2 systems, namely the geothermal area of Pusuk Bukit and Simbolon-Samosir. These hydrothermal systems are separated within 10 km and lie about 200 km of Medan or 80 km or Tarutung. Both Pusuk Bukit and Simbolon-Samosir are the hydrothermal systems associated with volcano tectonic depression of Toba caldera. The lithologies are dominated by volcanic products of pyroclastic, lava and intrusion, also sedimentary rocks. Indeed, the heat source of Pusuk Bukit and Simbolon-Samosir are associated with young volcanic system beneath Toba. The geothermal system of Pusuk Bukit has surface manifestations of steaming ground with altered ground and steam vents, and hot springs having temperature of 80-90°C and acid pH. Due south, the geothermal prospect of Simbolon-Samosir discharges warm seepage, 42-74°C warm and hot spring and small area of steaming ground.

Location

Lake Toba is located administratively in North Sumatra Province, Indonesia. It is geographically located on 02°20'00"-02°55'00" North Latitude and 98°30'00"-99°15'00" East Longitude. It can be accessed by 4-hours land route from Medan (the capital city of North Sumatra Province) to Parapat (the nearest city from Lake Toba). Lake Toba is known as the largest volcanic lake on earth formed by an explosive eruption about 74,000 years ago. On the surrounding area of Lake Toba, geothermal manifestations are largely found. These manifestations are usually accompanied by alteration. The most extensive manifestations are located on Pusuk Bukit and Simbolon-Samosir area on the western part of the lake.
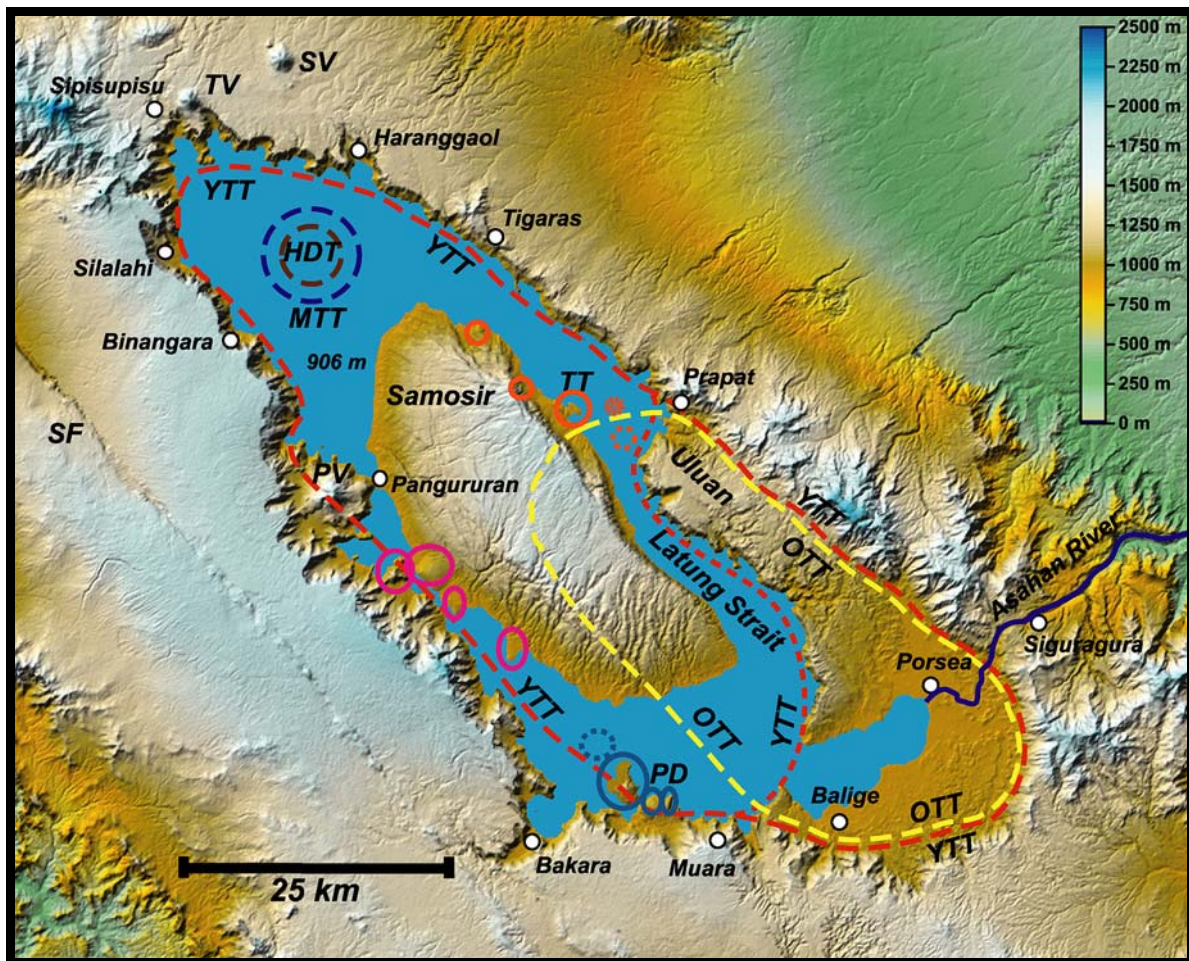
Figure 1: Distribution of pre-caldera volcanic rocks and caldera-fill rocks. Calderas are indicated by dashed line where brown line=HDT, yellow line=OTT, dark blue line=MTT, red line=YTT (Chesner, 2011).

Geology

Lake Toba is a part of Toba Caldera Complex. Toba Caldera is one of the biggest volcanic caldera formed in Quaternary period. The size of the caldera is 100 x 30 km which was formed by a single eruption event 74,000 years ago. This eruption emitted approximately 2,800 km^3 magma and became cataclysmic event during Quaternary period. The effect of this eruption was felt almost on the entire part of South East Asia as temperature changes and environmental damages. Based on Chesner on 2011, the history of Toba Caldera formation and evolution was started at 1.3 Ma when the oldest volcanic rock unit formed before the caldera-forming eruption (Fig.1). The rock units in Toba Caldera Complex are explained as follows:

- Pre-Caldera Andecite
  This is the oldest volcanic rock dated 1.3 Ma based on K-Ar dating (Yokoyama and Hehanussa, 1981 in Chesner, 2011). The rocks are pyroxene andesites and basaltic andesites. The outcrops can be found mostly on the northern part of Lake Toba. This rock unit is represented a large stratovolcano on the northern part of present caldera.

- Haranggaol Dacite Tuff (HDT)
  This rock unit is densely welded dacitic tuff and represents the beginning of caldera-forming eruption. Dating by fission track method gave 1.2 Ma of age and interpreted as crater-lake type caldera eruption from the pre-caldera stratovolcano from which Pre-Caldera Andecite was erupted.

- Oldest Toba Tuff (OTT)
  Oldest Toba Tuff is the first three quartz-bearing Toba tuffs which has 840 ka in age by ^{40}Ar/^{39}Ar dating method. The outcrops can be found on the southern part of Lake Toba with densely welded rhyolite tuff in lithology. Based on the distribution of outcrops, the source of its eruption is estimated in the southern part of present Toba Caldera.

- Middle Toba Tuff (MTT)
  Distribution of Middle Toba Tuff outcrops on the northern part Lake Toba indicated that it has same eruption source with Haranggaol Dacite Tuff. By ^{40}Ar/^{39}Ar dating method, the age of this rock unit is 501 ka. The lithology of this rock unit is rhyolitic tuff.

- Youngest Toba Tuff (YTT)
  Youngest Toba Tuff is the latest quartz-bearing tuff with 74 ka in age. The source of the eruption is approximately a linear vent system in southeastern part beneath Latung Strait. This eruption was the biggest which finally formed the present Toba Caldera. The eruption ejected about 2,800 m^3 magma during the eruption and produced rhyolitic to rhyodacitic rocks. It covered all previous calderas and most of the stratovolcano on the north.

After the activity of Youngest Toba Tuff eruption, several activities have been taken place in Toba caldera. The activities are as follows:

- Lake filling

- Lacustrine sedimentation

- Resurgence

- Formation of several lava domes, i.e. Samosir, Pusuk Bukit etc

Geothermal surface manifestation

Surface geothermal manifestations located on Pusuk Bukit and Simbolon-Samosir area have similar types, i.e. steaming grounds, steam vents, hot springs and altered grounds. Alteration type in these areas is argilic with silica residue deposits on the surface of active steaming grounds. The host rocks are pyroclastic breccias, tuff and lapilli. The total area of the alteration is about 5 km^2 on Pusuk Bukit. The alteration is located on the northeastern part. On Simbolon-Samosir area, the total alteration area is 7 km^2 located on Rianiate. Not only steaming grounds are found but also steam vents with 80-90°C temperature and sulphur deposits near the vents. Hot springs in Pusuk Bukit are fond with boiling condition (80-90°C) and acidic pH. On Simbolon area, the hot springs have neutral pH and located on higher elevation.

References

Chesner, C. A., 2011. *The Toba Caldera Complex*, Quaternary International (2011), doi:10.1016/j.quaint.2011.09.025.

3D Numerical Modelling of Chingshui Geothermal Reservoir in Taiwan

Lee, B. H.[1], Guo, T. R.[1], Lee, C. R.[1], Liu, C. H.[1], Ouyang, S.[1], O'Sullivan, M. J.[2], Yeh, A.[2]

[1]Industrial Technology Research Institute, Taiwan, R.O.C., [2] The University of Auckland, New Zealand

bohenglee@itri.org.tw

Introduction

In Taiwan, the first geothermal power plant of 3MWe capacity was built in Chingshui geothermal field in 1981. This power plant was decommissioned in 1992 due to continued decline in production. Although some geothermal exploration and field production had been exercised in the past, the production potential of Chingshui geothermal reservoir is still not well understood (Lee, 1994; Fan et al., 2005; Tong et al., 2008;). The situation actually creates problems in the design of new production wells, particularly in terms of determining appropriate well locations and wellbore traces. The purpose of this study is aimed to simulate the natural state and production performance based on a conceptual model of Chingshui geothermal reservoir. Moreover, the computer simulation was undertaken for assessing and predicting the reservoir response to planned development.

Chingshui geothermal conceptual model

Based on the geophysical data with knowledge of the geology in the Chingshui geothermal area (Fan et al., 2005; Tong et al., 2008), this study arranges a 3D view of the fault systems in the vicinity of Chingshui as shown in Figure 1. The geothermal reservoir, with a NW-SE trend and about 1.5 km in length, might be associated with the fracture zone of the Chingshuihsi fault and is bounded by the G fault and the Xiaonanao fault in the north and south, respectively.

There are twenty one wells were drilled in Chingshui geothermal area. Nineteen deep production wells were drilled by the CPC and ITRI in the past, and two additional 500m and 1100m boreholes was drilled in 2006 and 2011 by the ITRI. Only eleven wells were drilled in fracture zone (IC-4, 5, 9, 12, 13, 14, 16, 18, 19, 20, and 21), and these wells can be verified data for simulation. The other wells were drilled out of fracture zone. In addition, Chingshui geothermal conceptual model has been verified by fifteen wells logging data and cuttings within the verified area (Figure 1). The well logs collected from fifteen boreholes thermal reservoir in detail. Wells IC-1 and 17 located at western of Chingshuihsi fault, and IC-18 located away from Chingshuihsi fault. These three wells have high temperature, but insufficient quantity of hot water and no obvious feed zones; this implies that these three wells do not penetrate the feed zone in the geothermal reservoir. Thus, the geothermal reservoir is clustered with feed zones, which are confined in an area 260 m in width, $N21^{o}W$, and dip 80° to the NE. This is in agreement with the results of MT and gravity interpretation (Tong et al., 2008).
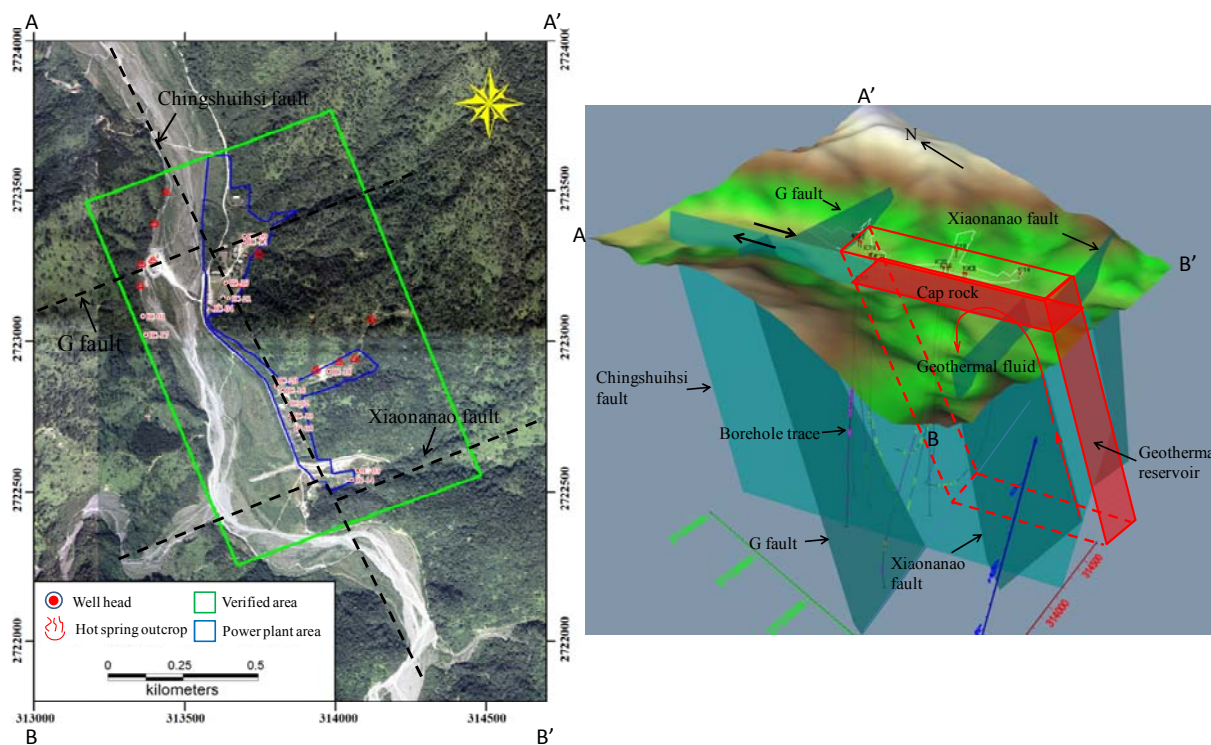
Figure 1: The geothermal conceptual model of the Chingshui area. The geothermal reservoir might be associated with the fracture zone of the Chingshuihsi fault, and it is bounded by the G fault and the Xiaonanao fault in the north and south, respectively.

Numerical modelling

A numerical model of the Chingshui geothermal reservoir was developed and implemented by AUTOUGH2 computer code with EW module (O'Sullivan, 2008). The model covers a total area of 6.9 km^2 with E-W direction 2,284m and S-N direction 3,016m (Figure 2), and extends vertically from elevation of -2,400m a.s.l to 400m a.s.l. The model has 14,280 grid blocks in l4 horizontal layers. The boundary conditions and distributions of permeability was obtained by trial and error matching of the initial temperature based on conceptual model. Other hydraulic and thermal properties were obtained from exploration drilling and well testing (Table 1).
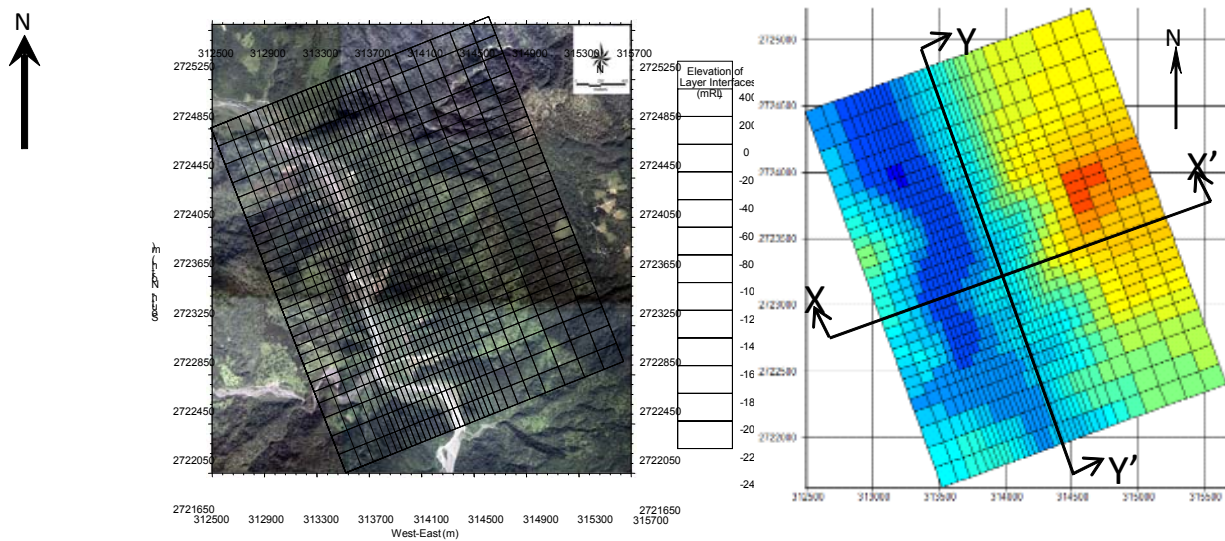
Figure 2: *Coverage area of Chingshui geothermal model*

Table 1: The input parameters of Chingshui geothermal reservoir model

Rock type	Porosity	Permeability k_{xyz} (m^2)	Grid blocks and layers	Thermal properties	Boundary condition
LOW	0.01	0.5^{-15}	X=34 block (2284m) Y=30 block (3016m) Z=14 layer (mRL-2400)	Heat source: 0.18 W/m2 Rock thermal conductivity: 3.0 W/m2°C	Conductive heat is losses from the top layers to the atmosphere. At the top of the model are specified using an infinitely large block saturated with water at 15°C. There are no inflow and outflow from peripheral boundaries. High temperature fluid recharges at a rate of 12 kg/s of 260°C from the bottom layer.
MID	0.05	5^{-15}			
HIG	0.10	2.5^{-14}			
HIG18	0.10	2.0^{-14}			
HIG04	0.10	3.0^{-14}			
HIG09	0.10	1.0^{-14}			

Key Results

Chingshui geothermal numerical model was calibrated by repeating simulations until a good match was obtained with the natural state condition in the reservoir (Figure 3). The computed results were compared against temperature measured in twelve wells. The temperature distribution and surface outflows of heat and mass in the model are also compared with measured field data and the permeability structure of the model is adjusted to achieve a satisfactory match.

The result of simulation in natural state shows the reservoir temperature of 200°C at 1500m depth can be extracted (Figure 4). Finally, the future scenario was conducted to determine location and depth of wells. The field can sustain a power generation of 3MWe with six 1500m productions and one 2500m deep reinjection well for thirty years.
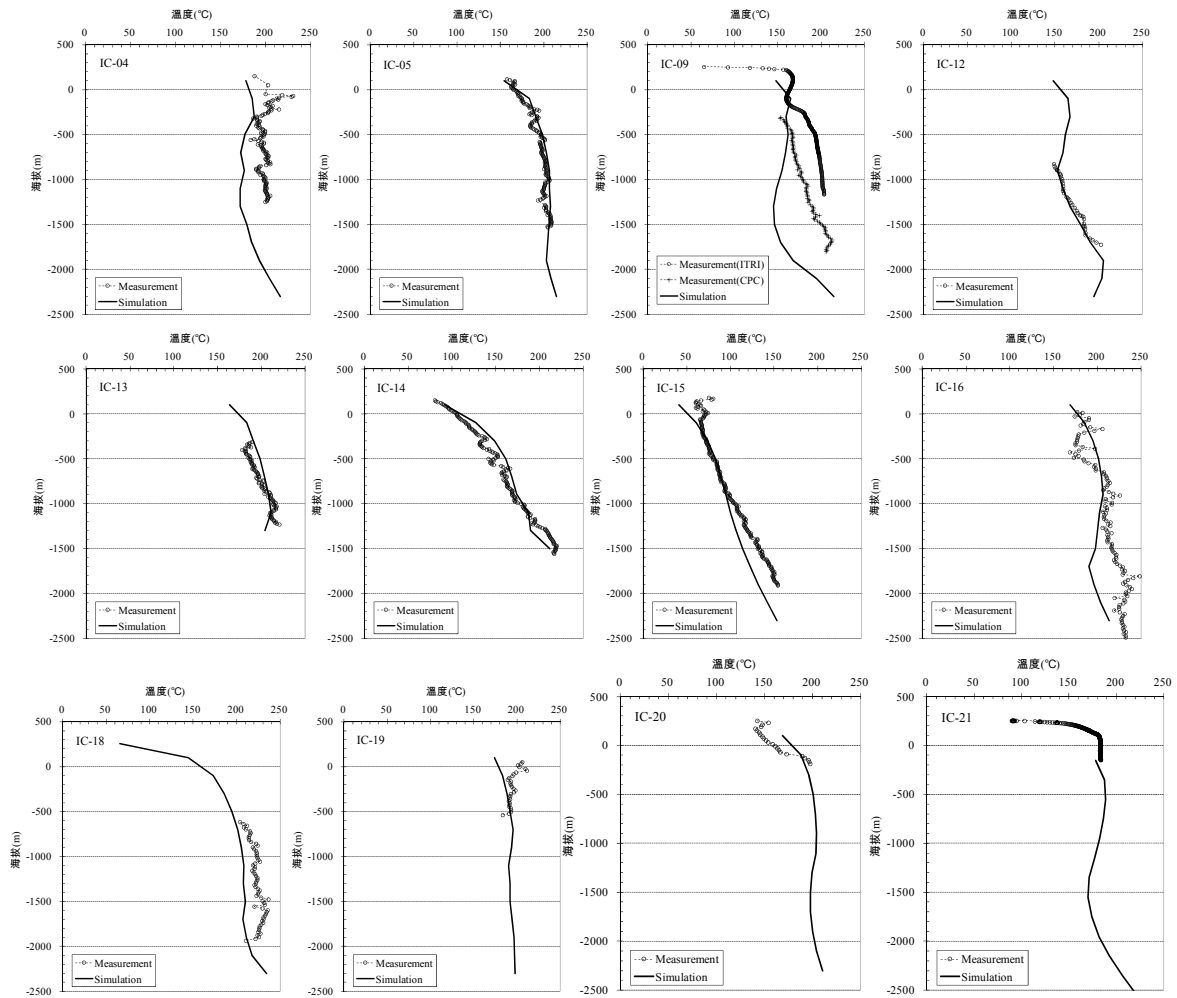
Figure 3: Measured and simulated natural state temperature in Chingshui geothermal area
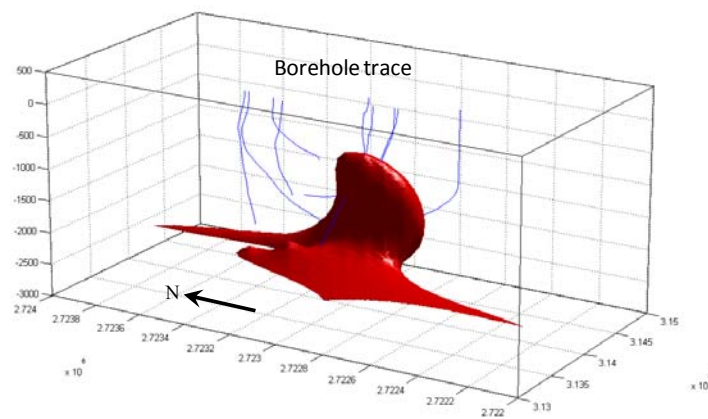
Figure 4: 1500m borehole trace can reach 200°C isothermal surface in Chingshui geothermal reservoir
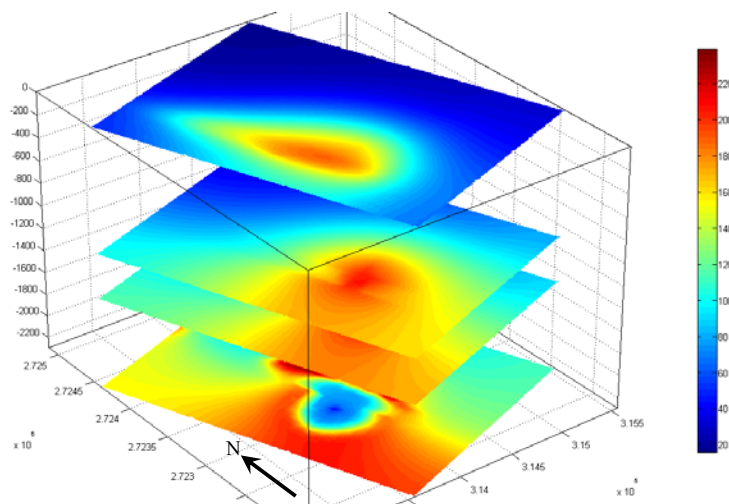
Figure 5: *Simulated temperature changes after 30 years of six 1500m production well and one 2500m deep reinjection well in Chingshui geothermal reservoir.*

References

Lee, C. R. (1994), "Compilation of the geothermal prospects data in Taiwan during 1966-1979," Bureau of Energy Report, R.O.C., p.500.

Fan, K.C., Kuo, M.C., Liang, K.F., Lee, C.S., and Chiang, S.C., (2005), "Interpretation of a well interference test at the Chingshui geothermal field, Taiwan," Geothermics,Vol. 34, pp.99–118.

Tong, L.T., Ouyang, S., Guo, T.R., Lee, C.R., Hu, K.H., Lee, C.L., and Wang, C.J. (2008), "Insight into the Geothermal Structure in Chingshui, Yilan, Taiwan," Terrestrial, Atmospheric and Oceanic Sciences, Vol.19, No.4, pp.413-424.

O'Sullivan, M.J., (2008), "AUTOUGH2 Notes", Department of Engineering Science, The University of Auckland, p.34.

Synthetic thermal modelling of hot rock geothermal systems

Lescinsky, D.T. [1], Budd, A.R. [1], and Kirkby, A.L. [1]

[1]Geoscience Australia

David.Lescinsky@ga.gov.au

Keywords: finite difference thermal modelling, synthetic modelling, hot rock geothermal systems

Project description

Currently it is difficult to assess the quality of Australian geothermal exploration targets, particularly for those with very limited amounts of available geological data. To rectify this, Geoscience Australia (GA) is developing a knowledge-based tool that incorporates diverse observational data and theory. This tool will be used for evaluating geothermal potential across the continent and for identifying areas that warrant additional investigation. An important first step in the development of this tool is synthetic thermal modelling. Synthetic modelling has been used to perform sensitivity analysis, determine the importance of different geothermal parameters and the values of these parameters necessary to produce specific temperatures at depth. The results of the synthetic modelling are presented here.

Model design and assumptions

A series of synthetic models were constructed to simulate a wide range of geological scenarios where heat transfer occurred exclusively by conduction. Lithologic components of the models included: a granite heat source; an insulating sedimentary overburden; and a thickness of basement rock consisting of upper crust to 15 km depth and lower crust to the base of the model at 25 km depth. Granite body dimensions were simplified by assuming the bodies were radially symmetrical and had a fixed power-law relationship between diameter (L_g) and thickness (H_g). This relationship can be expressed as $H_g \sim 0.66 \times L_g^{0.6}$ and was determined by fitting the data of Petford et al., 2000). Granite diameters were varied between 0 (no granite) and 150 km and sediment thickness (H_s) was varied between 0 (no sediment) and 6 km.

Each of the lithologic units was assumed to be homogeneous in respect to heat production and thermal conductivity. The values for these geothermal parameters were chosen to test the complete range of geologically reasonable conditions for hot rock geothermal systems, regardless of probability. Heat production values for the granites (HPR_g) ranged from 2.0 μW/m^3 to 10.0 μW/m^3 and for upper crust (HPR_{uc}) ranged from 1.0 μW/m^3 to 4.0 μW/m^3. Heat production values were fixed for the sediments (1.0 μW/m^3) and the lower crust (0.19 μW/m^3). Thermal conductivity values for the sediments (k_s) ranged from 1.0 W/mK to 3.0 W/mK. Thermal conductivities were fixed for the remaining lithologic units, 3.0 W/mK for granites and 2.4 W/mK for the upper and lower crust. The basal heat flow (HF_b) used in the simulations ranged from 30 mW/m^2 to 50 mW/m^2.

Key results

More than 250,000 discrete simulations were performed using the SHEMAT computer code (Clauser, 2003) to compute the thermal models. Python scripts developed in GA, as well as from the PyShemat scripting library (Wellmann et al., 2011) were used to facilitate the SHEMAT modelling. Temperature profiles were extracted from the computed 2D models and used during the analysis described below. The analysis focussed on depths less than 5.5 km in order to characterise the zone that can be reached by current drilling technology.

Sensitivity Analysis

Six separate variables were considered during the sensitivity analysis, these were: granite body size; granite heat production; sediment thickness; sediment thermal conductivity; upper crust heat production; and basal heat flow. Since model temperatures are primarily the result of a balance of heat production and thermal insulation, the role of these properties must be evaluated independently. However, it is possible to evaluate the relative importance of different factors associated with heat production and different factors associated with thermal insulation.

The amount of heat produced during a simulation is largely a function of the granite body size and the rate of heat production of the granite. An examination of the simulation results (Figure 1) reveals that granite body size is most important for small granites (< 20-30 km diameter) and at high rates of heat production (> 6.0-7.0 $\mu W/m^3$). In contrast, the rate of heat production is most important for large granites (> 50 km) and at low rates of heat production (< 4.0-5.0 $\mu W/m^3$).

Thermal insulation is related to the sediment thickness and thermal conductivity. As shown in Figure 2, sediment thickness is most important when the sediments are thin (< 1.5 km thick). Sediment thermal conductivity is most important for high values of thermal conductivity (> 2.0 W/mK) and for thick piles of sediment (when the sediments are thicker than the depth of interest, i.e., 4 km in Figures 1-2).

An examination of the remaining variables indicates that these have lesser influence on the modelling results. Basal heat flow has a modest effect on model temperatures, accounting for an increase of ~2°C each 1 mW/m^2 of added basal heat flow (Figure 3). Model temperatures in the range of interest are relatively insensitive to variations in heat production in the upper crust (Figure 4). The model temperature isotherms in Figure 4 largely overlap, indicating minimal influence of upper crustal heat production except for the smallest granite bodies.
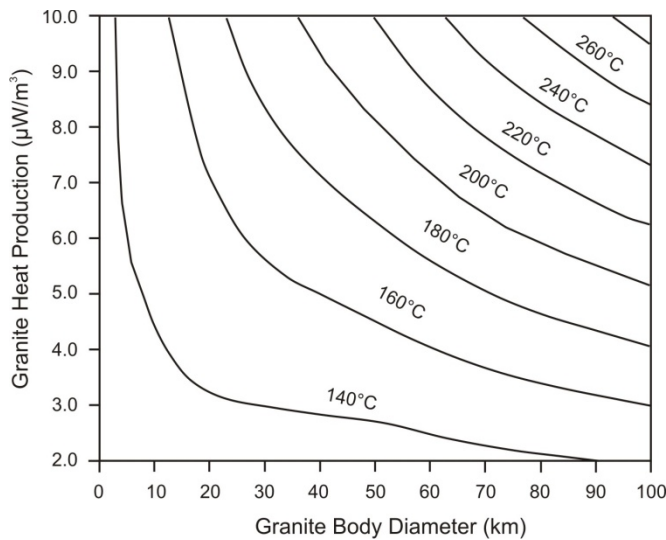
Figure 1: Plot of granite heat production and granite body diameter showing the model isotherms at 4 km depth for simulations with H_s = 3 km, k_s = 2 W/mK, HPR_{uc} = 2 $\mu W/m^3$, and HF_b = 40 mW/m^2. The relationships between granite heat production, granite diameter and model temperatures are described in the text.
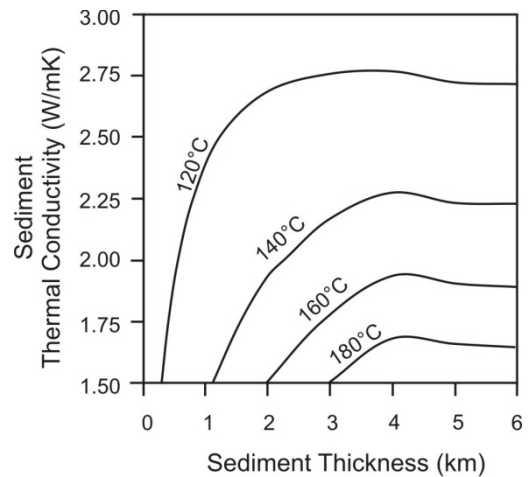
Figure 2: Plot of sediment thermal conductivity and sediment thickness showing the model isotherms at 4 km depth for simulations with L_g = 30 km, HPR_g = 4 $\mu W/m^3$, HPR_{uc} = 2 $\mu W/m^3$, and HF_b = 40 mW/m^2. The relationships between sediment thermal conductivity, sediment thickness and model temperatures are described in the text.
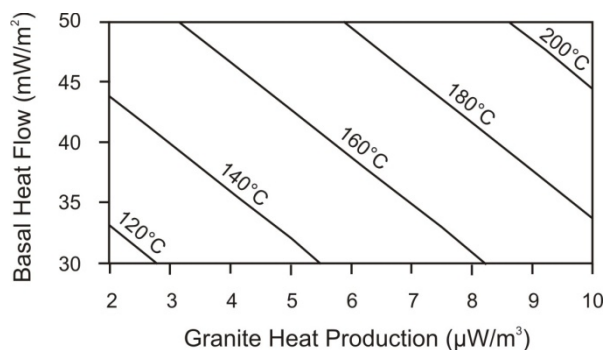
Figure 3: Plot of basal heat flow and granite heat production showing the model isotherms at 4 km depth for simulations with H_s = 3 km, k_s = 2.0 W/mK, L_g = 30 km, and HPR_{uc} = 1 µW/m³. The isotherms indicate a constant increase in temperature with increasing basal heat flow and with increasing granite heat production.
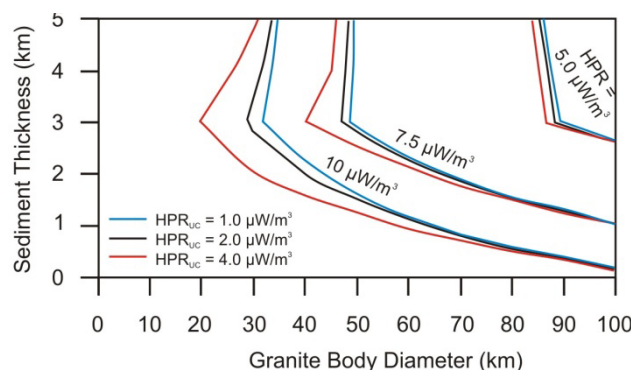
Figure 4: Plot of sediment thickness and granite body diameter showing the model temperature isotherms for 160°C at 3 km depth for simulations with k_s = 2.0 W/mK, and HF_b = 40 mW/m². The three coloured curves correspond to different values of HPR_{uc}: blue – 1.0 µW/m³; black – 2.0 µW/m³; and red – 4.0 µW/m³.. The isotherm curves bend upwards at 3 km sediment thickness indicating that model temperatures do not increase with further increases in sediment thickness.

While the majority of the simulations performed assumed the best-fit power-law relationship between granite body diameter and thickness (H_g ~ 0.66 × $L_g^{0.6}$), a number of simulations were performed to examine the importance of granite aspect ratio. Additional power-law relationships were constructed to bound the upper and lower ranges of granite body dimensions reported by Petford et al. (2000). A plot of the results (Figure 5) shows that for granites 30-40 km in diameter, model temperatures fall within ± 10°C of the best fit relationship at 3 km depth and ± 15°C at 5 km depth, indicating that the model temperatures are relatively insensitive to aspect ratio for granites with diameters < 40 km.

The simulation results shown in Figure 6 can be summarized as follows. For granite bodies less than 40 km in diameter (close to the upper limit for granites in Australia) and a basal heat flow of 40 mW/m², target temperatures of 160°C can be achieved at 3 km depth when: granite heat production > 5.0 µW/m³; sediment thickness > 3 km; and sediment thermal conductivity < 2.0 W/mK (Figure 6). Higher values of basal heat flow increase the range of acceptable parameter values.

Implications for Exploration

Results of the synthetic geothermal modelling indicate that "average" geological conditions in Australia are insufficient to generate and/or trap economically viable heat, and therefore, exploration should focus on locating anomalous geological conditions. Across Australia, sediment thickness is the best mapped of the four most important parameters, in large part due to geophysical investigations such as SEEBASE™ (Loutit et al., 2005). Large portions of Australia have sediment thicknesses greater than 1.5 km and locations with sediment thicknesses greater than 3 km (the minimum sediment thickness based on synthetic modelling) are relatively well known. In contrast, the distribution of sediment thermal conductivities is poorly resolved. Existing studies (e.g., Ayling and Lewis, 2010; Meixner et al., 2011, 2012) indicate that the thermal conductivity values of Australian basins are predominantly > 2.25 W/mK except in areas with significant quantities of coal or lignite (where coal accounts for ~> 3% of stratigraphy, assuming thermal conductivities of coal of 0.2-0.5 W/mK; Herrin and Deming, 1996). Although thermal conductivity is temperature dependent, temperatures of ~ 220°C will only result in minor decreases in thermal conductivity (~0.50-0.25 W/mK for rocks initially 3.0-2.0 W/mK heated; Lee and Deming, 1998)
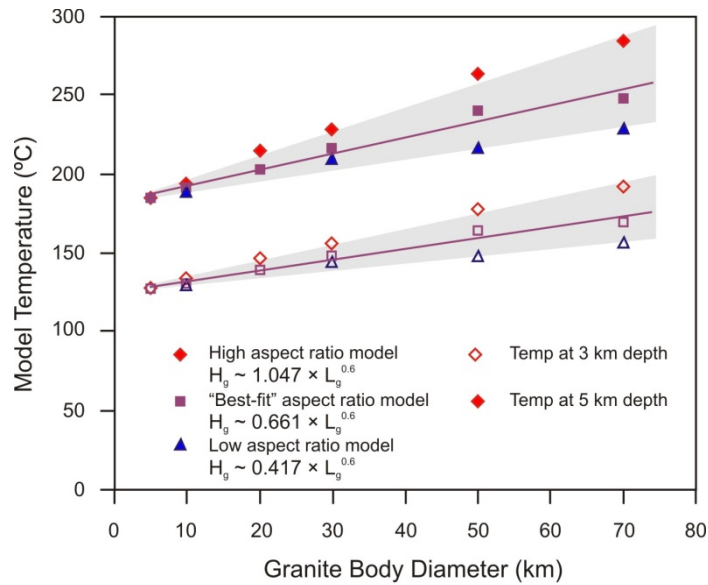
Figure 5: *Plot of model temperatures (open symbols – 3 km depth; closed symbols – 5 km depth) and granite body diameters for simulations using aspect ratios that bracket the range of granites in nature. All simulations were performed with HPR_g = 5 μW/m^3, k_s = 2.0 W/mK, HF_b = 30 mW/m^2, and HPR_{uc} = 1 μW/m^3. Model temperatures for 3 km depth are for simulations with H_s = 3 km and model temperatures for 5 km depth are for simulations with H_s = 5 km. The shaded areas corresponding to the range in model temperatures, which expand at larger granite body diameters. For granite bodies with L_g = 40 km, the model temperature range is ±10°C at 3 km depth and ±15°C at 5 km depth.*

Few discrete granite bodies have been identified in Australia that exceed 40 km in diameter. The majority of large mapped granites consist of multiple bodies that have coalesced and are difficult to differentiate. Although there tends to be little control on the thickness of the coalesced bodies, they are most likely to form large thin plates. An evaluation of simulation results using granite bodies with fixed thicknesses and varying diameters, indicates that these large bodies can reasonably be modelled using a characteristic individual granite body diameter and that the added lateral extent does not significantly increase the model temperatures (Figure 7). Due to the paucity of granites in excess of 30-40 km diameter (and anassociated increase in thickness), it is necessary to rely on high values of heat production to generate sufficient heat. An examination of Geoscience Australia's OZCHEM geochemistry database reveals that ~8% of the analysed Australian granites have heat production values of ≥ 7.5 μW/m^3. Determining the extent of these and other high heat producing granites therefore becomes important.

The results of this study highlight the need to better constrain geologically relevant parameter values in regions of interest in Australia. Of particular importance, techniques are needed to determine the location and size of individual buried granites, the magnitude of the basal heat flow, and the presence of coal.
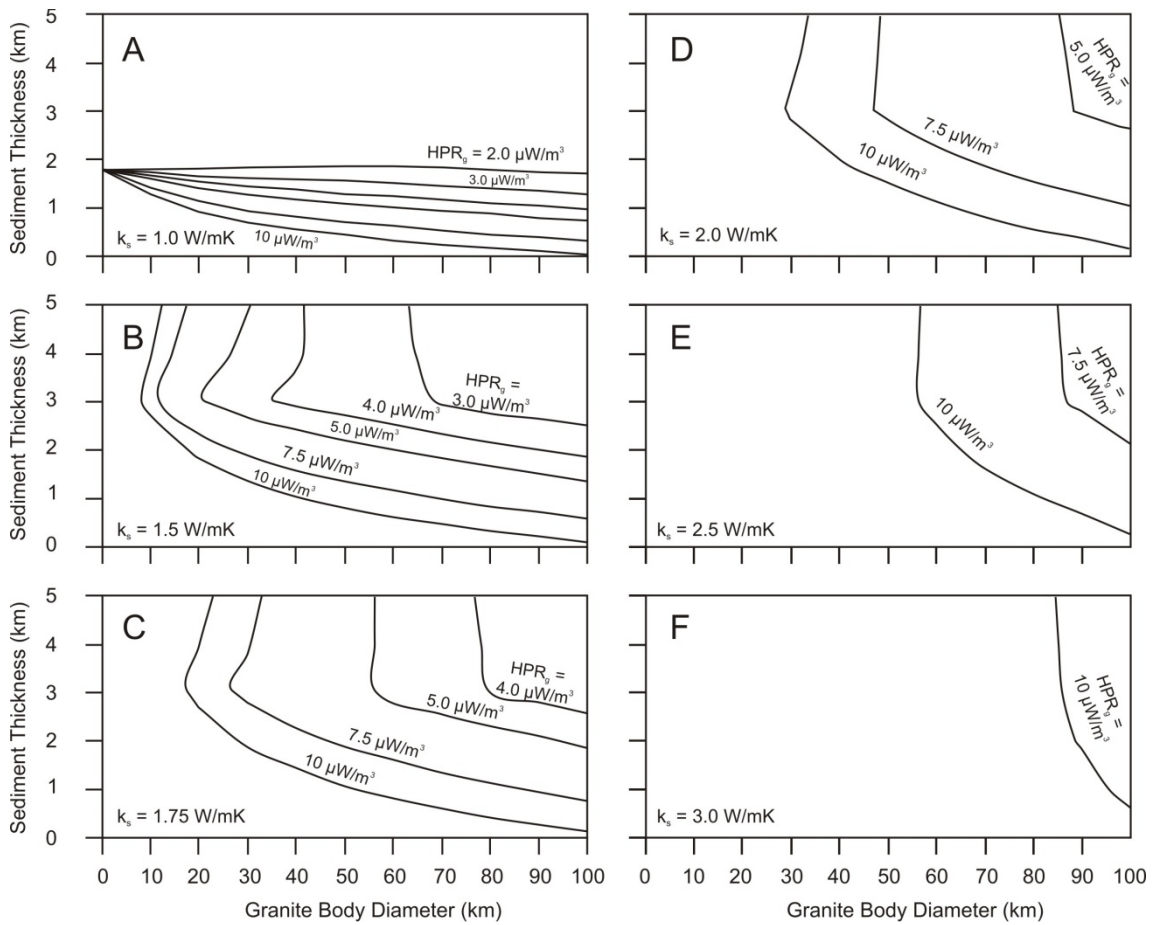
Figure 6: *Plots of sediment thickness and granite diameter showing variations in model parameters (HPR_g and k_s) which produced temperatures of 160°C at 3 km depth. Upper crustal heat production of 2 µW/m³, and basal heat flow of 40 mW/m² were kept constant. Graphs correspond to different values of k_s: A) k_s = 1.0 W/mK; B) k_s = 1.5 W/mK; C) k_s = 1.75 W/mK; D) k_s = 2.0 W/mK; E) k_s = 2.5 W/mK; and F) k_s = 3.0 W/mK. The isotherm curves bend upwards at 3 km sediment thickness indicating that model temperatures do not increase with further increases in sediment thickness. The 3 km sediment thickness corresponds to the 3 km observation depth*
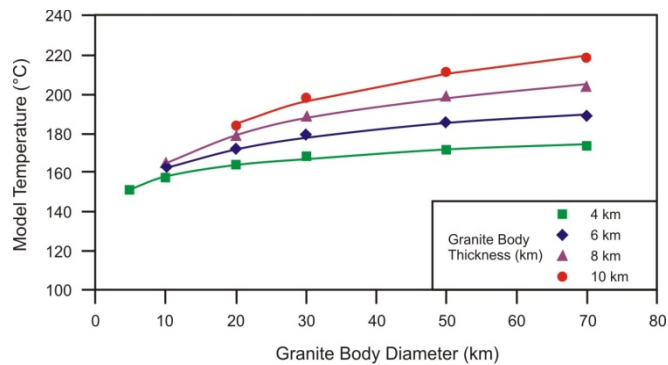
Figure 7: *Plot of model temperature at 4 km depth and granite body diameter for simulations with HPR_g = 5 µW/m³, k_s = 2.0 W/mK, HF_b = 30 mW/m², and HPR_uc = 1 µW/m³. Symbols correspond to different values of H_g: circles – 4 km; diamonds – 6 km; triangles – 8 km; and circles – 10 km. The curves fitting the data demonstrate a logarithmic decline in temperature increase with increasing granite body diameter.*

References

Ayling, B.F., and Lewis, B. (2010). Geothermal Systems, in: Huston, D.L. (ed). An assessment of the uranium and geothermal potential of north Queensland. Record 2010/14. Geoscience Australia: Canberra.

Clauser, C. (Ed.) (2003).Numerical simulation of reactive flow in hot aquifers. SHEMAT and Processing SHEMAT. Springer Verlag, Heidelberg-Berlin, 332 p.

Herrin, J.M. and Deming, D. (1996). Thermal conductivity of U.S. coals. J. Geophys. Res., 101(B11), 25381-25386.

Lee, Y., and Deming, D. (1998). Evaluation of thermal conductivity temperature corrections applied in terrestrial heat flow studies. J. Geophys. Res., 103(B2), 2447-2454.

Loutit, T., Pryer, L., Henley, P., Gardner, P. (2005). The OZ SEEBASE™ Project: A new view of Australia's Phanerozoic basins. PESA News, August/September 2005, 12-13.

Meixner, A.J., Kirkby, A., Champion, D.C., Weber, R., Connolly, D., and Gerner, E., 2011. Geothermal Systems, in: Huston, D. L. and van der Wielan, S. E. (eds). An assessment of the uranium and geothermal prospectivity of east-central South Australia. Record 2011/34. Geoscience Australia: Canberra.

Meixner, A.J., Kirkby, A.L., Lescinsky, D.T., and Horspool, N., 2012. The Cooper Basin 3D map version 2: Thermal modelling and temperature uncertainty. Record 2012/60. Geoscience Australia: Canberra.

Petford, N., Cruden, A.R., McCaffrey, K.J.W, and Vigneresse, J.-L. (2000). Granite magma formation, transport and emplacement in the Earth's crust. Nature, 408, 669-673.

Wellmann, J.F., Croucher, A., and Regenauer-Lieb, K., (2011). Python scripting libraries for subsurface fluid and heat flow simulations with Tough2 and SHEMAT. Computers & Geosciences, 43, 197-206.

Queensland's Coastal Geothermal Energy Initiative: shallow drilling as a means of assessing geothermal potential

L.K. O'Connor, S.N. Sargent, B. Talebi and M. Maxwell

Geological Survey of Queensland, Department of Natural Resources and Mines

lauren.o'connor@dnrm.qld.gov.au

The Coastal Geothermal Energy Initiative (CGEI) implemented a shallow drilling and heat flow investigation program across Queensland's coastal regions. The program sought to determine the most successful means of sampling and hole completion, and to assess the geothermal potential of selected geological settings.

Ten fully-cored boreholes were drilled into sedimentary basins and metasedimentary terranes of northern and eastern Queensland, from which temperature and thermal conductivity data were collected. These data were used to determine heat flow – a useful tool for assessing geothermal potential.

Thermal conductivity analysis of fresh core with preservation of *in situ* moisture content better represent rocks under formation conditions and resulted in values for sedimentary strata much lower than those previously published. The published values are consistent with the spread of values obtained for metasediments. The collection of multiple precision temperature logs demonstrated the effect of aquifers and minor permeable units on the thermal profile of a borehole when not properly isolated. Grouting of the borehole annulus can overcome temperature distorting owing to influx of water from intersected aquifers.

Coal measures are ideal in hot rock geothermal systems as they provide excellent insulation, but they introduce difficulties in using a shallow drilling program to determine geothermal potential. Their high thermal resistance can mask heat flow. Deeper drilling is required to definitively penetrate all coal sequences, and enable a more accurate determination of heat flow.

The high thermal resistance of coal measures can allow even moderate heat sources to generate sufficiently high temperatures at depth to constitute viable geothermal targets. In the absence of high heat-producing intrusives, low to moderate heat-producing intrusives and the residual heat from Cainozoic tectonism and volcanism, overlain by thick coal measures, may constitute viable heat sources. As such, the geothermal potential of south-eastern Queensland may have been previously underestimated, and further research and exploration are required.

Introduction

Regional datasets such as Oztemp, released by Geoscience Australia in 2011, are commonly used to highlight areas with geothermal energy potential using pre-existing data. This dataset has highlighted the south-west portion of the state as having anomalously high temperatures at depth, suggesting substantial geothermal potential. Outside this region, data density and reliability diminish, limiting the accuracy with which the prospectivity of Queensland's coastal regions can be assessed. Thus, the collection of new data is critical for better assessment of the geothermal potential of the state. In lieu of direct measurements of temperature at depth, temperature and thermal conductivity data collected from shallow drilling may be used to determine heat flow – a useful tool through which temperatures can be modelled at greater depths. However, the confidence with which shallow drilling data can be used to represent surface heat flow of a target is a product of the methods of collection and analysis.

The CGEI sought to determine the best methods of sampling and hole completion for use in a shallow drilling program. CGEI collected thermal conductivity and temperature data through a regional drilling program. These data were used to determine conductive vertical heat flow, from which temperatures

were modelled to 5 km depth, and an assessment of the regional geothermal energy potential was made.

Ten fully-cored boreholes were drilled into sedimentary basins and metasedimentary terranes across northern and eastern Queensland (Figure 1), to a total depth from 320 to 500 m. The boreholes were cased to total depth with PVC or VAM steel casing, and the annulus was grouted to isolate aquifers and permeable layers to ensure a closed system. The boreholes were left to thermally stabilise for a minimum of six weeks after drilling before precision temperature logs were run. Core samples from representative rock types intersected in each borehole were collected for thermal conductivity analysis. Details of targeting, sampling, and methodologies have been provided by Fitzell *et al.* (2009); Talebi *et al.* (2010); Sargent *et al.* (2011). Talebi *et al.* (2012) describes methods of temperature modelling and detailed results of resource volume and thermal energy content.
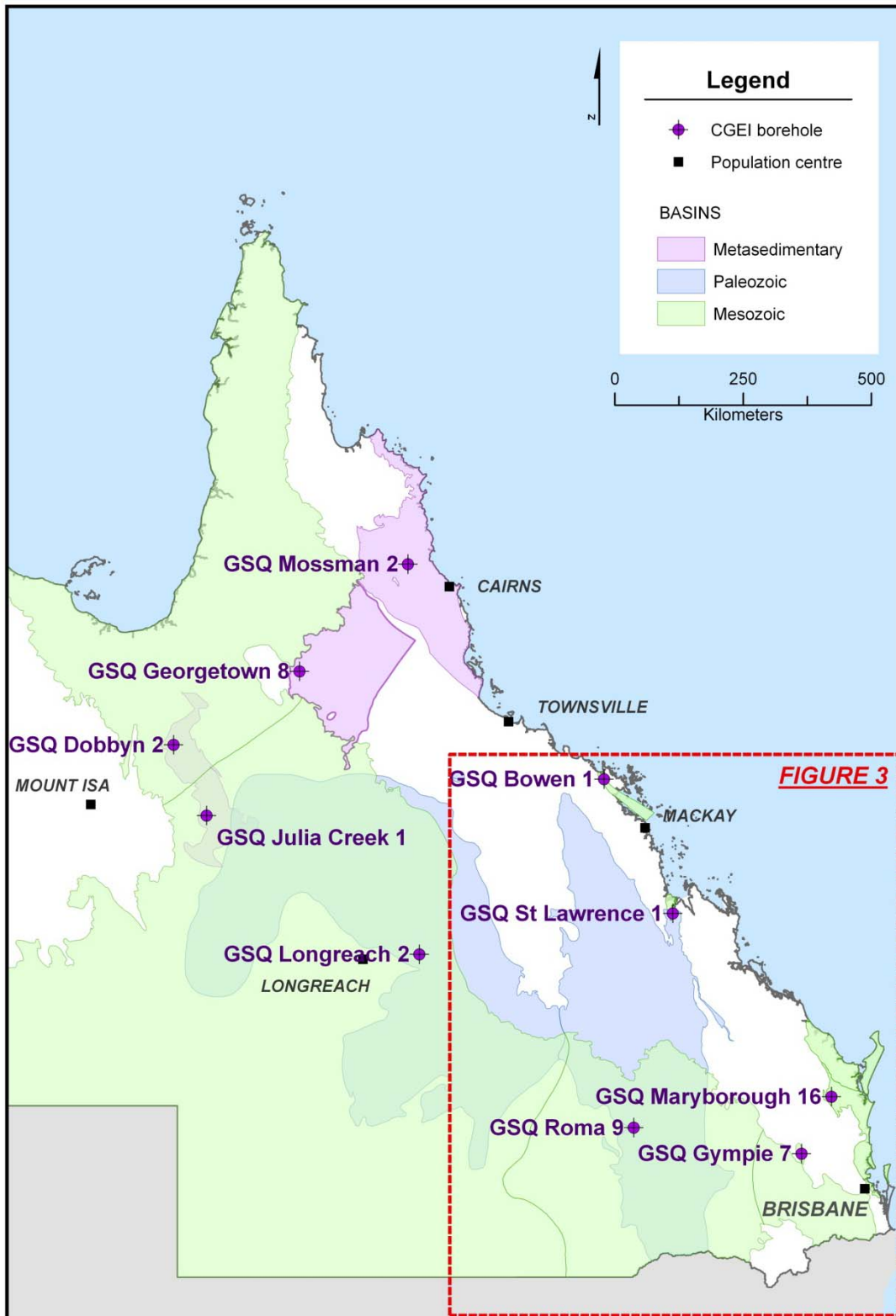
Figure 1 Sedimentary basins (blue, green) and metasedimentary terranes (purple) drilled in the CGEI program. Borehole locations are shown, with major towns and cities.

Aim

This paper examines the methods of data collection, the quality of the data collected and the subsequent heat flow and temperature modelling. The benefits and drawbacks of shallow drilling in eastern Queensland as a means of assessing regional geothermal potential are also discussed, and the effect of coal-bearing strata on temperature logging and heat flow modelling. The implications of the results of the CGEI program will also be discussed with respect to how the CGEI has assessed the geothermal potential of south-east Queensland (Figure 1).

Data collection and processing

Thermal conductivity analysis

Fresh core with preserved *in situ* moisture content is considered to better represent the rock under formation conditions. Analysis of these samples gave lower thermal conductivity than those of samples analysed under both wet and dry conditions.

Thermal conductivity of samples from by CGEI boreholes were lower than or in the lower part of the published range of values (Table 1). The published values are consistent with the spread of values obtained for metasediments intersected in the Georgetown Inlier, Hodgkinson Province and Millungera Basin. Similarity of values may be a reflection of the composition of the rocks – higher silica content, matrix composition or a higher degree of alteration of the rocks. Use of higher published values to sedimentary basin strata would lead to underestimation of the heat flow in these areas. The collection of *in situ* samples for thermal conductivity analysis is critical for determining accurate surface heat flow at a specific site.

Table 1 Comparison of thermal conductivity values. Published values from Beardsmore & Cull (2001).

Rock Type	Range of thermal conductivity values (W/mK)		
	Beardsmore & Cull (2001)	**Sedimentary Basins (CGEI)**	**Metasedimentary Terranes (CGEI)**
Sandstone	2.8 – 7.1	1.47 – 3.52	2.50 – 7.69
Siltstone	2.7 – 3.2	1.88 – 2.43	4.12 – 5.06
Mudstone	1.9 – 2.9	0.47 – 2.70	-

Temperature logging

The method of hole completion proved critical to obtaining a reliable temperature profile. Two methods of hole completion were used in this program. The first was to cement off aquifers as they were intersected, with the annulus of the borehole left uncemented. Subsequent temperature logging showed that fluid flow between even minor permeable units distorts the temperature profile. This demonstrated the difficulty in identifying minor aquifers while drilling. The failure to properly seal the aquifers meant that water could flow up the annulus distorting the temperature profile. Figure 2 shows where two permeable units were intersected in GSQ Longreach 2, which caused a sharp increase in temperature and a steep geothermal gradient between. The recompletion of this hole included cementing of the annulus to isolate any aquifers and permeable zones, which resulted in a steady temperature gradient (Figure 2).
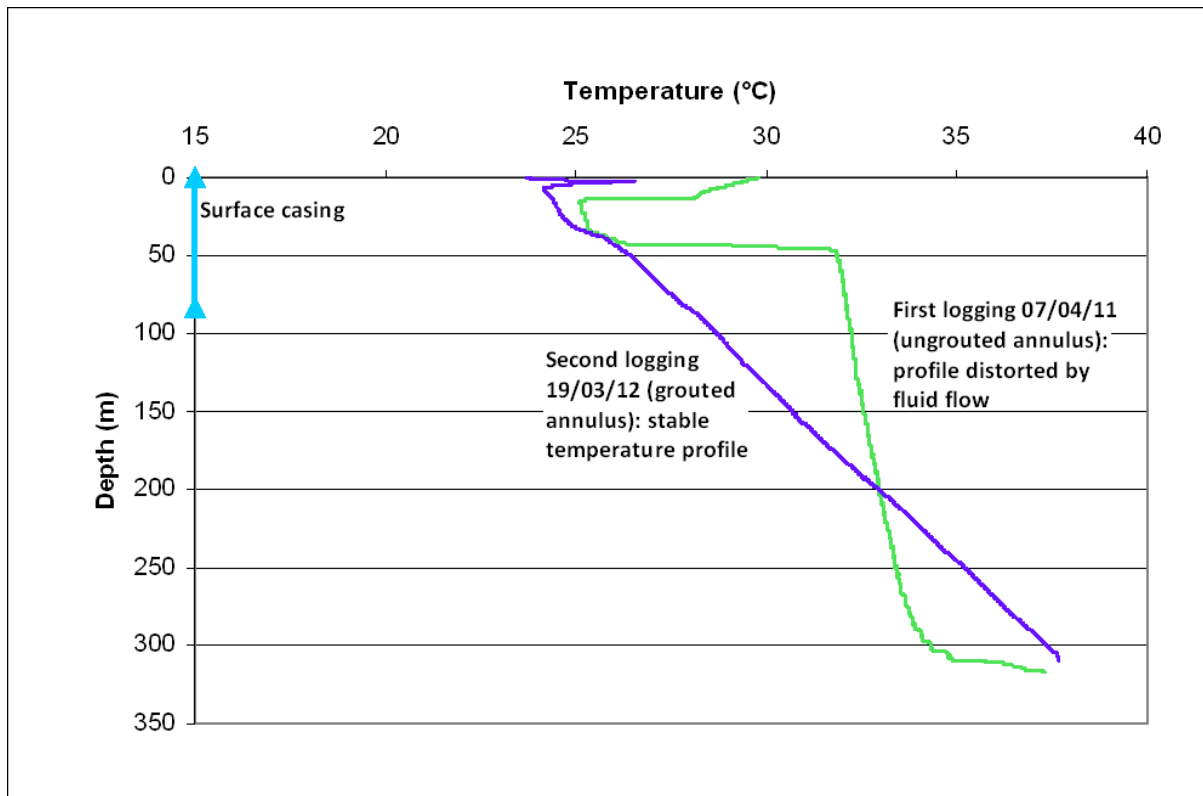
Figure 2 Temperature profile of GSQ Longreach 2. Two minor aquifers were intersected, and without grouting of the annulus, these caused a sharp increase in temperature within each aquifer and a steep geothermal gradient between (green line). By grouting the annulus of the borehole, flow between these units was controlled, and thermal equilibrium was achieved (purple line).

Modelling

Geothermal gradient data can be used for temperature extrapolations where heat flow data are lacking. As the thermal resistance of rock units is not constant to depth extrapolations based on gradients only may not produce reliable results. Where definitive thermal properties to 5 km depth are not available, a thorough review of geological and geophysical data was used to extrapolate stratigraphy to 5 km depth. Owing to the uncertainty associated with this approach, several stratigraphic scenarios were developed for each site, and then thermal conductivity values were assigned to the predicted rock types for temperature modelling at depth.

Geothermal potential of south-east Queensland

CGEI identified high heat flow and geothermal energy potential within the Hillsborough and Surat basins, with lower heat flow and less potential within the Nambour and Tarong basins. This difference in heat flow is postulated to be due to the presence of coal measures and thickness of the sedimentary cover of these basins.

The lowest determined heat flow was for the Tarong Basin, where thick coal and sedimentary sequences are interpreted to overlie the moderate heat producing Boondooma Igneous Complex. The entire basin sequence was not penetrated; therefore it is possible that further insulating sequences, potentially including coal, underlie the drilled sequences. This would significantly lower the heat flow within the drilled section, accounting for the anomalously low heat flow value.

Similarly, further coal sequences below the drilled section in the Nambour Basin would account for the average heat flow determined. A fault was intersected towards the bottom of the borehole making it

difficult to determine whether drilling intersected the entire coal sequence. These coal measures may have been a factor in previous estimates of low heat flow for this region.

Further targets included the low to moderate heat producing Roma Granites, and residual heat from Cainozoic tectonism and volcanism under the Hillsborough Basin, which would conventionally be considered less prospective than high heat producing intrusives. Moderate to high heat flow was determined for both these sites, with temperatures in excess of 200°C modelled at 5 km depth. This is related to the thermal resistance of the overlying sedimentary cover, where the intersected sequences contained coal and had thermal conductivity values below 2.6W/mK.

Coal measures are ideal in hot rock geothermal systems as they provide excellent insulation. The high thermal resistance property of coal can result with a localised low heat flow within the coal measures. In cases where the coal seams have not been penetrated by drilling, the low heat flow value may be inferred as reflecting poor geothermal energy potential.

Shallow drilling in coal basins, especially where a borehole does not extend below the coal measures, can be an added risk factor. This can be overcome by a good understanding of local geology and structure. Deeper drilling, penetrating the coal measures, should be undertaken in order to obtain the required data in order to determine the geothermal potential in these geological settings.

The stacked sedimentary basins in south-east Queensland commonly contain coal measures (Figure 3), which provide excellent insulation for potential heat sources. Results of the CGEI drilling program also demonstrate that given the high thermal resistance of these sedimentary sequences, sufficiently high temperatures can be generated by a range of heat sources.
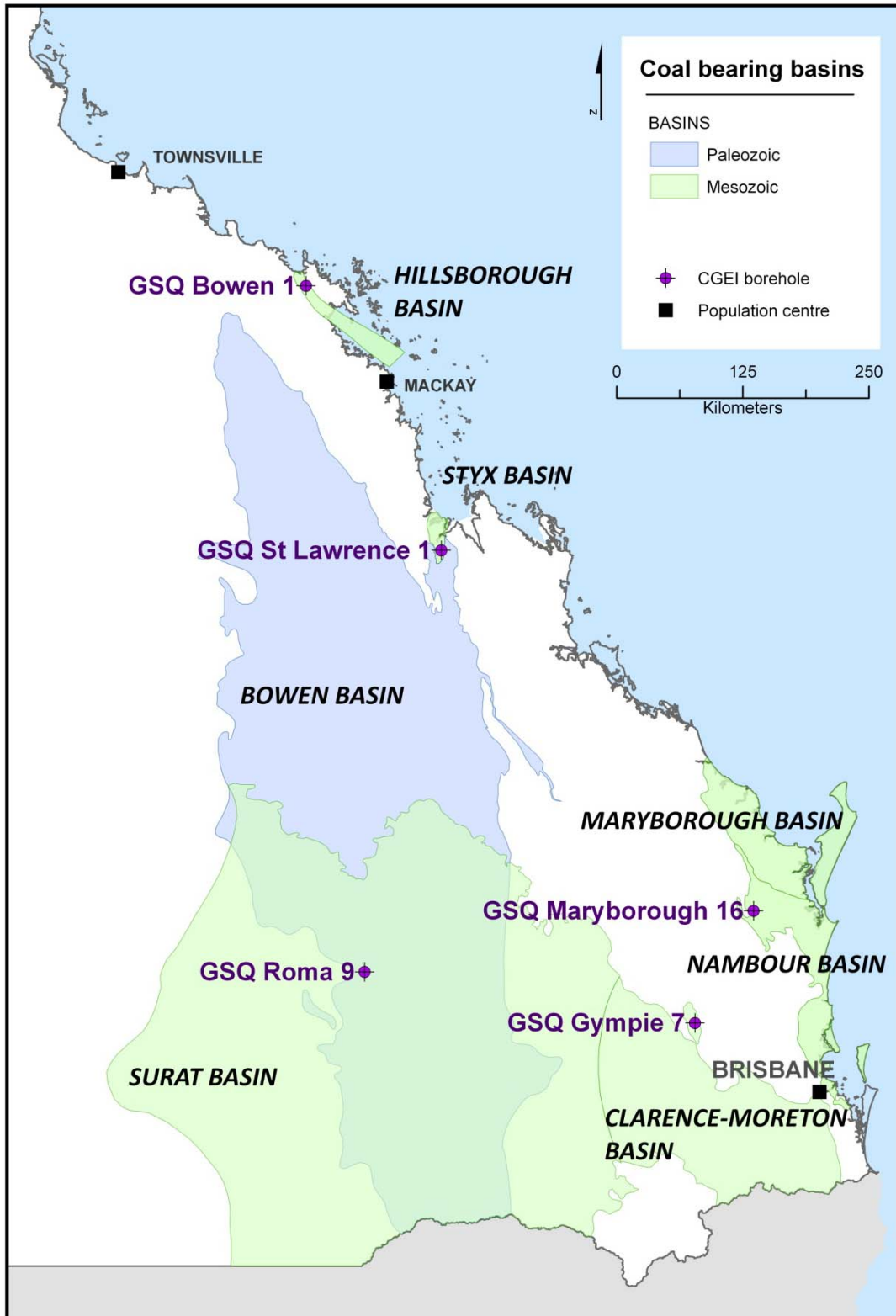
Figure 3 *CGEI boreholes in south-east Queensland and coal-bearing sedimentary basins.*

Conclusions and recommendations

Shallow drilling is an applicable method of collecting data for determining heat flow – a useful tool for assessing the geothermal prospectivity of a region. However, the use of high quality data is critical for precision and accuracy in the modelling of heat flow and temperature.

Complications may arise from shallow drilling in coal basins, as thick coal measures mask the heat flow regime and, as such, have the potential to distort heat flow and give a potentially misleading evaluation of geothermal potential. The risk factors associated with this may influence future shallow drilling in these regions, despite the benefit of these coal measures to the overall geothermal system. Drilling to penetrate all coal measures is required.

The collection of multiple precision temperature logs not only provides excellent quality data, but also allows for assessing whether the system has returned to a state of thermal equilibrium. The isolation of all aquifers intersected by a borehole is critical to the thermal stabilisation. Cementing the annulus provides the most efficient way of isolating these aquifers.

The CGEI program highlighted the differences between published thermal conductivity values and samples with preserved *in situ* moisture content. Sedimentary strata (from the Carpentaria, Eromanga, Surat, Bowen, Styx, Hillsborough, Nambour and Tarong basins) had much lower thermal conductivity than published thermal conductivity values. Published values better reflected measurements from metasedimentary terranes. The limitations associated with using published values for thermal conductivity needs to be recognised in determining the geothermal potential of an area.

High thermal resistance of the sedimentary sequences of south-east Queensland increase the geothermal prospectivity of the region. Even moderate heat sources present under these basins may generate sufficiently high temperatures at depth to be considered viable geothermal targets. The geothermal potential presented by these less traditional heat sources lends credence to the notion that despite the lack of high heat producing intrusives, the prospectivity of south-east Queensland may be much better than previously estimated.

References

Beardsmore, G.R. and Cull, J.P., 2001, *Crustal Heat Flow: a guide to measurement and modelling*, Cambridge University Press, 324pp.

Fitzell, M., Hamilton, S., Beeston, J., Cranfield, L., Nelson, K., Xavier, C. and Green P., 2009, *Approaches for identifying geothermal energy resources in coastal Queensland*, Proceedings of the 2009 Australian Geothermal Energy Conference, 6pp.

Sargent, S., Maxwell, M., Talebi, B. and O'Connor, L., 2011, *Queensland's Coastal Geothermal Energy Initiative: preliminary heat flow modelling results*, Proceedings of the 2011 Australian Geothermal Energy Conference, 6pp.

Talebi, B., Maxwell, M., Sargent, S. and Bowden, S., 2010, *Queensland Coastal Geothermal Energy Initiative – An Approach to a Regional Assessment*, Proceedings of the 2010 Australian Geothermal Energy Conference, 6pp.

Talebi, B., Sargent, S.N., O'Connor, L.K. and Maxwell, M., 2012: *Coastal Geothermal Energy Initiative: identifying hot rocks in cool areas,* Proceedings of the 2012 Australian Geothermal Energy Conference, *In press*.

Education and Demonstration of Direct Geothermal Energy (edDGE)

Payne, D. J. B.1,[5], Johnston, I. W.[2], Narsilio, G. A.[3], Colls, S.2, Valizadeh Kivi, A.[2] Wearing-Smith, M.[5], Noonan, G.[6]

[1] Australian Geothermal Energy Group, Technical Interest Group 7 (Direct Use Geothermal). [2] Golder Associates Chair of Geotechnical Engineering, Department of Infrastructure Engineering, University of Melbourne, Melbourne, Victoria 3010, Australia. [3] Senior Lecturer, Dep. of Infrastructure Engineering, University of Melbourne, Melbourne, Victoria 3010, Australia. [4] PhD student, Department of Infrastructure Engineering, University of Melbourne, Melbourne, Victoria 3010, Australia. [5] Direct Energy Australia Pty Ltd, Mezzanine Level, 225 Bourke St., Melbourne, Victoria 3001, Australia. [6] Geotechnical Engineering, 174 Turner St., Port Melbourne, Victoria 3207, Australia

Donald@eddge.com.au

Education & Demonstration of Direct Geothermal Energy (edDGE) has been founded as a $1.6 million pilot demonstration project for direct geothermal energy technology funded by the Victorian Government's Department of Primary Industries through the Energy Technology Innovation Strategy (ETIS): Sustainable Energy Pilot Demonstration (SEPD) Program and officially launched in April 2012. edDGE is governed as a partnership between the University of Melbourne, Geotech & Direct Energy Australia. edDGE will collect important data about the use of direct geothermal energy systems in Victorian conditions in order to help develop greater efficiency in installation practices and design. In-ground data will be collected from instruments placed in direct geothermal systems that will be installed in numerous new and retrofit buildings throughout Victoria. The project will also engage and educate the general community about direct geothermal energy, as well as provide specific training to the trades and professions so that the technology can be rolled out in Victoria and participate in the development of Australian Standards for design and installation of direct geothermal systems.

Principles of direct geothermal energy

Geothermal energy is renewable and available 24 hours a day, 365 days a year. It comes from two replenishing sources: the Earth's core in the case of hot-rock, usually several-kilometre-deep - power generation, and solar energy in the case of Geothermal Heat Pumps (GHPs, also referred to as Ground Source Heat Pumps, GeoExchange or Direct Geothermal systems, see Figure 1). About 50% of incoming solar energy is absorbed. GHPs harvest solar energy from the shallow Earth via ground loops circulating a fluid resulting in a more efficient use of energy and natural resources and providing an opportunity for people to live & work more sustainably.

Geothermal Heat Pumps (GHPs) can efficiently address heating, cooling, hot-water heating and pool heating for homes and businesses. Over 3 million GHPs are installed worldwide with concentrations in Europe and the US who embraced this technology in the 1970's. Australia is behind on the uptake of this technology – programs such as edDGE will assist with uptake. Demand-side reduction strategies such as the scale application of GHPs may effectively offset some of the transmission network upgrades.

edDGE projects

edDGE entails several sub-projects that are briefly described below:

- **Bio21 Science School:** new 1200m^2 two-storey building that will employ a direct geothermal system with 28 x 50m deep double-loop HDPE pipe bores providing 90 kW$_{th}$ thermal capacity to the building (see Figure 1).

- **Port Melbourne Office Retrofit:** 1500m^2 two-storey building which will be half retrofitted with Geothermal Heat Pumps to allow a side-by-side comparison of Air & Ground Source systems.

- **Victorian Properties:** Up to 40 new and retrofit buildings covering a range of Victorian conditions will have direct geothermal systems installed and include ground & performance monitoring.

- **Main Ridge Horizontal System:** Recently renovated 700m^2 residence with 70 kW$_{th}$ horizontal "slinky" system installed to heat & cool the building and swimming pool.

- **PICAC:** Plumbing Industry Climate Action Centre OH&S training facility is conditioned by a 35 kW$_{th}$ GHP system with temperature sensors installed in the ground to monitor ground loop performance.

- **Unimelb Campus Geothermal Test Facility:** 5 Ground Heat Exchangers (GHEs) are installed to 30m deep with extensive temperature monitoring to study different GHEs and performance.

Australian Standards for direct geothermal systems

Following industry consultation and workshops throughout 2011, development of an Australian Standard for design & installation of Ground Source Heat Pump Systems commenced in April 2012 with the formation of the EN-005 committee. The Ground Source Heat Pump Systems Standard has been allocated designation AS8800-20XX. Drafting of AS8800 Pt. 1 – GSHP system design is under way with headings and information from Canadian Standards Association (CSA) C448.0 and the International Ground Source Heat Pump Association (IGSHPA) being incorporated. The working group will further this draft and will continue the drafting process over the coming months. Final delivery of the standard is scheduled for January 2014.

The development of Australian Standards is expected to underpin further broader policy measures for direct geothermal systems. One example is captured by dialogue with the Office of the Renewable Energy Regulator (ORER) on the inclusion of GHPs in the Renewable Energy Target (RET) Small-scale Renewable Energy Scheme (SRES). Another is the inclusion in the various energy efficiency schemes such as the Victorian Energy Efficiency Target (VEET).
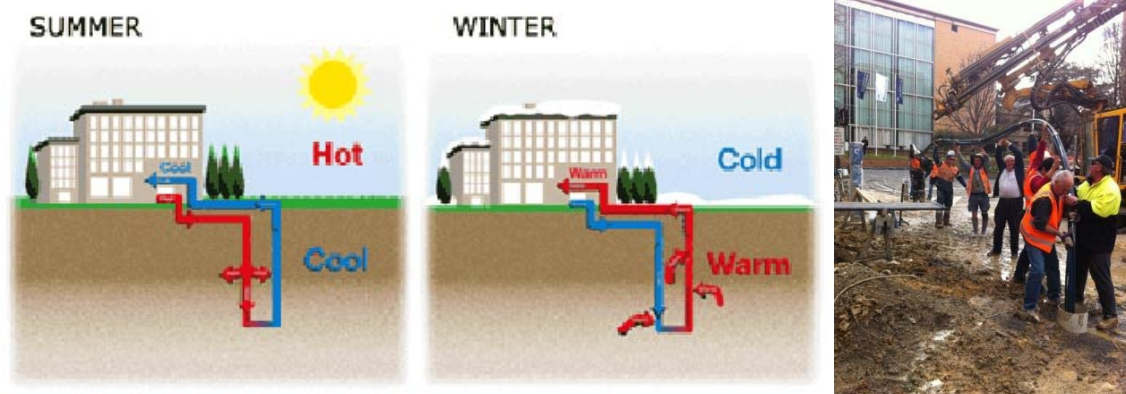
Figure 1: Illustration of the principles of direct geothermal heating & cooling (left, not to scale); Installation of one of 5 x 50m HDPE ground loops on campus at the University of Melbourne (right).

Acknowledgements

Evolution in the reliability of experimental geothermal data

Yuri Popov

Schlumberger Moscow Research Center

ypopov@slb.com

Introduction

We have conducted experiments in fourteen scientific deep drilling projects in Russia, Germany, USA, Mexico and other countries. This work has produced unique experimental data on the thermal characteristics of the crust in many different regions and geological situations, and has allowed us to refine the experimental geothermal methodology.

These deep continental drilling programs have provided experimental data (temperature, thermal gradient, rock thermal properties, and heat flow) to help define the thermal characteristics of the crust. A principal advantage of these scientific boreholes was that they permitted repeated temperature logging over long time intervals (often several years) after drilling or fluid injection ceased. Thus scientists were able to measure fully equilibrated thermal gradients, and study spatial and temporal variations in temperature and temperature gradient within individual rock formations. Scientific boreholes are usually cored, helping scientists in measuring thermal conductivity along large continuous sections of the borehole. As a result, deep and super-deep scientific boreholes prove invaluable in the determination of vertical heat flow distribution, one that can usually not be studied in commercial boreholes.

Our geothermal and petrophysical investigations included the super-deep boreholes Kola, Ural, Vorotilovo, Tyumen, and Yen-Yakha, in Russia; Saatly in Azerbaijan; and deep boreholes Kolva, Timano-Pechora, Tyrnyaus, in Russia; Krivoy Rog in Ukraine; Muruntau in Uzbekistan; Nordlingen-72 in Germany, a joint research project with J.Pohl and H.Soeffel; Yaxcopoil-1 in Mexico, a joint research project with H.Burkhardt, H.Wilhelm, J.Safanda, V.Cermak, P.Heidinger, and S.Mayr; and Eyreville in the USA, a joint research project with H.Wilhelm, H.Burkhardt, P.Heidinger, and S.Mayr.

The application of our new technique for rock thermal property measurements on more than 80,000 core samples from deep, super-deep and industrial boreholes with depths of 1,600 to 12,262 m have allowed us to compile a large rock thermal property database that accounts for rock anisotropy and heterogeneity, as well as formation pressure and temperature.

New technique for measurements of rock thermal properties

Numerous laboratory instruments for the measurement of rock thermal properties have been developed over the years, but most suffer from one or more of the following shortcomings:

1. influence on results due to the contact between rock sample and equipment, particularly for porous and fractured rocks,

2. poorly defined metrological parameters due to instrument uncertainty, more than 8% in most cases,

3. inability to account for rock heterogeneity and anisotropy due to selective and discreet sampling,

4. inability to measure thermal conductivity and thermal diffusivity simultaneously, moreover at formation pressure and temperature,

5. difficulty in conducting non-destructive measurements on samples,

With this in mind, we have developed a new tool that alleviates these problems.

Technique for non-destructive measurements on cores under laboratory conditions

The optical scanning method and instruments were developed for non-contact, non-destructive measurements of thermal conductivity and thermal diffusivity of rocks and minerals (Popov, 1983; Popov et al., 1999). This technology allowed us to provide economical, fast, detailed and reliable data of thermal conductivity, thermal diffusivity and volumetric heat capacity measured on thousands of cores from many scientific boreholes. In turn this data, along with corresponding thermal gradients permitted us in calculating heat flow values at 25-100 m intervals along every borehole.

A series of theoretical and experimental investigations was carried out to evaluate the potential of the optical scanner, leading to the construction of various prototypes. The principle of the optical scanner is based on scanning the surface of a sample with temperature sensors, in combination with a focused, mobile and constant heat source. The heat source and sensors move with the same speed relative to the sample and at a constant distance from each other (Figure 1). The contactless nature of the measurements ignores the influence of thermal resistance between rock sample, heat source and sensors thus providing high precision measurements.
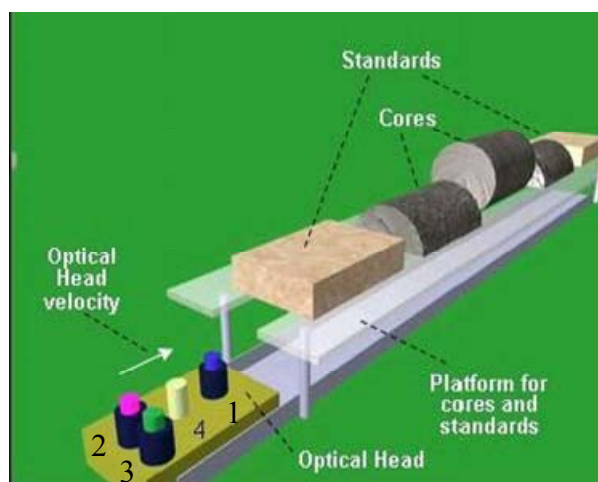
Figure 1: Schematic of the optical scanning device.

After scanning along three non-collinear and non-coplanar directions which are located on two non-parallel planes, the optical scanning technology permits to determine the thermal conductivity. For a sample with two-dimensional anisotropy, the principal values of conductivity can be determined from two non-collinear scans on one face, if this face is not parallel to the foliation. Thermal diffusivity tensor components of the samples under study are determined simultaneously.

The benefits of using the optical scanning method include: (1) short measurement time, typically 10 to 30 seconds, (2) contactless mode of measurement, (3) ability to measure on a flat or cylindrical sample surface, (4) ability to measure full core and core plugs, moreover without mechanical treatment, (5) simultaneous measurement of thermal conductivity and thermal diffusivity, (7) estimation of heterogeneity of rock samples, (8) high precision,1.5%, and accuracy, 1.5%, with a confidence probability of 0.95, of thermal conductivity measurements within the range of 0.1-70.0 $Wm^{-1}K^{-1}$, (9) high precision, 2%, and accuracy, 2%, of thermal diffusivity measurements within the range of $0.1x10^{-6}$ - $5.0x10^{-6}$ m^2s^{-1}, (10) large range of shape and sample sizes (1 cm to 70 cm in sample length).

A portable version of the instrument (Figure 2) was developed for measurements on full cores in laboratory and core storage facilities (Popov et al., 2012a). A laser version of the instrument was also developed for measurements on core plugs and small samples of rocks, typically 10x10x10 mm and larger, (Figure 3) (Popov et al., 2012a). An additional thermal scanner was also developed for high-resolution rock heterogeneity profiling on dry or fluid-saturated samples (Popov et al., 2012b). The

spatial resolution of thermal heterogeneity profiling is ~0.2 mm (Figure 4). All versions have the ability to measure simultaneously thermal conductivity and thermal diffusivity.

Figure 2. *Field optical scanning instrument for rock thermal property measurements on full size cores.*
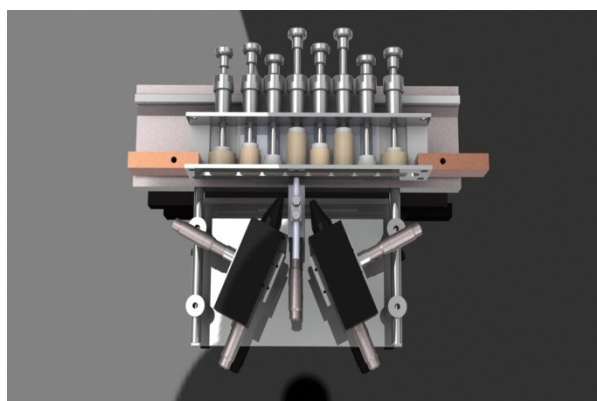
Figure 3. *Laser optical scanning instrument for thermal property measurements on core plugs.*

Measurements can be carried out on dry or fluid-saturated samples. In the case of cylindrical samples, scans are oriented along the core axis. Surface roughness of up to 1.0 mm is acceptable. In general, it is not necessary to polish the surface of the sample. However if the scanned surface is too rough, systematic errors can be corrected based on results from reference standards with a similar rough surface. The working surface of the sample is covered with an optical coating (25-40 μm thick) in order to minimize the influence of varying optical reflection coefficients. An important feature of the technology is the ability to change the thickness of the investigated surface layer depending on sample size and purpose of the experiment. In effect, a change of scanning speed and modifying the distance between the heat source and the sensors will permit to measure different thicknesses of the surface layer. The surface layer thickness also depends on the thermal properties of the sample and may reach 20-30 mm or more for samples with thermal conductivity exceeding 6-7 $Wm^{-1}K^{-1}$.
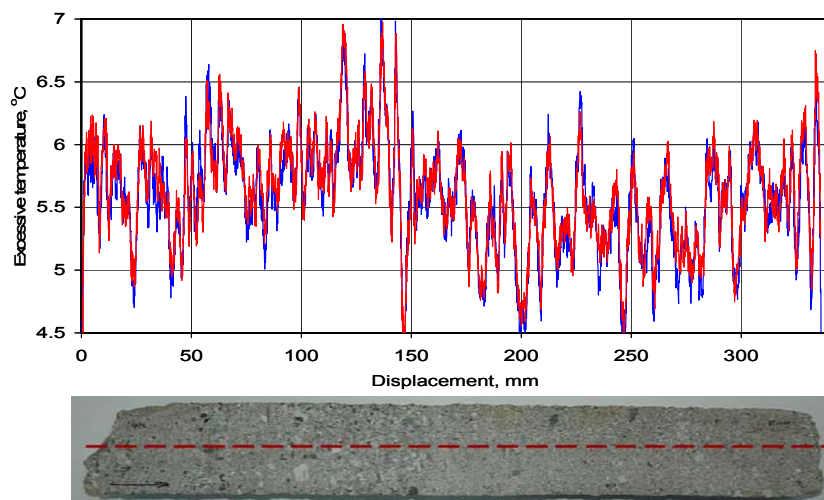
Figure 4: Reproducibility of high resolution optical scanning profiling results: temperature profiles (blue and red in the top graph) of two independent optical scans performed on the same gravelly sandstone sample.

After the scanning is completed, the following information is available for each sample:thermal conductivity, thermal diffusivity and volumetric heat capacity profiles along a single scanning line. In the case of two measurement, perpendicular to each other, on the same sample, the following information is available: individual thermal conductivity and thermal diffusivity as well as effective thermal conductivity and effective thermal diffusivity with related anisotropy factor. The thermal heterogeneity factor is defined as the standard deviation of local thermal conductivity values along each scanning line divided by an average value of the thermal conductivity of the rock sample. The rate of measurements is between 50 and 70 measurements per hour.

The new methods and instruments described herein have been used to perform measurements on collections including in excess of 200 rock forming minerals (single crystals and aggregates) in order to correct and extend the database of thermal properties of minerals, including their anisotropy. This resulted in more reliable information for the interpretation of rock thermal properties and the variation of those properties.

The new technology has provided measurements on cores from deep boreholes with typical core sampling intervals of 1-2 m. Significant vertical variations in rock thermal properties were established in every case not only for crystalline rocks but for sedimentary rocks as well. Numerous measurements on cores drilled in different geological structures, including geothermal energy fields, have shown that thermal properties vary significantly not only within rock formations (meter scale) but within cores samples as well (millimeter scale). An understanding of thermal anisotropy of rocks is essential in most cases (with anisotropy coefficient up to 6; anisotropy coefficients of 1.2-1.5 are typical for many rock types). This requires thermal property measurements to determine the principal components of the thermal property tensor. Rock thermal anisotropy has strong incidence on heat flow density estimates and interpretation of heat flow density variations.

The optical scanning technology application also reveals correlations of thermal properties with other physical properties such as porosity, permeability, sonic velocity, and electric resistivity. Those correlations help in reducing the uncertainties of thermal properties due to rock heterogeneity and anisotropy. Vast new information about correlations between thermal and other physical properties were compiled from measurements of some 80,000 full size cores and core plugs drawn from different sedimentary and crystalline rocks (Popov et al., 2003).

Technique for thermal property measurements at elevated pressure and temperature

The influence of in-situ rock formation pressure and temperature was also considered in the application of the instruments developed for rock thermal property (Popov et al., 2010). New research, both experimental and theoretical, was developed in addition to optical scanning technology to determine simultaneously thermal conductivity, thermal diffusivity and volumetric heat capacity of dense, highly porous and fractured rocks and non-consolidated rocks at formation thermo-dynamical conditions.

The instruments are now capable of measuring thermal conductivity (TC) and thermal diffusivity (TD) under the influence of temperature (up to $250^{o}C$), pore pressure, and two-component lithostatic pressure (up to 200 MPa). A novel approach in line-source method has been devised to provide simultaneous measurements of TC and TD tensor components within a single measurement cycle. Measuring thermal properties of rock samples, in a laboratory environment, to reflect those of in-situ rock formation is a complex problem since no reliable references exist. In our instance metrological testing of the instruments has been performed on set of 6 reference glass samples identical to those studied in industrial thermal physics: Pyroceram®, marbles, natural and synthetic single-crystal quartz with TC and TD values within ranges of respectively 0.71-10.7 $Wm^{-1}K^{-1}$ and 0.557×10^{-6} - 5.42×10^{-6} $m^2 s^{-1}$ (Popov et al., 2010). In addition, natural single-crystal quartz has been used as a reference for assessing the anisotropy of thermal conductivity and thermal diffusivity.

New data on heat flow density (HFD)

Temperature gradient recovery up to equilibrium occurs essentially faster than it was assumed earlier. The rate of temperature gradient recovery was found to be different for different formation layers (Popov et al., 1999). For some parts of a given formation the temperature gradient may reach equilibrium practically upon completion of drilling or fluid injection. This allows to determine a relatively robust heat flow density (HFD) value from temperature measurements performed in boreholes immediately upon completion of drilling. On the other hand an accurate estimation of formation recovery time profile along a borehole – and this implies several temperature measurements over time – can provide valuable information about the distribution of reservoir properties from the temperature logging data.

In most cases a correlation between temperature gradient and thermal conductivity determined for short depth intervals along the borehole does not follow the Fourier Law for steady-state conductive heat transfer. In other words it can be shown that vertical variations in temperature gradient do not correspond to the vertical variations in thermal conductivity. This implies that heat transfer in a formation of significant depths (more than 2-4 km) may not be in steady state and/or not purely conductive as routinely assumed. It was found in some instances that transient heat transport could be explained by active fluid migration as confirmed from hydrogeological data.

Thermal conductivity data with core sampling 1-2 m allowed us to determine a conductive component of the HFD within every 25-100 m interval along every borehole under investigation. Significant vertical variations in the HFD conductive component were established for all boreholes. The conductive component of the HFD can vary as much as 70-100%. Continental heat flow density values established from measurements in scientific deep and super-deep boreholes exceed significantly (in most cases by 30-100%) previous experimental estimates for shallow boreholes (see the Table 1 below). Similar heat flow density behaviours were established from measurements of the KTB super-deep borehole (Huenges and Zoth, 1991; Clauser et al., 1997).

Table 1: Heat flow density values estimated from temperature gradients and measured rock thermal conductivities.

Borehole	Depth reached, m	Formation type	Amount of cores for thermal property measurements	New data on heat flow density, W/m^2. Depth interval used for HFD estimation	Previous heat flow density estimates from measurements for shallower boreholes, W/m^2
Kola SG-3 (Russia)	12,262	Crystalline rocks	8,250	55-63 5,200-7,600 m	31-39
Ural SG-4 (Russia)	5,355	Folded area	4,414	57-64 3,000-4,000 m	21-28
Timano-Pechora (Russia)	6,904	Sedimentary basin	383	60-72 4,000-5,000 m	38-54
Kolva (Russia)	7,057	Sedimentary basin	1,016	63-78 5,200-6,000 m	36-47
Tyumen SG-6 (Russia)	7,502	Sedimentary basin	1,243	75-90 3,900-6,700 m	52-60
Tyrnyaus (Russia)	4,001	Crystalline rocks	1,008	135-165 1,300-1,500 m	85-120
Vorotilovo (Russia)	5,374	Impact structure	3,715	53-56 3,200-5,300 m	40-49
Saatly SG-1 (Russia)	8,200	Sedimentary basin	225	40-50 6,000-7,000 m	30-37
Noerdlingen-72 (Germany)	1,206	Impact structure	652	90-95 900-1,200 m	65-70
Yen-Yakha (Russia)	8,350	Sedimentary basin	383	78-96 6,000-8,000 m	52-60
Yaxcopoil-1	1,650	Impact structure	658	80-95 1,200-1,600 m	55-60
Eyreville (USA)	1,770	Impact structure	596	75-80 900-1,100 m	42-52
Yaxcopoil-1 (Mexico)	1,511	Impact structure	451	75-90 800-1,400 m	35-50

The vertical variations in HFD were further confirmed with new experimental data for boreholes Severo-Molokovo, Vysokovo, and Yarudeyskaya, as well as from the revision of previous experimental geothermic data from the Moscow Syncline (the East European platform) and the Ural region. The new results obtained from studying vertical variations in the heat flow density demonstrate an increase (30-60%) of the conductive component of the heat flow density within depths of 2,000-3,000 m. Comparing vertical distributions of heat flow density from historical experimental data for the Moscow Syncline, to those of our recent experiments allowed us to find similar trends whereby heat flow density increase with depth. Our recent estimates of HFD for the Moscow Syncline are 55-77 mW/m^2 and exceed the previous data (42-59 mW/m^2).

Experimental data for four impact structures – Puchezh-Katunk (Russia, Vorotilovo super-deep borehole), Ries (Germany, Noerdlingen-72 borehole), Chicxulub (Mexico, Yaxcopoil-1 borehole) and Chesapeake (USA, Eyreville borehole) – demonstrate an uneven distribution of the HFD along the boreholes. For Noerdlingen-72 a sharp HFD increase (up to 130 mW/m^2) is observed within a depth interval of 100-230 m. The HFD value then decreases to 66 mW/m^2 below, followed by an increase to 77 mW/m^2 within a deeper depth interval down to 1,150 m. This significant increase in HFD with depth

is also observed within the first 2,000 m of the Vorotilovo super-deep borehole. The combination of high quality data, both thermal conductivity and temperature gradient, for the Yaxcopoil-1 borehole allowed us to establish not large but a statistically significant trend in the HFD with variations from 55 to 95 mW/m^2.

Heat flow density estimates produced by experimental data from scientific deep and super-deep boreholes can significantly change our understanding of the nature of the thermal regime in the shallow crust. Our estimates demonstrate that the correct determination of terrestrial heat flow density requires boreholes of sufficient depths, detailed information on the vertical distribution of thermal conductivity and temperature gradient, thermal equilibrium of the rock formation under study and information about the variations in the temperature gradient, whether those variations are induced by advective heat transport, or time-dependent transient signals.

Conclusions

The optical scanning technology provides continuous, non-contact, high-resolution profiling of rock with simultaneous measurements of thermal conductivity and thermal diffusivity on anisotropic and heterogeneous rock samples.

Thermal heterogeneity of rock formations revealed from numerous thermal measurements demonstrates the necessity of a representative core collection with detailed core sampling along boreholes for shaping meaningful heat flow density estimates.

The new optical scanning instrument allows to determine simultaneously the thermal conductivity and diffusivity tensor components at elevated temperatures and pressures (pore, axial and confining pressure), in an attempt to replicate in-situ rock formation conditions.

Averaging thermal conductivities and thermal gradients over long depth intervals can lead to an underestimation of the heat flow density values.

An increase in heat flow density with depth is observed within the upper portions of most of the drillholes investigated, along with significant local variations.

New experimental data on the conductive component of heat flow density obtained from deep and super-deep boreholes shows that previous experimental data obtained from shallower boreholes of the same region are significantly underestimated.

References

Clauser, C., Giese, P., Huenges, E., Kohl, Th., Lehmann, H., Rybach, L., Safanda, J., Wilhelm, H., Windloff, K., Zoth, G., 1997. *The thermal regime of the crystalline continental crust: Implications from the KTB*. J. Geophys. Res. 102 (B8), 18417-18441.

Huenges, E., Zoth, G., 1991. *KTB Oberpfalz VB: temperature, thermal conductivity, and heat flow density*. Sci. Drilling, 2, 81-89.

Popov, Y., 1983. *Theoretical Models of the Method of Determination of the Thermal Properties of Rocks on the Basis of Movable Sources.*" Geologiya i Razvedka (Geology and Prospecting). 9, 97–105 (in Russian).

Popov, Y., Pevzner, S., Pimenov, V., and Romushkevich R., 1999. New geothermal data from the Kola superdeep well SG-3. Tectonophysics, 30, 177-196.

Popov, Y., Pribnow, D., Sass, J., Williams, C., and Burkhardt, H., 1999. *Characterisation of rock thermal conductivity by high-resolution optical scanning.* Geothermics, 28, 253-276.

Popov, Y., Tertychnyi, V., Romushkevich, R., Korobkov, D., and Pohl, J., 2003. *Interrelations between thermal conductivity and other physical properties of rocks: Experimental data.* Pure and Appl. Geophys. 160*, 1137-1161.

Popov, Y., Bayuk, I., Parshin, A., Miklashevskiy, D., Novikov, S., and Chekhonin, E., 2012a. *New methods and instruments for determination of reservoir thermal properties.* Proceedings of 37th Workshop on Geothermal Reservoir Engineering, Stanford, California, USA.

Popov, Y., Parshin, A., Chekhonin, E., Gorobtsov, D., Miklashevskiy, D., Korobkov, D., Suarez-Rivera, R., and Green, S., 2012b. *Rock Heterogeneity from Thermal Profiles using an Optical Scanning Technique.* Proceedings of 46th US Rock Mechanics / Geomechanics Symposium, Chicago, IL, USA.

Geothermal potential of the crust - the role of the Underworld

Quenette, S.[1], Beall, A.[1], Mather, B.[1], Moresi, L.[1]

[1]Monash University

steve.quenette@monash.edu

Abstract

Exploration for conventional reservoirs has been relatively easy, with expressions of resource found close to or even at the surface. Conversely, exploration for non-conventional systems relies on inherently increasing temperature with depth and the search for favourable geological environments that maximise the utility of this increase. Hence the research interest in broad geological settings. Unfortunately the confidence in our geological knowledge rapidly decreases with depth — we cannot readily or cost-effectively sample at depths beyond (lets say) a kilometre; drilling becomes far too expensive to achieve high lateral spatial resolution, and other remote sensing techniques suffer from loss of detail as we probe to further depths and through impeding materials. Can we employ more tools to refine our confidence?

Our group's approach has been to broaden and maximise the utility of information we do have (i.e. the joint geological-, geophysical- (and so on) data and models), and its assimilation with physics that capture the dominant underlying processes applied over heterogeneous and anisotropic regions. One can then reason on error, uncertainty and appropriateness of the processes within the constraints imposed by the data but in the context of favourable expressions at depth.

Here, we discuss computational modelling approaches to exploration, with application to geothermal reservoirs within basins or systems of basins. We discuss the software tool Underworld and its role in the process of questioning. We give examples in the different data-centric geothermal regimes of shallow heat-flow & temperature, and spatially distributed geotherm profiles. We also discuss the role of data-assimilation and sensitivity analysis as conduits to understanding uncertainty for various provinces of eastern Australia.

Underworld

Underworld (Moresi *et al*. 2007) is a 3D parallel geodynamic forward modelling framework, capable of deriving viscous / viscoplastic thermal, chemical and thermochemical models. It is highly adaptable software based on the *StGermain* (Quenette *et al*. 2007) implementation of a novel approach to programming. The *StGermain/Underworld* combination is designed specifically for families of related software for high performance computing. That is, scaling out the spatial dimensions from the reservoir scale to basins and systems of basins is a key property.

A fundamental differentiator of *Underworld* is the use of the Lagrangian Particle-In-Cell Finite Element Method, of which *Ellipsis* (Moresi *et al*. 2003) were the prototypes. It uses PETSc optimised numerical solvers (Balay *et al*. 1997, 2011), the MPI interface (Gropp & Lusk, 1996), and is regularly used at 100s and 1000s of processes for complex geodynamics-oriented simulations. *Underworld-GT* (Quenette et al. 2010) is the toolbox specialisation of *Underworld* that provides easier to use interfaces to the heat and fluid flow equations. *Underworld* also provides gLucifer, which enables the rendering of visualisations whilst computing (see Figure 1).
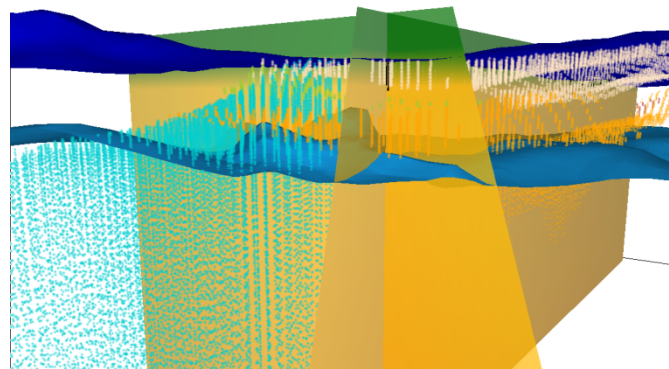
Figure 1: *A key property of Underworld is its ambidextrous ability for both mesh and particle reference frames. Shown here is a model with cut-planes at a borehole, with material displayed as particles, topography and an isotherm.*

Underworld-GT piloted the ability to import stratigraphic layers in the form of ASCII-CSV data, or GoCAD and Geomodeller voxel sets into *Underworld*. A similar mechanism has been used for seismicity data and topography data such as SRTM (Farr et al. 2007), and leading the development of an *Importer* toolbox to *Underworld*. *Underworld-GT* also includes a drill-core plugin, which is used to describe the location, length and orientation of synthetic drill-cores, as well as sampling information for results.

Questioning

Here we are interested in two facets of modelling. We are interested forward models of geothermal potential given novel abstractions of geology and physics, and we are interested in geothermal potential in terms of assessments with characterised uncertainty. Hence Underworld is a tool that enables an expert geologist to augment their intuition with physically based model exploration, through discrete uncertainty measures. Through the following examples we will demonstrate some of these facets.

Example 1 – Western Victoria

In this example we present part of three detailed models for Western Victoria: The Murray Basin, Otway Basin (see Figure 2), and Stawell models. Heat-flow measurements in these provinces suggest a highly heterogeneous near-surface heat-flow regime. Of interest is the geology (and the degree to which geology) at depth influences this near-surface regime. For this we calculate conductive heat transport using Underworld. Its flexible boundary conditions, for example, enable spatial heterogeneity of basal heat-flow. We then express uncertainty using parameter sensitivity and validation against near-surface publically available data.
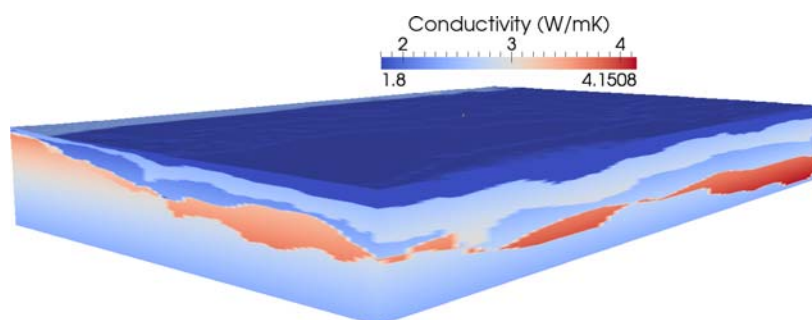
Figure 2: *is the modelled effective conductivity of the Otway basin, one of three basins under investigation in Western Victoria, and using one of several variable conductivity models.*

Results show that the distribution of crustal heat producing elements (HPEs) related to buried Proterozoic crust is an important influence on surface heat-flow variation and is complicated by lateral heat-flow effects. These models infer an anomalously high transient mantle heat-flow contribution.

Example 2 – Sydney Gunnedah

In this example, heat flow assessments are made for the Sydney and Gunnedah basin systems (Danis et al. 2010 & 2011), where for the Sydney basin approximately 50 drill-core thermal profiles (of 5 to 10 measurement points each) are available as constraints. We employ a data-assimilation approach, which produces optimal model conductivity and heat production as a distribution of misfits between the forward model actual down-hole temperature logs within a constraint. Similarly, sensitivity of the model resolution itself is assessed and controlled. Both contribute to the need for high performance computing.

Results show that consistency can be found across the spatially varying observation data, but also highlight regions of poor confidence or fit. Maps of temperature and variance at depth are also generated.
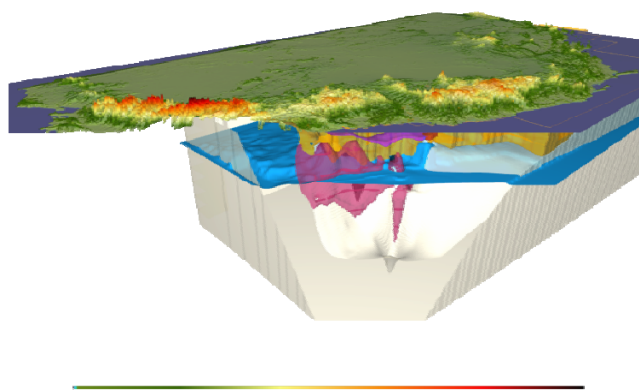
Figure 3: is a view of the Sydney-Gunnedah basin model with a topography overlay. This particular model also covers the Bowen basin region, a total area of 2000x1000kms. Each forward model realisation takes approximately 3minutes on 128processors on the NCI NF facility.

Closing remarks

Through Underworld, and as demonstrated by these examples, dynamical systems (such as heat flow) can be used to provide further confidence on geological models. Thus augmenting existing and well-established methods for exploration.

References

Balay S., Eijkhout V., Gropp W.D., McInnes L.C. & Smith B.F. 1997. Efficient Management of Parallelism in Object Oriented Numerical Software Libraries. In: E. Arge, A.M. Bruaset & H.P. Langtangen (Editors) Modern Software Tools in Scientific Computing. Birkhauser Press, 163-202.

Balay S., Buschelman K., Gropp W.D., Kaushik D., Knepley M.G., McInne, L.C., Smith B.F. & Zhang H. 2011. Portable, extensible toolkit for scientific computation. <http://www.mcs.anl.gov/petsc> (accessed 14 September 2011).

Danis C., O'Neill C. & Lackie M. 2010. Gunnedah Basin 3D architecture and upper crustal temperatures. *Australian Journal of Earth Sciences* 57, 483-505.

Danis C., O'Neill C., Lackie M., Twigg L. and Danis A. 2011. Deep 3D structure of the Sydney Basin using geophysical modelling. *Australian Journal of Earth Sciences* 58, 517-542.

Gropp W.D. & Lusk E. 1996. User's guide for mpich a portable implementation of MPI, ANL-96/6.

Farr, T. G., et al. (2007), The Shuttle Radar Topography Mission, Rev. Geophys., 45, RG2004, doi:10.1029/2005RG000183

Moresi L., Dufour F. & Mulhaus H.-B. 2003. A Langrangian integration point finite element method for large deformation modeling of viscoelastic geomaterials. *Journal of Computing Phys*ics, 184, 476–497.

Moresi L., Quenette S., Lemiale V., Meriaux C., Appelbe B., & Mulhaus H.-B. 2007. Computational approaches to studying non-linear dynamics of the crust and mantle. *Physics of the Earth and Planetary Interiors* 163, 69-82.

Quenette S., Moresi L., Sunter P.D. & Appelbe W.F. 2007. Explaining StGermain: an aspect orientated environment for building extensible computational mechanics modelling software. HIPS Workshop, Parallel and Distributed Processing Symposium, Proceedings of the 19th IEEE International.

Quenette S., Moresi L. 2010. Models based experimentation: numerical modelling of 3D basin scale architecture heat & fluid flow. AGU Fall Meeting Abstracts

Bayesian data fusion for geothermal exploration

Ramos, F.T. [1], Bonilla, E. V. [2,3], McCalman, L. [2], O'Callaghan [2], S., Reid, A. [2], Uther, W. [2], Sambridge, M. [3], and Rawling, T. [4]

[1]University of Sydney, [2]NICTA, [3]Australian National University, [4]University of Melbourne

fabio.ramos@sydney.edu.au

Project description

The process of finding the best locations for drilling in geothermal exploration requires the collection of vast amounts of information. Gravity, magnetism, seismic reflection, radiometric, magnetotellurics and drilling data are commonly used to infer specific properties of rocks such as temperature conductivity, permeability, porosity, density and fracture levels. The availability of the data does not necessarily ensure their best usage. From a statistical perspective, it is desirable to determine the degree of dependence between each of the data sources to fuse them in a single estimation framework for all the rock properties. This ensures the correct quantification of the predictive uncertainty, which leads to risk minimisation in drilling and better decision-making. This work aims to organise the information available in Australia for geothermal activities and develop a novel statistical framework for data fusion and joint estimation of rock properties relevant to the industry.

Methodology

The approach is divided into two main components; 1) the collection and organisation of the data in a data portal; and 2) statistical methods for join inversion and characterisation of geothermal targets. More details on these developments are presented below.

The Portal

A unique property of our machine learning techniques is that data from different sensors can be fused simultaneously and automatically. To facilitate this, we developed a portal system that could provide all available data from any sensors given a particular region in a single, machine-readable format suitable for the inference software.

Traditionally, datasets are stored in a variety of text-based and binary formats depending on the type of sensor (ArcGIS, ERS, SEG-Y etc.), in different projections and with idiosyncratic labelling systems. We saw the need for an open data format, which was flexible enough to allow different kinds of sensor or simulation data to be stored together and represented in a self-describing way. The format should be universal enough that a variety of open-source tools for reading it already existed. The HDF5 data format (www.hdfgroup.org) meets all these requirements and was chosen as the portal's output.

Communication with the portal occurs via a simple HTTP-based interface. Software can easily implement control of the portal directly, and we have also written a web front-end that allows the user to select, visualise, and download available datasets in a single HDF5 file, ready for input into our data fusion software. We also anticipate being able to serve and visualise results from our algorithms using this system.

Bayesian data fusion

The second phase of the project consists of developing the data fusion engine using statistical machine learning, in particular, nonparametric Bayesian methods (see e.g. Rasmussen and Williams, 2006). Nonparametric Bayesian methods are flexible and principled approaches to modelling

uncertainty in real-world problems, allowing the incorporation of information from various sensor modalities and different types of prior knowledge. Moreover, these techniques have the advantage of automatically determining statistical dependencies between input measurements (e.g. observations of the gravitational and magnetic fields) to jointly estimate other parameters involved in the underlying physical process (e.g. density and magnetic susceptibility).

Our first step towards the development of a unified non-parametric Bayesian framework for data fusion in geothermal exploration is the construction of probabilistic models for geophysical inversion problems. Our goal here is twofold. Firstly, we want to develop more accurate joint inversion methods that allow us to reason about physical properties of the earth by exploiting commonalities between different sensor modalities (e.g. gravity, magnetics, seismic) and by using prior information (e.g. from geological studies of a specific region). Secondly, we aim at *quantifying the uncertainty* of the different variables in the process. For example, rather than placing hard constraints on parameters based on previous geological studies, we can introduce this information probabilistically in our models. More importantly, the output of our methods is, in general, a full distribution over the parameter of interest.

Our methods can avoid over-fitting (i.e. poor generalization, see e.g. Mackay, 1992) and enable the use of kernels that capture nonlinear relationships, providing a simple but effective platform for multi-task learning and sensor data fusion in spatial stochastic processes.

These methods have opened major opportunities to overcome the challenges by extending the applicability of machine learning techniques to large-scale exploration problems, integrating data acquisition and data acquisition in a principled and unifying statistical model.

Geophysical Inversion with Gaussian Processes

Given a set of measurements such as gravity, magnetics and seismic data, and the location where they were obtained, a Gaussian process (GP) prior is placed over the space of functions mapping spatially dependent geophysical quantities (such as density) to measurements. Our goal is to reason about these quantities probabilistically. Hence we perform inversion by conditioning the distribution of the corresponding property (or parameter) on the observations yielding a posterior distribution that balances prior knowledge and data fit. The result is a probability distribution over the inverted quantity (for example, density) for any point in space. The method produces continuous outputs with an associated uncertainty, which can be used, for example, to reason about optimal locations where to acquire more measurements or to figure out the locations where to carry out new explorations (drilling) so that a predefined risk that depends on the desirable properties is minimized.

Results to date

Portal

The portal is the pipeline that feeds geophysical and geological datasets into our data fusion algorithms. As such, the first stage of the pipeline is to convert incoming files into a unified internal representation suitable for further processing. We currently use HDF5 for this internal representation, though as the volume of data stored increases a distributed file system might be chosen. The file importers also add metadata attributes such as the bounding box, sensor type, creation date, and description to a database, used by the backend to facilitate queries and requests.

The portal backend connects to this database and uses it to serve requests for a collection of datasets in a particular region. The communication protocol is an HTTP-based REST interface, a stateless protocol using URL requests easily implemented in a variety of languages. When a request is received by the backend, it opens the associated HDF5 files of all requested datasets, crops them to the region of interest, then re-writes a new HDF5 file that contains all this data in a single file. That output file is then sent to the user as a download.

Even though we anticipate our software directly interfacing with the portal system, we have developed a web interface to facilitate members of the geothermal community exploring the available data. The interface has standard functionality such as an interactive map that can be panned and zoomed with the mouse. Geo-referenced visualisations of the datasets and their bonding boxes are automatically

overlaid when selected. Regions of interest can be chosen on the map either by clicking and dragging with the mouse or entering co-ordinates directly. Check-boxes for each available dataset allow the user to determine the contents of the output file, which is collated on the server when the user hits 'download'. See Figure 1 for a screen-shot of the portal web interface.
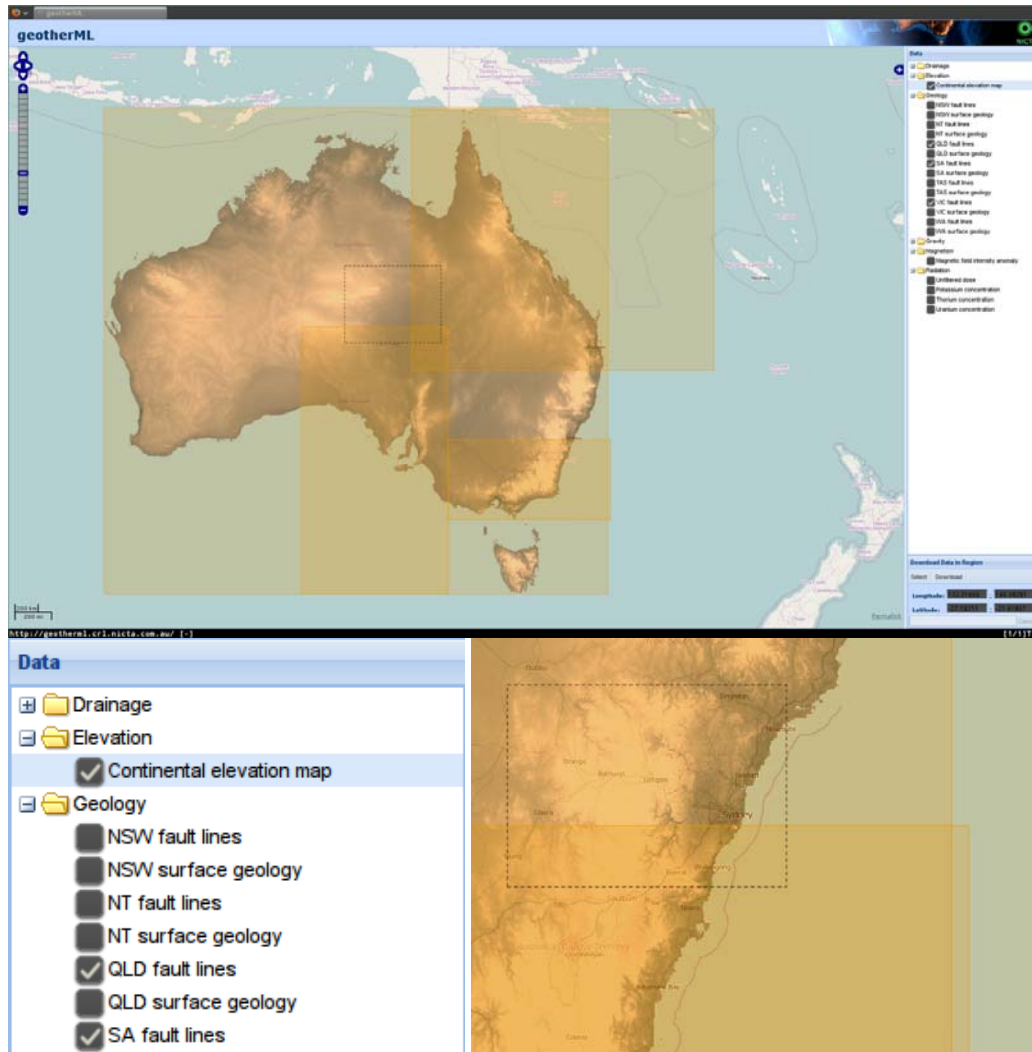
Figure 1: *Screenshots from the portal web interface. (Top) A figure depicting the portal web interface. A list of datasets is on the right, with check-boxes for selecting those in which the user is interested. The bottom right contains tools for selecting data in a region with the mouse, or entering lat/long coordinates manually. The central pane contains a zoomable visualisation including partially transparent shaded bounding boxes of the checked datasets, and a dotted line indicating the selected region. (Bottom left) A close-up of the list of datasets with checkboxes. (Bottom right) A close-up of a selected region on the map, with two overlapping bounding boxes and a region around Sydney currently selected.*

The portal is currently populated with representative datasets from Geoscience Australia, state governments, and geothermal companies. Data acquisition and conversion into the portal system is ongoing, but datasets with existing support include all public gravity station data, surface geology and fault lines from all states, and high-resolution gridded magnetics, topographics and radiation. We have already acquired and are currently in the process of converting additional magnetics, 2- and 3-D seismic lines, magnetotellurics, depth-to-basement models, various drill-hole measurements and micro-seismic. We anticipate eventually collecting all available data relevant to the geothermal exploration problem in Australia.

Inversion of gravity and magnetics with drill hole data

In this section we present preliminary results of our nonparametric Bayesian inversion method on a synthetic experiment regarding gravity data when additional magnetic data are presented along with drill hole observations. The goal is to reason about the density of the underlying anomaly responsible for the observed data.
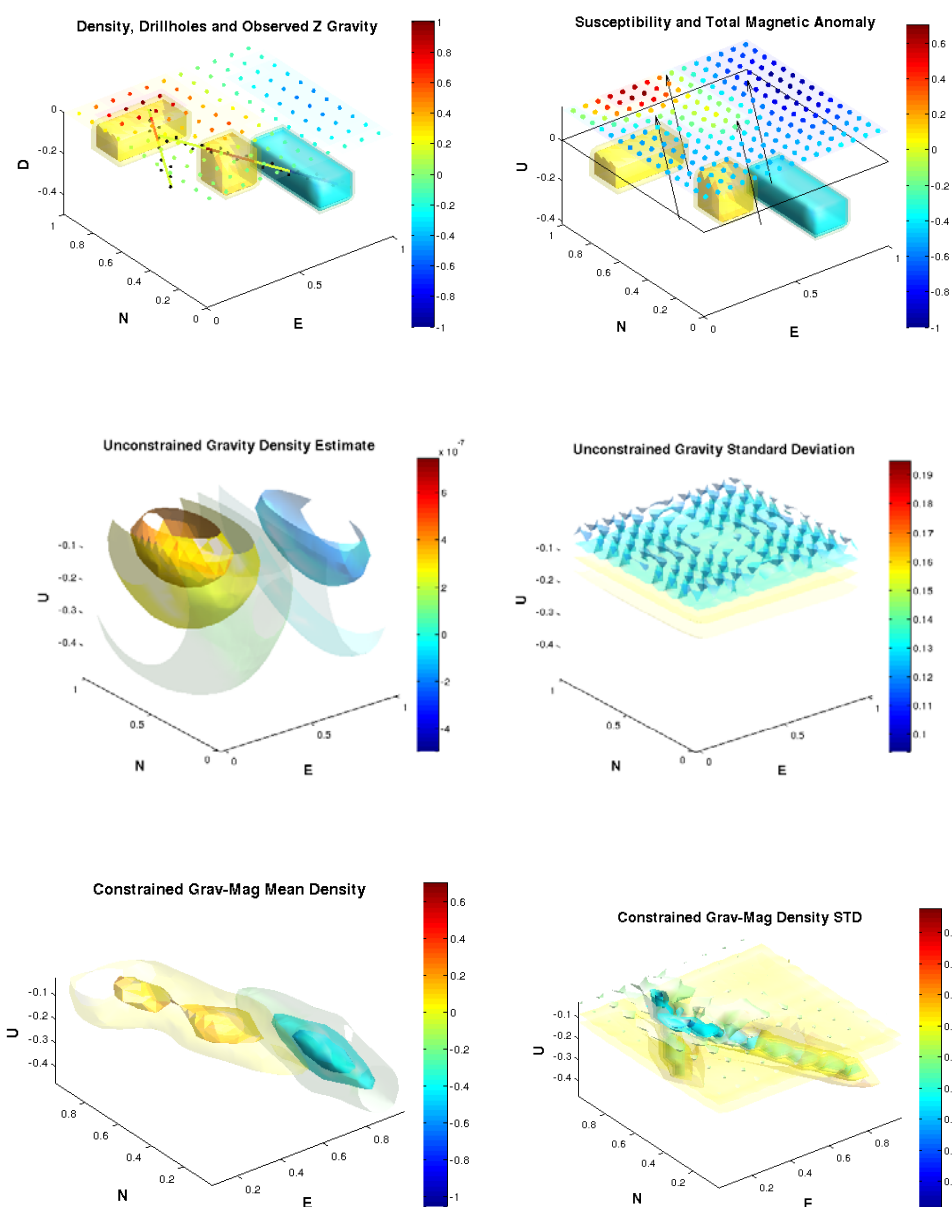
Figure 2: Density inversion scenario using a Matérn covariance function. (Top left) The density anomaly along with the gravity observations and drill hole observations. (Top right) Forward simulated Total Magnetic Anomaly observations for the same body. (Middle) Results of the unconstrained nonparametric Bayesian inversion with only gravity data showing the mean of the density distribution (left) and its standard deviation (right). (Bottom) Results of the nonparametric Bayesian inversion using gravity data, magnetic data and drill hole data showing the mean of the density distribution (left) and its standard deviation (right).

Figure 2 shows the results for a synthetic example of a density anomaly, the corresponding gravity observations and additional magnetic data and drill hole observations. These synthetic data have been generated with a linear forward model as in Li and Oldenburg (1998). Incorporating drill hole data in our model is straightforward as these can be considered as actual observations of the parameter of interest (i.e. density). Similarly, as our approach addresses probabilistic dependencies between the outputs (in this case gravity and magnetics) through the covariance (kernel) function, our technique provides a flexible way of performing joint inversions, where the relationships between the different modalities can be learnt from data.

We see that the constrained nonparametric Bayesian inversion, using drill hole observations and magnetic data, not only improves the quality of the mean of the density distribution but it also reduces the uncertainty around these predictions.

References

Li Y., and Oldenburg D.W., 1998. 3D inversion of gravity data. Geophysics, 63(1):109-119.

Mackay, D. J. C., 1992. Bayesian interpolation. Neural Computation, 4(3):415-447.

Rasmussen, C. E., and Williams C. K. I., 2006. Gaussian Processes for Machine Learning. MIT Press, Cambridge, Massachusetts.

Realisation of the geothermal potential of insulated coal basins: the challenge of integrated multi-use basin management.

Rawling, T.J. and Sandiford, M.

School of Earth Sciences, University of Melbourne

trawling@unimelb.edu.au

It is well known that coal is one of the best geological insulators with a thermal conductivity an order of magnitude lower than many other rock types. As a result basins that contain thick coal sequences have the potential to also contain valuable geothermal resources. A number of coal insulated basins exist in Australia, such as the Latrobe and Hunter basins. These basins have the added advantage that they already contain significant electricity generation infrastructure (coal burning generators) as well as associated power transmission capacity.

A number of geothermal companies currently have projects underway in these regions to develop both unconventional baseload geothermal systems a well as direct use applications associated with the existing coal-fired power generation systems, such as water pre-heating and coal drying.

However, geothermal energy is not the only new kid on the block in many of these basins and a number of other nascent energy industries are also trying to establish themselves alongside the traditional coal burners. These include geological storage of captured carbon, tight gas, coal gasification and liquefaction and coal seam gas. Each of these technologies is trying to utilise effectively the same pore space volume within the basin for very different ends, sometimes in a mutually exclusive manner. In addition they must also compete for the pore-space with other established users such as hydrocarbon extraction, mining, forestry and groundwater-based irrigation. In extreme cases multiple technologies are being deployed in exactly the same place (eg Buscheck et al. 2011)

A number of issues present themselves when it comes to developing "whole of basin" management strategies. The critical ones discussed here are:

1. Data quality, fidelity and coverage

2. 3D geological models

3. Integrated whole of basin simulation modelling fidelity

4. Risk modelling (financial as well as geological)

Data Quality. This would not seem to be a significant issue since it is clear that the traditional users of the deeper portions of these energy basins, the oil and gas industry, have generated vast geophysical and petrophysical datasets over the last 50 years. These datasets have been gathered at huge expense through geophysical data acquisition, drilling and mapping however they have limitations when it comes to applying them to the whole basin as they were typically gathered and developed with a very specific purpose in mind, usually the identification of exploration targets or the development of a known reservoir.

3D Geological Models. Similarly there are a variety of high quality 3D models available for the regions of these basins that are data rich and in particular those regions that contain significant petroleum resources (and as a result 3D seismic and drilling control). However very few, if any, high quality 3D models exist that contain enough detail to model interactions between various reservoirs as well as other locations within the basin where the pore-space may be used for other activities (ie groundwater use onshore, coal seam gas etc). There is a need to develop a new generation of sophisticated, high fidelity and high resolution 3D geological models of the whole basin that are designed exclusively for whole of basin modelling and management.
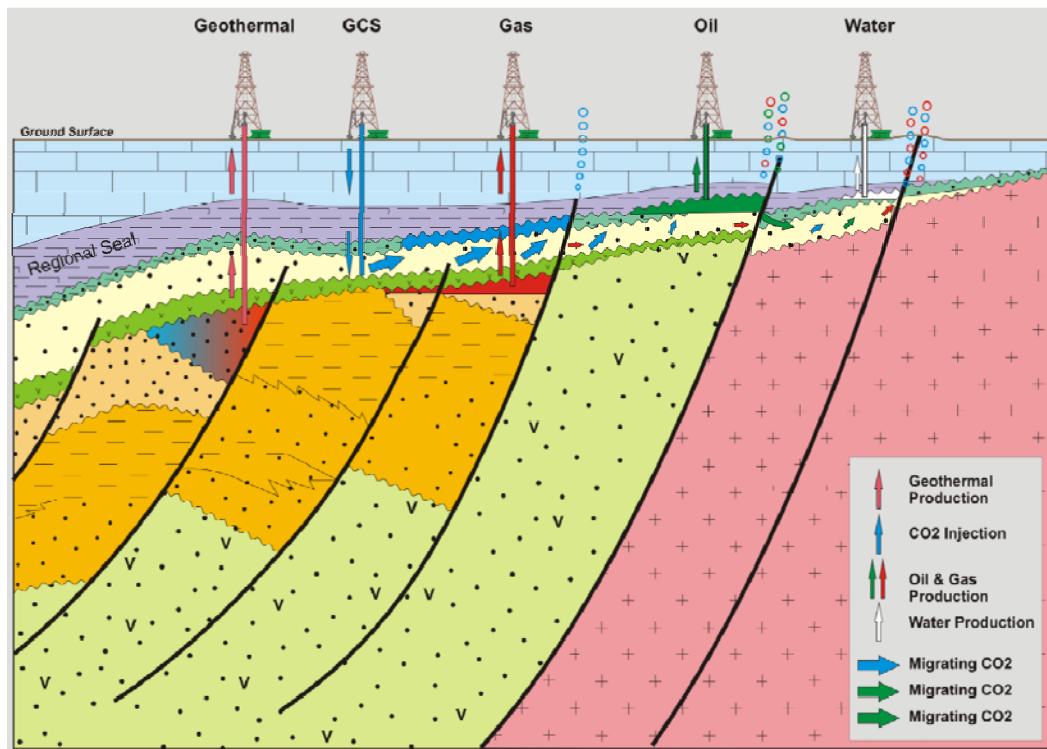
Figure 1. *Mutilple use of the pore-space within a basin. Diagram provided by the Victorian DPI.*

High Fidelity simulations. Once we have these 3D Geological models we are presented with our next dilemma. In order to successfully manage these basins what fluid and heat flow modelling software do we have access to that is scalable enough to allow us to model activity and interaction between these systems within the basins at the resolutions and timescales we need? Again a new generation of modelling software is required that will allow modelling of flow within narrow aquifer systems in groundwater and geothermal systems (potentially veins and faults on the 0.1 to 1m scale vertical) as well as interactions with larger reservoir systems offshore (on the 10 – 100m scale).

Risk modelling. Risk associated with new development in these basins will include both geological risk/hazard from things such as induced seismicity or indeed hazard associated with leakage of fluids to the surface. However risk in the basin management sense also includes risk to other developments due to activity or development. Understanding and planning these potential risks is critical to mitigate against sterilisation or damage to unrealised resources or accumulations.

Financial modelling. Finally and critically we need to integrate financial modelling with all these systems to be able to provide tools for making truly informed basin management systems. How do we value a reservoir that has potential for storing CO_2 today but may have a much higher value as a geothermal resource in the future?

We assess all of these issues and propose a way forward for the development of whole of basin datasets, models and management workflows so that informed basin management decisions can be made now and in the future that preserve the value of all of the new and traditional resources contained within the basin.

*References***:**

Buscheck Thomas A., Yunwei Sun, Yue Hao, Thomas J. Wolery, William Bourcier, Andrew F. B. Tompson, Edwin D. Jones, S. Julio Friedmann, and Roger D. Aines 2011. Combining Brine Extraction, Desalination, and Residual-Brine Reinjection with CO 2 Storage in Saline Formations: Implications for Pressure Management, Capacity, and Risk Mitigation. Energy Procedia 4 (2011) 4283–4290

Geothermal Energy in Australia Now

Klaus Regenauer-Lieb[1,2] and the WAGCoE Team

[1]CSIRO Earth Science and Resource Engineering. [2]The University of Western Australia

*corresponding author: Klaus.Regenauer-Lieb@uwa.edu.au

Introduction

Geothermal energy exploration in Australia has so far mainly focused on the future, however, little attention has been paid to the present, the geothermal opportunity on time scales as short as 3 years. The Western Australian Geothermal Centre was formed to address this overlooked opportunity and has completed the development of a number of novel technologies for the application of geothermal energy in not only electricity generation but also energy use displacement through 'direct heat' use. We use the unique opportunity of deep, hot sedimentary aquifers underlying the Western Australian coastline to underpin the promotion and execution of geothermal demonstration projects for this particular form of clean energy. We have delivered the first 3-D computer model (geologic and heat flow) of the entire Perth Basin focusing specifically on developing a high-resolution resource map for the Perth Metropolitan area. These studies have also delivered a complete and innovative workflow for geothermal resource identification with a fully quantified risk matrix for geothermal developments and industrial application. We propose to use the outcomes for an Australian initiative to build geothermal cities, starting with the opportunity of integrated power-water-heat solutions for remote areas and mine sites.

Geothermal Electricity Production in Australia now

The key problem in utilizing Geothermal Energy in Australia now lies in the unconventional nature of geothermal energy available in Australia. Other than the Undara Volcanic Province in Queensland and the Newer Volcanic Province (Mt Gambier System) in South Australia, there is no onshore volcanic system that is considered to be active. Therefore conventional (volcanic) geothermal energy is not a large-scale option for Australia. In the last decade over $0.5 Billion have therefore been invested in Australia to extract heat from the hot granitic basement which has the potential to deliver temperatures in excess of 200° C. The initiative has so far been partially successful but it is premature to assume that on the time frame of 3 years any of the current basement heat extraction schemes will be delivering electricity at scale to the grid.

The logical next step is to extract heat from the shallower sedimentary cover, which delivers heat with less than 200° C and often much lower. A simple consideration shows that for this temperature range electricity production alone does not make sense from an econo-thermal point of view. Figure 1 shows the theoretical limit of the efficiencies of binary cycle geothermal power plants using a trilateral heat engine and the real achieved efficiency (DiPippo, 2004). From an inspection of Figure 1 it becomes immediately apparent that the conversion of heat into mechanical energy and then electricity becomes less attractive for lower temperatures. We are throwing away at least 90% of the total heat content for the case of geothermal electricity production from hot sedimentary aquifers.
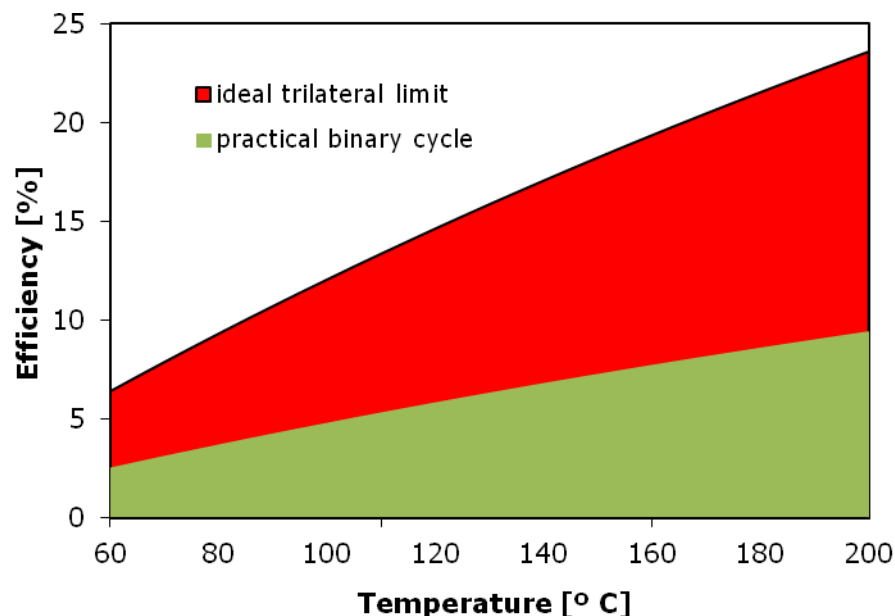
Figure 1: Theoretical limit and practical efficiencies of binary cycle heat engines used by the geothermal industry (diPippo 2004)

From an econo-thermal point of view it is not acceptable to throw away 90% of the commodity heat that the geothermal well is producing. In addition, there is expenditure for parasitic pumping energy, which must be subtracted from the 10% left over het converted to electricity if the sole purpose would be to produce geothermal electricity. This logic applies to all low-grade heat sources not just geothermal. However, in our current legislation clean electricity generation is considered as the only valuable one because of its societal acceptance, while its original form of energy, namely heat, is not appreciated.

One of the appealing concepts of electricity generation is that it makes heat/energy transportable in a refined form. How then can we use low-grade geothermal energy at scale in Australia now? There are two alternatives: i.) use heat directly (geothermal city concept, remote communities, mine sites) and avoiding the transport problem and , ii) use heat to drive a thermo-chemical process where the end product can be transported (e.g. geothermal desalination). Both alternatives were investigated by the Western Australian Geothermal Centre of Excellence. Highlights of the research done over the last three years are summarized below. WAGCoE has delivered a geothermal heat based energy system concept that can be used as a viable economical route to include electricity production as a by-product in a much broader heat based energy concept. The concept could become a template for a much broader national initiative to deliver geothermal energy to the Australian household. This strategy is ready to be deployed immediately.

Geothermal Energy System Concept in Australia now

The Western Australian Geothermal Centre of Excellence (WAGCoE) was a State Centre of Excellence (2009-2012) established to provide capacity within the State to lead the exploration and exploitation of geothermal heat in a modern society.

WAGCoE formed as an unincorporated joint venture between The University of Western Australia, CSIRO and Curtin University.

By exploring for and utilising low-grade heat in a permeable sedimentary environment, WAGCOE addressed an overlooked opportunity for broadening the footprint of geothermal energy utilisation in an urban environment.

WAGCoE's research programs aimed to:

- provide geothermal zero emission desalinated water

- enable technology to provide air conditioning and power energy to power 'geothermal cities'

- develop demonstration projects for a new era of energy development in WA

- deepen geological understanding and exploitation of sedimentary geothermal fields

- seed a major national initiative in geothermal.

WAGCoE provided a world-class research and training environment for students and professionals in geothermal energy systems and promote synergies between key strength areas in the WA geoscience community.

At the successful conclusion of WA State Government support in 2012, the WAGCoE core partners agreed to continue to collaborate in this field of research and build on the foundation successes of WAGCoE. This includes commitment to participate in the national Geothermal Research Initiative (GRI).

The key outputs of WAGCoE are summarised below:

1. The main international impact of WAGCoE is its recognition by the Geothermal Energy Association (GEA), which as a result of WAGCoE's work has identified Perth as one (number 5) of the top ten "Geothermal Cities" of the world.

    http://www.geo-energy.org/pdf/press_releases/Copenhagen_Release.pdf

2. Perth is entering the geothermal community with a new twist – as the first geothermally cooled city (Wang et al., 2013) with plans to test Perth's geothermal resources at depth and to demonstrate geothermally powered heating and air-conditioning units at the Australian Resources Research Centre and the adjacent Pawsey Centre. This project has brought approximately $20m of federal Education Infrastructure Fund (EIF) funding into the State and is currently being developed as a geothermal demonstration project by the CSIRO.

    http://ecogeneration.com.au/news/the_seska_geothermal_project/075448/

3. The core intellectual property (IP) generated by WAGCoE underpins the exploration and assessment of the unique geothermal resources of the deep, hot sedimentary systems underlying much of the Western Australian coastline, from Augusta to Geraldton (the Perth Basin) and other basins in the North such as the Carnarvon Basin, Canning Basin and the Bonaparte Basin as well as the inland Officer Basin. We have completed high level assessments of all Western Australian basins as well as the first 3-D computer model (geologic and heat flow) of the entire Perth Basin focussing specifically on developing a high resolution resource map for the Perth mMetropolitan area. These studies have also delivered a complete and innovative workflow for geothermal resource identification with a fully quantified risk matrix for geothermal developments.

    https://wagcoe.ivec.org/geonetwork/srv/en/main.home

4. The Centre was instrumental in building the national Geothermal Research Initiative founded in Perth in 2011 and is convening the Australian participation in the International Partnership for Geothermal Technologies, Reservoir Modelling Workgroup.

    http://internationalgeothermal.org/Working_Groups/Modeling.html

5. WAGCoE has had exceptional and high quality research research output both in terms of papers (in excess of 90 papers) and completed PhD's geothermal diploma/honours/masters programs as well as a curricula for annual short courses. Simultaneously WA 's State high school courses have been developed in collaboration with SPICE and EES. WAGCoE has already established a vibrant geothermal focus in WA most visible in the Western Australian Geothermal Energy Symposium (WAGES).

   http://www.wageothermalsymposium.com.au/

6. WAGCoE is also actively promoting new patents arising through the synergies between its key partners. One invention is the new concept of heat rejection into aquifer systems using the method of chaotic mixing (CSIRO funded). Another patented technology provides geothermal and low grade heat desalinated water (Wang et al., 2011) and is currently under construction and to be demonstrated both at the National Centre of Excellence for Desalination in Rockingham NCED and at a refinery plant in the south Perth Basin with UWA in the lead (NCED funded). The third invention entitled "Controlled Coupled Cracking" (C3) has been developed during the Premier's Fellowship of the WAGCoE Director and has be submitted as a provisional patent by CSIRO (CSIRO and UWA funded).

   http://www.patentmaps.com/inventor/Chua_Hui_Tong_1.html

The Centre has also been pursuing the support of remote and aboriginal communities with smaller scale geothermal projects to assist with Western Australia's unique public infrastructure challenges. Finally, the Centre has opened exciting opportunities to provide future large –scale off grid power and water infrastructure for securing the economic viability of the WA mining industry.

Geothermal research remains a vital and active component of the world-class geoscience precinct that exists in Perth. WAGCoE has been the catalyst to stimulate, accelerate and position the research capability in key research institutions in WA as well as nationally in an area of research, education and commercial demonstration that is fundamentally important to Australia's energy future.

References

DiPippo, R. (2004), Second law assessment of binary plants for power generation from low-temperature geothermal fluids, *Geothermics*, *33*, 565-586.

Wang, X., et al. (2013), Application of geothermal absorption air-conditioning system: A case study, *Applied Thermal Engineering*, *50*, 71-80.

Wang, X., et al. (2011), Low grade heat driven multi-effect distillation technology, *International Journal of Heat and Mass Transfer*, *54*(25-26), 5497- 5503.

The Paralana Engineered Geothermal Project – Case history and results of the hydraulic fracture stimulation

Peter REID[1], Mathieu MESSEILLER[1], and Michael HASTING[2]

[1] Petratherm Limited, [2] Hasting Micro-Seismic Consulting

preid@petratherm.com.au

Introduction

The Paralana Engineered Geothermal Project is located 600 kilometres north of the city of Adelaide in South Australia (Figure 1). The project is testing for viable geothermal sources generated by the radiogenic decay of high heat producing Mesoproterozoic basement rocks of the Mt Painter Complex (Figure 2). Petratherm Limited in joint venture with a major oil and gas company, Beach Energy, are initially seeking to build a 3.5 MWe commercial power development to supply a local off-grid mine, with the long term objective of providing large scale (300 MWe+) power through the national grid.
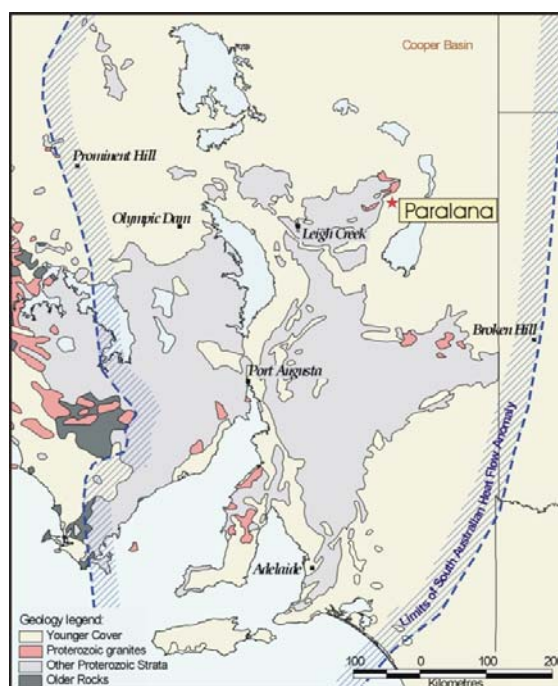
Figure 1: Regional Locality Map

Deep Drilling

In the second half of 2009 a deep geothermal well, Paralana 2, primarily designed to be an injector well, was drilled to 4003 metres (G.L) AHD (Figure 2). During drilling of the well, several zones of over-pressured fluid between 3670 - 3864 metres were encountered. The well was originally designed to be steel cased but due to well breakout issues in the lower portion of the well, a result of the abovementioned over-pressured brines, the final casing string was set at 3725 metres. The strategy is to perforate the casing at selected target intervals and perform hydraulic stimulations to increase the chance of achieving a commercial flow rate, a key commercial barrier for EGS developments around the world.
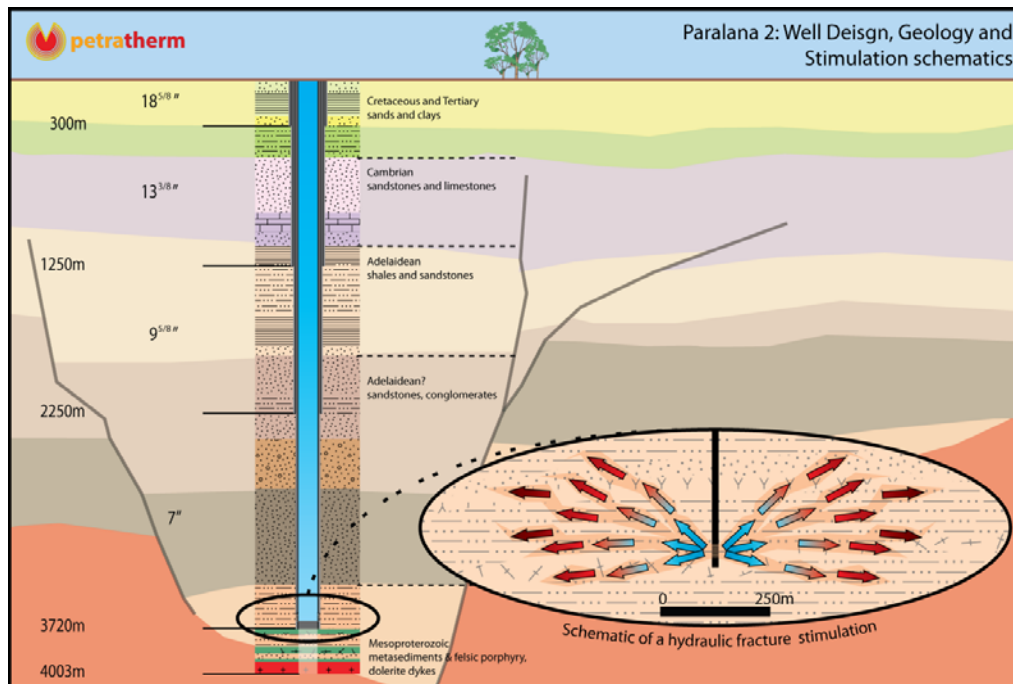
Figure 2: Paralana Well Completion and Geological log

Micro-Seismic Array

The Paralana micro-earthquake (MEQ) monitoring array has been operational since April 2008, initially recording the background seismicity in the region, prior to ground operations.

The array combines sensitive downhole sondes with surface seismometers to enable the interpretation of a wide spectrum of seismic events (Figure 3). For the hydraulic stimulation in July 2011, the array was upgraded to a real-time monitoring network to enable analysis of micro-seismic events and to manage induced seismic risk.
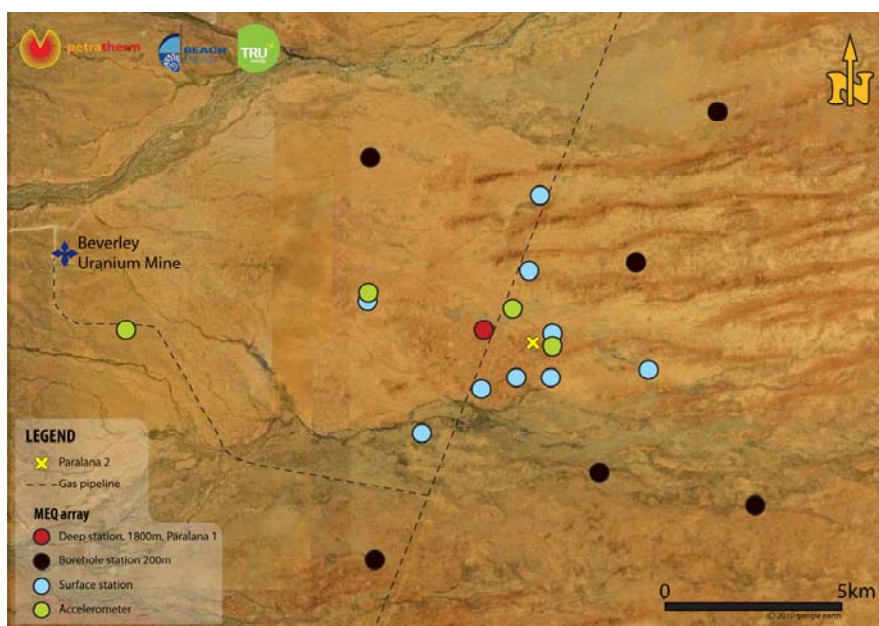
Figure 3: Google Earth image of Paralana area, showing distribution of micro seismic array

Four ground accelerometers were also added to the array and were located to measure peak ground velocity with respect to local surface infrastructure. The ground accelerometer data was used in real time to manage the injection operating process and induced seismic risk.

Diagnostic Fracture Injection Test (DFIT)

In January 2011, the Paralana 2 deep well's casing was perforated over the 3679 - 3685 metres interval, corresponding to the zone where the wireline logging did not indicate the presence of a permeable structure. This was trialled to initiate a complex frac in competent formations around the well bore. The perforation was followed by a small volume stepped injection test that successfully broke down the formation. Injection rates ranged between 1.3 and 5.3 l/sec providing base information to plan the main fracture stimulation works. On completion of the injectivity test, the measured stable well head pressure was 3,940 psi. The high pressure suggests connection to a pre-existing over-pressured zone contained in the reservoir rock.

Fracture Stimulation – July 2011

In July 2011 fracture stimulation works were successfully completed. Over a five day period, 3.1 million litres of fracturing fluid were pumped into the Paralana 2 well at pressures up to 9,000 psi. Initial injection rates were low (3 l/sec), but steady improvement occurred over the period principally through the injection of several acid treatments. The reservoir rock sequence contains only trace carbonate so it thought the increased injection rates are principally due to the breakdown of casing cement in and around the injection zone. Near the end of the injection period a maximum sustained pump rate of 27 litres per second was achieved.

The Stimulation produced over 11,000 micro-earthquakes detected by the Micro seismic network (Figure 4). The primary aim of the fracture stimulation, was to create fractures in the subsurface at least 500 metres from the Paralana 2 well was achieved, with stimulated zone extending approximately 900 metres to the northeast and east of the Paralana 2 well and at a depths ranging between 3,500 to 4,100 metres.
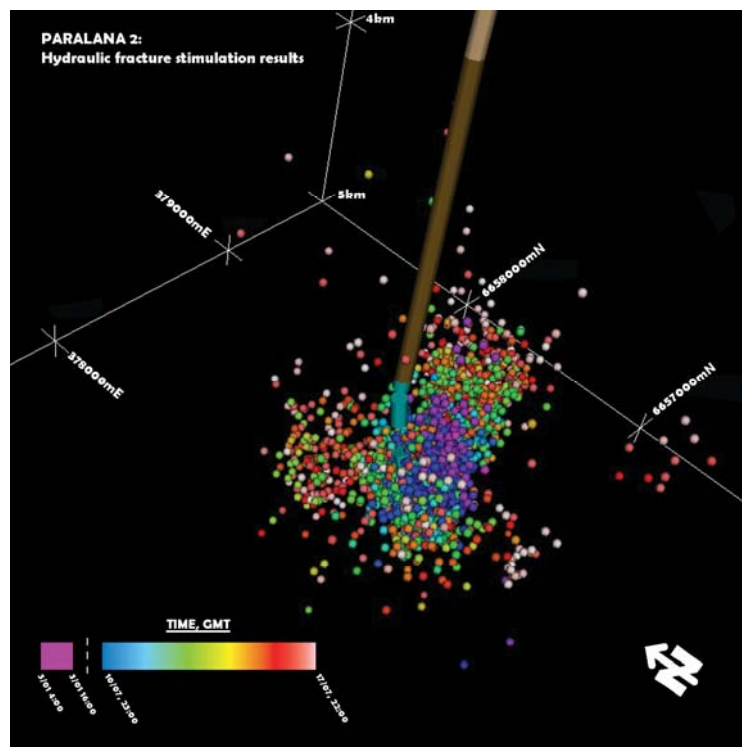
Figure 4: Oblique view of the fracture cloud looking down and towards the northeast

The fracture network comprises at least 4 main structures, with the principal area of growth, a northeast trending en-echelon style tensile opening fracture which dips steeply to the northwest. This feature seems to be bounded either side by steep north-northeast trending structures.

On completion of the stimulation, the calculated stable wellhead pressure remained at approximately 4000 psi. Hence it appears that the stimulated volume is over-pressured and connected into a naturally over-pressured zone. This may assist in the recovery of hot fluids from the reservoir.

The largest seismic event detected during the stimulation was magnitude 2.6 on the Richter scale with 98% of the micro-seismic events detected being below 1.0. The magnitude 2.6 was felt as a short and slight vibration by some staff members near the well bore. Companies and people in the surrounding area did not feel the event. The Richter Magnitude 2.6 event corresponded with a peak particle velocity of 2.36 mm per second, which falls within the green operating zone of the induced seismicity risk management plan.

Paralana 2 Flow Test

Paralana 2 well flow testing was completed successfully in October 2011. Approximately 1.3 million litres of fluid was produced over a seven day period with natural flow rates of up to 6 litres per second. After flowing for seven days, the bottom hole flowing fluid temperature at the perforated interval 3679-85 metres was recorded as 171 degrees Celsius, which is in line with expectations. The geothermal brines were analysed to assist the determination of safe management procedures for any future scale and/or corrosion issues once in long term production. The flow test confirmed the existence of a natural geothermal system at Paralana which may aid future energy recovery from the hot rocks at depth.

Next Stage of Works: Completion of the Circulation Loop

The next critical stage of works is the drilling and completion of Paralana 3 into the stimulated volume of rock to complete the fluid circulation loop. A second round of extensive hydraulic stimulation will follow to increase the reservoir volume and connection to the well bores to ensure a commercial fluid circulation rate of approximately 75 litres/sec can be achieved. Stimulation works may include increasing the perforation interval, drilling out the lower casing shoe and fraccing into the open bottom hole section, increased frac pressures, use of acid and proppant, and injecting much larger volumes than previously trialled. This will be followed by long term circulation testing and finally installation of the initial geothermal plant.

Towards an understanding of social acceptance for the development of geothermal energy in Australia

Romanach, L.M. [1], Carr-Cornish, S. [1] Ashworth, P[1]

[1]Commonwealth Scientific and Industrial Research Organisation (CSIRO)

Lygia.Romanach@csiro.au

Many countries worldwide are committed to reducing their carbon emissions by increasing the share of low-emission energy technologies in their energy portfolio. As part of this change, it has been increasingly recognised that social acceptance of such technologies will be essential in achieving this goal (Wustenhagen et al., 2007). This paper draws on previous work on the social acceptance of low-emission energy technologies to highlight the issues that may impact public support for the development of geothermal energy in Australia.

Keywords: social acceptance, risk, perception, trust

Social acceptance of emerging technologies

Social acceptance of emerging technologies is essential for the successful deployment of these technologies. Within the energy domain, there have been many examples of public concerns openly being expressed towards the deployment of energy technologies around the world. Apart from well known opposition to nuclear power plants (Pickett, 2002), public opposition has also been expressed in relation to wind energy developments (Kaldellis, 2005), carbon capture and storage technology (Van Alphen et al., 2007) and geothermal energy (Gherang Community & Environment Group, 2010; Popovski, 2003).

In order to understand such concerns, a number of studies have been conducted worldwide investigating the social acceptance of energy technologies. Those studies show that social acceptance is complex and subject to a range of factors. Factors that explain public attitudes towards emerging technologies include the level of public understanding of their local environment and the science in question, as well as the broader context in which the technology is discussed. However the social acceptance of emerging technologies goes beyond just knowledge itself. It involves issues such as public perceptions of the risks and benefits of the technology (McComas et al., 2008), trust in the institutions associated with the technology (Bauer et al., 2007), beliefs about energy issues and climate change (Steg et al., 2005), sense of place and project proximity (Devine-Wright, 2012) as well as procedural justice (Bradbury et al., 2009).

Social acceptance of geothermal energy in Australia

In Australia, it has been suggested that geothermal energy has an important role to play in increasing Australia's low-emission energy mix because of its significant energy potential (Arif Syed, 2010). Like other emerging low-emission energy technologies, the social acceptance of geothermal energy has been recognised as a critical component for the industry to achieve large scale demonstration and deployment. Geothermal energy tends to receive general support from the public, most likely due to a common trend to support renewable energy sources in preference to more traditional fossil fuel based forms of energy generation. However, recent studies show that the Australian public have a low level of knowledge about geothermal energy (Dowd et al., 2011) and support for the development of geothermal technology is lower than more familiar low-emission energy technologies such as wind or solar (Dowd et al., 2011; Evans et al., 2010).

Factors that affect social acceptance of energy technologies

As suggested by previous research, public acceptance of energy technologies is complex and shaped by several factors (Midden and Huijts, 2009). Such factors include the public's perceptions of risks and

benefits, their trust in the institutions controlling and deploying the technology, as well as opportunities for public engagement about the technology. In order to understand how the public perceive the risks and benefits of geothermal technology and its associated impacts on their local community, a two-part framework for evaluating social acceptance of geothermal energy projects is presented in Figure 1. Part A of the framework takes into consideration the factors that affect general support for the development of geothermal resources in Australia while Part B of the framework takes into consideration the factors that determine public support for specific geothermal projects. The factors included in the model are briefly discussed below.

Figure 1: A two part framework for evaluating social acceptance of geothermal energy technology in Australia

Knowledge of geothermal energy

Research into public acceptance of energy technologies, including nuclear, biomass and carbon capture and storage, confirm that public support is influenced by more than just scientific knowledge (Huijts et al., 2007). In addition, previous research has shown that it is important to consider knowledge in a broader context. For example, a study conducted by Wynne (1992) has shown that when the scientific community fails to understand the local community's own knowledge about their local environment, there is a lack of trust from the local community about the experts' scientific knowledge. When investigating public knowledge about a particular technology it is important to consider the multiplicity and diversity of the various publics within a community, the knowledge and "local expertise" of lay groups and the limitations of technical knowledge when applied to new settings (Irwin and Michael, 2003). While ordinary citizens will not necessarily develop an in-depth understanding of every technology, it is important to communicate with the public about science and technology in order to support the right of the public to be informed (Hamstra, 1999). However, uninformed citizens will continue to rely on the judgement of others such as regulatory bodies, interested groups and the media to form their opinion about particular technological issues (Scheufele and Lewenstein, 2005). As stressed by Savadori et al. (2004), 'the less we know about an activity the more we need to rely on others to make decisions'. The issue of trust, most particularly, the level of public trust in the institutions controlling and deploying the technology, is further discussed in this paper.

Perceived risks and benefits

Understanding how the public perceive the risks and benefits of a technology is critical, as the public perception about it strongly influences the level of public support for the technology's implementation (Ashworth et al., 2009). Risk assessment therefore plays an important role in informing the public about new technologies (Slovic, 1987) and several studies to date have investigated the role of risk

and benefit perceptions on the public acceptance of emerging technologies (McComas et al., 2008). Emerging technologies are often inherently uncertain and therefore their associated risks can be largely unknown (Slovic, 1987). In addition, people perceive risks differently and therefore risk perception is subject to each individual's own personal characteristics (Slovic, 1987). In order to understand social acceptance of emerging technologies, it is important to therefore consider risk as a social construct. This means recognising that 'risk' might mean different things to different people and that it cannot be measured independently of people's minds and culture (Finucane and Holup, 2005:1604). This view is supported by Ashworth et al. (2012) who found that while some people evaluate energy project benefits as greater than the risks, others evaluate those same risks as being greater than the benefits.

Previous research in Australia has shown that the potential public concerns about the use of geothermal energy in Australia include water usage and seismic activity instigated by geothermal drilling (Dowd et al., 2011). In regard to specific projects being developed in Australia, the risks identified to date are predominantly local in nature and include issues such as noise and visual impact, impact on property values and the local environment, impact of plant construction on local community, increased large vehicle traffic, impact on existing infrastructure such as power lines, air pollution, health, and public engagement process and transparency (Gherang Community & Environment Group, 2010).

On the other hand, the public perceived benefits of geothermal energy identified so far are mainly global in nature, and include the fact that geothermal is a low emission energy technology, has the capacity to generate base-load renewable energy and to increase Australia's energy security (Gherang Community & Environment Group, 2010). This disparity between local risks versus global benefits is not unique to geothermal and has already been identified in relation to the deployment of carbon capture and storage technology (Ashworth et al., 2012).

Beliefs about climate change and energy issues

The acceptability of low carbon energy policies is also influenced by a person's environmental values, beliefs and norms (Steg et al., 2005). This is particularly relevant for geothermal energy as the perceived benefits of the technology are mainly global in nature. This means that support for low-emission technologies such as geothermal might benefit from being placed in context with biospheric values (Steg et al., 2005). Based on Steg et al. (2005), the framework we have developed to investigate the social acceptance of geothermal energy is presented in Figure 1. The framework assumes that individuals that have increased general environmental awareness, increased responsibility for the problems resulting from high energy consumption patterns, and a willingness to take corrective actions to lower carbon emissions will be more likely to support the development of low-emission technologies such as geothermal.

Trust in institutions

Research on the social acceptance of low emission energy technologies, such as carbon capture and storage, has shown that the level of public trust in the organisations involved in decision making is critical in predicting people's acceptance of the technology (Terwel et al., 2009). This is because the level of public trust in those organisations affects how they perceive the risks of the technology and their overall acceptance of it (Terwel et al., 2009). It is also important for relevant institutions to address public concerns about the technology as a failure to address those concerns will negatively affect public trust in those institutions.

Sense of place and project proximity to built-up areas

Social research on the public acceptance of energy technologies has demonstrated that support for energy developments often depends on the location of the energy project, with some studies showing that individuals tend to hold more negative attitudes when energy developments are proposed for their local residential area than they would normally (Terwel and Daamen, 2012). To address this issue, several studies have investigated the effect of the "not in my back yard" (NIMBY) concept in relation to this opposition to energy projects. The assumption is that individuals tend to hold greater concerns

when developments are proposed in their local area. However, Terwel and Daamen (2012) argue that the reasons for opposing energy developments go beyond NIMBYism and involve a 'range of social and personal factors affecting human interactions with social and political institutions'. This view is supported by Devine-Wright (2005) who argues that a multidimensional framework that goes beyond the NIMBYism concept is required to understand how contextual, social, economical and personal factors shape public perceptions of energy technologies. As suggested by Devine-Wright (2005), the framework we have developed to understand social acceptance of geothermal energy technology presented in Figure 1 is divided into two parts. Part A determines general support for geothermal technology while Part B determines support for specific projects. Examining the factors that affect general support for geothermal technology as well as support for specific projects will allow for a greater understanding about whether people who are against the implementation of energy projects in their local area are also against the implementation of energy projects nationally.

Procedural justice of engagement process

The term procedural justice refers to 'the extent to which the dynamics of the decision process are judged to be fair' (Lind and Tyler, 1988). Research conducted by Bradbury et al. (2009) on social acceptance of carbon capture and storage found that public acceptance is critically dependent on how the technology risks will be managed. In this context, the public is concerned about whether the development and implementation of the project process will be fair and transparent and whether there will be mechanisms and contacts in place for them to voice their concerns (Bradbury et al., 2009).

Moving forward: addressing public concerns about energy technologies

Research has shown that it is important to engage with the public in the early stages of technology development (Ashworth et al., 2012; Ashworth and Cormick, 2011). Early engagement with the community through a variety of mechanisms has emerged as the best approach to facilitate meaningful participation, to empower the community and to build trust in the institutions deploying the technology (Ashworth et al., 2012). However, experience has shown that simply engaging early does not assure project success. Several factors are known to influence the effectiveness of community communication and consultation process confirming that this is a complex task (Desbarats et al., 2010). Ashworth et al. (2012) have conducted a comparative analysis of five international carbon capture and storage projects and highlighted a number of factors related to overall project management that increased the likelihood of acceptance. First, the study highlights that it is important to take into account the social context of each community, which means spending time on getting to know the community and identifying the benefits that will have value to them (Ashworth et al., 2012). This is critical because the characteristics of each community will determine how the risks and benefits of the technology are likely to be perceived within that community. As stressed by Irwin and Michael (2003), public attitudes towards science and technology might be influenced by the fact that people are part of a certain community and movement, or due to the fact that people draw upon their traditional or local knowledge to form their opinion about technological issues. Second, it is important to understand what and how to communicate and engage with the community (Ashworth et al., 2012). And finally, it is also important to consider what sources of information the public consult or rely upon, as the level of public trust in these information sources is critical for social acceptance to occur.

Conclusion

Due to the fact that geothermal energy technology is largely unknown by the general public in Australia, improving the Australian public's knowledge of the potential applications and contribution to Australia's energy mix will be the first important step in shaping public support for geothermal energy in Australia. Further to this and as outlined above, early identification of the issues that may impact public support for geothermal energy technology and developing an understanding of the issues that are relevant to each community can only help in ensuring its successful advancement.

References

Arif Syed, J. M., Sally Thorpe and Kate Penney, 2010, Australian energy projections to 2029-30.

Ashworth, P., Bradbury, J., Wade, S., Feenstra, C. F. J. Y., Greenberg, S., Hund, G., and Mikunda, T., 2012, What's in store: Lessons from implementing CCS: International Journal of Greenhouse Gas Control, v. 9, p. 402-409.

Ashworth, P., and Cormick, C., 2011, Emerging Legal and Regulatory Issues, in Havercroft, I., Macrory, R., and Stewart, R. B., eds., Carbon capture and storage : emerging legal and regulatory issues: Oxford, Hart, p. 251-263.

Ashworth, P., Pisarski, A., and Thambimuthu, K., 2009, Public acceptance of carbon dioxide capture and storage in a proposed demonstration area: Proceedings of the Institution of Mechanical Engineers, Part A: Journal of Power and Energy, v. 223, no. 3, p. 299-304.

Bauer, M. W., Allum, N., and Miller, S., 2007, What can we learn from 25 years of PUS survey research? Liberating and expanding the agenda: Public Understanding of Science, v. 16, no. 1, p. 79-95.

Bradbury, J., Ray, I., Peterson, T., Wade, S., Wong-Parodi, G., and Feldpausch, A., 2009, The Role of Social Factors in Shaping Public Perceptions of CCS: Results of Multi-State Focus Group Interviews in the US: Greenhouse Gas Control Technologies 9, v. 1, no. 1, p. 4665-4672.

Desbarats, J., Upham, P., Riesch, H., Reiner, D., Brunsting, S., de Best-Waldhober, M., Duetschke, E., Oltra, C., Sala, R., and McLachlan, C., 2010, Review of the Public Participation Practices for CCS and Non-CCS Projects in Europe.

Devine-Wright, P., 2005, Beyond NIMBYism: towards an integrated framework for understanding public perceptions of wind energy: Wind Energy, v. 8, no. 2, p. 125-139.

Devine-Wright, P., 2012, Explaining "NIMBY" Objections to a Power Line: The Role of Personal, Place Attachment and Project-Related Factors: Environment and Behavior.

Dowd, A.-M., Boughen, N., Ashworth, P., and Carr-Cornish, S., 2011, Geothermal technology in Australia: Investigating social acceptance: Energy Policy, v. 39, no. 10, p. 6301-6307.

Evans, A., Strezov, V., and Evans, T., 2010, Comparing the sustainability parameters of renewable, nuclear and fossil fuel electricity generation technologies, 21st World Energy Congress: Montreal

Finucane, M. L., and Holup, J. L., 2005, Psychosocial and cultural factors affecting the perceived risk of genetically modified food: an overview of the literature: Social Science & Medicine, v. 60, no. 7, p. 1603-1612.

Gherang Community & Environment Group, 2010, Summary Results of the "What Do You Think Survey". Community views on the proposal by Greenearth Energy to develop multiple geothermal power plants near Gherang.

Hamstra, A. M., 1999, Studying public perceptions of biotechnology: helicopter or microscope?, in Dierkes, M., and Grote, C. V., eds., Between understanding and trust: the public, science and technology: Amsterdam, Harwood Academic, p. 179-200.

Huijts, N. M. A., Midden, C. J. H., and Meijnders, A. L., 2007, Social acceptance of carbon dioxide storage: Energy Policy, v. 35, no. 5, p. 2780-2789.

Irwin, A., and Michael, M., 2003, Science, social theory and public knowledge, Maidenhead ; Philadelphia, Open University Press, xiv, 175 p. p.:

Kaldellis, J. K., 2005, Social attitude towards wind energy applications in Greece: Energy Policy, v. 33, no. 5, p. 595-602.

Lind, E. A., and Tyler, T. R., 1988, The social psychology of procedural justice, New York ; London, Plenum.

McComas, K. A., Besley, J. C., and Yang, Z., 2008, Risky business perceived behavior of local scientists and community support for their research: Risk Analysis, v. 28, no. 6, p. 1539-1552.

Midden, C. J. H., and Huijts, N. M. A., 2009, The Role of Trust in the Affective Evaluation of Novel Risks: The Case of CO2 Storage: Risk Analysis, v. 29, no. 5, p. 743-751.

Pickett, S. E., 2002, Japan's nuclear energy policy: from firm commitment to difficult dilemma addressing growing stocks of plutonium, program delays, domestic opposition and international pressure: Energy Policy, v. 30, no. 15, p. 1337-1355.

Popovski, K., 2003, Political and public acceptance of geothermal energy, IGC2003 - Short Course. Geothermal training programme: Iceland, The United Nations University.

Savadori, L., Savio, S., Nicotra, E., Rumiati, R., Finucane, M., and Slovic, P., 2004, Expert and public perception of risk from biotechnology: Risk Analysis, v. 24, no. 5, p. 1289-1299.

Scheufele, D. A., and Lewenstein, B. V., 2005, The public and nanotechnology: How citizens make sense of emerging technologies: Journal of Nanoparticle Research, v. 7, no. 6, p. 659-667.

Slovic, P., 1987, Perception of risk: Science Communication, v. 236, p. 280-285.

Steg, L., Dreijerink, L., and Abrahamse, W., 2005, Factors influencing the acceptability of energy policies: A test of VBN theory: Journal of Environmental Psychology, v. 25, no. 4, p. 415-425.

Terwel, B. W., and Daamen, D. D. L., 2012, Initial public reactions to carbon capture and storage (CCS): differentiating general and local views: Climate Policy, v. 12, no. 3, p. 288-300.

Terwel, B. W., Harinck, F., Ellemers, N., and Daamen, D. D. L., 2009, Competence-Based and Integrity-Based Trust as Predictors of Acceptance of Carbon Dioxide Capture and Storage (CCS): Risk Analysis, v. 29, no. 8, p. 1129-1140.

Van Alphen, K., Voorst, Q. V. T., Hekkert, M. P., and Smits, R. E. H. M., 2007, Societal acceptance of carbon capture and storage technologies: Energy Policy, v. 35, no. 8, p. 4368-4380.

Wustenhagen, R., Wolsink, M., and Burer, M. J., 2007, Social acceptance of renewable energy innovation: An introduction to the concept: Energy Policy, v. 35, no. 5, p. 2683-2691.

Wynne, B., 1992, Misunderstood misunderstanding: social identities and public uptake of science: Public Understanding of Science, v. 1, no. 3, p. 281-304.

Local Thermal Non-Equilibrium heat transfer in fractures: the realistic approach in geothermal reservoir simulations

Hamid Roshan, Martin S. Andersen, Ian R. Acworth

Connected Waters Initiative, School of Civil and Environmental Engineering, University of New South Wales & National Centre for Groundwater Research and Training

h.roshan@unsw.edu.au

Abstract

It is well known that the fracture systems have a significant impact on fluid flow and heat transfer in geothermal reservoirs. As the matrix of crystalline rocks is generally of extremely low permeability the fluid flow is predominantly through fractures. Therefore the simulation of the fluid flow and heat transfer in fractured rocks is of special interest to the geothermal industry.

The amount of heat which can be extracted from a geothermal system over the production period greatly depends on the thermal interaction between the rock and fluid. To describe this heat exchange there are two main approaches for solving the heat transfer equation: local thermal equilibrium (LTE) and local thermal non-equilibrium (LTNE). Numerous numerical models have been developed so far to deal with fluid and heat flow in fractured porous media. While these models use the LTE assumption, the recent model developments gravitate towards the more realistic approach of LTNE. However, the LTNE assumption used in these models originates from the field of porous media experimentation and was not developed for fracture rock environments.

In this study a finite element reservoir model has been developed incorporating the LTNE approach for the heat exchange between the fracture walls and the fluid. The proposed model is applied to a typical situation of a naturally fractured geothermal system with realistic operational pressure losses and the extraction water temperatures and thermal drawdown are calculated. The obtained results are then compared with an identical reservoir model but with the LTNE assumption derived from porous media.

The results of this study show that the average matrix temperature from the porous media LTNE is much lower than that of the fracture LTNE over the production period. In fact the results illustrate that the porous media LTNE reaches almost instantaneous thermal equilibrium while in the fracture LTNE, the thermal equilibrium takes longer period of time to reach. Therefore the porous media LTNE assumption may be a potential misrepresentation when it is used to simulate fractured geothermal systems especially for lower flow velocities in the fractures.

Keyword: Local thermal non-equilibrium, Geothermal systems, Fractured reservoir, Heat flow

Methodology

Understanding the hydraulic flow and heat transfer in hot fractured rocks are important for geothermal energy production [*Ghassemi and Suresh Kumar*, 2007; *Kolditz and Clauser*, 1998]. While many efforts have been made to study the coupled fluid flow and heat transfer in fractured rocks, a fundamental concept seems to be lacking: whether local thermal equilibrium is attained or not [*Koh et al.*, 2011]. In recent years the concept of local thermal non-equilibrium has been taken from chemical and mechanical engineering applications and incorporated into the field of geothermal energy [*Celli et al.*, 2010; *Gelet et al.*, 2012; *Shaik et al.*, 2011]. While using the approach of local thermal non-equilibrium has now been adopted by the industry, further fundamental research is still required. The assumption of local thermal non-equilibrium, related to geothermal energy extraction, is incorporated into the numerical models in two different approaches: considering a constant heat transfer rate between the rock and fluid [*Shaik et al.*, 2011] and the use the porous media local thermal non-equilibrium assumption [*Gelet et al.*, 2012]. In the first approach the heat transfer is not directly a

function of fluid and rock properties but a constant value and therefore is not justified within the framework of thermodynamics. In the second approach the applied correlations are obtained from the porous material heat research (i.e. pack beds) which has not been justified for fractured rock. Some potential shortcomings for applying the porous media LTNE correlations to fractured rocks are:

- These correlations may not be applicable for the heat transfer at low Reynolds numbers

- Generally a system of gas and glass bead is used to conduct such tests whereas a geothermal reservoir consists of minerals and a liquid.

- Finally and most importantly, porous media have a much higher tortuosity and larger contact area than the fractured rock systems. This causes the different heat transfer rate between the rock material and the fluid and also induces a very different thermal dispersion.

Considering above points, the heat transfer in a fractured reservoir was modelled numerically by either incorporating the porous media (*Case A*) or the fracture (*Case B*) local thermal non-equilibrium . In order to conduct the numerical analysis (for both case A and B), a randomly oriented fracture network is generated and finely meshed into elements (Fig. 1a). Then each element permeability tensor was calculated using the method proposed by Kasap and Lake [1990] and fed into the fluid flow equation to calculate pore pressures and velocities. Fig. 1b shows the velocity distribution after reaching steady state fluid flow in the fractured reservoir. The obtained directional velocities from the fluid flow equation of the fractured media are then used to calculate the heat transfer in the rock and the fluid separately for each element for both porous media and fracture LTNE.

In case A, the obtained velocities are fed into the porous media LTNE correlation to predict the rate of heat transfer between rock and fluid regardless of whether those elements contain fractures or not whereas in case B, the porous media correlation is replaced by the fracture LTNE correlation if the element contains one or more fractures. It is noteworthy that in the proposed correlations for both fracture and porous media LTNE, the element velocity is the main variable controlling the rate of heat transfer between the rock and the fluid.

Fig. 1c presents the temperatures of the production fluid and average matrix temperature after 12 years of production for both the porous media and fracture LTNE. From Fig. 1c, it can be seen that after 12 years of production, the average matrix temperature from the porous media LTNE is almost 40ºC lower than the average temperature from the fracture LTNE. From this figure it is also seen that the production fluid temperature drops sharply to almost 140ºC for the case of the porous media LTNE while the temperature has only dropped to around 190ºC for the fracture LTNE after 12 years. It can be also pointed out that the fluid thermal breakthrough for the fracture LTNE occurs 2 years after that of the porous media LTNE.

Results

It can therefore be concluded that the rate of heat transfer is lower for a fracture system, or in other words: the thermal equilibrium between the fluid and the elements with fractures takes a longer time to be attained compared to that of a porous media (Fig. 1d). This in turn causes the average matrix temperature for the fracture LTNE to drop at a slower rate which gives a longer life of the production operation for this case. However the amount of captured heat from the fracture walls depends on the fluid velocity (higher fluid velocity causes higher thermal convection rate but fluid stays in the reservoir for a shorter period of time).

Acknowledgment
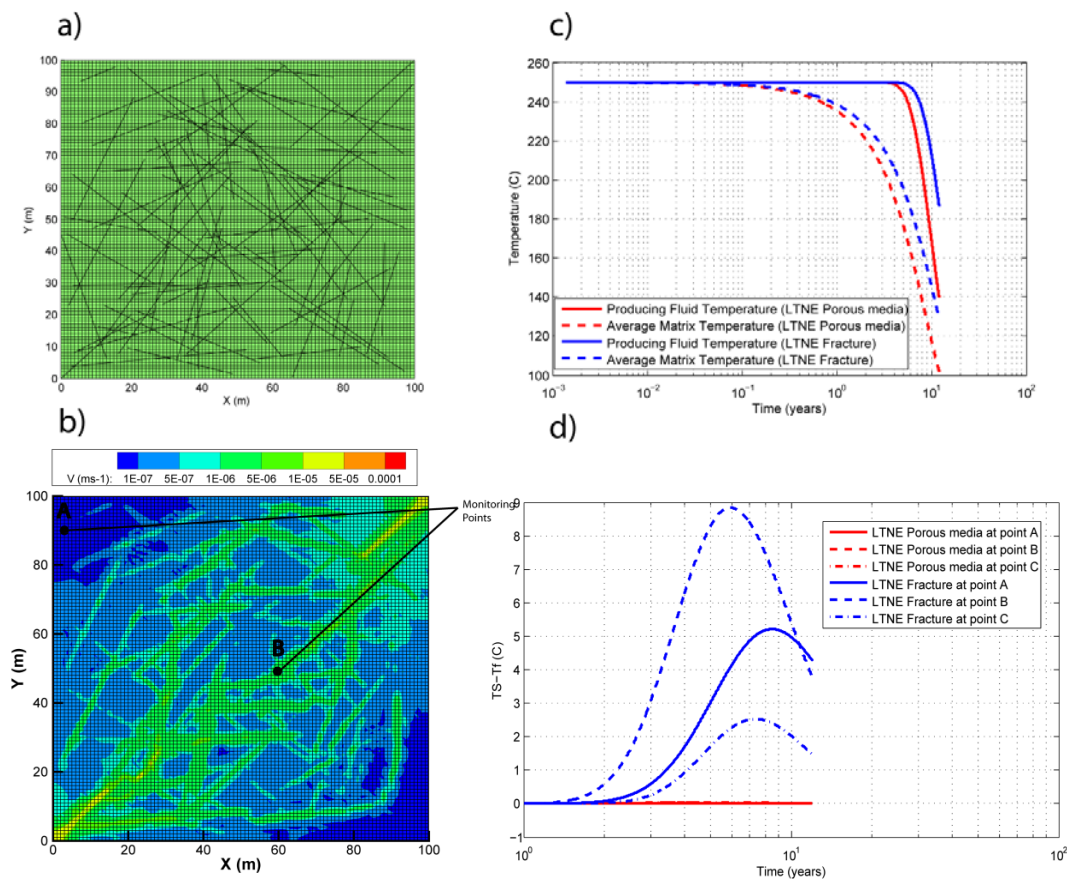
Fig. 1. *a) Randomly oriented fracture network, b) 2D velocity field after reaching steady state fluid flow, c) temperature difference between fluid and rock at monitoring points, d) production fluid and average matrix temperature for LTNE porous media and LTNE fracture.*

References

Celli, M., D. A. S. Rees, and A. Barletta (2010), The effect of local thermal non-equilibrium on forced convection boundary layer flow from a heated surface in porous media, *International Journal of Heat and Mass Transfer, 53*(17-18), 3533-3539.

Gelet, R., B. Loret, and N. Khalili (2012), A thermo-hydro-mechanical coupled model in local thermal non-equilibrium for fractured HDR reservoir with double porosity, *J. Geophys. Res., 117*(B7), B07205, doi:10.1029/2012JB009161.

Ghassemi, A., and G. Suresh Kumar (2007), Changes in fracture aperture and fluid pressure due to thermal stress and silica dissolution/precipitation induced by heat extraction from subsurface rocks, *Geothermics*, *36*(2), 115-140.

Kasap, E., and L. W. Lake (1990), Calculating the Effective Permeability Tensor of a Gridblock, *SPE Formation Evaluation, 5*(2), 192-200, doi:10.2118/18434-pa.

Koh, J., H. Roshan, and S. S. Rahman (2011), A numerical study on the long term thermo-poroelastic effects of cold water injection into naturally fractured geothermal reservoirs, *Computers and Geotechnics, In Press, Corrected Proof,* doi:DOI: 10.1016/j.compgeo.2011.03.007.

Kolditz, O., and C. Clauser (1998), Numerical simulation of flow and heat transfer in fractured crystalline rocks: Application to the Hot Dry Rock site in Rosemanowes (U.K.), *Geothermics*, 27(1), 1-23.

Shaik, A. R., S. S. Rahman, N. H. Tran, and T. Tran (2011), Numerical simulation of Fluid-Rock coupling heat transfer in naturally fractured geothermal system, *Applied Thermal Engineering, 31*(10), 1600-1606, doi:10.1016/j.applthermaleng.2011.01.038.

Modification of Compressible Flow Equation for One Phase Steam Geothermal

Rudi., Hendrarsakti, J., Syihab, Z. and Ashat, A.

Bandung Institute of Technology

rudi.siburian@yahoo.com

Keywords : compressible, incompressible, one phase steam, geothermal

Abstract

Modeling of one phase steam in geothermal well is usually using an equation derived with assumption of incompressible fluid flow. This equation actually is addressed to analyze fluids with small compressibility such as water, whose density change is very small and can be neglected. Previous studies suggested that this equation can be used to analyze steam flow when the velocity is relatively low, about 103 m/s (0.3 Mach number). Based on observation data, velocity of flowing fluid in MBB-3 reached 115 m/s. When the velocity approaches or exceeds 0.3 Mach number (Ma), a good match between model and data observation is difficult to achieve.

To achieve a better wellbore steam flow model, we need to develop an equation based of compressible fluids was developed. This modified compressible equation was derived from combination of continuity, momentum, and energy equations.

This modified compressible equation as a result from this research was validated with observation data from MBB-3 well of Wayang Windu field, and also compared to model from Cullender and Smith correlation. The result shows that the modified compressible flow model gives better agreement with observation data compared both previous incompressible equation and Cullender and Smith correlation.

Introduction

This study initiated after problem found on some one phase geothermal well such as in Kamojang, Darajat and for this study, MBB-3 well Wayang Windu field, West Java, Indonesia. Based on MBB-3, the result of flow modelling of this well is not in good match. When calculating bottom hole pressure (Pwf) with measured data in wellhead (top-down modelling), the result from model is smaller then the measured data. And when When calculating well head pressure (Whp) with measured data in bottom hole (bottom-up modelling), the result from model is higher then the measured data. Same problem also appear when quantitatively well modelling from PTS data (Pressure, Temperature dan Spinner) is in proceed. Pressure, temperature and mass flowrate curve between measured data and model in not in good match (Figure 4).

Problem on this MBB-3 might be happened because on some abnormal things on wellbore. Cause of this abnormality might be from casing damage, the consequence is diameter used as calculation is different from its measured data. Another guess is, the problem might be happened because of well head pressure is relatively low, so pressure differences is getting bigger, effecting fluid flow velocity become so high.

MBB-3 is a one phase steam well. Figure 1 and 2 will describe pressure, temperature and saturation temperature of this well versus its measured depth. Whereas Figure 3 adan tabel 1 provides casing configuration of MBB-3 well. MBB-3 is a 1938 m directional well with, 10-3/4 slotted liner at the bottom, 13-3/8 casing at the top as production casing and the angel reached 60°.
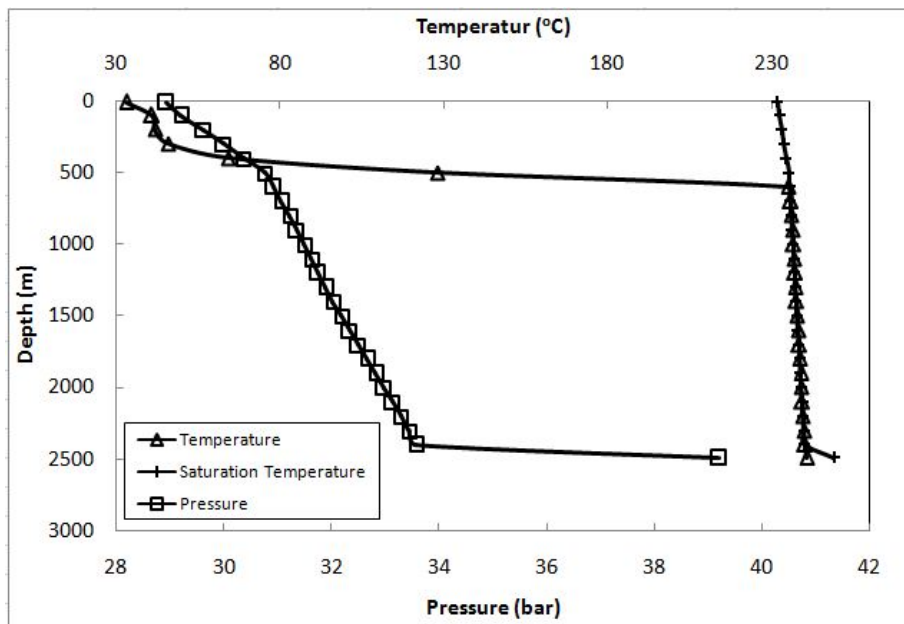
Figure 1: *PT shut In of MBB-3*
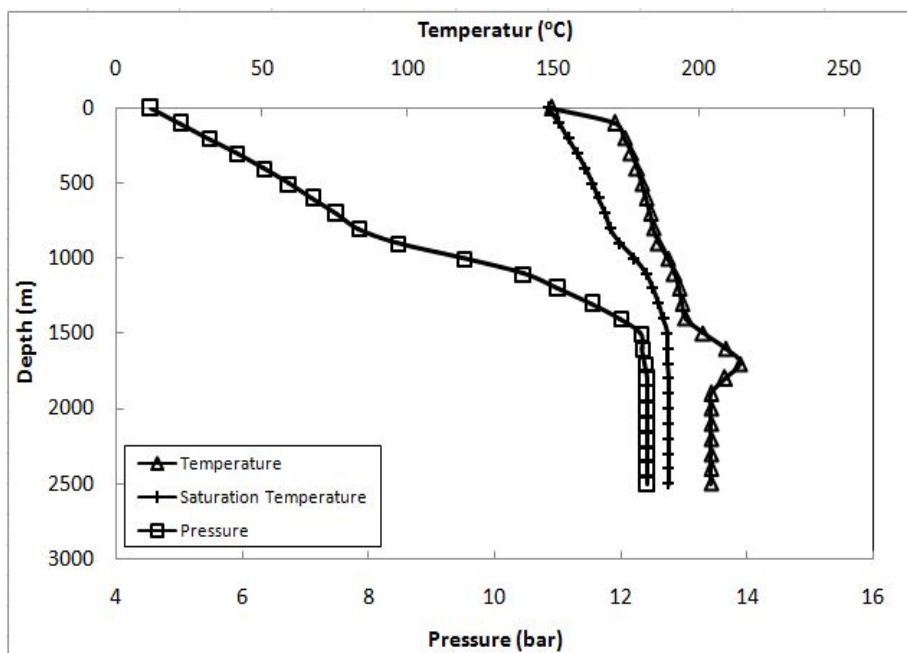
Figure 2: *PT Flowing of MBB-3*

Table 1: Geometry of MBB-3

Depth (m)		Casing ID (m)	Roughness(m)	Angle, °
0	516	0.315	0.000045	5
516	890	0.315	0.000045	25
858	1938	0.255	0	60
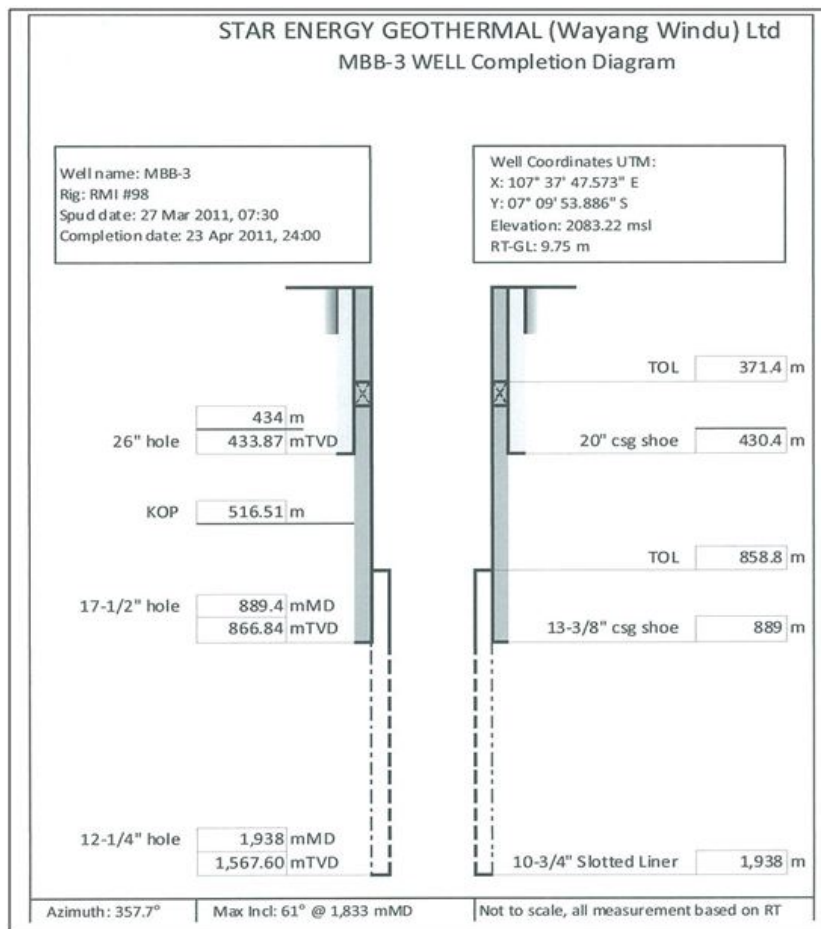
Figure 3: *Casing Configuration of MBB-3*
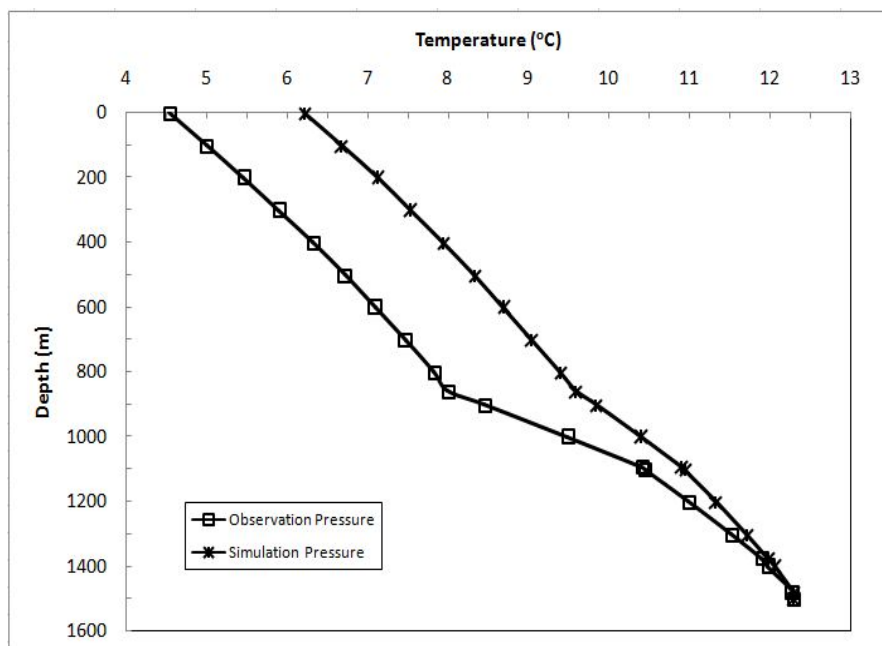
Figure 4: *MBB-3 Pressure Observation and Simulation (Indrinanto, 2012)*

Flow Modellling Problem in Well MBB-3

The basic pressure drop equation usually used on geothermal and oil & gas industry untill today is equation as form of elevation, friction dan acceleration ;

$$\frac{dp}{dz} = g\rho\cos\theta + \frac{f\rho v^2}{2d} + \frac{\rho v dv}{dz}$$
(Equation. 1)

This equation actually for incompressible flow which derived from continuity and momentum equation (Hasan - Kabir, 2002), but still can be used for compressible flow if the flow velocity is below ± 0.3 of its speed of sound, about 100 m/s (Fox – McDonald, 2003). When the velocity of the fluid getting closer to 0.3 of its speed of sound (Mach Number), problem like we have in well MBB-3 might be because of this incompressible equation.

As can be seen at Figure. 4, there is gap/ difference between observation and simulation curve. Maximum flow velocity recorded on this well is 115 m/s (Figure 5), which is already higher than 0.3 Mach number (Ma). Figure. 4 is well modelling start from bottom of well to the top of the well, usually called bottom-up modelling.
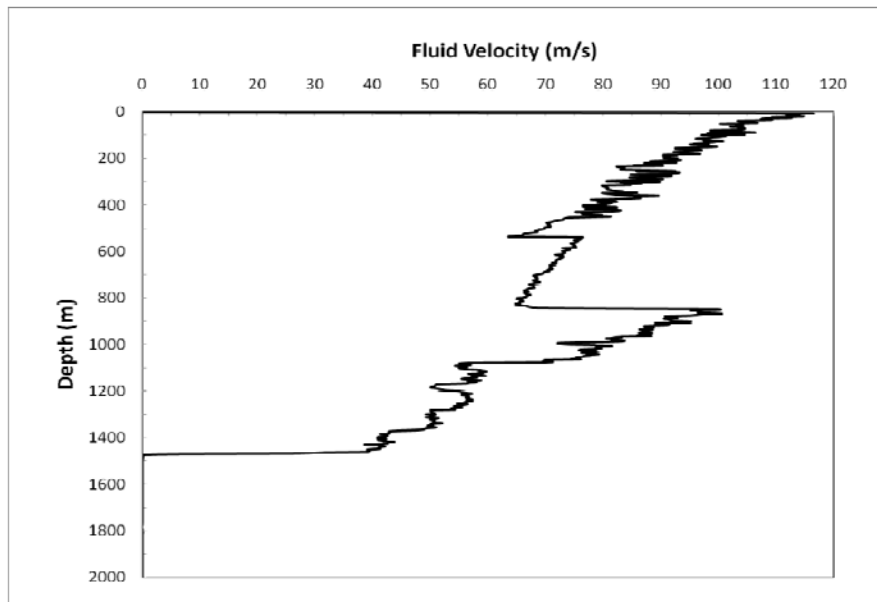
Figure 5: *Fluid Velocity in Well MBB-3*

Equation Modification

When velocity is near or larger than 0.3 Ma, the flow should treat as compressible flow, which means the equation should build from three basic equation ; continuity, momentum dan energy equation (White, Fluid Mechanics). Based on this statement, here under our approach to solve compressible flow on well MBB-3.

At first, the energy equation as shown at Equation. 2, need to change to pressure per-depth equation based as shown at Equation. 3, so later we can combine it with equation 1.

$$h_1 + \frac{1}{2}v_1^2 + gz_1 = h_2 + \frac{1}{2}v_2^2 + gz_2$$
(Equation. 2)

$$\frac{\rho_1 h_1}{dz} + \frac{1}{2dz}\rho_1 v_1^2 + \frac{\rho_1 g z_1}{dz} = \frac{\rho_2 h_2}{dz} + \frac{1}{2dz}\rho_2 v_2^2 + \frac{\rho_2 g z_2}{dz}$$
(Equation. 3)

Change in potensial energy for gas is very small, and so can be neglected, as shown at Equation. 4.

$$\frac{\rho_1 h_1}{dz} + \frac{1}{2dz} \rho_1 v_1^{\,2} = \frac{\rho_2 h_2}{dz} + \frac{1}{2dz} \rho_2 v_2^{\,2}$$

(Equation. 4)

And if we assumed the flow is isentalpic, the result is Equation. 5, 6 and 7.

$$\frac{\rho_1 v_1^{\,2}}{2dz} = \frac{\rho_2 v_2^{\,2}}{2dz}$$

(Equation. 5)

$$\frac{\rho_1 v_1^{\,2}}{2dz} - \frac{\rho_2 v_2^{\,2}}{2dz} = 0$$

(Equation. 6)

$$\frac{\rho_1 v_1^{\,2} - \rho_2 v_2^{\,2}}{2dz} = 0$$

(Equation. 7)

Continuity equation in well MBB-3 can be simplified as shown at Equation. 8 and then Equation 9.

$$\rho_1 v_1 = \rho_2 v_2$$

(Equation. 8)

$$\rho_2 = \frac{\rho_1 v_1}{v_2}$$

(Equation. 9)

With substitution Equation. 9 to Equation 7, as shown at Equation 10 and 11, the result is Equation 12.

$$\frac{\rho_1 v_1^{\,2} - \dfrac{\rho_1 v_1}{v_2} v_2^{\,2}}{2dz} = 0$$

(Equation. 10)

$$\frac{\rho_1 v_1^{\,2} - \rho_1 v_1 v_2}{2dz} = \frac{\rho_1 v_1 (v_1 - v_2)}{2dz} = 0$$

(Equation. 11)

$$\frac{\rho_1 v_1 dv}{2dz} = 0$$

(Equation. 12)

Combining Equation. 1 and Equation. 12 we will have Equation 13 and Equation 14.

$$0 = g\rho \cos\theta + \frac{f \rho v^2}{2d} + \frac{\rho v dv}{dz} + \frac{1}{2} \frac{\rho v dv}{dz} - \frac{dp}{dz}$$

(Equation. 13)

$$\frac{dp}{dz} = g\rho \cos\theta + \frac{f \rho v^2}{2d} + \frac{3}{2} \frac{\rho v dv}{dz}$$

(Equation. 14)

Equation. 14 is the final result that we will use to try to solve modelling problem in well MBB-3.

Result

We call Equation. 14 as *Modified-Compressible Equation*. Modelling MBB-3 well with this new equation resulting better pressure curve compare to incompressible equation (Equation. 1) as shown at Figure. 6. Although, the result from modified compressible is still far from perfect matching with observation data.

In addition, we also utilized Cullender & Smith (C&S) correlation to modelling well MBB-3. The result as shown at Figure. 6 is C&S correlation has better value than incompressible flow, but our modified-compressible equation is still better than this C&R correlation.
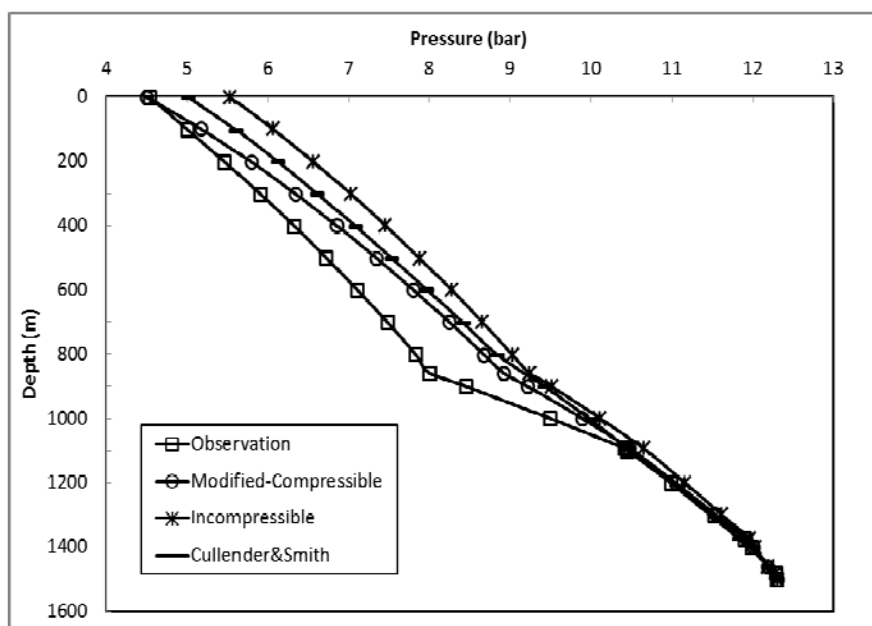
Figure 6: *Pressure of Observation, Modified Compressible, Incompressible and Cullender&Smith Correlation*

Conclusion

The main motivation for this study is to achieve better wellbore modelling result to approach data observation as near as possible. The result is the modified-compressible equation has the best result compare to incompressible equation and C&R correlation, but the result itself is still far from perfect.

Therefore, further study is still needed to achieve better result, either its to build another new/ modified equation or other things such as friction factor if possible.

Nomenclature

p = Pressure (bar)

z = depth (m)

ρ = density (kg/m^3)

g = gravitational acceleration (m/s^2)

θ = angle of well

f = friction factor, dimensionless

v = fluid flow velocity (m/s)

d = well casing inner diameter (m)

References

A.R. Hasan, C.S. Kabir. 2002, Fluid Flow and Heat Transfer in Wellbores. Society of Petroleum Engineers,Texas.

Chi U. Ikoku. 1992, Natural Gas Production Engineering. Malabar, Florida.

Frank M. White, Fluid Mechanics, 4th edition, University of Rhode Island.

Kermit E. Brown, H. Dale Beggs. 1997, The Technology of Artificial Lift Methods. Volume 1, Tulsa, Oklahoma.

M. H. Cullender, R. V. Smith. 1956, Practical Solution of Gas-Flow Equations for Wells and Pipelines With Large Temperature Gradients. Petroleum Branch Fall Meeting, Los Angeles.

Robert W. Fox, Alan T. McDonald. 2003, Introduction to Fluid Mechanics. 6th edition.

Tarek ahmed. 1946, Hydrocarbon Phase Behavior. Houston, Texas.

Yudi Indrinanto FX. 2012. Analisa Hasil Interpretasi Survei Pressure, Temperature dan Spinner Serta Parameter Pemboran Terhadap Penentuan Karakteristik Feed Zone Sumur MBB-3 di Lapangan Panas Bumi Wayang Windu. ITB, Bandung.

A stochastic model for the fracture network in the Habanero enhanced geothermal system

Seifollahi, S., Dowd, P-A and Xu, C

University of Adelaide

Sattar.seifollahi@adelaide.edu.au

Fracture Network Modelling (FNM) plays an important role in many areas where the characterization of discontinuities in deep ground is required. Applications of the FNM include, but not limited, hydrocarbon reservoir production, mineral extraction, tunnelling, underground storage or disposal of hazardous wastes and geothermal systems. One important step in FNM is to estimate the density of fractures and geometries and properties of individual fractures such as the size and orientation. Due to the lack of data, the tortuous nature of fractures and the great uncertainty involved in practice, the only feasible approach is via a stochastic modelling. This paper describes a general optimization approach to modelling the fracture network in a geothermal reservoir, conditioned on the seismic events several kilometres beneath the surface detected during the fracture stimulation process. Two key aspects of our method are the construction of an appropriate objective function and the derivation of an efficient updating scheme, which still remain to be the two challenging issues of most global optimization techniques. In our application, the objective function consists of two important components: the minimisation of squared distances of the seismic points to the fracture model and the minimisation of number of fractures or the amount of fracturing, which corresponds to the least consumption of fracturing energy. The model updating process includes several proposals for perturbing the parameters of individual fractures and also to alter the size of the fracture network in order to get a global optimal solution. As a case study, the model is applied to Geodynamics' Habanero reservoir in the Cooper Basin of South Australia.

Keywords: global optimization, simulated annealing, stochastic fracture modelling, enhanced geothermal systems, hot dry rock

Introduction

Earlier mathematical models for fracture networks include continuum models that assume a fractured rock mass can be represented as an "equivalent porous medium" (Long and Witherspoon, 1985; Odling, 1992) and discrete fracture models that rely on a detailed description of discontinuity geometry (Dershowitz and LaPointe, 1994; Einstein 2003; Mardia et al., 2007a). In a discrete fracture model, the characterization of a fracture network is still a very challenging problem as the whole fracture system is not observable on any meaningful scale and the system can only be described via a stochastic model. Stochastic modelling is a general approach in which the fracture characteristics such as location, size and orientation are treated as random variables with inferred probability distributions.

In modelling practice, it is impossible to represent all fractures by tortuous surfaces and some simplification is required. Common approaches for fracture geometry include circular discs, elliptical discs, planer polygons or planes with infinite extents. Here we use an ellipse to represent a fracture, i.e. $H = (x, y, z, \alpha, \beta, \gamma, a, b)$ where x, y, z are the coordinates of the fracture centre point, α, β the dip direction and dip angle of the plane, γ the rotation angle of the major axis against the dip direction of the ellipse, and a, b the major and minor axes of the ellipse. This configuration, even with the 'best' fitted model, can not intersect all seismic points due to fracture tortuosity but the distance of the points to fracture planes can be used as one of the criteria to assess the goodness-of-fit of the fracture model. The seismic events in this context refer to those detected during the stimulation process at the development stage of a geothermal reservoir.

Recently, a Markov chain Monte Carlo (MCMC) approach has been used to condition a fracture model to borehole data in 2D application (Mardia et al, 2007b). The model, then, was extended to 3D

applications, where the early results are promising (Mardia et al, 2007a). In both works, the number of fractures varies during the learning process. Another extension of MCMC in FNM is to condition the fracture model on the seismic events recorded during fracture stimulation of the reservoir (Xu et al., 2011). In this model the number of fractures is fixed in advance and it doesn't vary during the optimization process. Therefore, determining an optimal number of fractures to properly fit the seismic event points is one of the remaining challenging issues in this approach. In the work presented in this paper, we address this issue via a general optimization model by defining proper objective functions and using two sets of proposals: one for updating the parameters of individual fractures and the other for adjusting the number of fractures in the model.

Distance-Directional Transform

The Distance-Directional Transform (DD-Transform), originally proposed for line detection by Seifollahi et al. (2012), is extended to 3D applications in our approach to generate parameters of new fractures. In 2D applications, the approach can generate the midpoint and the orientation of fractures. It incorporates the distance and the orientation and represents the best orientations of planes embedded in the points. In the following extended version, the approach is used to detect five parameters (out of eight) of the fracture, which are the centre coordinates, (x, y, z) the dip direction and the dip angle. Other three parameters of the fracture (size of the ellipse and rotation) can be generated by specified distributions. Suppose D denotes the conditioning data points, then the steps of the DD-Transform are as follows:

- Set $A = 0$, where A is an $N \times 3$ matrix, and N is the number of points in D

- Select the point $p_i \in D, i = 1, ..., N$.

- Initialize $A^i = 0$ where A^i is an $i_d \times i_a$ matrix; i_d and i_a correspond to the possible indices of the dip direction and dip angle; here $i_d = 360$ and. $i_a = 90$ For $s = 1, 2, ..., S$ do the following:

  a) Select two points. $p_i, p_{j'} \in D, j, j' \neq i$

  b) Determine a plane passing through the points p_i, p_j and $p_{j'}$.

  c) Calculate the dip direction and dip angle of the plane and update $(k, l)^{th}$ element of the matrix

  $$A^i_{kl} = A^i_{kl} + \min\left(b, d_{ij}^{-\alpha} + d_{ij'}^{-\alpha}\right)$$

  where k and l correspond to the index of dip direction and dip angle, respectively, $d_{ij}^{-\alpha}, d_{ij'}^{-\alpha}$ are the distances of p_i to p_j and $p_{j'}$ α and b are two positive constants (here $b = 10$, $\alpha = 0.5$).

- Sort A^i in terms of the highest values. Store the row corresponding to the highest value in i^{th} row of matrix A. If $i \geq N$ go to the next step; otherwise, repeat from second line.

- Sort the rows of A in a descending order with respect to the values obtained in previous step.

- The ith row of A corresponds to the parameters of the ith best new fracture, which includes the dip direction, dip angle and the index of the centre.

Stochastic optimization model

We propose an optimization approach to construct a fracture map fitted to the seismic point cloud with the best possible goodness-of-fit and a most reasonable size. In the initialization step, a prior map,

$H = \left\{ H^i \right\}_{i=1}^{m}$ of fractures is generated, where H^i is an ellipse as a first approximation of the ith fracture and m is the number of fractures. The centres of initial fractures are selected from the seismic points at random. Other parameters of the fractures are generated by their specified probability distributions. Prior distributions for the dip direction, dip angle and rotation angle considered are uniform distributions. For priors for the major and minor axes, lognormal distributions are used.

After the initialization stage, we post-process the fracture map by optimization using the simulated annealing technique. The measure of goodness-of-fit, or objective function for the simulated annealing, consists of two parts: the minimization of the sum of squared distances of the points to the fitted fracture model and the minimization of the number of fractures or the amount of fracturing. The first part is defined as

$$f_d(w) \equiv \sum_{j=1}^{N} d\left(p_j, H_{k*}\right) \qquad k* = \arg\min\left(d\left(p_j, H_k\right)\right) \tag{1}$$

where N is the number of points, j and k stand for the jth point and k^{th} fracture in the network and $d(...)$ represents the orthogonal least squared distance. Minimization of (1) is an essential step to produce an accurate model close enough to the point cloud. The second part of the objective function is expressed as

$$f_{AF} \equiv \sum_{i=1}^{n} \left\{ \frac{(1 + a_i b_i) \times w_p}{1 + N_i \times w_p} \right\} \tag{2}$$

where n is the number of fractures, a_i and b_i are the major and minor axes of ith fracture and w_p is a constant number (here $w_p = 100$).

Two categories of proposals are incorporated in the optimisation process to determine a global optimal solution of the FNM. The first category is related to the parameters of individual fractures, and the second category is used to determine an optimal size of the fracture system (i.e, number of fractures in this case). In the first category, the parameters of individual fractures (the centre, dip direction, dip angle, rotation angle, major and minor axes) are changed, while the aim in the second category is to propose adding new fractures or removing redundant fractures by using the proposals "Split", "Replacement", "Joint" or "Removal".

Based on the consideration of various proposals, the new association between points and fractures is set and the value of the objective function is recalculated by considering the values that are modified by the perturbation. If the change represents a reduction in the objective function, the transformation to the new state is accepted. If it represents an increase in the objective function, the transformation is accepted with a specified probability, p,

$$p = \exp\left(\frac{-f^{new} - f^{old}}{T} \right) \tag{3}$$

where f^{new} and f^{old} are the objective function value in the new and old configurations, T is a control parameter, which corresponds to absolute temperature in the physical process of annealing.

The details of perturbation/modification proposals are as follows:

Centre: The aim is to perturb the centre of a candidate fracture by shifting the location through a direction, d, to one of the associated points of the fracture.

$$(x, y, z) = (x, y, z) + rd$$

where $d \in R^3$ and $r (r \sim U[0,0.1])$ is the step size to determine the amount of the perturbation. Both the candidate fracture and the associated points are chosen at random.

Orientation: The orientation, here, consists of three components, the dip direction, dip angle and rotation angle. The proposal is repeated for each component independently. For a given component, a pair of fractures is selected at random and their corresponding orientation parameters are exchanged.

Major-axis and Minor-axis: Two fractures, H^i and $H^j (i \neq j)$ are chosen at random. The major axes of the selected fractures as well as the minor axes are exchanged independently.

Joint: The steps of the joint proposal are as follows:

- Choose two fractures based on a similarity measure in terms of their parameters (closeness)

- Apply DD-Transform on the associated points of the candidate fractures to find the centre, dip direction and dip angle of a new fracture.

- Generate the rotation angle and major and minor axes from their specific distributions.

Removal: A fracture is chosen from the network based on the lowest density (the ratio of the number of the associated points to the area of the ellipse). The candidate fracture is removed from the network.

Replacement: The steps of the proposal are as follows:

- Choose a set of fractures based on their associated errors, i.e., select fractures with at least one point with the distance to the associated fracture greater than a threshold.

- Apply DD-Transform on the associated points of each fracture selected in previous step to find the "best" orientations of planes passing through all the points concerned.

- Find the highest value in the first column of the matrix. The index of the row corresponding to the highest value represents the candidate fracture and the elements of that row represent the parameters, x, y, z, α and β of the new fracture.

- Generate the other three parameters of the new fracture from their specified distributions.

- Replace the candidate fracture with the new one.

Split: This proposal has similar steps as in the "Replacement" proposal. The key difference is that two new fractures are generated to replace one old fracture. The difference in orientations of the two new fractures should be greater than a threshold in order to represent two distinct fractures.

Habanero reservoir dataset
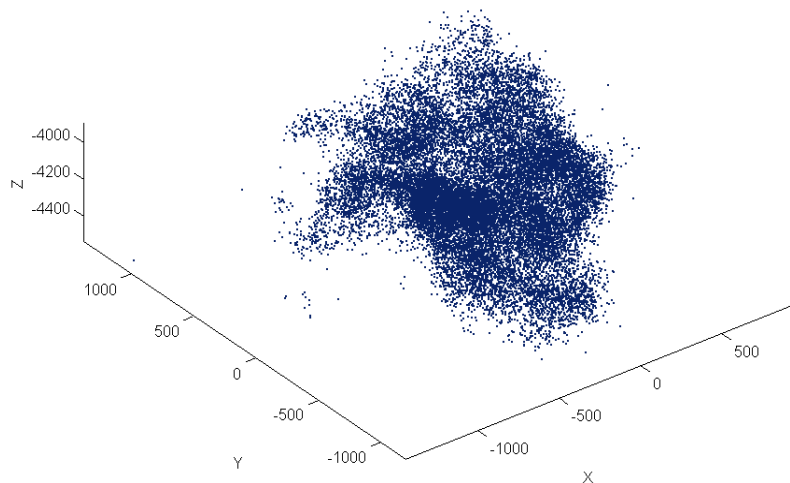
Figure 1: *Hypocentre locations of the seismic events*

The Habanero wells are the key components of Geodynamics' HDR geothermal project in the Cooper Basin, South Australia. These wells have been drilled to depths of about 4400m below the surface or about 700m into the bedrock where temperatures reach 250 °C (Baisch et al., 2006). The dataset used in this study is the Q-Con dataset which contains a total of 23,232 seismic events covering an approximate area of 2.5 km^2. The absolute hypocentre locations of these events are shown in Figure 1.

The resulting fractures after optimization (30000 iterations of simulated annealing) are shown in Figure 2 which represents an optimal realization to the given point cloud. The number of fractures after optimization is 521 compared to 613 fractures in the work of Baisch et al., 2006, and Xu et al., 2011.
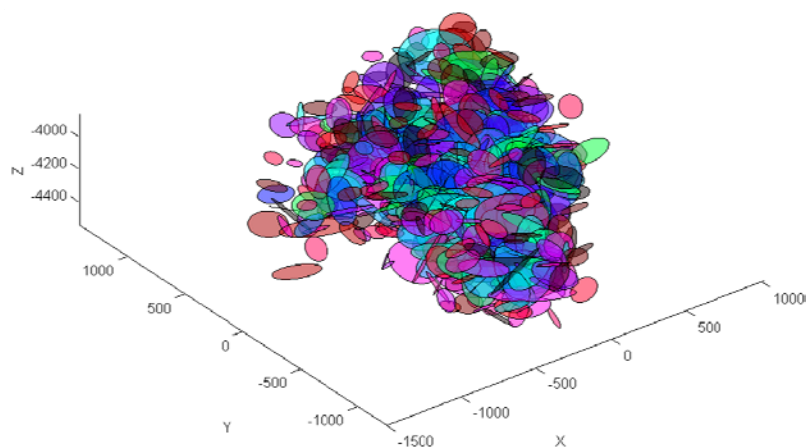
Figure 2: *Habanero fracture model after optimization*

Figure 3 demonstrates the distributions of major and minor axes of the detected fractures which follow a lognormal distribution. The distribution of the point associations is demonstrated in Figure 4. Figure 5 shows the distribution of error, in which the horizontal axis is the error of the points to the nearest fractures.
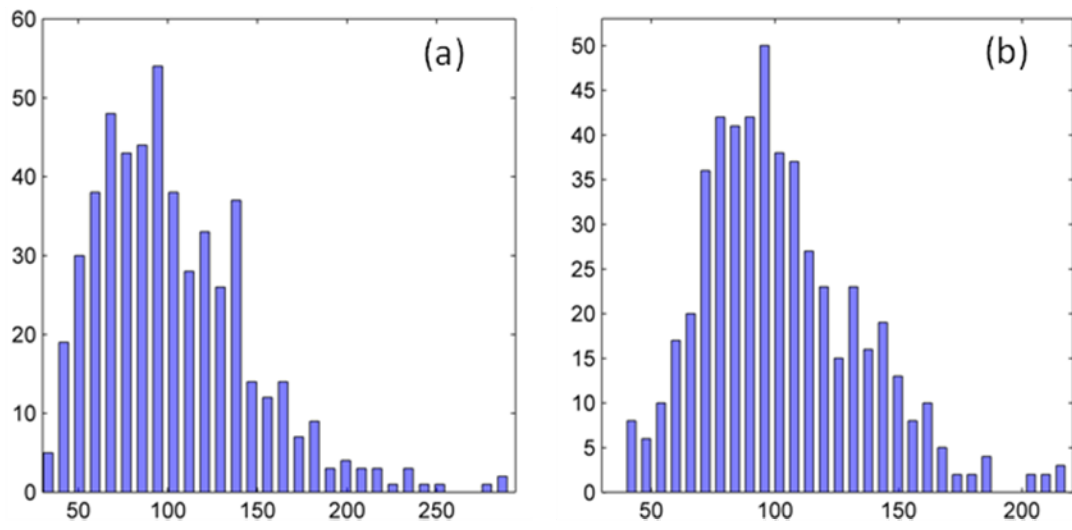
Figure 3: Distribution of size (parameters a and b) of obtained fractures
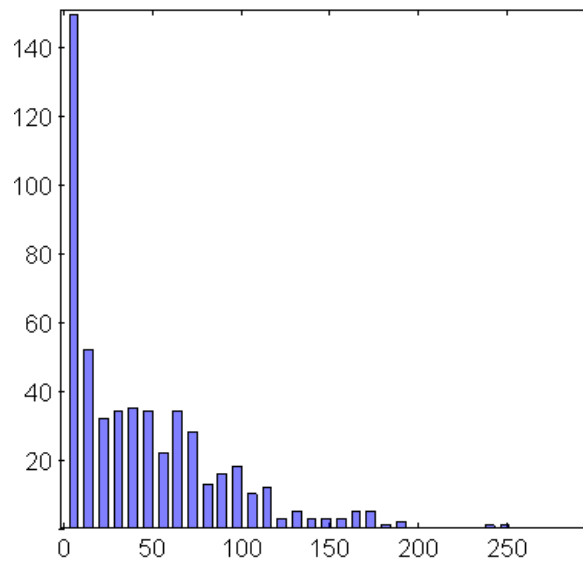
Figure 4: Distribution of the point association
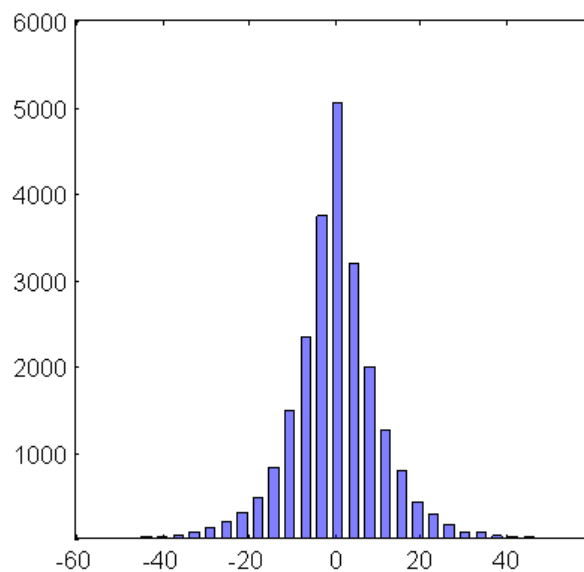
Figure 5: *Distribution of the distances of the points to the fractures*

Conclusions

A global optimization approach has been proposed to generate a remarkably good fit of a fracture map to seismic points recorded during fracture stimulation of the geothermal reservoir. A constructive contribution of the approach is that it addresses two main issues in the optimisation of a fracture model, i.e., a suitable objective function and a model modification system, which still remain as the two major challenging aspects of any global optimization technique. A new method, called DD-Transform, is developed to initialize the parameters of the new generated fractures.

The work demonstrates the effectiveness of the optimization approach for fracture modelling conditional on seismic events. By increasing the number of iterations of simulated annealing, it is expected to get more accurate solution. Work is now proceeding to deal with the time domain feature of the events to get a more realistic and reliable fracture model for the EGS system.

Acknowledgment

References

Baisch S., Weidler R., Vörös R., Wyborn D., and Graaf L-de (2006). Induced Seismicity during the Stimulation of a Geothermal HFR Reservoir in the Cooper Basin, Australia. Bulletin of the Seismological Society of America, 96(6):2242–2256.

Dershowitz W., and LaPointe P. (1994). Discrete fracture approaches for oil and gas applications. In: Nelson PP, Laubach SE (eds) Proceedings of the Northern American rock mechanics symposium, Austin, TX. Balkema, Rotterdam, pp 19–30.

Dowd P. A., Xu C., Mardia K. V., and Fowell R. J. (2007). A comparison of methods for the simulation of rock fractures. Mathematical Geology, 39:697-714.

Einstein H. H. (2003). Uncertainty in rock mechanics and rock engineering—then and now. In: Proceedings of the 10th international congress of the ISRM. The South African institute of mining and metallurgy symposium series S33, vol. 1, pp 281–293.

Kirkpatrick S., Gelatt-J C. D., and Vecchi MP (1983). Optimization by simulated annealing. Science, 220:671-680.

Long J. C. S., and Witherspoon P. A. (1985). The relationship of the degree of interconnection to permeability in fracture networks. J Geophys Res B 90(4):3087-3098.

Mardia K. V., Nyirongo V. B., Walder A. N., Xu C., Dowd P. A., Fowell R. J., and Kent J. T. (2007a). Markov Chain Monte Carlo implementation of rock fracture modelling. Mathematical Geology, 39:355-381.

Mardia K. V., Walder A. N., Xu C., Dowd P. A., Fowell R. J., Nyirongo V. B., and Kent J. T. (2007b). A line finding assignment problem and rock fracture modelling. Bayesian Statistics and its Applications, Eds. Upadhaya, S.K., Singh, U., Dey, D.K. (Eds), Anamaya Pubs, New Delhi pp 319-330.

Odling N. E. (1992). Permeability and simulation of natural fracture patterns, in Structural and Tectonic modelling and its application to petroleum geology. Nor Pet Soc Spec Publ 1:365–380.

Seifollahi S., Fadakar-A Y., Dowd P. A., and Xu C. (*2012) Multi-objective Stochastic Optimization in Fracture Network Modelling. *Submitted.

Xu C., Dowd P. A., and Wyborn D. (2011). Optimised fracture model for Habanero reservoir. In Proceeding of the Australian Geothermal Conference 2010 (Geoscience Australia: Adelaide).

Queensland's Coastal Geothermal Energy Initiative: identifying hot rocks in cool areas

Talebi, B., Sargent, S.N., O'Connor, L.K. and Maxwell, M.

Geological Survey of Queensland, Department of Natural Resources and Mines

behnam.talebi@dnrm.qld.gov.au

The Coastal Geothermal Energy Initiative (CGEI) drilling program commenced in November 2010 and concluded in July 2012, with the completion of 10 boreholes fully cored to depths of between 320 and 500 metres. A variety of geological settings along the State's north and east coasts had been targeted in the drilling program to collect new pre-competitive geoscientific datasets for geothermal energy.

The new datasets collected from the CGEI drilling program have indicated moderate to high heat flow values, between 71 and 113 mW/m^2, which are higher than previous estimates. These values are above the global average and highlight possible geothermal energy potential across the Millungera, Surat, Hillsborough and Maryborough basins. Using the newly established heat flow data, modelled temperatures of 204-239°C are predicted at 5 km depths based on which, total thermal energy content as well as equivalent electric power generation potential has been estimated for the highlighted regions in each basin. As an example, geothermal energy assessment of the Millungera Basin is presented here in more detail. A similar approach was applied to other highlighted basins to assess their potential.

Detailed exploration programs are required to refine geothermal energy potential across the highlighted basins. The viability of exploration programs within the highlighted basins is favourable due to the close proximity to centres of population, industry including mining or power transmission lines.

Keywords: Queensland, geothermal energy, drilling, heat flow, thermal energy, Monte Carlo simulation.

Project Background

Queensland's known geothermal energy resources are located in the far south-west of the state, beneath the Cooper and Eromanga basins. This is a long way from the existing national electricity grid and major population centres, preventing economic viability of the resources in the near term. The $5 million CGEI was established to investigate additional sources of hot rocks for geothermal energy close to existing electricity infrastructure along the State's northern and eastern coastal strips. The CGEI included a shallow drilling program to collect pre-competitive geoscientific datasets. The main purposes of this initiative were firstly to increase knowledge of the crustal temperatures along the north and east coasts where geothermal energy has been less investigated to date, and secondly to facilitate reduction of exploration risks and assist potential explorers to explore for and develop this source of clean energy close to the electricity grid in Queensland.

Data Collection

A precise crustal heat flow determination program was planned as part of the CGEI drilling program to evaluate the geothermal prospectivity of selected geological provinces along the Queensland coast. Moderate to high heat producing intrusives of Proterozoic age, residual heat from Cainozoic volcanism and rifting, and younger low to moderate heat producing intrusives overlain by sedimentary basins with thick coal measures, were targeted for further investigation through the drilling program. The geological setting of the selected targets had been previously discussed in detail in several papers and is not considered further here (Fitzell et al, 2009; Talebi et al, 2010). The drilling program commenced in November 2010 and concluded in July 2012, with the successful completion of 10 boreholes fully cored to depths of 320-500 metres (Figure 1).

Precision downhole temperature logging was undertaken 6-8 weeks after hole completion, when the hole returned to its thermally equilibrated state, and detailed thermal conductivity analysis of the core samples had been completed for all boreholes. The data have been used to determine vertical conductive heat flow in each borehole using inversion modelling technique. Temperature dependence of thermal conductivity data had also been taken into account, following the method of Sekiguchi (1984). The modelling process has indicated moderate to high vertical conductive heat flow of 71-113 mW/m^2, which is higher than previous estimates (Table 1). These values are above the global average and imply possible geothermal energy potential in the respective target drilled.
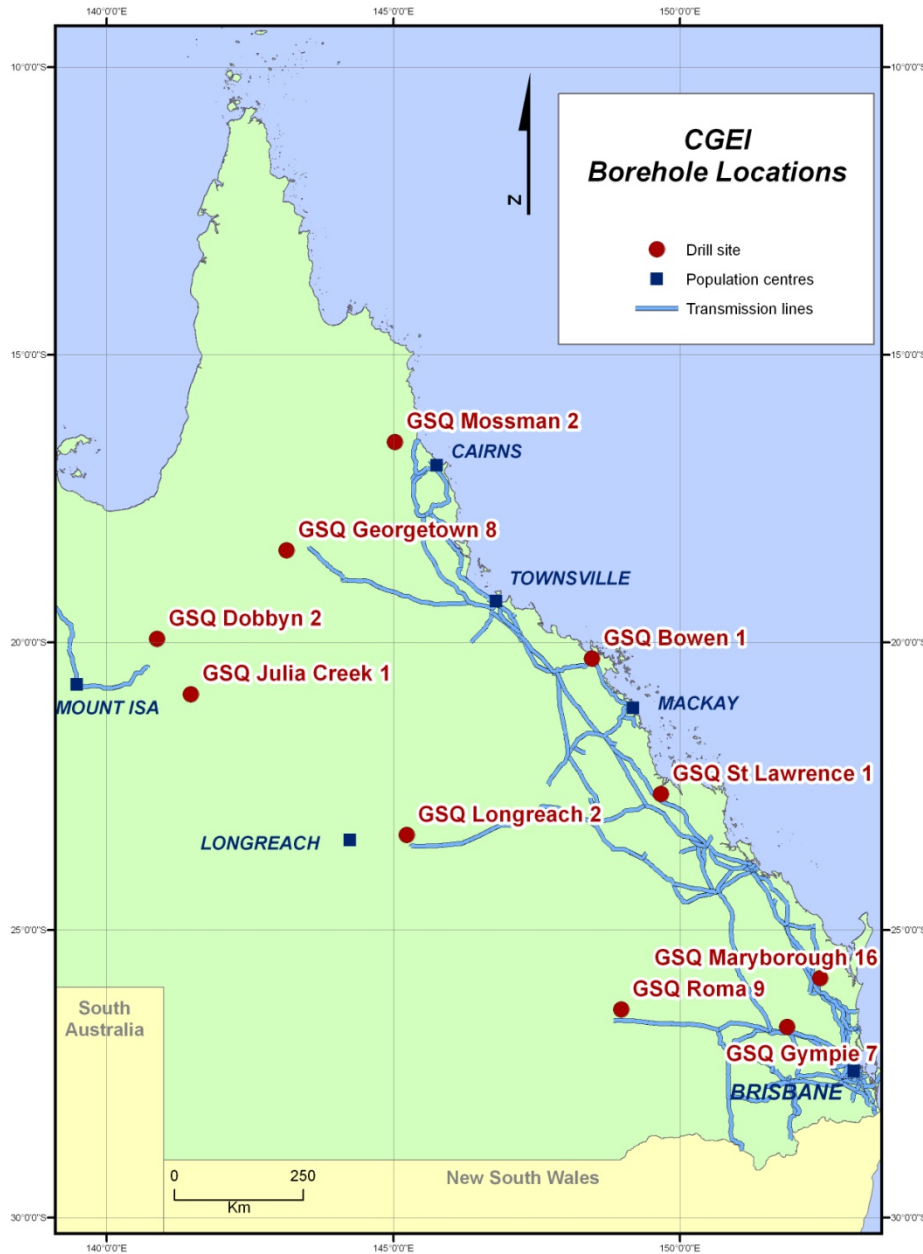
Figure 1: Location of CGEI boreholes

Table 1: A summary of all modelled heat flow values for CGEI boreholes.

Tectonic Unit	Borehole Name	Total Depth (mGL)	Modelled Interval (m)	Harmonic Mean Conductivity (W/mK)	Mean temp. gradient (°C/km)	Heat Flow (mW/m^2)
Millungera Basin - south	Julia Creek 1	500	120-480	2.19±0.08	52.82	113.0±2.8
Millungera Basin - north	Dobbyn 2	500	91-500	1.68±0.04	66.31	107.0±1.7
Surat Basin – Roma Shelf	Roma 9	336	106-336	2.11±0.10	39.04	82.2±2.4
Hillsborough Basin	Bowen 1	321	89-321	2.14±0.11	33.06	71.0±2.3
Maryborough Basin	Maryborough 16	387	61-380	1.97±0.13	34.37	67.4±2.9
Eromanga Basin	Longreach 2	327	84-310	1.40±0.06	41.75	60.0±2.5
Tarong Basin	Gympie 7	338	54-337	1.18±0.08	31.78	37.5±1.5
Styx Basin	St Lawrence 1	340	90-338	1.51±0.04	42.66	64.3±1.1
Georgetown Inlier	Georgetown 8	320	43-265	3.74±0.12	16.09	56.5±1.0
Hodgkinson Province	Mossman 2	339	62-265	3.96±0.08	19.80	77.0±0.9

Uncertainty in the heat flow is calculated by propagating the relative uncertainty in the average thermal conductivity of the rock units intersected.

Temperature Projection

Determination of subsurface temperature at target depth is a key parameter when assessing geothermal energy potential of a target area. In lieu of deep drilling and direct measurements, downward extrapolation of steady-state temperature to a depth *z* can be performed by:

$$T_z = T_0 + q_0 \cdot \int_0^z \frac{d_z}{\lambda_z}$$

Where λ and *d* are the thermal conductivity and thickness of the regarded interval; T_0 and T_z represent the temperature at the top and bottom of the interval, respectively. The heat flow at the top of the interval is q_0 and is assumed purely conductive and therefore constant to depth *z*. Although this linear relationship is a simplification of a complex dynamic system, it is a reasonable first order approximation in the absence of direct measurements at depth.

In the case of CGEI boreholes, the established conductive heat flow values have been used to predict temperatures at greater depths. First, the geological succession to 5km was inferred from geological and geophysical data to estimate the stratigraphic thicknesses and bulk thermal conductivities to that depth using the weighted harmonic means of values measured in this initiative or assigned from published data. It is considered that 5km is deemed an economically drillable depth for electricity generation from a geothermal energy resource. Temperatures at 5km depths were then modelled in one dimension assuming that the established conductive heat flow values remain relatively constant and predictable with depth, with negligible advection. Table 2 shows the input parameters used in the temperature modelling at 5km depth for the Millungera Basin in the vicinity of borehole GSQ Julia Creek 1. Figure 2 is plot of the modelled temperatures at depth beneath the same borehole in conjunction with the geological cross section of the inferred resource area.

Table 2: Input parameters used in the 1D-modelling of temperature to 5km depth beneath the borehole GSQ Julia Creek 1, Millungera Basin.

Tectonic Unit	Age	Bulk lithology	Bulk thermal conductivity (W/mK)	Depth interval (m)
Eromanga Basin	Jurassic - Cretaceous	Mudstone	1.37±0.06	120-236
		Mudstone	1.53±0.05	236-310
Millungera Basin	Palaeo-Mesoproterozoic	Quartzose Sandstone	5.43±0.16	310-1500
Williams Supersuite	Mesoproterozoic	Granitoid	3.20±0.73	1500-3500
Soldiers Cap Group	Palaeoproterzoic	Metasediment	3.26±0.87	3500-5000

The modelled temperatures at 5 km depth range from 204 to 239°C across the Millungera, Surat, Hillsborough and Maryborough basins implying possible geothermal energy potential within these basins. Using the same modelling approach, depth to a cut-off temperature of 150°C – the minimum temperature of the resource which could allow commercial deliverability from a production well – has also been estimated for each basin. This depth is used to determine thickness of the inferred resource when assessing geothermal energy potential in the next section. Results of temperature projection at 5 km and depth estimation to the cut-off temperature are summarised in Table 3. Uncertainty in the projected temperatures calculated solely by propagating the relative uncertainty in the average thermal conductivity of the rock units predicted to 5 km.

Table 3: Temperature and depth projections for CGEI boreholes, based on the established heat flow data from Table 1

Tectonic Unit	Borehole Name	Depth to Cut-off temperature – 150°C (m)	Modelled temperature at 5km (°C)
Millungera Basin - south	Julia Creek 1	3178	239 ± 18
Millungera Basin - north	Dobbyn 2	3630	212 ± 15
Surat Basin – Roma Shelf	Roma 9	3615	204 ± 14
Hillsborough Basin	Bowen 1	3879	204 ± 16
Maryborough Basin	Maryborough 16	3342	206 ± 14
Eromanga Basin	Longreach 2	5390	140 ± 13
Tarong Basin	Gympie 7	8063	106 ± 9
Styx Basin	St Lawrence 1	4734	170 ± 16
Georgetown Inlier	Georgetown 8	6437	122 ± 6
Hodgkinson Province	Mossman 2	4810	156 ± 10

Heat does not always flow vertically in areas where significant lateral contrasts in thermal conductivity exist. Similarly, lateral variations in heat producing elements will also cause local variations in heat flow. Therefore, 1D-modelling of heat flow and temperature may not produce accurate results. For the CGEI targets, lateral contrasts in thermal conductivity as well as heat producing elements must be investigated in more than one dimension in future work.
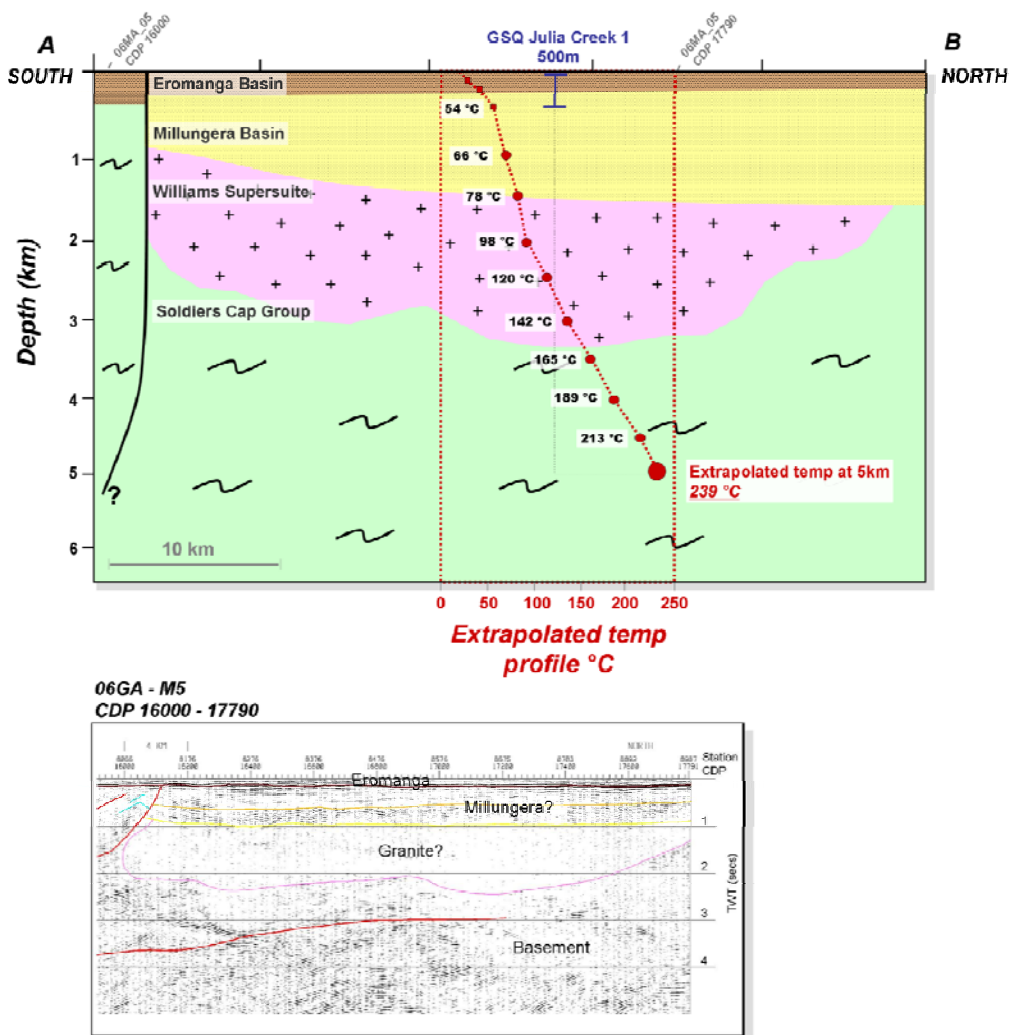
Figure 2: *Temperature extrapolation at 5km depth beneath Julia Creek 1, Millungera Basin, based on heat flow of 113 mW/m^{2}, in conjunction with geological and seismic cross sections. For the broader area refer to Figure 4.*

Geothermal Energy Assessment

An important factor in the assessment of geothermal energy potential of a target area is the evaluation of the volume of the geothermal system in question. For the CGEI targets, a volumetric approach has been used as the preferred method for geothermal energy assessment. This method is patterned from the works applied by the United States Geological Survey (USGS) on the assessment of geothermal energy resources of the United States (Muffler, 1979). In the application of the volumetric method, it is assumed, for simplicity, that the volume is a box, with a surface area A in the x-y plane and thickness z_1-z_0 along the z-axis, where z_1 and z_0 are the lower and upper limits of the geothermal system, respectively. Again for simplicity, it can be assumed that the heat capacity and temperature are homogeneous in the x-y plane and are only dependent on depth. The thermal energy content of the system can then be calculated by integrating the product of the estimated heat capacity per unit-volume, C_z, and the difference between the estimated temperature curve, T_z, in the system and the reference temperature, T_0, i.e.:

$$Q = A \int_{z_0}^{z_1} C_z [T_z - T_0] d_z$$

If one assumes that the temperature curve is close to being linear then calculation of the thermal energy is based on the assumption that the temperature is also homogeneous in the *z* direction and therefore constant over the whole system. This constant would then be the mean temperature of the resource, the average between the cut-off temperature and the temperature at the base of the system. Thus, the thermal energy content of the geothermal system containing single phase liquid, say water, can be estimated by the equation below:

$$Q = [(1-\Phi).\rho_r C_r + \Phi \rho_w C_w].V.(T_R - T_r)$$

where:

Q   Total thermal energy, Joule (J)

Φ Rock porosity, (%)

ρr Rock density, kg/m^3

ρw Water density, kg/m^3

Cr   Rock specific heat capacity, J/kg°C

Cw Water specific heat capacity, J/kg°C

V   Rock (resource) volume, m^3, (=AH) where

   A=Rock (resource) surface area, m^2

   H=Rock (resource) thickness, m

TR Rock (resource) average temperature, °C

Tr   Reference (rejection) temperature, °C

For the highlighted CGEI regions, porosity and presence of fluid (water/steam) at depth are unknown. Furthermore, Sanyal and Sarmiento (2005) indicated that heat in the rock is known to strongly dominate the above equation, even for high porosity rocks with fluid contents. Therefore, it is assumed that the inferred resource rocks of the CGEI targets have negligible porosity hence negligible fluid content thus a more simplistic equation is adopted for the thermal energy estimates presented here, in the following form:

$$Q \approx \rho_r C_r V (T_R - T_r) \qquad\qquad (1)$$

Thermal energy assessment

There are a number of input parameters and assumptions which need to be defined for a thermal energy assessment effort. These parameters and assumptions have been rationalised for the highlighted areas as follows:

Resource mean temperature, (T_R), is taken as the average between the cut-off temperature (150°C) and the temperature at the base of the resource, 5km depth, listed in Table 3. Currently, there is not enough information to conclude that there is significant lateral temperature variation in the highlighted areas so the resource mean temperature, for simplicity, is assumed to be homogeneous and constant in the entire volume of the respective area.

Reference temperature, (T_r), is the temperature relative to which the thermal energy will be estimated. The choice of the reference temperature is very important since it has a large effect on the estimation of thermal energy. Some choose a reference temperature equivalent to the minimum temperature of the geothermal fluid for the intended utilization. For electricity generation purposes, it is often defined as the temperature of the geothermal fluid after heat extraction process in the power plant, also called rejection temperature. For the purpose of this assessment and in the absence of any more definitive information, the reference temperature has been set at 70°C, which is a typical temperature for rejected fluid by an Organic Rankine Cycle (ORC) binary plant with air cooling system.

Specific heat capacity, (C_r), of the CGEI inferred resource rocks at the cut-off temperature of 150°C and above is estimated between 900 and 1000 J/kg°C for plutonic/metamorphic or sedimentary rocks, based on an interpretation of the data presented by Vosteen and Schellschmidt (2003) in Figure 3.
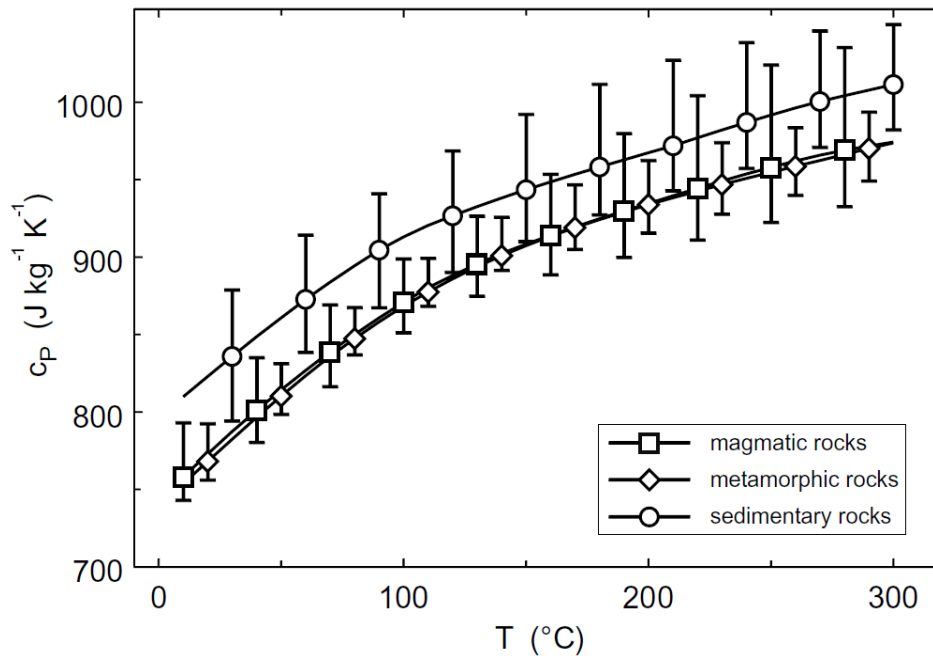
Figure 3: *Mean values and ranges of variation of specific heat capacity ($C\rho$) at constant pressure as a function of temperature for magmatic, metamorphic and sedimentary rocks (Vosteen and Schellschmidt, 2003)*

Density, (ρ_r), of the CGEI inferred resource rocks is taken between 2600 and 2900 kg/m^3 which, based on the GSQ database, is a reasonable approximation for many quartzo-feldspathic rocks within the highlighted areas.

Surface area of the resource, (A), is often defined from available geophysical surveys. For a hot rock project, the area of the resource is defined by the lateral extent of the granitic basement. Both inferred geology and surface development constraints (such as topography and land-use) have been given consideration in the estimation of the surface area of the inferred resources for the highlighted areas. Figure 4 shows the surface area of the resource in the Millungera Basin inferred from the integration of available geophysics data including gravity, MT and seismic.

Resource thickness, (H), is estimated by the depth at which the cut-off temperature of 150 °C is exceeded to the base of the resource i.e. to 5 km depth.

Using the above parameters and simplified equation (1), total thermal energy content of the highlighted areas has been estimated and reported in petajouls (PJ) in this paper. Both the input paramters and estimated thermal energy are presented in Table 4.
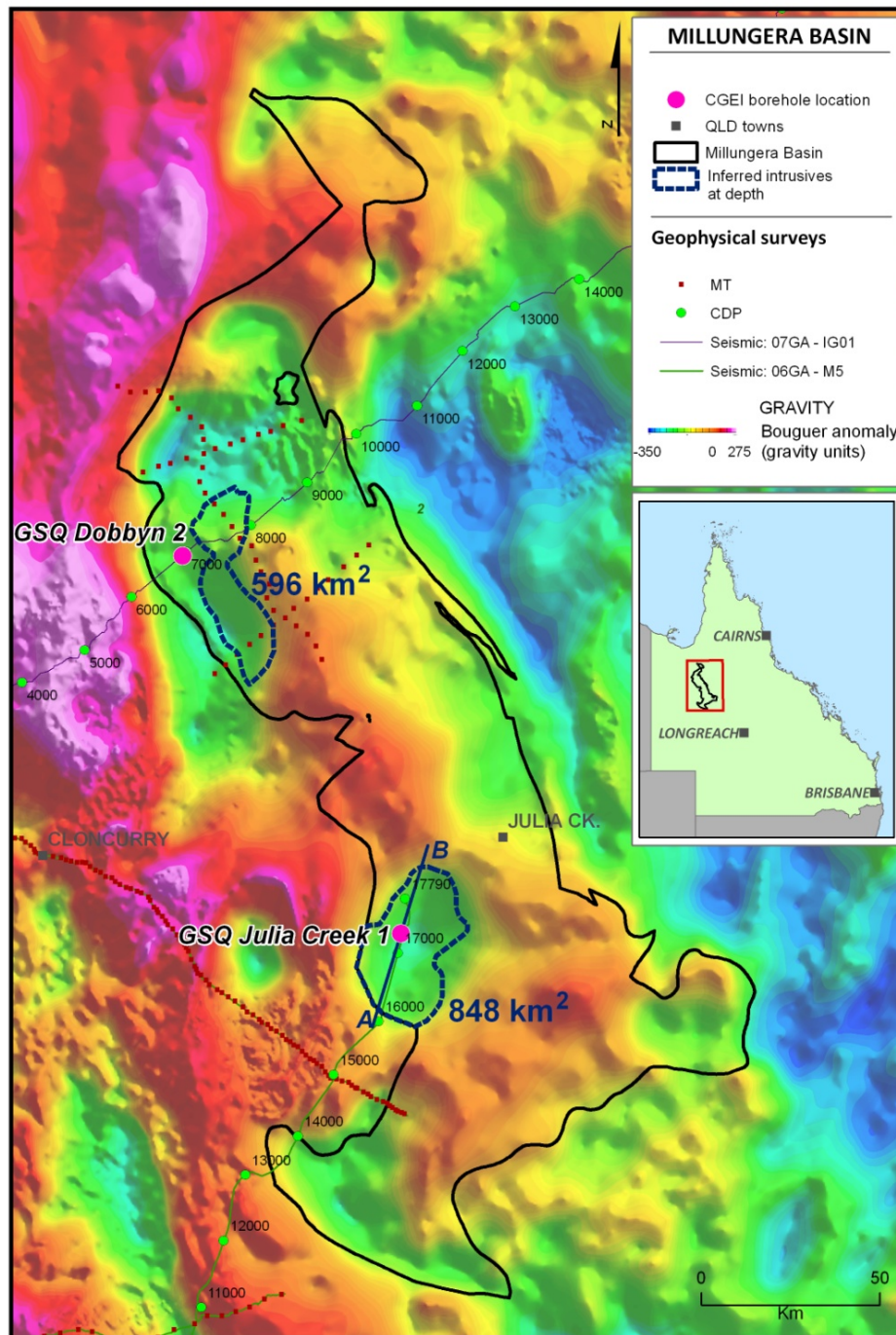
Figure 4: *Inferred intrusive (resource) from gravity, seismic and MT surveys in the Millungera Basin. For cross section A-B, refer to Figure 2.*

Table 4: Input parameters used to estimate stored thermal energy in the inferred resources of CGEI targets. Reference temperature is assumed 70°C in all cases.

Tectonic Unit	Inferred resource thickness (m)	Resource mean temp. (°C)	Resource surface area (km^2)	Rock density (kg/m^3)	Rock specific heat capacity (J/kg°C)	Thermal energy estimate (PJ)
Millungera Basin - south	1822	195	848	2880	1000	553995
Millungera Basin - north	1370	181	596	2880	1000	261025
Surat Basin	1385	177	430	2680	910	155410
Hillsborough Basin	1121	177	464	2870	900	143758
Maryborough Basin	1542	185	342	2680	900	145644

Electric power generation potential

For comparitive purposes and to present a more tangible figure, the estimated thermal energy of CGEI inferred resources is reported in terms of equivalent electric power generation potential. There are a few parameters that govern the conversion process of thermal energy to electricity. These parameters are discussed and rationalised below for the highlighted areas.

Recovery factor: Only a small fraction of the total stored thermal energy in a geothermal system is recoverable and can be converted to electricity. While conceptually simple, recovery factor is very difficult to predict and is hard to define. Even in convective geothermal reservoirs with long production histories, there is no definitive guideline in the literature as to how the recovery factor should be defined or determined (e.g. Grant, 2000). Generally, recovery factors vary between 5-50% depending on the geological conditions mainly porosity, with an average value of 25% for hydrothermal resources (Muffler, 1979) and 40-50% for Enhanced Geothermal Systems (EGS) (Sanyal and Butler, 2005). In 2007, Williams used a theoretical approach and suggested a range of 5-20% as recovery factor for both natural fracture dominated resources and EGS systems. At this stage there is no sound basis for predicting the net recovery factors for the thermal energy estimates of the highlighted areas. Therefore, a conservative value of 5% has been assumed as the recovery factor in the calculations for the areas.

Thermal conversion efficiency: From the recoverable thermal energy of the geothermal system, only a small portion can be converted to electricity, and this is determined by the thermal conversion efficiency of the power plant in use. The conversion efficiency of geothermal power plants is mainly dependent upon the temperature of the geothermal fluid. Compared with conventional fossil-fuel or nuclear powered plants, which operate with superheat steam over temperature ranges of about 550°C, geothermal power plants operate over relatively lower temperature ranges, generally between 150 and 250°C. At these relatively low temperatures, thermal conversion efficiencies are inherently lower than conventional power plants.

With the low temperatures generally around 150°C and the use of ORC binary power plants, the conversion efficiency of geothermal plants can typically vary between 7% and 12%. For higher temperatures, the conversion efficiency can reach well over 12% (Figure 5). Given the fact that the inferred resource temperature of the highlighted areas has not been measured directly, the net thermal conversion efficiency can not be determined at this stage, however, 7% has been assumed as a conservative value for thermal conversion efficiency in the calculations for the areas.
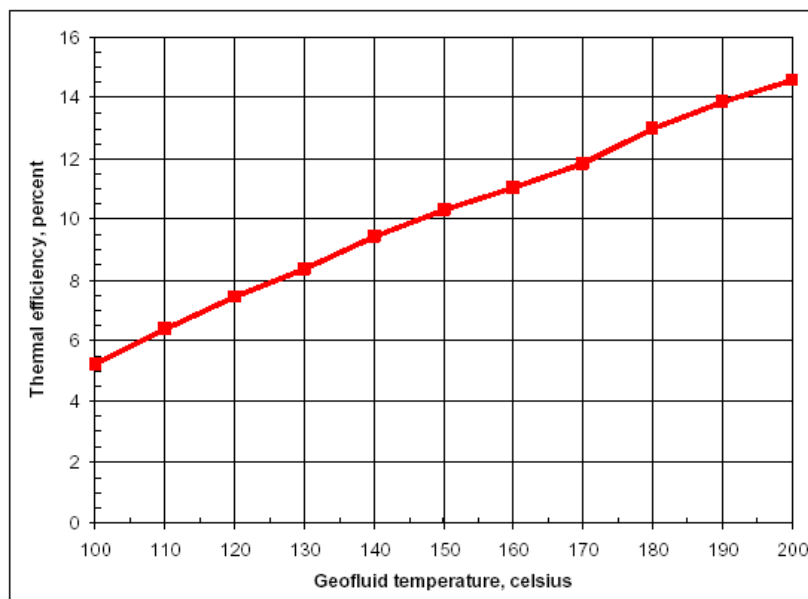
Figure 5: *Level of typical thermal efficiencies for electricity generation of ORC binary plants (Bertani R., 2010)*

Plant capacity factor: The percentage of time a power plant operates is the plant's capacity factor. Base load geothermal power plants typically produce electricity about 90% of the time, but can be operated up to 98% of the time in some cases. It is assumed that 90% would be reasonable capacity factor when calculating electric power potential of the highlighted areas from the estimated recoverable thermal energy.

Plant/project economic life: The economic life of a geothermal plant/project is the period it takes the whole investment to be recovered within its target internal rate of return. This is usually between 25-30 years. Therefore, it is a common practice to assess potential of a geothermal resource over an economic life time span of 25 years.

In summary, the assumptions used to convert the estimated thermal energy to equivalent electric power generation potential in the highlighted areas are:

- Thermal energy recovery factor: 5%

- Plant thermal conversion efficiency: 7%

- Plant capacity factor: 90%

- Plant/Project economic life: 25 years

Based on the above parameters and assumptions, the gross electric power generation potential is estimated to be between 700 and 2700 MWe for the highlighted areas (Table 5).

Obviously the estimates are purely based on a hypothetical case, and therefore should not be taken as an implication that the authors endorse the parameters and assumptions for using in any decision making effort or practical application. These parameters, assumptions and estimates should be revised once detailed exploratory work is undertaken in the future and when more direct measurements at subsurface conditions are available for the highlighted regions.

Table 5: Estimates of recoverable thermal energy and equivalent electric power potential of the highlighted areas.

Tectonic Unit	Inferred resource - recoverable heat estimate (PJ)	Equivalent gross electric power generation potential (MWe)
Millungera Basin – south	27700	2730
Millungera Basin – north	13051	1290
Surat Basin	7770	760
Hillsborough Basin	7188	710
Maryborough Basin	7282	720

Uncertainty Distribution

Because of the limited data and large uncertainty on the assumptions used, some degree of caution and conservatism has also been taken into account in the estimates. This approach, which accounts for the risk factor, can be quantified with reasonable approximation using the Monte Carlo simulation. It applies a probabilistic method of evaluating the estimated thermal energy or equivalent power output that captures uncertainty. Given the complexity and heterogeneity of the geological formations of most geothermal systems, this method is preferred over the usual deterministic approach which assumes a single value for each parameter to represent the whole system. Instead of assigning a "fixed" value to an input parameter, numbers within the range of the distribution model are randomly selected and drawn for each cycle of calculation. The Monte Carlo simulation performs the calculation and determines the estimate based on frequency distribution of the random variables, which are dependent on the number of times a value is extracted from the uncertainty models of the input parameters. To obtain a good representation of the distribution, sampling is usually done through 1000 iterations with continuous calculation. The results are then analysed in terms of the probability of occurrence of the estimated thermal energy or equivalent power output in the range of values over the resulting population.

Availability of sufficient quantitative data is required to justify application of the probability approach in estimating thermal energy content of the highlighted areas. However, to provide an indication of likely uncertainties in the estimates, the assigned input parameters have been categorised as "most likely", "worst guess" and "best guess" scenarios for the Monte Carlo simulation. The assumed input parameters used in the simulation for the Millungera Basin beneath the GSQ Julia Creek 1 borehole are summarised in Table 6.

Figure 6 shows the result of the Monte Carlo simulation for the estimated thermal energy in the vicinity of GSQ Julia Creek 1 drilled in the Millungera Basin. The simulation result is presented as a plot of relative and cumulative frequency distribution against the estimated thermal energy. In fact, it shows that the probability that thermal energy could be greater than 440,000 PJ is 90%. In other words, the risk that the inferred resource could not sustain 440,000 PJ is less than 10%.

The results of the simulation for all the highlighted areas are summarised in Table 7. There is no doubt that the reliability of results from Monte Carlo simulation highly depends on the type, amount, and quality of geoscientific data, which are also dependent on the stage of development and maturity of the target area. Generally, the reliability increases as the target area is drilled with direct measurements and more quantitative data becomes available.

Table 6: Input parameters used in the Monte Carlo simulation to estimate thermal energy in the Millungera Basin, vicinity of borehole Julia Creek 1.

Input Parameters	Worst Guess	Most Likely	Best Guess	Unit
Resource Surface Area	750	848	900	km^2
Resource Thickness	1650	1822	2000	m
Resource mean temperature	180	195	210	°C
Rock Density	2600	2880	2900	kg/m^3
Rock Specific Heat Capacity	900	1000	1100	J/kg°C
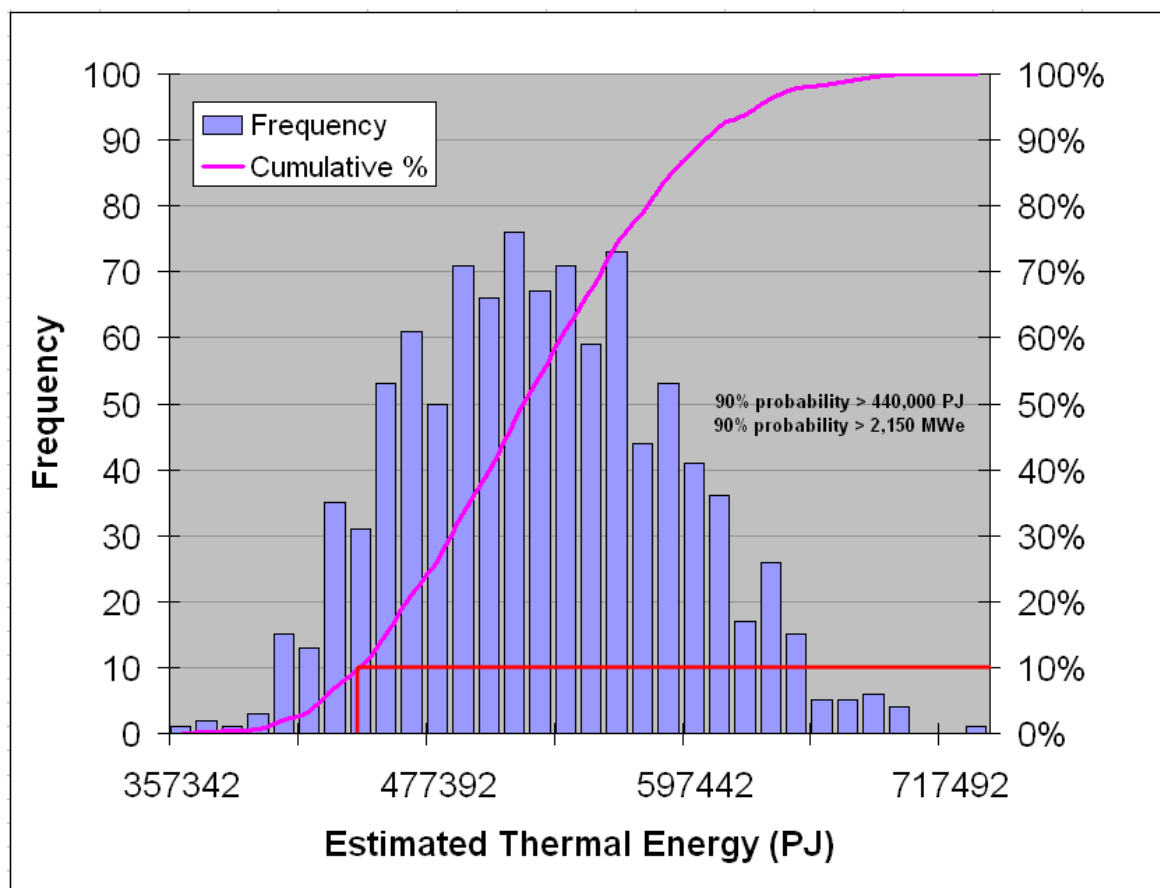
Figure 6: *Result from Monte Carlo simulation, probability of stored thermal energy within the Millungera Basin, vicinity of borehole Julia Creek 1.*

Table 7: Result from Monte Carlo simulation, estimation of stored thermal energy and equivalent power output for the highlighted areas with 90% probability.

Tectonic Unit	Total Thermal Energy - PJ (90% probability)	Electric Power Potential - MWe (90% probability)
Millungera Basin – south	>440,000	>2,150
Millungera Basin – north	>205,000	>1,015
Surat Basin	>130,000	>640
Hillsborough Basin	>110,000	>545
Maryborough Basin	>119,000	>585

Discussion and Conclusion

The CGEI was established to investigate geothermal energy potential close to potential market and the electricity network where electricity demand is increasing significantly and geothermal energy has been less investigated to date. Ten higher ranked geological settings were selected along northern and eastern Queensland to determine vertical conductive heat flow through a shallow drilling program. The newly established heat flow data ranges from 71 to 113 mW/m^2 across Millungera, Surat, Hillsborough and Maryborough basins implying possible geothermal energy potential within these basins. These were previously considered to have a normal crustal heat flow with low geothermal energy potential. Using the new heat flow dataset, temperatures of 204-239°C have been predicted at 5km depth in one-dimension in the selected regions. Due to the lack of information and for simplicity, it was assumed that the heat flow remains relatively constant with depth, and that the modelled temperatures are homogeneous in the vertical direction and therefore constant over the entire system. Based on the modelled temperatures at greater depths, total thermal energy content is estimated between 144,000 and 554,000 PJ at the selected targets using the volumetric approach under stated assumptions. The distribution of the heat per unit volume ranges between 260 and 360 PJ/km^3 which is relatively similar to the energy density reported for other geothermal prospects in Australia. The highlighted areas may be prospective for both EGS and Hot Sedimentary Aquifer (HSA) development depending on the rock type intersected at the target temperature and also mitigating other risk factors such as poor permeability.

Equivalent gross electric power generation potential of the highlighted areas has been estimated from the recoverable thermal energy based on certain assumptions. The estimates show power generation potential of 700-2700 MWe in the highlighted regions. The Monte Carlo analysis has indicated that the electric power generation potential of 585-2150 MWe can be expected from the highlighted basins with 90% probability. Obviously, the estimates are purely based on a hypothetical case under certain assumptions due to the lack of sufficient quantitative data, and therefore should be revised once detailed exploration programs are undertaken in the future and direct measurements at greater depths are available.

Overall, the method for estimating thermal energy has limitations. It provides no information about the practicalities of development, particularly whether there may be resource-specific constraints such as poor permeability, scaling or corrosion problems. However, it can still give an understandable, rational basis for comparing the size of different geothermal resources, taking into account both volume and temperature.

Individual well completion reports of CGEI boreholes are being released progressively as they are completed. A final report to outline the assessment of geothermal energy potential across the State's north and east coasts is due for publication by mid 2013. All the reports will be publically available through the Queensland Government's Digital Exploration Reports (QDEX) on-line system.

Recommendations

Following recommendations are made in order to refine geothermal energy potential in the highlighted basins:

- Spatial distribution of heat flow data needs to be increased in each area by incorporating all wells or boreholes previously drilled or currently being drilled as well as drilling new holes if necessary. This would require precision temperature logging to be undertaken in the holes and more extensive measurements of rock thermal conductivity to be made.

- A three-dimensional geological model of each area needs to be developed for facilitating 3D heat flow modelling to better constrain the 3D distribution of the temperature field. This would require triaxial thermal conductivity analysis of rock samples to investigate effects of anisotropy.

- Extensive stress field study is required across the highlighted basins at both regional and prospect scales for initiating numerical hydro-mechanical modelling to constrain expected geothermal reservoir growth direction.

- Exploratory drilling is required to validate the prospectivity of the identified areas. This would initially require drilling of low-cost slim-holes to 2-3km depth to verify predicted temperatures at depth, confirm geological succession, perform downhole logging and revise geothermal resource assessment.

- An engineering feasibility study needs to be undertaken by collating and integrating all the available geoscientific data, engineering and economic parameters to evaluate commercial viability of geothermal energy development programs in the highlighted basins individually.

References

Beardsmore, G. R., and Cull, J. P., 2001, Crustal Heat Flow: A Guide to Measurement and Modelling, Cambridge University Press, 324pp.

Bertani, R., 2010, Geothermal power plant efficiency: EUROSTAT consultation, TP Geoelec, 3rd Meeting, Pisa, Italy.

Cull, J. P. and Beardsmore, G. R., 1992, Statistical methods for estimates of heat flow in Australia, Journal of Exploration Geophysics 23, 83-86.

Fitzell, M., Hamilton, S., Beeston, J., Cranfield, L., Nelson, K., Xavier, C. and Green P., 2009, Approaches for identifying geothermal energy resources in coastal Queensland, Proceedings of the 2009 Australian Geothermal Energy Conference, 6pp.

Grant, M.A., 2000, Geothermal Resource Proving Criteria, Proceedings World Geothermal Congress 2000, 2581-2584.

Korsch, R.J., Struckmeyer, H.I.M., Kirkby A., Hutton, L.J., Carr, L.K., Hoffmann, K.L., Chopping, R., Roy, I.G., Fitzell, M., Totterdell, J.M., Nicoll, M.G. and Talebi, B., 2011, Energy Potential of the Millungera Basin: A Newly Discovered Basin in north Queensland, APPEA Journal 2011, 295-332.

Muffler, P., 1979, Assessment of geothermal resources of the United States-1978, USGS circular 790, 164p.

Muffler, P. and Cataldi, R., 1978, Methods for regional assessment of geothermal resources. Geothermics, 7, 53-89.

Rybach, L., 1989, Heat flow techniques in geothermal exploration, First Break Vol. 7, No.1, 9-16.

Sanyal, S. K. and Butler, S. J., 2005, An Analysis of Power Generation Prospects from Enhanced Geothermal Systems, Geothermal Resources Council Transactions, 29.

Sanyal, S.K. and Sarmiento, Z. F., 2005, Booking Geothermal Energy Reserves, Geothermal Resources Council Transactions, 29.

Sargent, S., Maxwell, M., Talebi, B. and O'Connor, L., 2011, Queensland's Coastal Geothermal Energy Initiative: preliminary heat flow modelling results, Proceedings of the 2011 Australian Geothermal Energy Conference, 6pp.

Sekiguchi, K., 1984, A method for determining terrestrial heat flow in oil basinal areas: Tectonophysics, 103, 67–79.

Somerville, M., Wyborn, D., Chopra, P., Rahman, S., Estrella, D. and Van der Meulen, T., 1994, Hot Dry Rocks Feasibility Study, Energy Research and Development Corporation, Report 243, 133pp.

Talebi, B., Maxwell, M., Sargent, S. and Bowden, S., 2010, Queensland Coastal Geothermal Energy Initiative – An Approach to a Regional Assessment, Proceedings of the 2010 Australian Geothermal Energy Conference, 6pp.

Vosteen, H.-D. and Schellschmidt, R., 2003, Influence of temperature on thermal conductivity, thermal capacity and thermal diffusivity for different types of rock. Physics and Chemistry of the Earth, 28, 499-509.

Williams, C. F., 2007, Updated methods for estimating recovery factors for geothermal resources, Proceedings, 32nd Workshop on Geothermal Reservoir Engineering, Stanford University, SGP-TR-183, 7pp.

Electromagnetic monitoring of fluid injection – lessons learned

Thiel, S.[1],*, Peacock, J.R.[1], MacFarlane, J.[1], Heinson, G.[1]

[1] Center for 4D Electrical Earth Imaging, University of Adelaide, SA 5005

*Corresponding author: stephan.thiel@adelaide.edu.au

Abstract

Magnetotelluric data acquired over the Paralana project has provided valuable insight into the resistivity distribution across geothermal sedimentary basins. The time-lapse MT measurements during an EGS fluid injection trace the preferential fluid connection in a NNE direction aligned with the regional stress field. The results add information to existing micro-seismic measurements by providing the preferential fluid-filled fracture connection at depth. New results using 2D forward magnetotelluric anisotropy codes are able to reproduce the direction of enhanced fluid flow by fitting measured against modelled phase tensor residuals. Future surveys will need to address limited resolution issues between EM measurements from the surface compared to standard micro-seismic monitoring techniques.

Introduction

EGS systems are an alternative to conventional hydrothermal systems as seen in New Zealand and Iceland for energy production. Creating fluid reservoirs at depths has been established at Habanero and Paralana, South Australia to create a volume of hot fluids for extraction. Prior knowledge of the extent and direction of fluid connection at depth is still a matter of research and relation to regional stresses and pre-existing faults are suggested. Conventional industry standard monitoring techniques of fluid injection involve microseismic monitoring (Wohlenberg and Keppler, 1987), sensitive to fracture opening events as a result of the fluid injection pressure.

Recent results from electromagnetic monitoring of a fluid injection at Paralana (Figure 1) indicate that a volume of 3.1 million litres of injected fluids at 3.6 km depth are sufficient to detect changes above measurement error in MT response at the surface (Peacock et al., 2012). The response changes calculated from successive 24 h blocks of frequency domain MT responses are spatially and temporally coherent and coincide with the injection schedule. Inversions of the MT responses relate the changes in the frequency domain to depth and estimates result in a conductive block at around 2.8 km depth, a few hundred metres shallower than the injected fluid. The discrepancy is due to the uncertainties in the inverse process and its non-uniqueness about the data. While the depth estimation is still matter of ongoing research, the use of invariant phase tensor representation of the measured impedance tensor Z (E=ZB) allows for a rigorous estimation of the directional dependence of the time-lapse measurements in view of the temporal changes. Peacock et al. (2012) show that time-lapse MT measurements result in preferred NNE orientation of current change of measurements taken a few days after fluid pumping began. The preferred orientation seems consistent from measurements weeks after the injection (Peacock et al., 2012a) and is aligned with the regional stress field.

Microseismic monitoring of the Paralana fluid injection appears to support the findings with seismic events aligned preferably in the NNE direction. The faults appear to be only a few hundred metres apart questioning the accuracy of surface MT measurements to individually resolve these faults. We propose that MT is still sensitive to these features without having the resolution to individually map the faults. The expected effect is similar to assuming electrical anisotropy of the fluid injection volume.
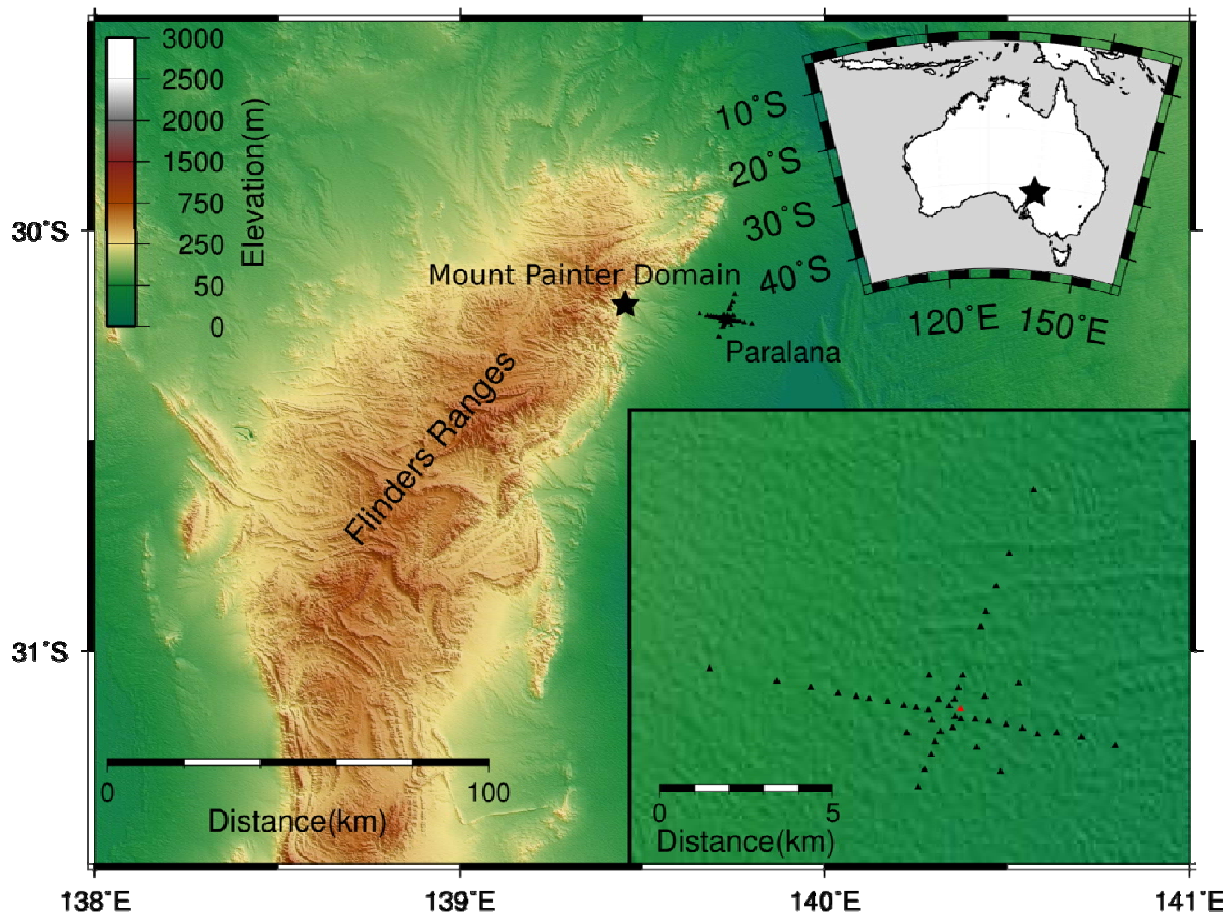
Figure 11: *Survey layout of the Paralana MT survey across the fluid injection site of the Paralana EGS system. The EW line is chosen for 2D anisotropic forward modelling of the injection volume at 3.6 km depth.*

Anisotropy modelling

In order to reproduce an electrical anisotropy response due to fluid injection the 2D forward anisotropy code by Pek & Verner (1997) was employed to simulate electromagnetic fields as a response to a fluid injection scenario at 3.6 km depth. The 2D model domain extending in the EW direction across the Paralana injection site is populated with isotropic (equal in all measurement directions) resistivity changing with depth (1D) following 2D inversion results of the observed MT data across the injection site Paralana 2. The top layer extends to 900 m with resistivity of 10 ohm.m, underlain by the basement and compacted sediments with an isotropic resistivity of 500 ohm.m. The anisotropic fluid injection volume is situated at a depth of 3.6 km with dimensions of 1km wide and 600 m high. The resistivities are equal for the resistivity in the x-direction (north) and z-direction (vertical) but are more resistive in the y-direction. Usual values assigned to the x-, and z- direction vary between 0.01 ohm.m and 100 ohm.m while maintaining a 500 ohm.m resistivity in the y-direction, equal to the background resistivity. In addition to changing the principal resistivities, the strike and dip angle of the resistivity structure is altered to match the observed responses. The best fit between modelled and observed responses is achieved by using an anisotropy strike angle of N10°E parallel to the regional stress field (Figure 2).

$$\rho_x = 0.01\ \Omega m \qquad \alpha_S = 10°$$
$$\rho_y = 500.00\ \Omega m \quad \alpha_D = 30°$$
$$\rho_z = 0.01\ \Omega m \qquad \alpha_{SL} = 0°$$
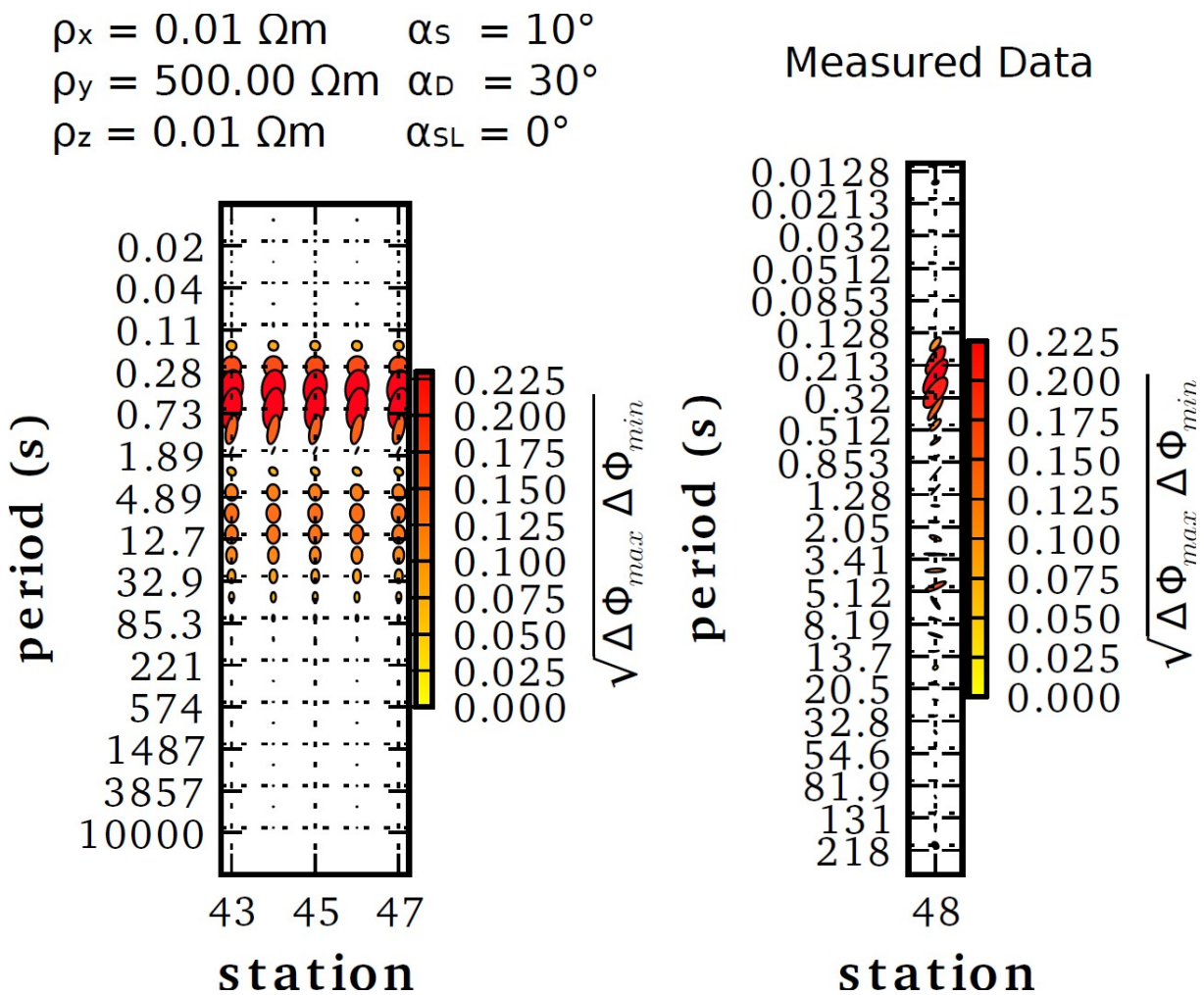
Figure 2: *Comparison of phase tensor residuals for anisotropy modelled (left) and observed (right) stations adjacent to the injection well. Responses are the difference between pre-injection and post-injection magnetotelluric responses. Orientations of the major axes denote direction of maximum connection of fluids and therefore electric currents as a result of fluid injection. An injection body with highest conductivity defined at a strike of N10°E and a 30° dip results in observed phase tensor residuals that match the observed responses.*

Conclusion

The estimation of extent from a fluid injection experiment remains an outstanding research question. Electromagnetic methods offer a useful complementary data set to microseismic monitoring. While microseismics images a high-resolution event cloud of fracture opening, magnetotelluric imaging is directly sensitive to the fluid volume and shows distinct directional dependence aligned with the regional stress field. Observed MT responses are ideally represented using anisotropy due to the lack of resolution of small fractures at depth, which however still produce a polarised MT response. MT anisotropic forward modelling is able to reproduce preferred fracture alignment and results compare well with observed MT responses at Paralana and with the measured microseismic cloud.

References

M. A. Hasting, J. Albaric, V. Oye, P. Reid, M. Messeiller and E. Llanos, 2011, *Micro-seismic monitoring during stimulation at Paralana-2 South Australia*: presented at 2011 Fall Meeting, AGU, San Francisco, California, 2012

Peacock, J. R.; Thiel, S.; Reid, P. and Heinson, G. *Magnetotelluric monitoring of a fluid injection: Example from an enhanced geothermal system*, Geophysical Research Letters, 2012, 39, L18403

Peacock, J.R., Thiel, S.; Reid, P. and Heinson, G. *Time-lapse magnetotelluric monitoring of an enhanced*

geothermal system, Geophysics, accepted

Pek, J. & Verner, T. *Finite-difference modelling of magnetotelluric fields in two-dimensional anisotropic media,* Geophysical Journal International*, Blackwell Publishing Ltd, 1997*, 128*, 505-521

Wohlenberg, J., and H. Keppler (1987), *Monitoring and interpretation of seismic observations in hot dry rock geothermal energy systems*, Geothermics, 16, 441–445.

Great Artesian Basin Heat Source Characterisation in the Light of Recent Helium Isotope Studies

Uysal, I.T [1], Siegel, C [1], Yuce, G [1] and Italiano, F [2]

[1]QGECE, [2]IstitutoNazionale di Geofisica e Vulcanologia, sezione di Palermo, Italy

t.uysal@uq.edu.au

Keywords: Great Artesian Basin, Millungera, Galilee and Cooper Basins, helium and carbon isotopes, mantle fluids

Introduction

Great Artesian Basin (GAB) in eastern Australia has a potential for geothermal development as shown by a variety of different methods in recent years. Temperatures at 5km depth have been interpreted to be very high (>230 °C). Measurements from shallow water boreholes show high near surface temperatures (up to 95 °C) (Radke et al., 2000). High heat flow has been attributed to the radioactive decay of U, Th, and K stored in the basement granitic rocks below the thermally insulating sedimentary rocks of the Eromanga, Cooper, Galilee and Millungera Basins. The Big Lake Suite granite underlying the Cooper Basin is regarded as the primary source of the heat in northeast South Australia and southwest Queensland. A wide diversity of basement granites are identified in central Queensland, with heat production values from 1.5 to 4 $\mu W/m^3$ and emplacement ages 400-860 Ma. The basement granites thus contrast with those at Innamincka with ~7-9.7 $\mu W/m^3$ heat production values and ~330-310 Ma emplacement ages (Siegel et al., 2012). The low average heat production values and low abundance of basement granites across southwest Queensland requires additional heat sources. Overall, the Cooper Basin is one of the Australian sedimentary basins with the highest subsurface CO_2 content with mantle-like carbon isotope signatures, which is consistent with CO_2 originated from the mantle (Boreham et al., 2001). This feature, together with the relatively low abundance of basement granites and the high temperatures across SW Queensland, raises the question of whether high thermal gradients in the GAB can be related to a mantle-derived heat flux.
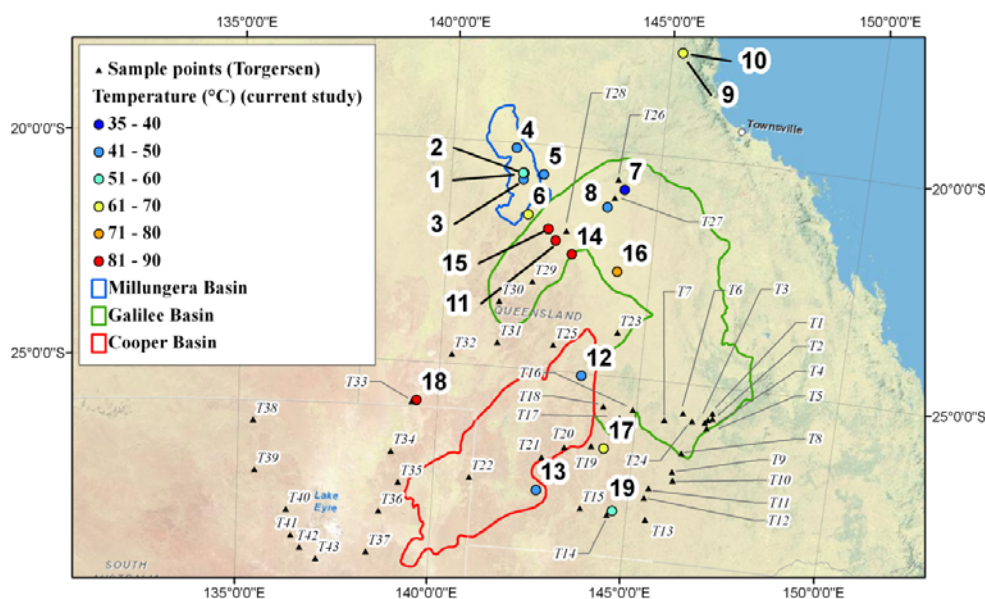

Figure 1: *Samples location over the investigated Millungera, Galilee and Cooper basins. Samples ID are the same as in tables 1-3. Black small triangles and numbers show the distribution of samples reported by Torgersen et al., 1992. Outlet temperatures are shown in various colours (see legend).*

QGECE Heat Source Discovery and Characterisation Program conducted a regional study of gases dissolved in artesian thermal waters collected throughout the Galilee and Millungera Basins and the northern part of the Cooper Basin in SW Queensland (Fig.1). The aim of this study was to verify a mantle fluid flux in eastern Australian sedimentary basins. Water samples were collected from 19 artesian wells in November 2011 and December 2012, and analyzed for dissolved gas contents (He, CO_2, CH_4, N_2 and O_2), and He and C isotopes to constrain the origin of volatiles released from artesian waters (Fig. 1) (Italiano et al., 2012).

Results and discussion

The isotopic composition of helium dissolved in almost all the samples denotes a crustal origin besides very low atmospheric contamination in agreement with previous determinations (e.g. Torgersen et al., 1992; Kulongosky et al., 2008). Closer examination of the data reveals that samples with high ^{4}He/^{20}Ne (denoting negligible atmospheric contamination) show ^{3}He enrichment from a source different from the air-saturated water (Italiano et al., 2012). This is the case of samples from Galilee Basin marked by values of 0.1Ra (Winton and Quilpie) and 0.09Ra (Longreach), where ^{3}He content seems to be three to five times higher to the respect of the other samples and an order of magnitude above the typical ratio for radiogenic production as expected for granites (0.01Ra). Although our data suggests that the helium contribution from the mantle to the GAB is limited to between 0.5% and 2.5%, the narrow range of δ^{13}C (from -5.89‰ to -6.11‰) in the Cooper Basin suggests a considerable amount of mantle degassing, consistent with the area's anomalously high heat flow. The lower helium isotopic ratios to the respect of those detected at the Galilee Basin can be the effect of contamination of mantle-derived fluids by radiogenic He derived from the granitic basement, and diluted as they diffuse through the > 3km-thick sequence of the (equally radiogenic) GAB aquifers. The helium content, significantly higher at Cooper Basin than at the others supports this outlook. The estimated 0.5-2.5% mantle component (this paper and also Torgersen and Clarke, 1985) is likely to be a conservative estimation, partly because of dilution, and partly because the regional ^{3}He/^{4}He crustal background is likely to be lower than the 0.01 Ra used as the radiogenic end-member in our calculations.

Elevated ^{3}He/^{4}He ratios with respect to crustal values as presented in our study (see also Torgersen et al., 1992) is consistent with the thinnest crust in the Australian continent, which is ca. 30 km and less, occurs in the southern extension of the study area in southwest Queensland and northeast South Australia (Kennett et al., 2011) that also coincides with high temperature anomalies (Chopra and Holgate, 2005) and low seismic velocity anomalies (Saygin and Kennett, 2010, 2012). Recent seismic tomography studies suggest that deep crustal fracturing and degassing and hence heat release from the mantle occurs at smaller scale than the whole GAB (Saygin and Kennett, 2010, 2012). The ambient seismic noise of the Australian continent indicates close spatial relationship between the features of the group wave speed anomaly map and the characteristics of major geological provinces of Australia. Low wave speeds are attributed to the thickness of sedimentary cover and/or elevated temperatures (Saygin and Kennett, 2010, 2012). For the shortest periods, anomalies are mostly associated with thick sedimentary sequences. At the longer periods, reduced wave speeds are most likely due to elevated temperatures. The Cooper Basin region includes a sharp low velocity anomaly (139°-141°E; 27°-29° S) with further strong anomalies corresponding to the western Cooper Basin (Poolowanna Trough, Simpson Desert Basin) and parts of the Galilee Basin. Strong low velocity anomalies are related to short seismic periods of up to 8.3s, whereas somewhat weaker anomalies correspond to the 12.5s period, which may indicate the role of high temperatures, crustal fracturing and/or upward migration of deep fluids and volatiles (E. Saygin, 2012, personal communication).

Implications and conclusion

The presented He isotope and geochemical data indicate multiple volatile sources including spatially variable proportions of deeply-derived (endogenic) fluids in the GAB. The ^{3}He/^{4}He values higher than typical crustal values of 0.01-0.05Ra indicate deep mantle-derived fluid uprise to the GAB through the ductile lower crust and brittle upper crust. Considering the general assumption that the fluid passage through the impermeable ductile lower crust is difficult (cf., Kennedy and van Soest, 2007), the

fundamental question that should be dealt with in future is how the mantle He was injected into the crustal-fluid system in a continental interplate tectonic setting far away from Tertiary volcanic centres (more than 500 km). In regions void of active or recently active volcanism, as is the case in the study area, amagmatic flow of mantle fluids through the ductile lower crust can occur due to the creation of permeable pathways as a result of crustal deformations (Kulongoski et al., 2005; Kennedy and van Soest, 2007). The role of faults as conduits and seals between sub-basins, and as preferential paths of deep-originated fluids that may include mantle-derived ^{3}He and CO_2 has to be considered in future studies, and the possible fluids/faults relationships should be investigated and interpreted at a scale compatible with the fault extension (normally from a few tens to a hundred km). The conventional idea of continental geothermal resources being dependent on only radiogenic heat is insufficient to explain observations and thus mantle heating via crustal thinning/fracturing may be an important contributor.

References

Boreham C.J., Hope J.M. and Hartung-Kagi B. (2001). Understanding source, distribution and preservation of Australian natural gas: a geochemical perspective, APPEA Jour. 2001, 523-547.

Chopra P & Holgate FL. 2005. A GIS Analysis of Temperature in the Australian Crust. Proceedings of the World Geothermal Congress 2005, Antalya, Turkey.

Italiano, F., Yuce, G., Uysal, I.T., Gasparon M., and Morelli, G. (2012). A new insight into mantle contribution and basin settings in the Great Artesian Basin, Australia: Evidence from dissolved gas phases in artesian waters. Earth and Planetary Science Letters, in review.

Radke BM, Ferguson J, Cresswell RG, Ransley TR, Habermehl MA (2000) Hydrochemistry and implied hydrodynamics of the Cadnaowie – Hooray Aquifer, Great Artesian Basin. Bureau of Rural Sciences, Canberra ISBN 0 642 47554 7.

Kennedy, B.M. and van Soest, M.C. (2007), Flow of mantle fluids through the ductile lower crust: helium isotope trends. Science 318, 1433-1436.

Kennett B.L.N., Salmon M., Saygin E. and AusMoho Working Group, 2011. AusMoho: the variation in Moho depth in Australia, Geophys.J.Int., 187, 946-958.

Kulongoski, J.T., Hilton, D.R., Izbicki, J.A., (2005). Source and movement of helium in the eastern Morongo groundwater Basin: the influence of regional tectonics on crustal and mantle helium fluxes. Geochimica et Cosmochimica Acta 69, 3857–3872.

Kulongoski J T., Hilton D R., Cresswell R G., Hostetler S, Jacobson G (2008) Helium-4 characteristics of groundwaters from Central Australia: Comparative chronology with chlorine-36 and carbon-14 dating techniques. Journal of Hydrology (2008) 348, 176– 194.

Saygin E. and Kennett B.L.N. (2010) Ambient noise tomography for the Australian Continent, Tectonophys., 481, 116-125.

Saygin, E., and Kennett B.L.N., (2012) Crustal structure of Australia from ambient seismic noise tomography, J. Geophys. Res., 117, B01304; doi:10.1029/2011JB008403.

Siegel, C., Bryan, S., Purdy, D., Allen, C., Uysal, T., and Gust, D. (2012). The origin of the temperature anomaly in SW Queensland Australia: High Heat Producing Granites or efficient insulation cover? 34th International Geological Congress 2012

Torgersen T., Clarke W.B. (1985) Helium accumulation in groundwater, I: An evaluation of sources and the continental flux of crustal 4He in the Great Artesian Basin, Australia. Geochim. Cosmochim. Acta, 49, 1211-1218.

Torgersen T., Habermehl, M. A. and W. B. Clarke (1992). Crustal helium fluxes and heat flow in the Great Artesian Basin, Australia. Chemical Geology 102, 139-152.

Performance of air-cooled organic Rankine cycle plants using temperature distributions from arid parts of South Australia

Varney, J.J [1] and Bean, N [1]

[1]University of Adelaide

Josephine.Varney@adelaide.edu.au

Keywords: air-cooling, ambient temperature, binary Rankine Cycle, super-critical heat exchanger

Abstract

Air-cooling is necessary for geothermal plays in dry areas and ambient air temperature significantly affects the power output of air-cooled thermal power plants. Hence, a method for determining the effect of ambient air temperature on subcritical and supercritical, air-cooled binary Rankine cycles using moderate temperature geothermal fluid and various working fluids is presented. Part of this method, includes a method for maximizing working fluid flow from a supercritical heat exchanger. In the example presented isobutane is used as the working fluid, while the geothermal fluid temperature and flowrate are set at 150°C and 126kg/s. Results of this analysis show that for every 14°C increase in ambient air temperature, above the ambient temperature used for design purposes, there is ~20% loss in brine efficiency; while conversely, there is no gain in brine efficiency for any drop in ambient air temperature below the ambient air temperature used for design purposes. Using the ambient air temperature distribution from Leigh Creek, Australia, this analysis shows that an optimally designed plant produces 6% more energy annually than a plant designed using the mean ambient temperature.

Introduction

Air-cooling is necessary for geothermal plays in the South Australian desert and other dry areas. Ambient air temperature significantly affects the power output of air-cooled thermal power plants, and so a method for quantifying and predicting this effect is needed. This paper presents a method for determining the effect of ambient air temperature on subcritical and supercritical, air-cooled binary Rankine cycle plants. This model is built using basic thermodynamic principals only and does not use or rely on industry standard models such as GETEM or ASPEN. This significantly reduces the number of inherent assumptions and the subsequent complexity, making cause and effect clearer.

Since each site can have only one plant, it can only be optimally designed for one ambient air temperature. Therefore, the plant must run in off-design conditions when the current ambient air temperature is higher or lower than the design ambient temperature. Assuming a geothermal fluid temperature of 150°C, the results of this analysis show that for every 1°C increase in immediate ambient air temperature, above the design ambient temperature, there is ~1.5% loss in brine efficiency. While conversely, there is no gain in brine efficiency if the current ambient air temperature drops below the design ambient air temperature.

Using the ambient air temperature distribution from Leigh Creek, South Australia, further analysis shows that an optimally designed plant produces 6% more energy, annually, than a plant designed for the mean ambient temperature. Similar results are obtained for geothermal fluid temperatures up to 250°C, using temperature distributions from Moomba, Roxby Downs and the Coonawarra.

Method

The majority of Australia's 366 existing geothermal exploration licences are located in arid to semi-arid areas of the continent, targeting relatively low enthalpy EGS and HSA targets. In this context, it is likely that binary Rankine cycles and air-cooling will be the most viable technologies for electricity

production from many projects. Hence, we chose, in this paper, to model an air-cooled binary Rankine cycle plant.

A binary Rankine cycle plant has two separate circulating fluids: the *geothermal fluid* which brings the heat from deep in the earth to the surface, and the *working fluid* which takes heat from the geothermal fluid and uses this heat to generate electricity (see Figure 1).


Figure 1: *Schematic for an air-cooled binary Rankine cycle*

Although not commonly mentioned, all Rankine cycles have another fluid, the *cooling fluid*; this is the fluid which removes heat from the vaporized working fluid, allowing it to condense and then be pumped back up to pressure. Generally, this cooling fluid is water because it has excellent thermodynamic properties for cooling, it is stable, abundant and cheap (which explains why 99% of the power plants in the USA use water cooling [5, p. 12]). However, where water is scarce, ambient air is used for cooling because it is also stable, abundant and cheap (although its thermodynamic properties, for cooling purposes, are not as good as water).

The working fluid in a Rankine cycle goes through four separate *processes*, changing the fluid into four different *states*. At State 1 the working fluid is a low pressure, low temperature saturated liquid, it is then pumped up to high pressure liquid (State 2), and then heated to become a high pressure vapor (State 3). Pressure and temperature, of the working fluid, drop across the turbine (to produce mechanical energy) to leave a low temperature, low pressure vapor in State 4. This vapor is then condensed to become the low pressure, low temperature saturated liquid of State 1, and the cycle starts again.

An *ideal* Rankine cycle assumes that the pump and the turbine operate isentropically, and that the condenser and the heat exchanger operate at constant pressure. Determining the power output from an ideal Rankine cycle is well known and widely covered in textbooks [1, 9, 2] so we will not go into it in detail here (for more information see paper 'Building a model to investigate the effect of varying ambient air temperature on air-cooled organic Rankine cycle plant performance' also presented at AGEC2012). Simply, if the following are known:

1. temperature of the saturated liquid at State 1,

2. temperature and pressure of the vapor at State 3,

3. working fluid mass flowrate,

the net-power generated by the ideal Rankine cycle can be determined.

Results

For a given set of plant conditions ($m^{GThF}, T_a^{GThF}, p_b^{GThF}$, working fluid and $T_{design\ amb}$) and an ambient temperature distribution it is possible to determine the energy output of an air-cooled binary Rankine cycle.

First, we examined the effect of ambient air temperature on brine efficiency for four different geothermal fluid temperatures (150°C, 175°C, 200°C, 225°C and 250°C). These results show the effect of an ambient temperature on a given day; so, on any site on any day, if you have these design conditions, this is the brine efficiency you can expect.

These results (see Figure 2), show that ambient air temperature has a significant impact on the power output of air-cooled binary Rankine cycle plants, for thermal uid temperatures of 150°C - 225°C. More specifically, according to our modeling, these plants lose around 10-15% brine efficiency for every 10°C increase in actual ambient air temperature, above the design ambient air temperature. Further, when the actual ambient air temperature is colder than the design ambient air temperature, there is no increase in brine efficiency.

Each graph in Figure 2 shows, what we call here the `maximum line', the maximum brine efficiency for all ambient air temperatures (i.e. this line assumes a new plant was designed for each point on this line). The maximum line is compared, in this Figure, to two individual plant designs, with design ambient air temperatures of 10°C and 20°C. Clearly, the brine efficiency for a single plant, will meet the `optimal line' at the design ambient air temperature. From Figure 7, it is also easy to see that a plant loses significantly more, in comparison to the optimal line, at temperatures which are colder than the design ambient air temperature, than it does from temperatures which are hotter than this temperature.

However, Figure 2 doesn't answer the question, `What is the best plant design for a specific temperature distribution?' Most air-cooled binary plants are designed at the mean ambient temperature. Looking at Figure 7 it is difficult, if not impossible, to decide if this is the best choice for your site. To be able to quantify the effect of ambient temperature at a given site, it is necessary to consider the temperature distribution for that site.

From the Australian Bureau of Meteorology we obtained half-hourly temperature data from three sites in South Australia: Leigh Creek, Moomba and the Coonawarra; and used this data to calculate a yearly time average of the actual brine efficiency for a range of design ambient temperatures. The *yearly time average brine efficiency* is the sum of the actual brine efficiencies for each temperature in a calendar year multiplied by the time at that temperature divided by the time in a year. So, for a plant that under ideal conditions (i.e. you had the design ambient air temperature every moment of every day of the year) has a brine efficiency of 120kJ/kg, once you consider the actual ambient temperature distribution for that site the plant may only produce on *average* 116kJ/kg.

The yearly time averaged brine efficiency results for Moomba are shown in Figure 3, the results for Leigh Creek are shown in Figure 4, and the results for the Coonawarra are shown in Figure 5. These results show that yearly time averaged brine efficiency plateaus or even drops off at colder design ambient temperatures, while it decreases sharply with hotter design ambient temperatures. This sharp decrease begins around 5-10°C colder than the site's mean temperature.

Many air-cooled binary Rankine cycle plants choose the mean ambient air temperature (at their site) to use as their design ambient air temperature. Our results show that building a plant using a design ambient air temperature of ~10°C colder than mean yearly air temperature would increase the yearly time averaged brine efficiency by 5-8%.
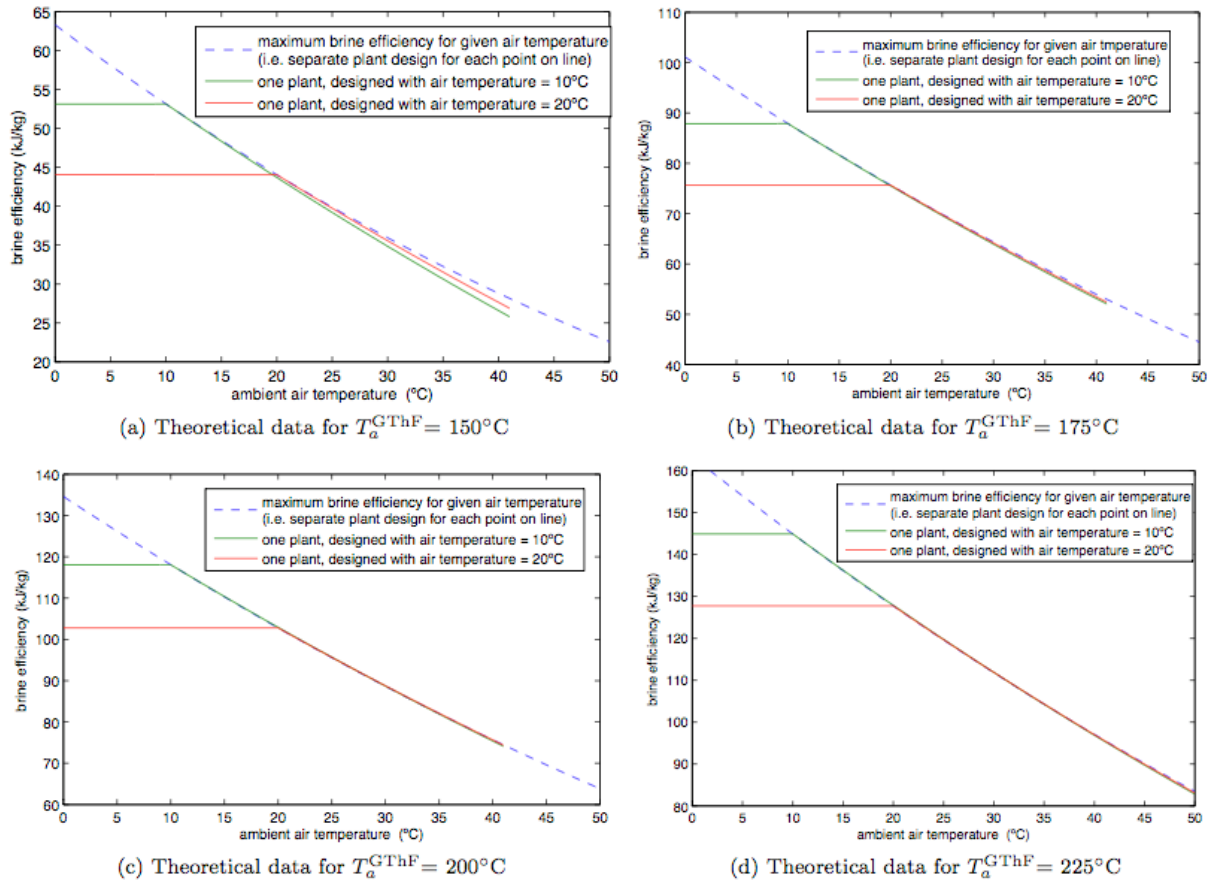
Figure 2: Theoretical data for various geothermal fluid temperatures

- A blue dashed line for maximum brine efficiency for the given air temperature (i.e. a separate plant design for each point on the line). This line is roughly linear and brine efficiency descends with increasing air temperature, for all geothermal fluid temperature options.

- A green line representing one plant designed with an air temperature of 10°C. This line is horizontal from the left of the graph, until it meets the maximum brine efficiency line. It then fairly closely follows the maximum brine efficiency line. For plots a and b, however it drops increasingly below this line with increasing ambient temperature.

- A red line representing one plant designed with an air temperature of 20°C. This line follows the same curve as the green line above. However, since it starts on the left at a lower point, it is always lower than the green line until it meets the maximum brine efficiency line, there after it is always above the green line (since it has started is movement away from the blue line at a later point that then green line).]
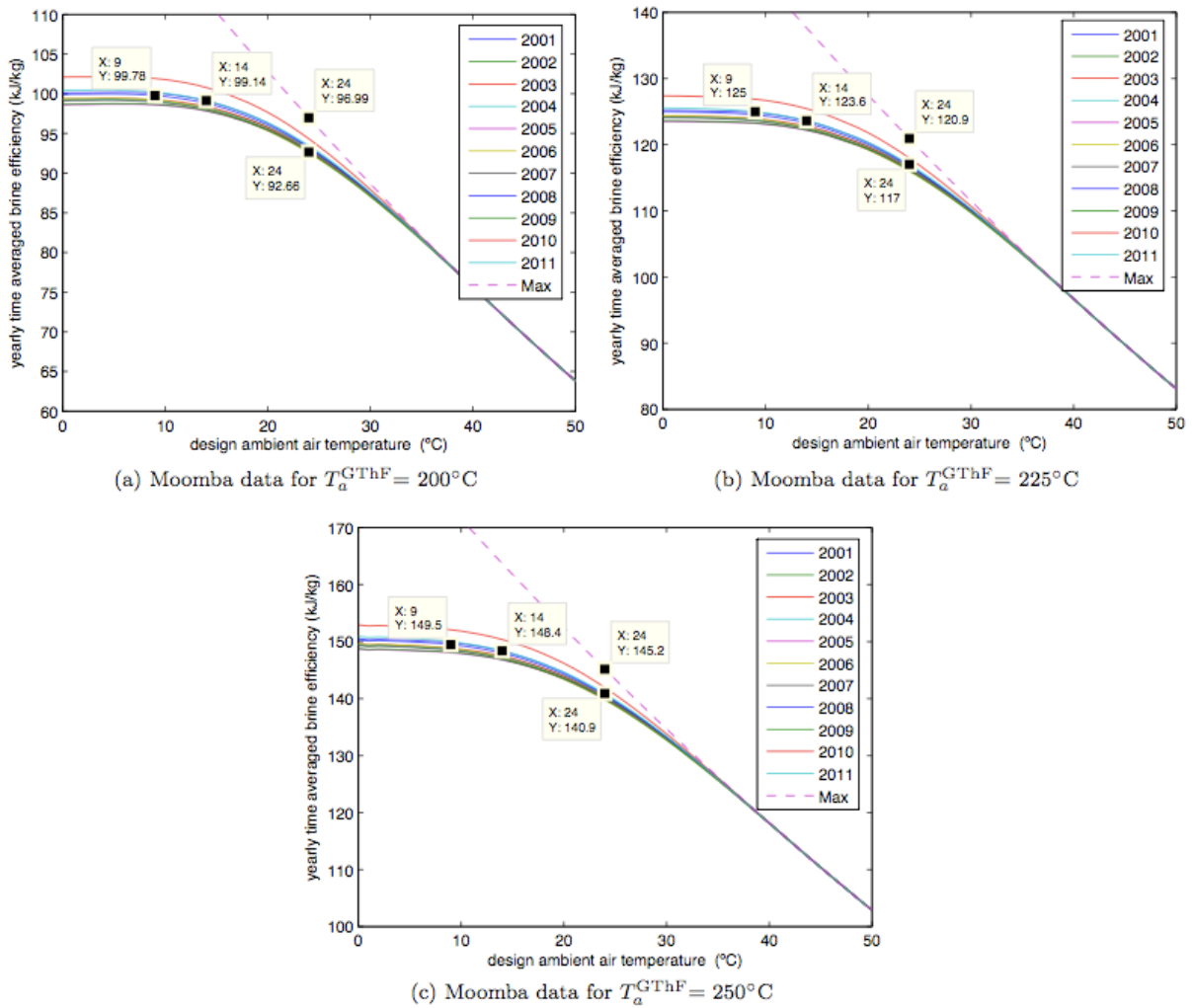
Figure 3: *Moomba site data for various geothermal fluid temperatures. The mean temperature at Moomba is 24°C. (Please note: The maximum brine efficiency line is the same line as shown in Figure (2), it is put here for ease of reference, but does not take into account any site data.)*
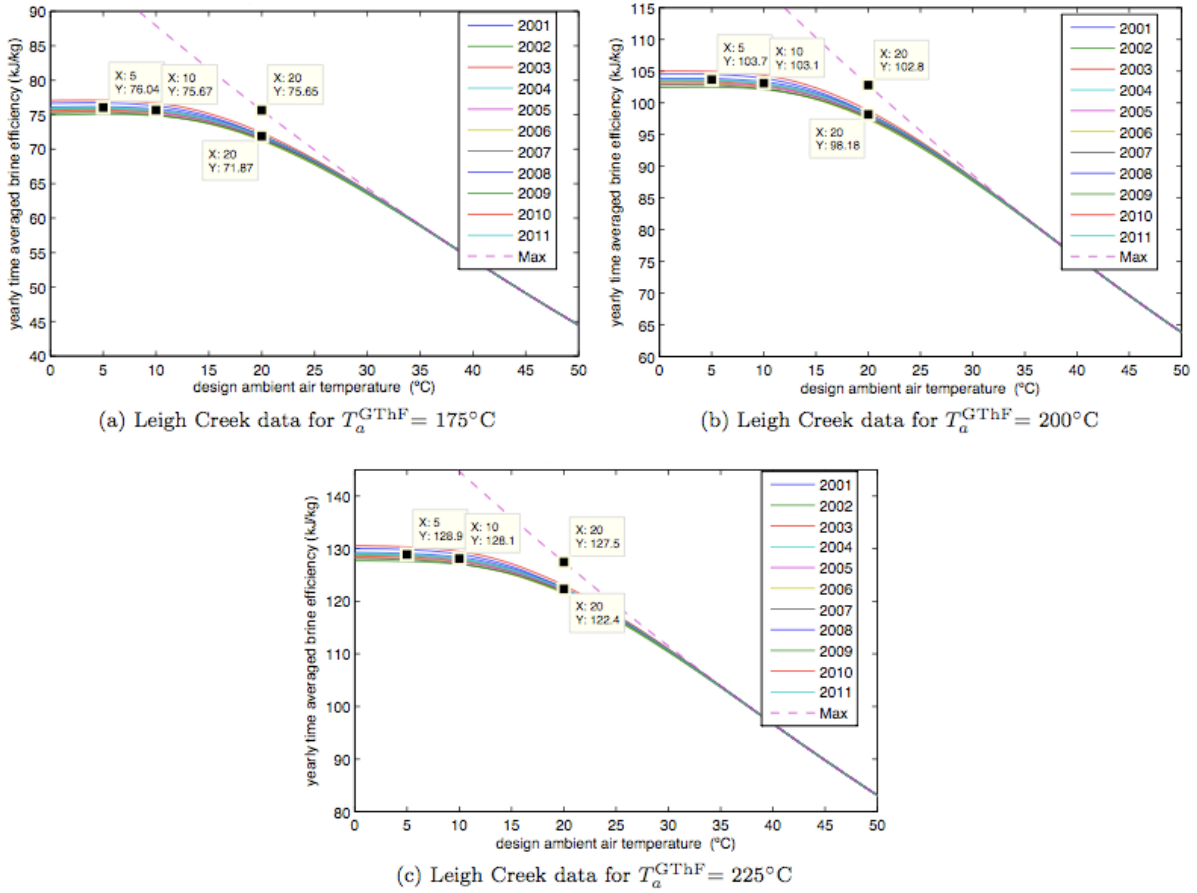
Figure 4: *Leigh Creek site data for various geothermal fluid temperatures. The mean temperature at Leigh Creek is 20°C. (Please note: The maximum brine efficiency line is the same line as shown in Figure (2), it is put here for ease of reference, but does not take into account any site data.)*
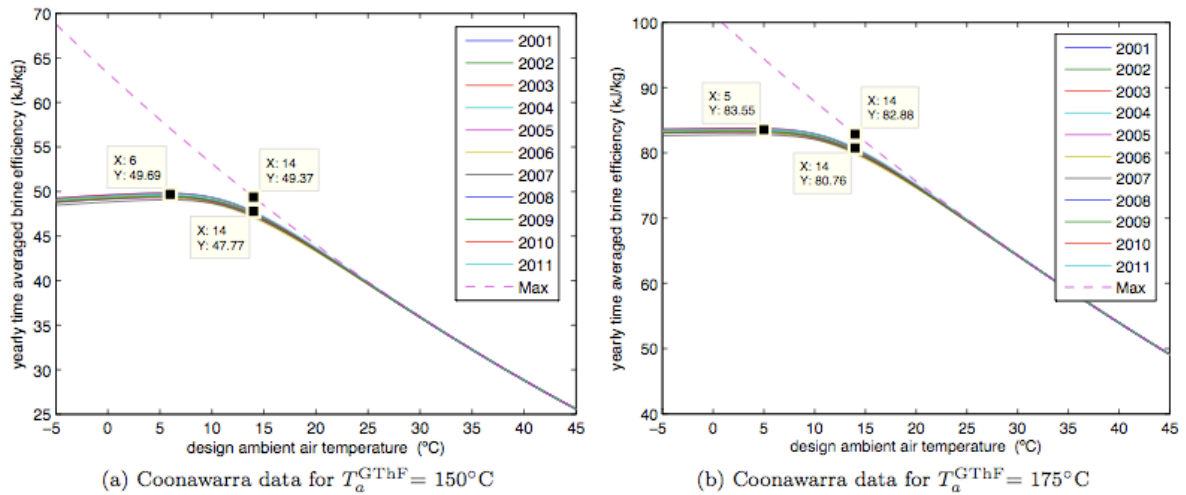
Figure 5: *Coonawarra site data for 150°C and 175°C geothermal fluid temperatures. The mean temperature in the Coonawarra is 14°C. (Please note: The maximum brine efficiency line is the same line as shown in Figure (2), it is put here for ease of reference, but does not take into account any site data.)*

Conclusion

Air-cooled binary Rankine cycle plants are significantly and adversely affected by varying ambient air temperature. However, while this loss is fundamentally due to the thermodynamics of the Rankine cycle, considering a site's temperature distribution and the off-design effects of this distribution can allow for better choice in initial plant design.

By designing for a temperature which is colder than the mean site temperature a plant's output can be increased by 5-8%. Since, designing for a lower ambient temperature will increase initial plant costs (due to the requirement for a larger heat exchanger), in the final analysis, the capital costs will need to be weighed against ongoing improved production capabilities.

List of abbreviations

h	enthalpy (J/kg)
m	mass flowrate (kg/s)
p	pressure (kPa)
s	entropy (J/(kg/K))
c_p	heat capacity at constant pressure (J/(kg K))
P	power (W)
Q	heat flow per second (J/s)
T	temperature (°C)
ΔT	temperature difference (°C)
η_{brine}	brine efficiency (W-h/kg)
η_{th}	thermal efficiency (dimensionless)

Superscripts

CF	cooling fluid
GThF	geothermal fluid
cold	cold fluid
hot	hot fluid

Subscripts

1,2,3,4	State 1, 2, 3 or 4
a,b,c,d	State a, b, c or d
Amb	ambient state
in	heat added to the cycle
PP-C	pinch point in the condenser
PP-HX	pinch point in the heat exchanger

Acknowledgements

References

Cenegel, Y.A., and A.B. Boles, 1989. "Thermodynamics an Engineering Approach.' McGraw-Hill, 5th Edition.

DiPippo, R., 2008. "Geothermal Power Plants: Principals, Applications, Case Studies and Environmental Impact." Elsevier, 2nd Edition.

U.S. Energy Information Administration (EIA), April 2011. "Annual energy outlook 2011 with projections to 2035." U.S. Energy Information Administration (EIA).

Entingh, D.J., July 2006. "DOE Geothermal Electricity Technology Evaluation Model (GETEM): Volume 1 – Technical Reference Manual." Department of Energy.

Stiegel, G.J., A. McNemar, B. Schimmoller, M. Nemeth, J. Murphy, and L. Manfredo, August 2006. "Estimation freshwater needs to meet future thermoelectric generation requirements." National Energy Technology Laboratory, Department of Energy (USA).

Mines, G., 2000. "Summary of investigations of the modified turbine inlet conditions in a binary power plant." Proceedings of GRC 2000 Annual Meeting.

Morris, C., April 2012, Personal correspondence.

Wendt, D., and G. Mines, September 2010. "Interim Report: Air Cooled Condensers for Next Generation Geothermal Power Plants Improved Binary Cycle Performance." Idaho National Laboratory.

Van Wylen, G.J., and R.E. Sonntag, 1958. "Fundamentals of Classical Thermodynamics." John Wiley and Sons, Inc, 3rd Edition.

Building a model to investigate the effect of varying ambient air temperature on air-cooled organic Rankine cycle plant performance

Varney, J.J [1] and Bean, N [1]

[1]The University of Adelaide

Josephine.Varney@adelaide.edu.au

Keywords: air-cooling, ambient temperature, binary Rankine Cycle, super-critical heat exchanger

Abstract

Air-cooling is necessary for geothermal plays in dry areas and ambient air temperature significantly affects the power output of air-cooled thermal power plants. Hence, a method for determining the effect of ambient air temperature on subcritical and supercritical, air-cooled binary Rankine cycles using moderate temperature geothermal fluid and various working fluids is presented. Part of this method, includes a method for maximizing working fluid flow from a supercritical heat exchanger. In the example presented isobutane is used as the working fluid, while the geothermal fluid temperature and flowrate are set at 150°C and 126kg/s. Results of this analysis show that for every 14°C increase in ambient air temperature, above the ambient temperature used for design purposes, there is ~20% loss in brine efficiency; while conversely, there is no gain in brine efficiency for any drop in ambient air temperature below the ambient air temperature used for design purposes. Using the ambient air temperature distribution from Leigh Creek, Australia, this analysis shows that an optimally designed plant produces 6% more energy annually than a plant designed using the mean ambient temperature.

Introduction

Air-cooling is necessary for geothermal plays in the South Australian desert and other dry areas. Ambient air temperature significantly affects the power output of air-cooled thermal power plants, and so a method for quantifying and predicting this effect is needed. This paper presents a method for determining the effect of ambient air temperature on subcritical and supercritical, air-cooled binary Rankine cycle plants. This model is built using basic thermodynamic principals only and does not use or rely on industry standard models such as GETEM or ASPEN. This significantly reduces the number of inherent assumptions and the subsequent complexity, making cause and effect clearer.

Since each site can have only one plant, it can only be optimally designed for one ambient air temperature. Therefore, the plant must run in off-design conditions when the current ambient air temperature is higher or lower than the design ambient temperature. Assuming a geothermal fluid temperature of 150°C, the results of this analysis show that for every 1°C increase in immediate ambient air temperature, above the design ambient temperature, there is ~1.5% loss in brine efficiency. While conversely, there is no gain in brine efficiency if the current ambient air temperature drops below the design ambient air temperature.

Using the ambient air temperature distribution from Leigh Creek, South Australia, further analysis shows that an optimally designed plant produces 6% more energy, annually, than a plant designed for the mean ambient temperature. Similar results are obtained for geothermal fluid temperatures up to 250°C, using temperature distributions from Moomba, Roxby Downs and the Coonawarra.

Method

The majority of Australia's 366 existing geothermal exploration licences are located in arid to semi-arid areas of the continent, targeting relatively low enthalpy EGS and HSA targets. In this context, it is likely that binary Rankine cycles and air-cooling will be the most viable technologies for electricity production from many projects. Hence, we chose, in this paper, to model an air-cooled binary Rankine cycle plant.

A binary Rankine cycle plant has two separate circulating fluids: the *geothermal fluid* which brings the heat from deep in the earth to the surface, and the *working fluid* which takes heat from the geothermal fluid and uses this heat to generate electricity (see Figure 1).

Figure 1: *Schematic for an air-cooled binary Rankine cycle*

Although not commonly mentioned, all Rankine cycles have another fluid, the *cooling fluid;* this is the fluid which removes heat from the vaporized working fluid, allowing it to condense and then be pumped back up to pressure. Generally, this cooling fluid is water because it has excellent thermodynamic properties for cooling, it is stable, abundant and cheap (which explains why 99% of the power plants in the USA use water cooling [5, p. 12]). However, where water is scarce, ambient air is used for cooling because it is also stable, abundant and cheap (although its thermodynamic properties, for cooling purposes, are not as good as water).

The working fluid in a Rankine cycle goes through four separate *processes*, changing the fluid into four different *states*. At State 1 the working fluid is a low pressure, low temperature saturated liquid, it is then pumped up to high pressure liquid (State 2), and then heated to become a high pressure vapour (State 3). Pressure and temperature, of the working fluid, drop across the turbine (to produce mechanical energy) to leave a low temperature, low pressure vapour in State 4. This vapour is then condensed to become the low pressure, low temperature saturated liquid of State 1, and the cycle starts again.

An *ideal* Rankine cycle assumes that the pump and the turbine operate isentropically, and that the condenser and the heat exchanger operate at constant pressure. Determining the power output from an ideal Rankine cycle is well known and widely covered in textbooks [1, 9, 2] so we will not go into it in detail here. Simply, if the following are known:

(iv) temperature of the saturated liquid at State 1,

(v) temperature and pressure of the vapour at State 3,

(vi) working fluid mass flowrate,

the net-power generated by the ideal Rankine cycle can be determined.

Determining the temperature at State 1

To maximize the power output from a Rankine cycle plant, it is necessary to have the minimum possible temperature at State 1. For an air-cooled Rankine cycle plant the minimum temperature at State 1, and hence the chosen temperature for State 1, is given by

$$T_1^{WF} = T_c^{CF} + \Delta T_{PP-C}$$
$$= T_{Amb} + \Delta T_{PP-C}$$

This equation assumes there is no restriction on the mass flowrate of air or size of the condenser. Given the abundance of air and the remote location of the Australian plants this is a reasonable assumption.

Determining the temperature and pressure at State 3

For a given T_1 there are many feasible turbine-inlet (or State 3) temperatures and pressures. Determining the turbine-inlet temperature and pressure which generates the maximum net-power is not a trivial exercise and is discussed later. However, as a first step in the optimisation process, a turbine-inlet temperature and pressure are chosen from a feasible range. The feasible range ensures: the fluid is completely vaporised (or a supercritical fluid), that T_3^{WF} are p_3^{WF} are within the working fluids operating range and that both T_3^{WF} are p_3^{WF} are greater than T_4^{WF} are p_4^{WF} respectively. Further, we required the turbine to operate completely in the 'dry' region.

Determining the working fluid mass flowrate

To generate maximum power using a Rankine cycle with a given turbine-inlet temperature and pressure, the maximum working fluid flowrate must be used. In a binary Rankine cycle the working fluid flowrate is limited by the heat exchanger, so this step must be maximized to generate maximum power.

In order to function, a heat exchanger needs two things:

1. Heat Balance

   In an ideal heat exchanger, all the heat from the hot fluid is absorbed by the cold fluid. When a heat exchanger operates at constant pressure, the heat balance equation simplifies to

   $$m^{hot} \Delta h^{hot} = m^{cold} \Delta h^{cold} \qquad (1)$$

   for any section of the heat exchanger.

2. Driving Force

   The place in a heat exchanger where the two fluids have the minimum temperature difference is called the pinch point [2, p.162]. When designing a heat exchanger the minimum temperature difference at the pinch point is set (usually between 5-10°C). The hot fluid must then always be hotter than the cold fluid plus the minimum temperature difference at the pinch point, throughout the entire length of the heat exchanger. So, for any point x along the length of the heat exchanger,

   $$T^{hot}(x) \ge T^{cold}(x) + \Delta T_{PP-HX} \qquad (2)$$

To achieve the maximum flowrate in a heat exchanger, the position of the pinch point (along the length of the heat exchanger) must be chosen optimally. The maximum working fluid flowrate is then calculated using this optimal pinch point, T_3^{WF}, T_a^{GThF} and m^{GThF} as inputs into equation (1).
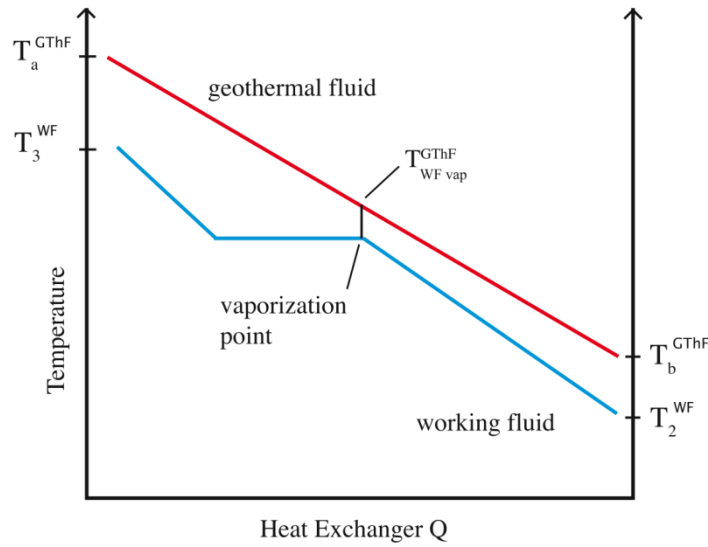
Figure 2: *Subcritical heat exchanger schematic*

It is well known that the optimal position of the pinch point, in a heat exchanger in a *subcritical* binary Rankine cycle, must be at either the working fluid vaporization point or at either end point of the heat exchanger [2, p.162] (see Figure 2). Hence, determining the maximum working fluid flowrate is fairly straight forward in this case.

In a heat exchanger in a *supercritical* binary Rankine cycle, the working fluid (as shown in Figure 3) has a gentle curve, reflecting a constantly changing heat capacity. This means that there is no obvious choice for the optimal position for the pinch point, along the length of the heat exchanger

We choose to address this problem in the following way.

1. Given the temperature and pressure information for States 2, 3 and a, and m^{GThF}, it is possible, using equation (1), to write the working fluid flowrate as a function simply of the cold geothermal fluid temperature,

$$m^{WF} = f\left(T_b^{GThF}\right)$$

2. However, calculating the working fluid flowrate using equation (1), without knowing (or using) the pinch point, means that we cannot be sure that equation (2) holds for the entire heat exchanger. So, for any given T_b^{GThF}, to ensure that equation (2) holds for the entire heat exchanger, the following method is used:

    a) Use equation (1) to calculate the working fluid flowrate, as follows

$$m^{WF} = m^{GThF} \frac{\left(h_a^{GThF} - h_b^{GThF}\right)}{\left(h_3^{WF} - h_2^{WF}\right)} \qquad (1)$$

    b) Divide the heat exchanger into i segments of equal heat balance. Given that the m^{WF} was calculated using equation (3), we know that the heat balance equation (equation (1)) holds for each segment with

$$\Delta h_{segment}^{GThF} = \frac{h_a^{GThF} - h_b^{GThF}}{i}$$

$$\Delta w_{segment}^{WF} = \frac{h_3^{WF} - h_2^{WF}}{i}$$

c) Using the fixed working fluid pressures in the heat exchanger (p_a^{GthF} and p_3^{WF}), and the enthalpy at the beginning and end of each segment, create segmented approximations of the temperature profiles of the geothermal and working fluids.

d) Using these temperature profiles as inputs into equation (2), determine if equation (2) holds for all x, and hence if the heat exchanger is feasible.

3. By setting all the infeasible working fluid flowrates to a negative number (say -1), we create a new function, equation (4), and the maximum working fluid flowrate is the maximum of this function:

$$m^{WF} = f\left(T_b^{GThF}\right) \qquad \text{If heat exchanger is feasible,}$$

$$\text{-1 otherwise.} \qquad\qquad\qquad (2)$$

4. We can also infer that the maximum working fluid flowrate must lie somewhere in the range mapped by,

$$T_b^{GThF} \in \left[T_2^{WF} + \Delta T_{PP\_HX}, T_a^{GThF}\right]$$

5. Finding the maximum of this function, is in fact quite simple, as it is one dimensional and unimodal, and the domain of the function is bounded. This can be done using any 1-dimensional constrained optimisation routine.

However, great care must be taken with the precision of the optimisation step, because small inaccuracies in m^{WF} are amplified in the power surface and results in significantly jagged (non-smooth) surface, which is inaccurate and very difficult to optimise.
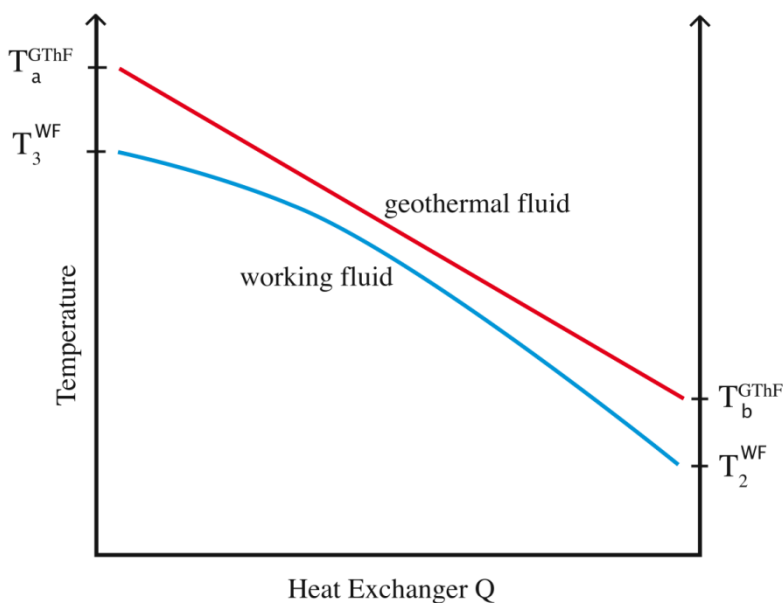
Figure 3: *Supercritical heat exchanger schematic*

The optimisation process

Figure 4 outlines the optimisation process we use to maximize the net-power from an air-cooled binary Rankine cycle plant. For a given set of, what we have called, *plant conditions* (geothermal fluid temperature, pressure and flowrate, ambient temperature and choice of working fluid) we iteratively, found the State 3 temperature and pressure (from within a specified feasible range) that produced the maximum net-power.

In essence, we have created a function for net-power using State 3 temperature and entropy as the only variables, $Power = g\left(T_3^{WF}, s_3^{WF}\right)$, this means to find the maximum net-power we need to solve a 2D optimisation problem, in which is embedded the maximum working fluid flowrate calculation. In order to do this using any standard constrained optimisation routine, we transformed the feasible region from a non-linear region to a linear region.

In order to calculate the power generated from an ideal Rankine cycle it is necessary to make a number of assumptions related to design efficiencies, pinch points etc. The values we use are listed here:

(i)   Isentropic turbine efficiency - 85%

(ii)   Mechanical turbine efficiency - 95%

(iii) Pump efficiency - 70%

(iv) Condenser pinch point - 7.5°C

(v)   Heat exchanger pinch point - 5°C

We also choose to require all cycles to be *dry*, that is that no expansion (in the turbine) occurs in the two-phase region.
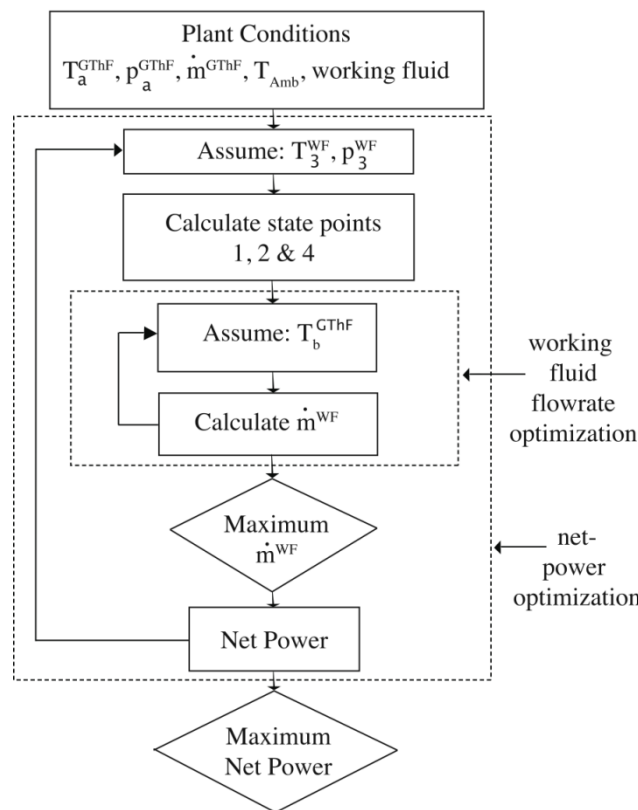
Figure 4: Flowchart of the optimisation procedure

Determining the effect of ambient air temperature

In order to determine the effect of ambient air temperature, it is important to realize that any site will have only one power plant. The power plant will be built to run optimally for a *given set of plant conditions.* This means that when the ambient air temperature varies, the plant will run *off-design.*

In our modelling, we vary the ambient air temperature but keep all other plant conditions constant. In response to the varying ambient air temperature, we make the following assumptions for a plant running in these off-design conditions:

(i)   State 3 temperature and pressure, and working fluid flowrate remain at design conditions.

(ii)   If the actual ambient air temperature is greater than the design ambient air temperature, then the turbine back-pressure (p_4^{WF}) is increased to ensure that the working fluid is a saturated liquid at State 1. The net-power is then recalculated. This is required in practice because the fluid entering the pump must be a liquid for the pump to work properly.

(iii)   If the actual ambient temperature is lower than the design ambient temperature, then the turbine back-pressure (p_4^{WF}) is kept at the design back-pressure. This is because lowering the turbine back-pressure at State 4, would result in a lower temperature at State 2, which, given the design of the heat exchanger, would make it impossible to achieve the design temperature at State 3.

As outlined in Figure 5, to determine the effect of ambient temperature, we first set the plant conditions: the temperature, pressure and flowrate of the geothermal fluid, the design ambient temperature (this is what we are calling ambient temperature used for plant design purposes), and the type of working fluid. From this, we calculate the optimal plant design conditions, in particular, turbine inlet temperature and pressure and the working fluid flowrate. The plant design conditions, together with the off-design assumptions are then used to calculate the power (or energy) produced for varying daily ambient air temperatures.
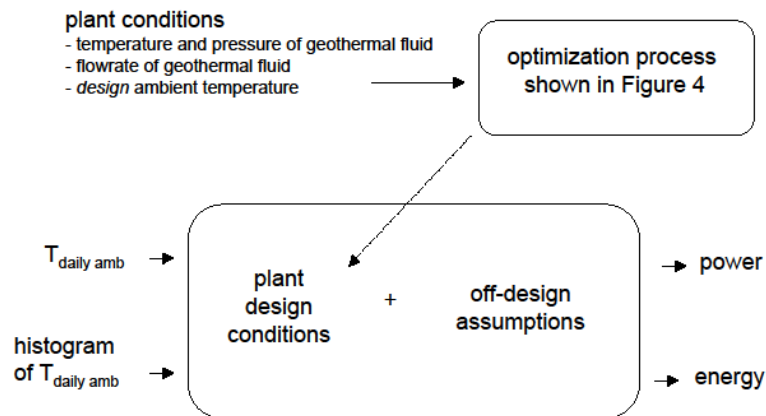
Figure 5: Flowchart for the off-design calculations

Performance Measures

Power plant performance is often judged using thermal efficiency, where thermal efficiency is

$$\eta_{th} = \frac{P_{turbine} - P_{pump}}{Q_{in}} \qquad (3)$$

For traditional coal-fired power plants this is a useful measure of performance, as the top line reflects revenue and the bottom line reflects the cost of coal, which is the largest portion of variable operations and maintenance costs in a coal fired power plant [3, p. 75].

In EGS and HSA power plants, Q_{in} , is the amount of heat withdrawn from the geothermal fluid to generate electricity. However, most of the costs in EGS and HSA plays are directly linked to the flowrate of the geothermal fluid, not how much heat can subsequently be removed from it to generate electricity.

Mines [6] often uses, what he terms, *brine efficiency* to reflect the performance of geothermal power plants, where brine efficiency is defined as

$$\eta_{brine} = \frac{P_{turbine} - P_{pump}}{m^{GThF}}$$

In our opinion, this is a more useful measure of performance for EGS and HSA plays for five reasons:

1. Capital cost is directly linked to the number of wells drilled, and each well-pair drilled generates a geothermal fluid flowrate.

2. The parasitic power required to run these plants, is predicted to be the largest portion of variable operations and maintenance costs, which again, is linked to geothermal fluid flowrate.

3. It removes the need to assume a geothermal fluid flowrate, one of the largest unknowns in these plays at the moment.

4. The results scale linearly with geothermal fluid flowrate. So, in relative terms brine efficiency results will be the same as power results which have assumed a specific geothermal fluid flowrate.

5. Power can easily be calculated given flowrate, as follows:

$$Power = \eta_{brine} \times m^{GThf}$$

For example, in SI units,

$$kW = \frac{kJ}{kg} \times \frac{kg}{s}$$

Validation

To check the assumptions we made for a plant running in off-design conditions, we compared our calculated data to real data from the Mammoth Pacific Plant, California, USA [6]. The Mammoth plant data was used because it was the only publicly available data linking ambient air temperature to plant power output, from an air-cooled binary geothermal power plant using isobutane that we could find. Also, please note, we have used non-SI units, in this section only, for ease of comparison with Mammoth plant data.

At Mammoth, the geothermal fluid temperature ranges from 300-350°F, and their air-cooled binary system operates using isobutane as its working fluid. Figure 5a shows brine efficiency versus ambient temperature. The grey triangles show results from the plant's normal operating conditions (in 2000), the red squares show results from, what we will call, *Mines wet-cycle trial* [6]. In his wet-cycle trial Mines changed the state at State 3 (i.e. the T_3^{WF} and p_3^{WF}), so that the isobutane was no longer completely dry in the turbine. Since we have assumed a dry turbine, the grey triangles are the data we need to compare with.

It can be seen from Figure 6, that on a plot of brine efficiency versus ambient air temperature, our data qualitatively agrees with the real-world Mammoth data. Quantitatively, our data some-what over-estimates the Mammoth data, but this is to be expected given that we have assumed an ideal plant. Our data also over estimates the effect of ambient temperature; the Mammoth plant loses ~17% over 25°F (from 38°F to 63°F), where our data loses 23% over the same range. This indicates that our off design assumptions are a little too harsh and/or that the Mammoth plant use some strategies, in hot weather, to mitigate the loss of power generation. For example, turning up the fans and/or spraying cooling water to aid fan cooling. These methods have the effect of reducing ΔT_{PP-C} (where we assumed this value is constant).

In their modelling, Wendt and Mines [8] show brine efficiency dropping ~20% (over 25°F) above the plant design point. However, their modelling with temperatures colder than the design point differs significantly from our modelling, due to their inclusion of a variable nozzle design in the turbine.

We believe our model is sufficiently close, both qualitatively and quantitatively, to real world data to provide meaningful insights into the effect of ambient air temperature on the performance of air-cooled, binary Rankine cycle power plants.

a)

**b)**
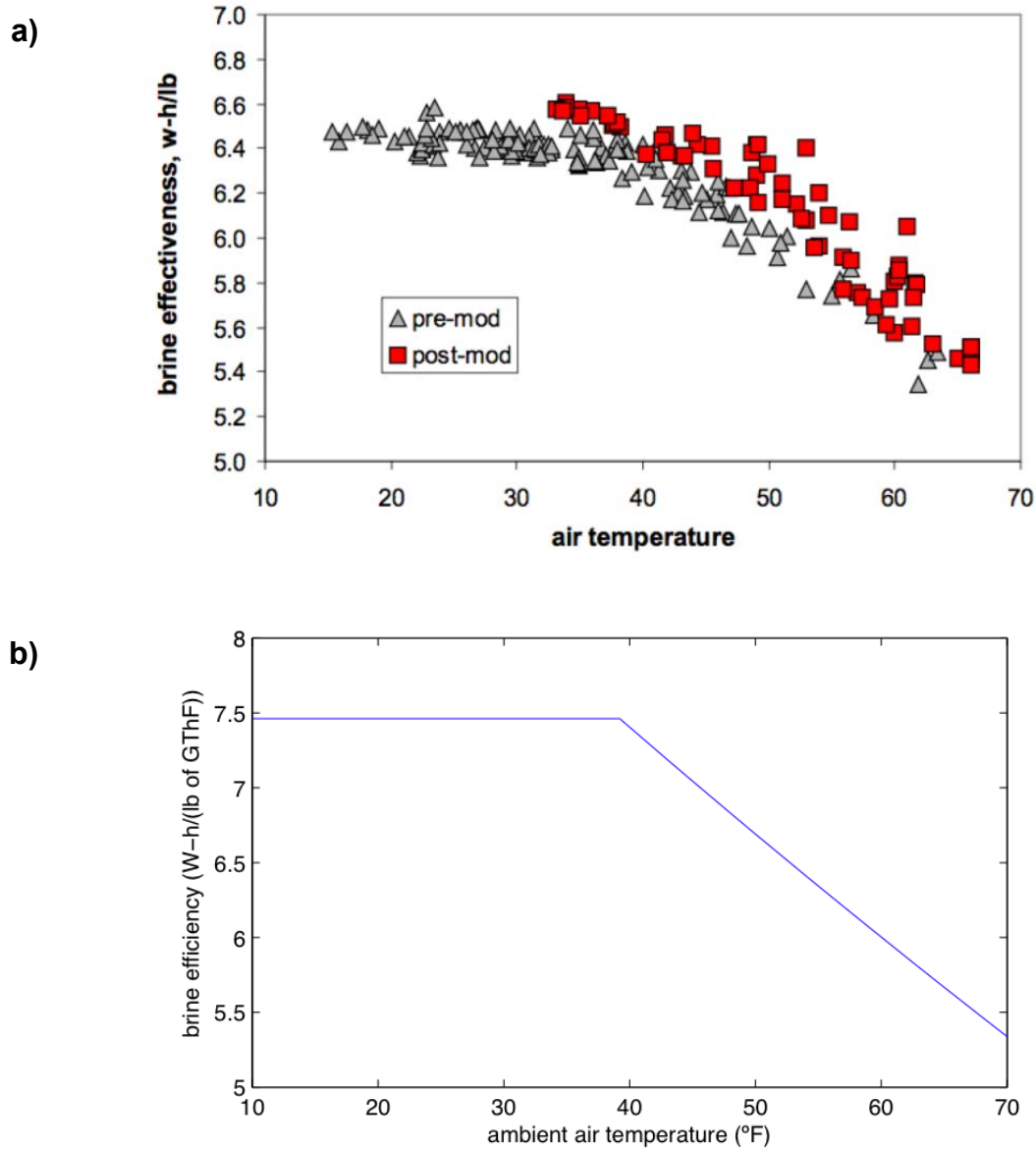
Figure 6: Validation Results. (a) Mammoth Plant Data [6]. (b)Effect of ambient air temperature on brine efficiency

(using: T_e^{GThF} *=300°F, ambient air temperature for design purposes of 38°F, and isobutane as a working fluid)*

Results

The results of this work are presented in the paper 'Performance of air-cooled organic Rankine cycle plants using temperature distributions from arid parts of South Australia' also presented at AGEC.

Conclusion

Air-cooled binary Rankine cycle plants are significantly and adversely affected by varying ambient air temperature. However, while this loss is fundamentally due to the thermodynamics of the Rankine cycle, considering the temperature distribution and the off-design effects of this distribution can allow for better choice in initial plant design.

By designing for a temperature which is colder than the mean site temperature a plant's output can be increased by 5-8%. Since, designing for a lower ambient temperature will increase initial plant costs (due to the requirement for a larger heat exchanger), in the final analysis, the capital costs will need to be weighed against ongoing improved production capabilities.

List of abbreviations

h	enthalpy (J/kg)
m	mass flowrate (kg/s)
p	pressure (kPa)
s	entropy (J/(kg/K))
c_p	heat capacity at constant pressure (J/(kg K))
P	power (W)
Q	heat flow per second (J/s)
T	temperature (°C)
ΔT	temperature difference (°C)
η_{brine}	brine efficiency (W-h/kg)
η_{th}	thermal efficiency (dimensionless)

Superscripts

CF	cooling fluid
GThF	geothermal fluid
cold	cold fluid
hot	hot fluid

Subscripts

1,2,3,4	State 1, 2, 3 or 4
a,b,c,d	State a, b, c or d
Amb	ambient state
in	heat added to the cycle
PP-C	pinch point in the condenser
PP-HX	pinch point in the heat exchanger

Acknowledgements

References

Cenegel, Y.A., and A.B. Boles, 1989. "Thermodynamics an Engineering Approach.' McGraw-Hill, 5th Edition.

DiPippo, R., 2008. "Geothermal Power Plants: Principals, Applications, Case Studies and Environmental Impact." Elsevier, 2nd Edition.

U.S. Energy Information Administration (EIA), April 2011. "Annual energy outlook 2011 with projections to 2035." U.S. Energy Information Administration (EIA).

Entingh, D.J., July 2006. "DOE Geothermal Electricity Technology Evaluation Model (GETEM): Volume 1 – Technical Reference Manual." Department of Energy.

Stiegel, G.J., A. McNemar, B. Schimmoller, M. Nemeth, J. Murphy, and L. Manfredo, August 2006. "Estimation freshwater needs to meet future thermoelectric generation requirements." National Energy Technology Laboratory, Department of Energy (USA).

Mines, G., 2000. "Summary of investigations of the modified turbine inlet conditions in a binary power plant." Proceedings of GRC 2000 Annual Meeting.

Morris, C., April 2012, Personal correspondence.

Wendt, D., and G. Mines, September 2010. "Interim Report: Air Cooled Condensers for Next Generation Geothermal Power Plants Improved Binary Cycle Performance." Idaho National Laboratory.

Van Wylen, G.J., and R.E. Sonntag, 1958. "Fundamentals of Classical Thermodynamics." John Wiley and Sons, Inc, 3rd Edition.

Numerical simulations of borehole breakouts using Discrete Element Method

Yucang Wang, Deepak Adhikary, Andy Wilkins

CSIRO Earth Science and Resource Engineering, Queensland Centre for Advanced Technologies

Yucang.Wang@csiro.au

Introduction

One of the challenges in geothermal energy extraction is how to stimulate and sustain the flow of fluid through the geothermal field and how to generate an efficient hydraulic subsurface heat exchanger system. Efficient drilling and completion and maintenance of geothermal wells are very important to the success of a geothermal project. During the drilling of circular holes in rock, borehole breakouts can occur near the borehole. Borehole breakouts are failures of rock adjacent to the borehole surface due to in situ stress concentration. They often result in the cross-sectional elongations in the direction of the minimum principle stress orthogonal to the borehole axis resulting in huge financial losses to industry.

An understanding of the mechanism causing borehole breakouts is paramount in efforts to design stable wellbores. In the previous studies, two major different modes of failure have been suggested as the mechanism leading to breakouts. In the first case, tensile cracks initiate in the vicinity of the borehole and propagate in the direction of the maximum compressive stress, causing a series of cracks parallel to the borehole wall, and finally leading to buckling and spalling (Lee and Haimson,1993). The second one is shearing type failure (Haimson and song, 1993). It is identified by shear fracture zones originating at the borehole wall and extending well into rock. The shear bands can cause breakout when they intersect some distance behind the borehole wall.

Another kind of modes reported recently by Haimson (Haimson, 2001) is compaction failure, which is observed in highly porous sandstone. In this case, fracture-like failure bands formed in the direction of the minimum principle stress. It is thought that the failure bands are caused by progressive compaction failure (particle crushing and pore collapses) of the rock.

In this study we simulate borehole breakouts using Esys_Particle (Wang and Alonso-Marroquin, 2009), an open-source Discrete Element Method (DEM) code. We are mostly focused on fracture patterns, especially sensitivity of breakout shape to the loading conditions. In DEM simulations, the evolution of contacts is automatically identified and updated at each time step. It is suitable to model the phenomena which involve large deformation and dynamic effects.

2-D Simulations of borehole breakouts

A cross-section of the borehole, under the loading of stress σ_H and σ_h, is modelled using the Esys_Particle code. The simulations consist of 190,000 -200,000 particles of sizes ranging from 0.1 to 1 unit. The sample is loaded by four walls moving at a low speed which generate the increasing stress but keep a constant σ_h/σ_H ratio.

Simulation results

In the case of uni-axial compression, $\sigma_h/\sigma_H = 0$, tensile stress will concentrate and extensile cracks will develop. Fig. 1 shows the stable development of tensile cracks, parallel to the loading direction, until overall collapse occurs.
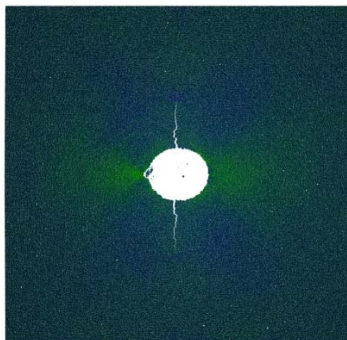
Figure 1 *Fracture development under uni-axial compression , Tensile cracks develop and extend the loading direction (the direction of σ_H)*

In the case of bi-axial compression with unequal far-field stresses, the tensile cracks in Fig. 1 are easily inhibited. Fig. 2 shows one of the typical simulations of breakout development. At time step of 41500, two conjugate cracks, dominated by shear fractures, start at the left side of surface of the borehole, intersect and release the crushed grains. With the removal of some particles and continuous loading, stresses concentrate at the corner of the previous fault intersection. This causes shear fracture in the middle part, with some tensile cracks extended to the surface area, producing another major layer of fracture. Finally at the right side of the wall a group of shear conjugate fracture develops progressively forming a "dog eared" shape.
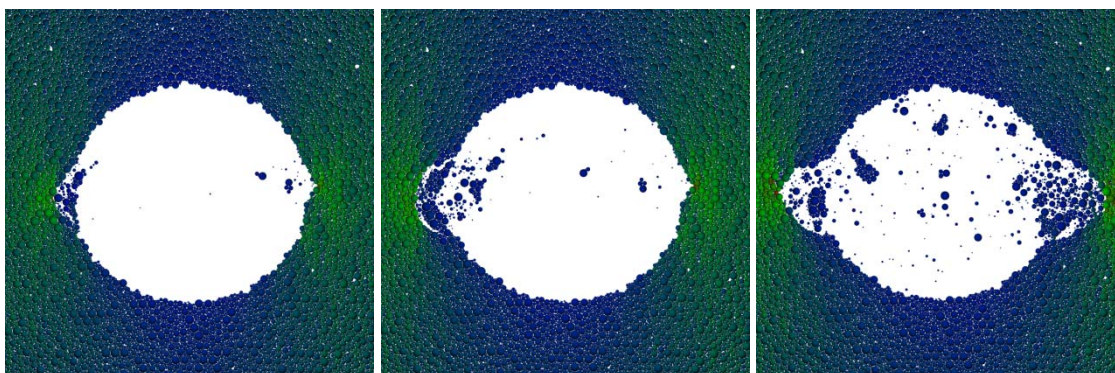
Figure 2 *Progressive fracture development under bi-axial compression at time step 41500, 43000 and 49000 . $\sigma_h/\sigma_H = 0.2$. Dog-eared shaped breakouts are formed*

With uniform far-field stresses, $\sigma_H = \sigma_h$. If σ_H and σ_h are monotonically increased, the rock close to the wall will be subjected to unconfined compression. Shear cracks will develop close to the borehole wall. In the simulation, it is observed that such shear cracks initiate at the borehole wall and distribute randomly around the borehole circumference. With the increasing of loading, some of these cracks stop to develop, while some continue to grow, extending into the rock in the direction of high shear stress, after a short distance turning direction to a direction subparallel to the borehole wall, and releasing grains from the matrix (Fig.3).
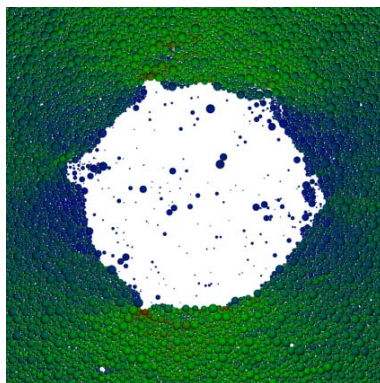
Figure 3 *Fracture development under bi-axial compression at time step 45000, 47500 and 49500.*
$\sigma_h / \sigma_H = 1$ *. There is no directional preference of breakouts under uniform principle stress*

Esys_Particle is also found to be capable of reproducing compact failure band. With certain particle packing, the long and narrow breakouts could be observed. These breakouts could be seen to extend for a long distance in the direction perpendicular to the major compressive stress(Fig. 4). The mechanisms of failure leading to this slot-shaped breakouts are still not fully understood. Haimson (2001) proposed that this type of failure is due to the pore collapse or grain debonding in the highly porous rocks. Further studies are required to fully understand the necessary conditions for this phenomenon to occur.
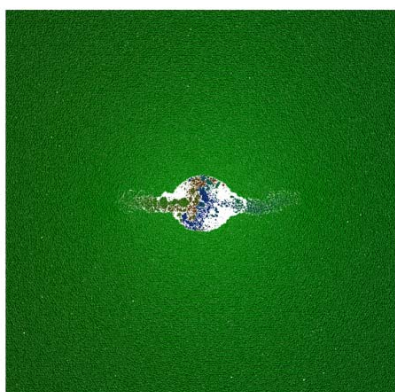
Figure 4 *Development of compaction breakout. Long and narrow slot-shaped breakouts are observed, perpendicular to the major compressive stress* σ_H

Summary and discussions

In this study, 2-D borehole breakouts are simulated using the Esys_Particle code. The simulations are performed under uni-axial compression, bi-axial compression with unequal and equal far-field stresses. Fracture initiation, development and spalling are well reproduced. The particular geometry of the fracture pattern is dependent on the applied load. We observed the typical "dog-ear" shaped breakouts, as well as slot-shaped compaction bands which were recently reported in the literature. There is no directional preference of breakouts under uniform principle stress environment. The satisfactory results suggest that the Esys_Particle code produces reliable results which are consistent with laboratory tests, and therefore is capable of modeling the progressive failure related to borehole breakouts.

The current study is just qualitative rather than quantitative, i.e. the input parameters are not calibrated against the laboratory data yet. The effects of input parameters to the breakout need to be investigated. This study is the first step towards developing a fully coupled T (thermal) – H (hydraulic) - M (mechanical) code which can be used to model geothermal extraction, including hydraulic fracture, fluid and heat flow and heat exchange between rocks and fluid.

References

Lee, M., and Haimson, B. (1993). Laboratory study of borehole breakouts in Lac Du Bonnet Granite: a case of extensile failure mechanism. Int. J. Rock Mech. Sci. Geomech. Abstr., 30,1039-1045.

Haimson, B., and Song, I. (1993). Laboratory study of borehole breakouts in Cordova Cream: a case of shear failure mechanism. Int. J. Rock Mech. Sci. Geomech. Abstr., 30,1047-1056.

Haimson, B. (2007). Micromechanisms of borehole instability leading to breakouts in rocks. Int. J. Rock Mech. Sci. Geomech. Abstr., 44,157-173.

Wang. Y. C., and Alonso-Marroquin, F. (2009). A finite deformation method for discrete modelling: particle rotation and parameter calibration. Granular Matter 11, 331-343.

Probabilistic Assessment of Geothermal Resource Bases

J. Florian Wellmann[1*], Jonathan Poh[2] and Klaus Regenauer-Lieb[1,2,+]

[1]CSIRO Earth Science and Resource Engineering. [2]The University of Western Australia

*Corresponding author: florian.wellmann@csiro.au. [+] Presenting author

Introduction

The geothermal resource base is commonly evaluated on basis of the volumetric heat in place method (Muffler & Cataldi, 1978). Calculation of this measure depends on thermal rock properties, temperature, and the distribution and extent of suitable geothermal rock units in the subsurface. All these aspects are subject to uncertainty. We present here a probabilistic geothermal resource assessment that enables the consideration of these uncertainties. We propose that our method extends currently applied practices and provides an insight into the potential of a geothermal resource area based on a sound understanding of associated uncertainties.

In the following, the basic principle of our methodology is described and applied to a realistic case study for a geothermal resource base analysis in the North Perth Basin, Western Australia.

Volumetric heat in place method

The volumetric estimation of heat in place, also referred to as thermal energy in place is generally used as a measure to compare the geothermal resource base on larger scales, for example for different countries or states, and large company tenements (e.g. Hurter & Schellschmidt, 2003; Kohl et al., 2003; Tester et al. 2006; van Wees et al. 2010). It is based on the simple concept of evaluating the thermal energy Q stored in a volume V of a rock with homogeneous density ρ, heat capacity c, and porosity ϕ at a temperature difference ΔT to a usable base temperature (Muffler & Cataldi, 1978) and calculated as:

$$Q_{total} = [(1-\Phi)c_{pr}\rho_w + \Phi c_{pw}\rho_w]V\Delta T \qquad (1)$$

This calculated thermal energy in place is commonly considered as the "Geothermal Resource Base" (Muffler & Cataldi 1978, Tester et al. 2006). It should be noted that the second edition of the Australian Geothermal Reporting Code (AGRCC, 2010) redefines a Geothermal Resource strictly as that part of the energy in place that is recoverable, mainly to avoid over-interpretation by "non-technical people" of the large measures that are often derived (AGRCC, 2010). We consider the term geothermal resource base here in the original sense and evaluate in the following uncertainties related to the entire resource base, or the available heat/ thermal energy in place.

Estimates of uncertainties in the geothermal resource base

It is well known that geothermal resource evaluations are estimates that can contain a high degree of uncertainty. The Australian Geothermal Reporting Code (AGRCC, 2010) states that, if possible, the accuracy of a resource estimate should be provided, and encourages probabilistic estimates. In a recent presentation, Garg and Combs (2010) stated that probabilistic methods are commonly applied to heat in place studies, but rarely based on a real understanding on the relevant uncertainties, and therefore of limited use. However, in their own study, although considering data from real geothermal case studies as an input, they limit themselves to very simplified unrealistic structural geological setting, a simple "shoe-box" style geometry, for a consideration of geological uncertainties. A detailed study of the geothermal resource base (and extractable energy) has been performed by TNO for the entire Netherlands (van Wees, 2010). In this case, a structural geological setting has been evaluated from a very rich and dense dataset about the subsurface, even though the authors state that

significant uncertainties about the structures, especially at depth, remain. Nevertheless, these uncertainties were not considered in their probabilistic resource estimation, although the authors state that this would be a scope of future work.

Our method distinguishes itself in three important aspects from these previous approaches:

1. We explicitly respect and consider uncertainties in a realistic, full 3-D, structural geological model, built on basis of available geological and geophysical datasets;

2. The temperature field for the resource area is simulated, and therefore completely consistent with the distribution of thermal properties derived from the 3-D geological model;

3. Knowledge about the geological history and the tectonic evolution is respected, and associated uncertainties are part of our methodology.

Case study: North Perth Basin, WA

As a test of feasibility, we apply our methodology to a potential geothermal resource area in the North Perth Basin, Western Australia (Figure 1).
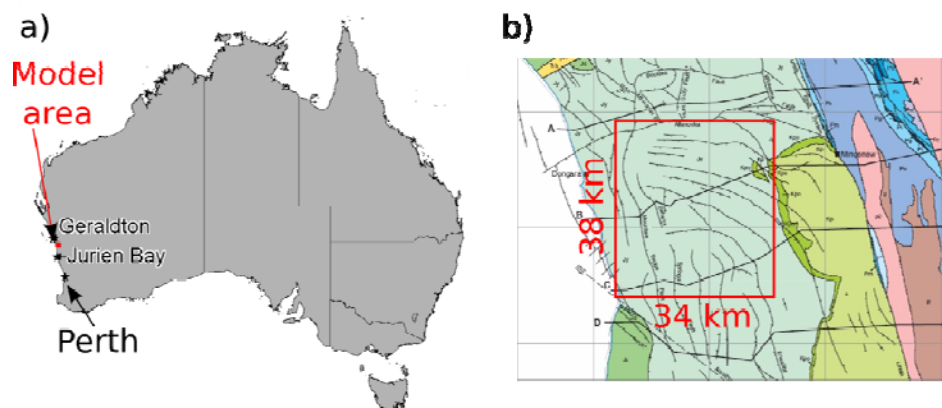
Figure 1: (a) Area of case study in the Perth Basin between Geraldton and Jurien Bay; (b) Model area over geological map from Mory and Iasky (1996), Plate 10; shown are also the positions of interpreted sections that were used to construct the model (see Figures 3 and 4).

The Perth Basin is an extensional basin at the Western side of the Australian Craton. It consists of sedimentary sequences from Silurian to Quaternary age with a thickness of up to 12 km (Mory & Iasky, 1996). The basin formed during two major phases of extension: a Permian extension, and an Early Cretaceous extension associated with the break-up of Gondwana. The complex tectonic history led to a partitioning of the basin into several fault compartments, commonly forming Horst-Graben structures, and intersecting patterns of predominantly normal faults.

The initial step of the work presented here was to construct a structural geological model for an area in the North Perth basin, based on interpreted seismic cross sections, maps of formation thickness (isopach) and depth (isohypse), drillhole information, and maps of major structures and geological units at the surface (all presented or referenced in Mory & Iasky, 1996). The geological model is constructed with the implicit potential-field method (Calcagno et al., 2009) implemented in Geomodeller (www.geomodeller.com). It extends 34 km in East-West direction and 38 km in North-South direction and covers the main sedimentary sequences that were considered as relevant in the context of a geothermal resource base evaluation (Figure 2).
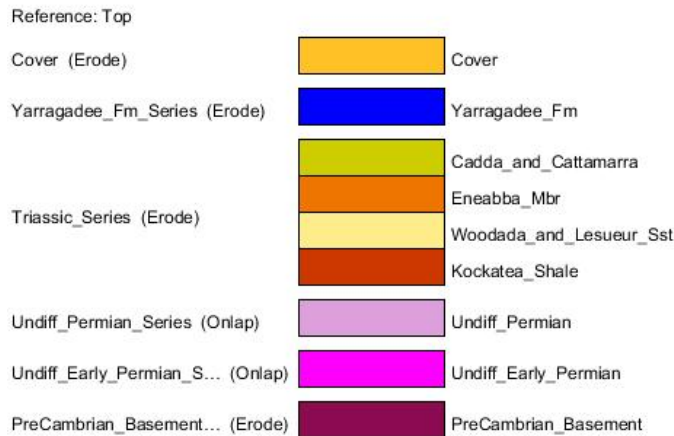
Figure 2: *Stratigraphic pile of geological model: geological units are defined to reflect units with significantly different rock parameters in the geothermal simulation and the subsequent heat in place analysis. Units that are combined in a series (left column) are assumed to be concordant. The sequence of the stratigraphic pile is respected in each model generated with Geomodeller (see Calcagno, 2008, for more details).*

The geological data (surface contact points and orientation measurements) are digitised in sections in the model. Great care was taken to reduce the number of geological constraints to the minimum required to correctly construct a structural geological model that is in accordance with all available data. The derived low-dimensional parameterisation of the geological model is an important prerequisite for the probabilistic method that we apply.

An interpreted geological section (Mory & Iasky 1996) that was used as an input for the structural modelling, with geological contact and orientation points, and the derived structural model is presented in Figure 3.
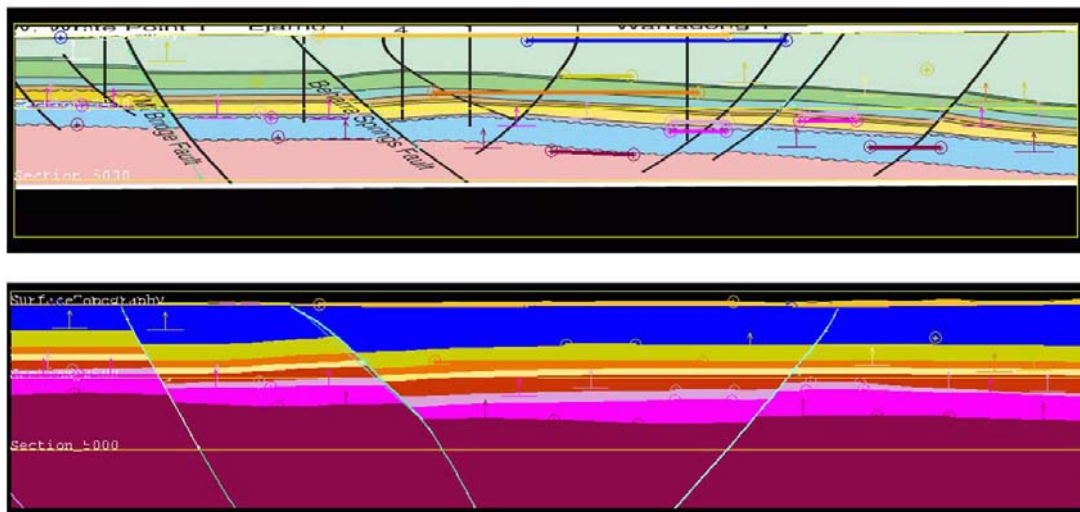
Figure 3: (top) *Cross Section B and geological contact points and orientation data; (bottom) representation of the section in the structural geological model. Note: bends in the position of the section (see Fig. 1b) can cause changes in apparent dip of faults and units.*

A representation of the simulated fault network in the area is shown in Figure 4a. The modelled fault network provides the basic separation into different fault compartment blocks (Fig. 4b). One major

source of uncertainties is related to the vertical offset between different fault compartments, i.e. to the subsidence of the blocks in the extensional phase (see Mory & Iasky, 1996). Uncertainty about the fault offset for the older geological units is of major relevance in the deeper (> 4 km) parts of the basin (mainly in compartments 4 and 5), as seismic coverage is poor and Mory & Iasky (1996) clearly state that great uncertainties exist and several horizons are only "phantomised" at depth.
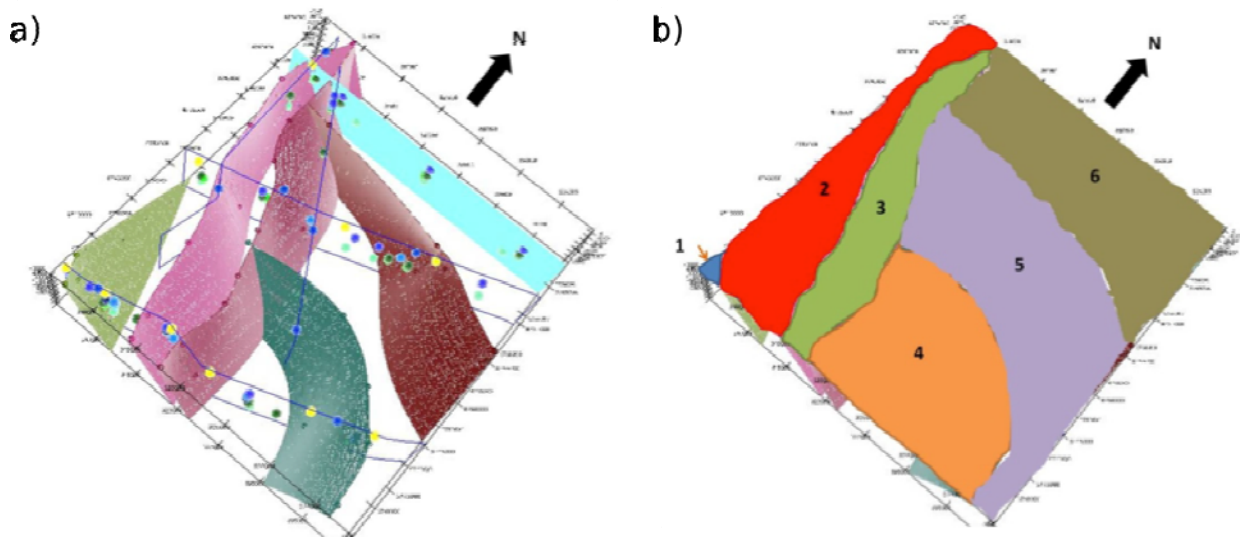
Figure 4: (a) 3D illustration of fault structures used in project area. (b) Uncertainties are assigned to fault compartments, respecting uncertainties of fault throw according to geological history and available structural geological data.

Probabilistic workflow

The geological model is subjected to an integrated geological uncertainty simulation workflow (Wellmann, 2010), where multiple possible geological models are automatically generated from the initial geological model and uncertainties assigned to the geological observations.

In the model presented here, great care was taken to generate multiple geological model realisations that are consistent with the geological history of the basin, i.e. the relative age of the geological units is respected, unconformities are only allowed where they make geological sense, and general isopach and isohypse layering is preserved throughout all model realisations.

Uncertainties are assigned to the structural geological data points defining surface contacts between two geological units. We identified three main sources of uncertainty:

1. Uncertainties related to fault throw in each of the fault compartments (see Fig. 3);

2. Uncertainties of the initial sedimentation thickness;

3. And, where applicable, uncertainties of sedimentation during tectonic processes.

Uncertainties are assigned as normal distributions with the initial value as mean, and standard deviations ranging from 500 – 800 m for the fault throw, and 25 – 100 m for uncertainties related to sedimentation thickness. For the results presented here, we generated 50 geological model realisations. All of these models are then discretised into a regular mesh structure (50 x 50 x 100 cells) for all subsequent steps.

Each of the discretised geological models is used as conceptual model for a subsequent geothermal simulation of conductive heat transport. Relevant rock properties (thermal conductivity, porosity and heat production rate) are assigned to the cells in the geothermal simulation according to the spatial

distribution of geological units. Thermal boundary conditions were fixed temperature at the top (20°C), constant heat flux at the base (0.76 W/m^2) and insulating lateral boundaries.

After the steady state temperature field is simulated for each model, the cell-based volumetric heat capacity is calculated using equation (1) with the local properties and the simulated temperature in each cell, for a base temperature T_0 of 20 ^{o}C. In the final step, the bulk heat in place for each geological unit is calculated with a summation over all cells of each unit.

Results

Results of the applied method can be derived for several stages of the workflow. Visualisations of geological unit probability for Early Permian, Lesueur Sandstone and Yarragadee are presented in Figure 5 as an example of the uncertainties in the structural geological model. The sections are approximately at the location of the "cross section B" of Figure 3. The increase of uncertainties with greater depth is visible in the difference of "fuzziness" for the boundaries of the geological units Yarragadee and Early Permian. Additionally, higher uncertainties exist in the Western parts of the fault blocks, reflecting less reliable data in this area.
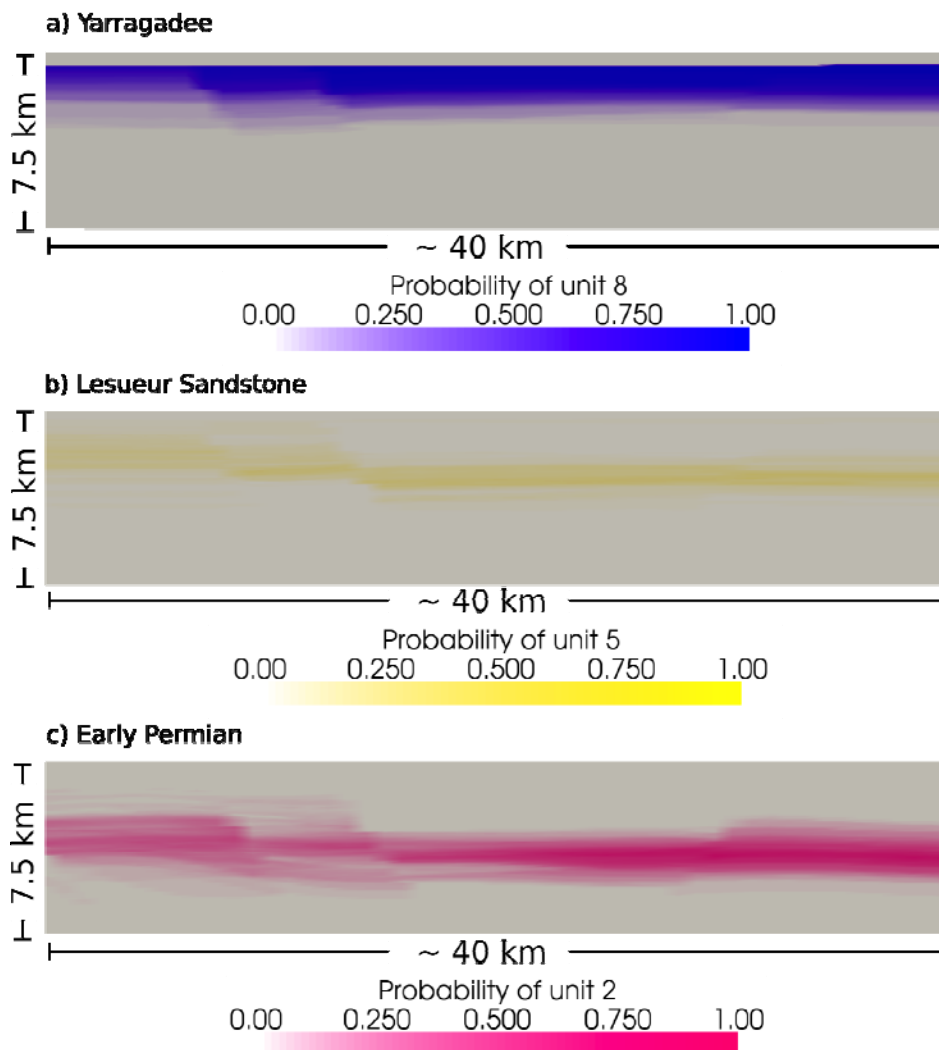

Figure 5: *visualisation of probabilities for three units of the geological model, approximately at the location of cross-section B (Fig. 3): the colour scale indicates the probability to obtain the geological unit, evaluated on the basis of all simulated geological models.*

The influence of the structural uncertainties on geothermal resource base estimations is presented in Figure 6 as histograms of bulk heat in place for the three geological units presented above. It is interesting to note that, although structural uncertainties are highest for the Early Permian (as the deepest geological unit shown here), the heat in place estimations vary only in a range of 20% with an expected value of approximately 260000 PJ. Estimations for the Lesueur Sandstone vary greatly from close to zero to 140000 PJ, with an expected value of around 50000 PJ. The distribution of heat in place estimates for the Yarragadee formation is close to a normal distribution with a sample mean (and an expected value) of approximately 200000 PJ and a (high) standard deviation of about 50000 PJ, leading to a significantly higher range of results than the Early Permian.
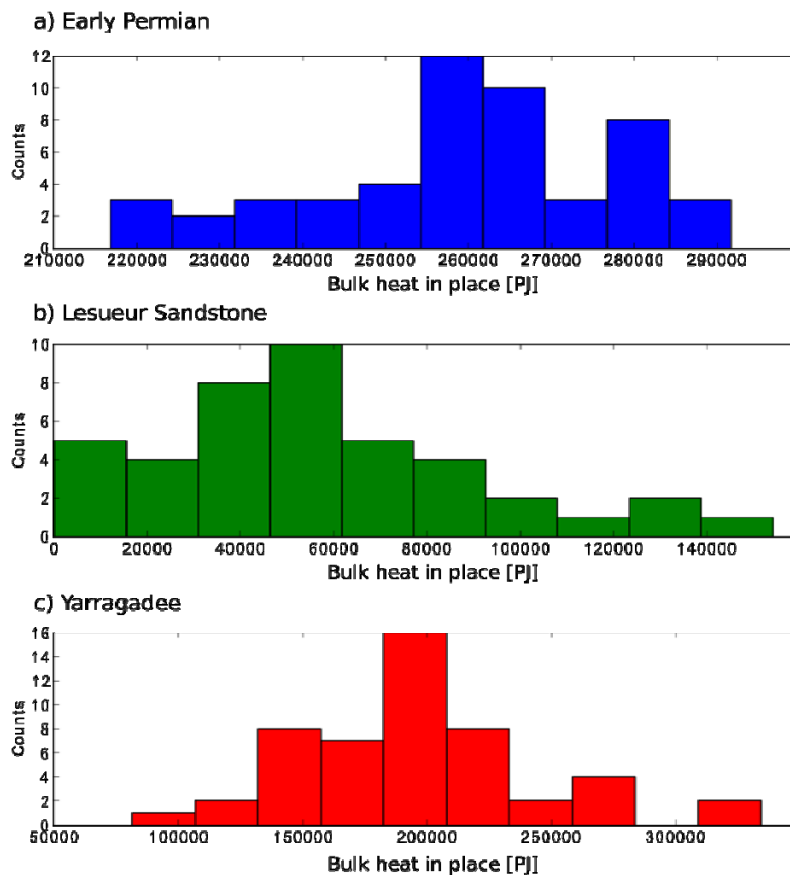
Figure 6: Histogram of bulk heat in place values for three of the geological units, determined from 50 realisations of the structural geological model. Uncertainties reflected in these histograms are solely due to uncertainties in the structural geological setting.

Discussion

The application our probabilistic geothermal resource base assessment to a case study in the North Perth Basin clearly shows how uncertainties about the subsurface structure lead to uncertainties in the estimated heat in place value. This result is not surprising as the volume of a considered resource area is a significant factor in the calculation of the available heat in place (eq. 1). However, uncertainties in the structural setting are not considered in standard probabilistic estimates of the geothermal resource base (e.g. Garg and Combs, 2010; van Wees et al. 2010).

We assume that a major reason why structural uncertainties were neglected to date is that no method exists for a straightforward integration of these types of uncertainties – at least not for the case of reasonably complex (and realistic) geological models. We bridged this gap with a recently developed method (Wellmann et al. 2011) that integrates state-of-the-art implicit structural geological modelling,

heat transport simulations, and geothermal resource base estimations into one framework, combining several commercial (Geomodeller and SHEMAT) and open-source codes (Python, PySHEMAT). The integration enables a flexible adaption to address scientific problems that require an automatic procedure combining all aspects. One example is the uncertainty propagation presented here. Additionally, it enables the integration of all aspects from geological modelling to heat transport evaluation in an inverse framework for automatic model calibration, sensitivity analysis, and hypothesis testing.

An interesting observation in the results is that uncertainties in the estimated heat in place for the shallow Yarragadee unit were relatively higher than uncertainties in the deeper, and structurally more uncertain, Early Permian. A potential reason for the higher variation in the shallower surface is that temperatures in the unit are lower – and uncertainties in the structural setting therefore more dominant.

An important aspect of all the presented methods is that, due to the flexibility of the method, it is possible to re-evaluate the results semi-automatically when new data become available. This aspect is, in our point of view, important in the context of geothermal resource estimations as defined in the Geothermal Code (AGRCC, 2010), as they provide a quantitative measure for the reduction of uncertainty in the progress of knowledge acquisition, and model optimisation.

References

AGRCC, 2010. *The Geothermal Reporting Code*, Second Edition. Adelaide, SA: The Australian Geothermal Reporting Code Committee (AGRCC). Available at: http://www.pir.sa.gov.au/geothermal/ageg/geothermal_reporting_code.

Calcagno, P. et al., 2008. *Geological modelling from field data and geological knowledge: Part I. Modelling method coupling 3D potential-field interpolation and geological rules: Recent Advances in Computational Geodynamics: Theory, Numerics and Applications.* Physics of the Earth and Planetary Interiors, 171(1-4), pp.147–157.

Garg, S.K. & Combs, J., 2010. *Appropriate Use of USGS Volumetric "Heat in Place" Method and Monte Carlo Calculations.* Proceedings, Thirty-Fourth Workshop on Geothermal Reservoir Engineering, SGP-TR-188, pp.1–7.

Hurter, S. & Schellschmidt, R., 2003. *Atlas of geothermal resources in Europe*. Geothermics, 32(4-6), pp.779–787.

Kohl, T., Andenmatten, N. & Rybach, L., 2003. Geothermal resource mapping—example from northern Switzerland. *Geothermics*, 32(4–6), pp.721–732.

Mory, J.A. & Iasky, P.R., 1996. *Stratigraphy and structure of the onshore northern Perth Basin, Western Australia.* Geological Survey of Western Australia, Report 46, pp.1–126

Muffler, P. & Cataldi, R., 1978. Methods for regional assessment of geothermal resources. *Geothermics*, 7(2-4), pp.53–89.

Tester, W.J., 2006. The Future of Geothermal Energy. pp.1–110.

van Wees, J.-D. et al., 2010. *ThermoGIS*, Utrecht: TNO. Available at: http://www.tno.nl.

Wellmann, J.F. et al., 2010. *Towards incorporating uncertainty of structural data in 3D geological inversion*. Tectonophysics, 490(3-4), pp.141–151.

Wellmann, J.F. et al., 2011. *Geothermal Resource Assessment: Combining Uncertainty Evaluation and Geothermal Simulation*. AAPG/SPE/SEG Hedberg Conference "Enhanced Geothermal Systems" March 14-18, 2011, Napa, California.

Modeling Heat Extraction by Fluid Circulation through an Array of Conductive

Wu, B., Bunger, A., Zhang, X., Jeffrey, G.R.

CSIRO Earth Science and Resource Engineering, 71 Normanby Road (Gate 7, Bushells building), Clayton, VIC 3168, Australia

bisheng.wu@csiro.au

Abstract

The number of and spacing between fractures in a geothermal reservoir is one of the most important factors in determining its output power and lifetime. In this paper, a mathematical model is developed to study the heat extraction by fluid circulation through an array of conductive fractures distributed in a reservoir in which the original temperature varies according to a prescribed geothermal gradient. Two geometric settings are studied using a numerical solution based on superposition of Green's functions. By comparing the average output temperatures (AOTs), it is found that, when the depth of the bottom fracture is fixed, there exists an optimal range of values for the fracture number and fracture spacing that maximise the output power and reservoir lifetime. Conversely, non-optimal placement of fractures can significantly decrease the lifetime power output of the reservoir. The implication is that appropriate engineering of the fracture array through which the working fluid circulates has a leading order impact on the performance of the reservoir, and well completion and stimulation methods that do not enable the fracture locations to be controlled are likely to lead to underperforming reservoirs.

Keywords: Multi-fracture geothermal reservoir, heat extraction, Green's functions, optimal fracture spacing, optimal fracture number

Introduction

Due to large sources of heat from the interior of the earth and low CO2 emissions associated with extraction compared to fossil fuel energy resources, enhanced geothermal systems (EGSs) have received a great deal of interest during the past 40 years. One cubic kilometre of hot granite at $250^{o}C$ has the stored energy equivalent of 40 million barrels of oil (Dopita and Williamson, 2009), but recovering this vast resource has proven challenging. Therefore, to improve the reservoir performance so as to maximise output power and reservoir lifetime has become an important topic in the reservoir design.

Heat extraction from geothermal reservoirs has been extensively studied. For some models with simple geometries, analytical solutions can be obtained based on the simplification of one- or two-dimensional assumption (Lauwerier 1955; Badvarsson, 1969, Gringarten and Ramey, 1973, Gringarten et al.,1975; Ziagos and Blackwell; Schulz,1991; Cheng et al., 2001).Other more complicated cases have to resort to numerical methods (Mcfarland 1975; Koldtz 1995; Mossop, 2001; Ghassemi, 2003). Tenma et al (2001) used the code FEHM (Finite Element Heat and Mass Transfer code) (Zyvoloski et al., 1983) to study a two-fracture system combined with a two-year circulation test in Hijiori HDR site of Japan, but focused on the comparison of the effect of using different reservoirs characteristic, rather than varying the number of fractures (reservoirs).

Although the above models have led to many useful insights, most of them consider only the case of a single fracture reservoir or homogeneous porous medium or assume that the initial temperature of the whole system is the same by ignoring the effect of the geothermal gradient. It is well known that the average temperature of the earth increases by 3 to 4 ^{o}C with increasing the depth by 100 meters. This means that for two fractures with a distance of 400 meters vertically between them, their temperature difference can reach 16 ^{o}C. Therefore, the above models cannot be applied to accurately model the cases where there are several subparallel horizontal fractures and the fracture spacing varies.

In the present model, the heat extraction from a parallel fracture array is studied by taking into account the effect of the geothermal gradient. The aim is to grasp the characteristic of a multiple fracture (reservoir) system and have a better understanding of the relationship between some input parameters and the reservoir performance.

Problem formulation

Figure 1 shows a fluid circulation crack model with multiple parallel penny-shaped fractures, all with the same radius. The vertical injection well is along the z axis shown in Figure 1 and four production wells are evenly distributed along the fracture periphery. The initial temperature of the system is assumed to be a function of the depth $T_0=A_0z+B_0$ (where A_0 is the geothermal gradient, B_0 is the ground temperature and z is the depth into the ground). At $t>0$, a fluid is circulated into the well with a total volumetric rate Q_{in} and at a temperature T_{in}. The fluid flows along the circular fractures and out at the production wells where a constant pressure p_0 is imposed. It is assumed that the heat flux from the rock to the air is q_1.

The radii of the wellbore and reservoir are r_w and r_e, respectively. The depths of the first fracture (the bottom one for Case I and the top one for Case II) and the fracture spacing are denoted by H and d, respectively. The number of fracture is N.
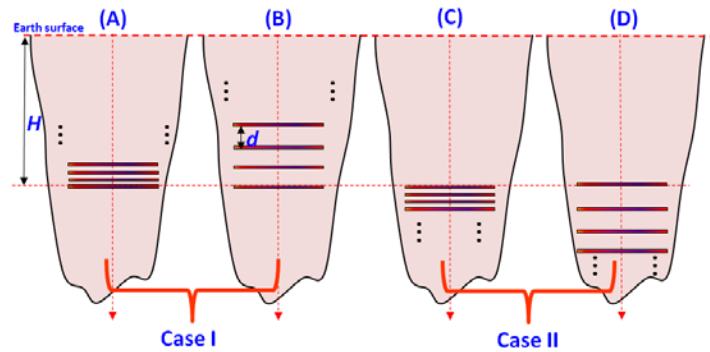
Figure 1: Geometry for a multi-layered geothermal reservoir model.

Some assumptions are made for the present model:

- The rock is homogenous, impermeable to fluid and isotropic, and the fluid is Newtonian;

- The properties (such as the density and viscosity) of the rock and the fluid are constant and independent of the temperature;

- The injection rate of each fracture is equal to the total injection rate Q_{in} divided by the fracture number N;

- The thermal induced stress is neglected and the fracture width is constant.

Governing equations and boundary conditions

Fluid pressure diffusion in the fracture

The pressure diffusion along the fracture can be described as

$$\frac{\partial p_f^\ell}{\partial t} = \frac{k^\ell}{\phi C_f \mu \omega^\ell} \nabla^2 p_f^\ell \ , \quad k^\ell = \frac{(\varpi^\ell)^3}{12}, \qquad (1)$$

where the symbol ∇^2 is Laplacian operator; ℓ $(\ell = 1 \ldots N)$ denotes the ℓth fracture; p_f^ℓ is the fluid pressure along the fracture ℓ; ϖ^ℓ and k^ℓ are the fracture aperture and fracture conductivity, respectively; the fracture aperture is generally less than 0.1 mm; ϕ is the porosity as fracture roughness can affect conductivity, μ and C_f are the fluid viscosity and fracture surface compressibility, respectively.

The fluid transport in the fracture obeys the Darcy law

$$\mathbf{q}_f^\ell = -\frac{k^\ell}{\mu}\nabla p_f^\ell,$$

(2)

where $\mathbf{q}_f^\ell$ is the fluid discharge with the unit of m²/s.

Heat transport in closed fractures

As the effect of the heat storage and thermal dispersion can be ignored (Cheng et al., 2001), the advection plays a dominant role in the heat balance equation for the fluid in the fracture

$$\rho_w c_w \mathbf{q}_f^\ell \square \nabla T_f^\ell + q_h^\ell = 0,$$

(3)

where the symbol ∇ is the gradient operator, T_f^ℓ is the fluid temperature, ρ_w and c_w are the fluid density and specific heat capacity, respectively; q_h^ℓ is the heat exchange rate across the ℓth fracture and can be expressed as

$$q_h^\ell = \lambda_r \left(\frac{\partial T_r^{\ell+1}}{\partial z} - \frac{\partial T_r^\ell}{\partial z} \right)\bigg|_{z = z_0^\ell}, \quad z_0^\ell = H - (\ell - 1)d,$$

(4)

where z_0^ℓ is the vertical coordinate of the ℓth fracture.

Heat diffusion in the rock

As the surrounding rock is impermeable and isotropic, the governing equation for the heat transport is expressed as

$$\frac{\partial T_r^*}{\partial t^*} = \kappa_r \nabla^2 T_r,$$

(5)

where the thermal diffusivity $\kappa_r = k_r / \rho_r c_r$ with ρ_r, c_r and k_r being the mass density, specific heat and thermal conductivity, respectively, of the rock.

Initial and boundary conditions

The fluid temperature at the injection point of each fracture can be measured

$$T_f^\ell = T_w, \quad r = r_w, \quad z = z_0^\ell.$$

(6)

The fluid temperature in the fracture is assumed to be equal to the rock temperature at the fracture walls

$$T_f^\ell = T_r \quad \text{on } z = z_0^\ell \text{ and } r_w < r < r_e.$$ (7)

The heat exchange rate between the surface of the earth and the air is

$$q_1 = \lambda_r \frac{\partial T_r}{\partial z}, \quad z = 0.$$ (8)

The injection rate for each fracture is known

$$Q_0 = \frac{Q_{in}}{N} = \frac{2\pi k^\ell}{\mu}\left(r \frac{\partial p_f^\ell}{\partial r}\right), \quad r = r_w,$$ (9)

and the pressure at all points along the outer circumference of each fracture (approximating production wells) is the same for all fractures

$$p_f^\ell = p_0, \quad r = r_e.$$ (10)

In addition, the initial temperature of the system and the fluid pressure are

$$T_r = T_0 \text{ and } p_f^\ell = p_0, \quad \text{when } t = 0.$$ (11)

Methods for the solutions

The approach for solving the present model is similar to that used by Abe et al. (1983) and Zhang et al. (2009). The heat exchange rate q_h^ℓ along the fracture is treated as a point sink/source. The total responses can be found by summing the point solution (Green's function) along all fractures. The temperature of the rock formation is attributed to three contributions: one from the initial condition, one from the heat exchange between the earth's surface and the air (which has little impact on the result), and the last one from the heat removed away by the flowing fluid, that is, the heat exchange rate between the rock and the fluid.

As the rate of heat taken away by the circulation of fluid is coupled to the fluid flow, it is necessary to obtain the fluid velocity first. By solving the governing equation (1) with the boundary conditions (9) and (10), the fluid pressure p_f^ℓ and thus the fluid discharge $\mathbf{q}_f^\ell$ via Eq. (2) is obtained.

The Green's function corresponding to a point heat source in a semi-infinite domain with boundary condition of the second kind (heat flux at the earth surface) is given as

$$\overline{G}_r = \frac{1}{\pi^{3/2} R^3} \xi^3 e^{-\xi^2} + \frac{1}{\pi^{3/2} R'^3} \xi'^3 e^{-\xi'^2},$$ 12)

which denotes the temperature at point (r,θ,z) due to an instantaneous point source at (r',θ',z') in the semi-infinite domain, and the variables are defined as

$$\xi = \frac{R}{\sqrt{4\kappa_r(t-t')}}, \quad R^2 = r^2 + r'^2 - 2rr'\cos(\theta - \theta') + (z - z')^2,$$

$$\xi' = \frac{R'}{\sqrt{4\kappa_r(t-t')}}, \quad R'^2 = r^2 + r'^2 - 2rr'\cos(\theta - \theta') + (z + z')^2.$$

Therefore, the rock temperature can be written as follows in terms of the Green's function

$$T_r = \int_{\Omega} T_0(x', y', z')\overline{G}_r \mid_{\tau=0} d\Omega + \frac{\kappa_r}{\lambda_r}\int_0^t d\tau \sum_{\ell=1} \int_{A^i} \overline{G}_r q_h^\ell dA - \frac{\kappa_r}{\lambda_r}\int_0^t d\tau \int_{\Gamma} \overline{G}_r q_1 d\Gamma.$$

$$(C_1, \text{ICs}) \qquad (C_2, \text{Heat sink}) \qquad (C_3, \text{BCs}) \qquad\qquad 3)$$

The above three parts for the rock temperature are simplified to be

$$C_1 = \frac{A_0}{\sqrt{\pi}}\sqrt{4\kappa_r t}e^{-\frac{z^2}{4\kappa_r t}} + zA_0\mathrm{erf}\left(\frac{z}{\sqrt{4\kappa_r t}}\right) + B_0,$$

$$C_2 = \frac{2\kappa_r}{\sqrt{\pi}\lambda_r}\sum_{\ell=1}^N \int_0^t \int_{r_w}^{r_e} \frac{q_h^\ell(r', t')}{[4\kappa_r(t-t')]^{3/2}} I_0\left[\frac{2rr'}{4\kappa_r(t-t')}\right] \times \left\{ e^{-\frac{r'^2 + r^2 + (z-z^s)^2}{4\kappa_r(t-t')}} + e^{-\frac{r'^2 + r^2 + (z+z^s)^2}{4\kappa_r(t-t')}} \right\} r'dr'dt',$$

$$C_3 = -\frac{q_1}{\sqrt{\pi}\lambda_r}\left\{ \sqrt{4\kappa_r t}\, e^{-\frac{z^2}{4\kappa_r t}} - \sqrt{z^2\pi}\,\mathrm{erfc}\left(\sqrt{\frac{z^2}{4\kappa_r t}}\right)\right\},$$

where I_0 is the modified Bessel function, $\mathrm{erf}()$ and $\mathrm{erfc}()$ are the error functions. Obviously, C_1 and C_3 are functions of z and can be calculated easily. Thus, the heat flux jump q_h^ℓ is the only unknown to be solved.

As the heat is transported axi-symmetrically in the fluid, we obtain the fluid temperature by integrating Eq. (3) from r_w to r

$$T_f^\ell = T_w^\ell - \frac{1}{\rho c_w}\int_{r_w}^r \frac{q_h^\ell(r', t)}{q_f^\ell(r', t)}dr'. \qquad\qquad 14)$$

By using the condition (7) that the fluid temperature is equal to the rock temperature, we obtain the following integral equations in terms of the heat exchange rate q_h^ℓ

$$C_1 + C_3 - T_w^\ell + \frac{1}{\rho_w c_w \varpi^\ell}\int_{r_w}^r \frac{q_h^\ell(r', t)}{q_f^\ell(r', t)}dr' + \frac{\kappa_r}{\pi\lambda_r}\sum_{\ell=1}^N \int_0^t \int_{r_w}^{r_e} q_h^\ell(r', t')Fdr'dt' = 0, \quad \text{at } z = z_0^\ell,$$

where the function F is defined as

$$F = \frac{1}{t_d} \left\{ e^{-\frac{(z^\ell - z^s)^2}{t_d}} + e^{-\frac{(z^\ell + z^s)^2}{t_d}} \right\} e^{-\frac{(r'-r)^2}{t_d}} \bar{I}_0 \left(\frac{2rr'}{t_d} \right) \sqrt{\frac{r'}{r}}, \quad t_d = 4\kappa_r (t - t').$$

The spatial domain (r_w, r_e) and time domain $(0, t)$ are divided into M and L sub-domains, respectively, and we obtain

$$C_1(z^\ell, t_W) + C_3(z^\ell, t_W) - T_w^\ell + \frac{1}{4\pi\lambda_r} \sum_{j=1}^{W} \sum_{i=1}^{M} \sum_{s=1}^{N} q_h^s(R_i, t_{d,j}) \int_{t_{d,j}}^{t_{d,j+1}} \int_{r_i'}^{r_{i+1}'} F dr' dt_d$$

$$+ \frac{1}{\rho c_w} \sum_{i=1}^{k} \frac{q_h^\ell(R_i, t_W)}{q_f^\ell(R_i, t_W)} (r_{i+1}' - r_i') = 0, \quad (k = 1 \cdots M, \quad \ell = 1, 2 \cdots N, \quad W = 1, 2 \cdots L).$$

15)

Therefore, from Eq. (15) the problem is converted to one of finding the unknown q_h^ℓ at specific positions and time t by solving a system of linear algebra equations. First, we choose a time step Δt starting from time t=0. Then we obtain the heat exchange rates along all fractures at t_1 by solving Eq. (15). After that we can update the time and solve the new heat exchange rates at t_2, t_3 ... t_{L-1} and t_L.

As each fracture has different output temperature, the AOT is calculated based on the following formula

$$AOT = \frac{1}{N} \sum_{\ell=1}^{N} T_{out}^\ell,$$

16)

where T_{out}^ℓ is the output temperature for the ℓth fracture.

Table 1 Parameters for the calculation

Parameter	Value	Parameter	Value
Wellbore radius r_w (m)	0.1	Depth of first fracture H (m)	4500
Well separation r_e (m)	500	Granite pore compressibility χ (Pa^{-1})	10^{-8}
Initial pressure p_0(MPa)	75	Fluid viscosity (Pa.s)	0.0002
Fracture aperture w (m)	0.001	Injection temperature ($^\circ$C)	90
Granite thermal conductivity λ_s (W m^{-1}K^{-1})	2.4	Geothermal gradient A_0 ($^\circ$C/m)	0.047
Granite density ρ_s(kg m^{-3})	2700	Surface temperature B_0 ($^\circ$C)	27
Granite specific heat c_s (J kg^{-1} K$^-$1)	1000	Granite initial temperature ($^\circ$C)	$A_0z + B_0$
Heat flux to the air q_1 (W/m^2)	0.06	Fracture number N	varies
Total injection rate Q_{in} (Kg/m^3)	0.060	Fracture spacing d (m)	varies

Verification of the present solution

To verify the present solutions, the calculated temperatures for the case with single fracture are compared with those obtained from TOUGH2 as shown in Figure 2. It can be seen that they are in first-order agreement.
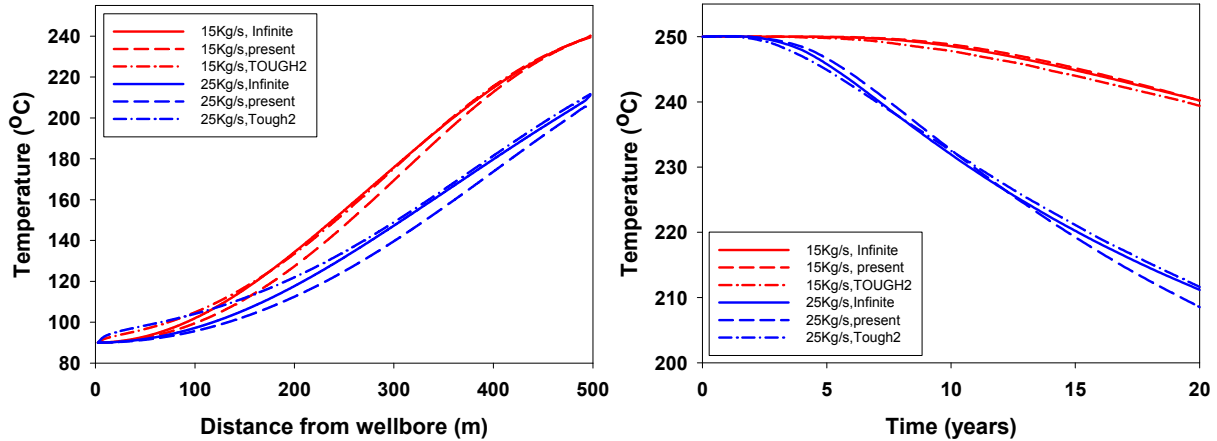

Figure 2: Comparison between the present calculation and TOUGH2 for the case with a single fracture and $A_0=0$, $B_0=250\,^{o}C$.

Numerical results

In order to study the effects of the number of fractures and fracture spacing on the reservoir performance, two case studies are carried out. In Case I as shown in Figure 1, we arrange N fractures at a spacing d upwards from the depth of the bottom fracture, while in Case II the spacing is applied downwards from the top fracture. The first fracture of two cases has the same depth. In all computations, the total injection rate is 60 kg/s and the individual injection rate for each fracture is 1/N of the total injection rate. The parameters for the present calculations are listed in Table 1.

Figure 3 shows the AOT for different numbers of fractures and fracture spacing in Case I. It can be seen from Figs 3(a) to 3(d) that the AOT in any of the multiple-fracture cases (blue curves) is larger than that in the single-fracture case (red curve). This indicates that the lifetime of the multiple fracture reservoirs is much longer than that of the single fracture reservoir as the multi-fracture system can supply a higher outlet temperature for a longer time.

For the cases shown in Figure 3, the AOT curve for d=2 m is close to the red curve for single fracture case. This means that the multiple fracture reservoir acts like a single fracture reservoir when the fracture spacing is sufficiently small. By increasing the fracture spacing the reservoir will exhibit the advantages arising from multiple fractures. For example, when d=50 meters, the increase in AOT is largely increased for large time period. However, if the spacing is beyond 50m, there is little difference between the AOTs. Moreover, there is a trend for the AOT to decrease at long production time when d is increased to be larger than 100 meters. This is due to the lower local rock temperature of the shallower fractures.
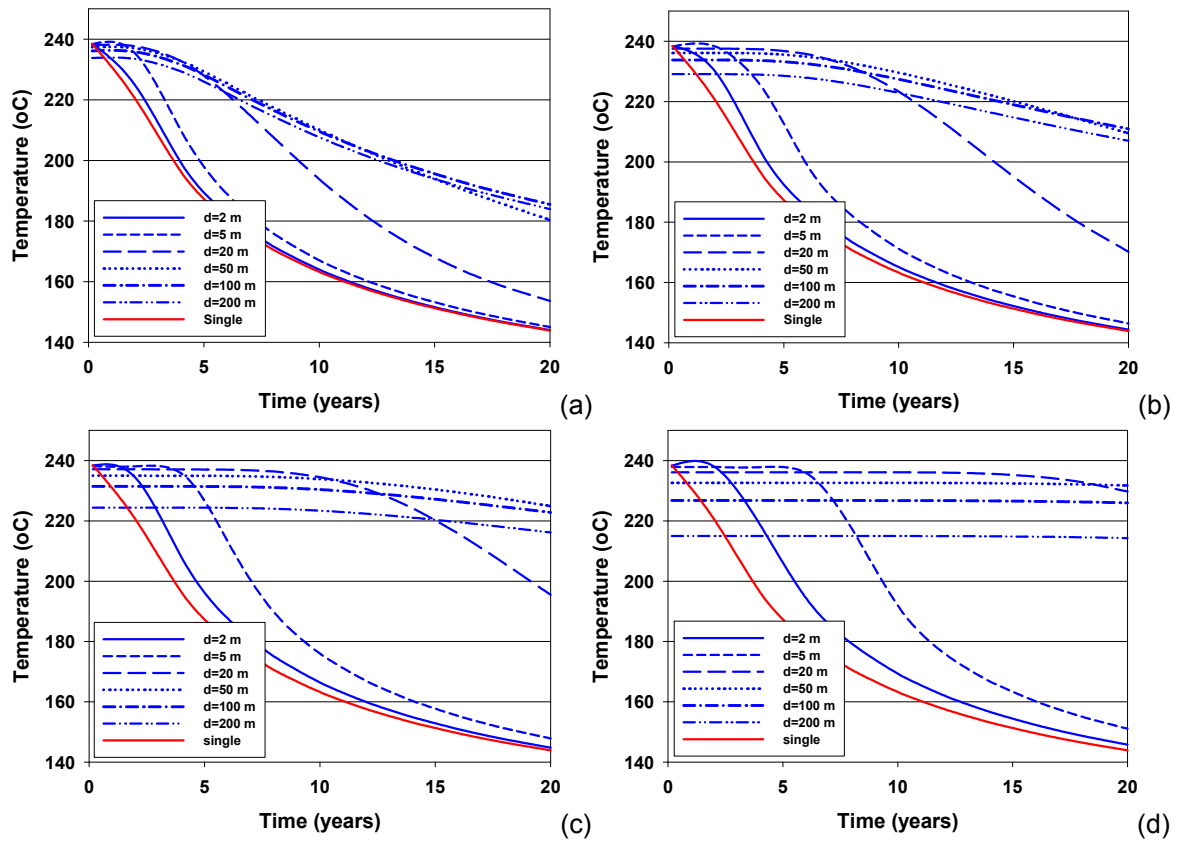
Figure 3: *AOTs under different number of fracture: (a) for N =2, (b) for N =3, (c) for N=4 and (d) for N=6.*

In addition, Figure 3 shows that simply increasing the fracture number does not produce the maximum temperature response in value and time. The curves in Figure 3(d) are obviously lower than their counterparts in Figure 3(c). This is to say, that the intuitive and often used stimulation strategy that is based on stimulating as many natural fractures as possible does not produce optimal reservoir performance.

To find the best choice of the fracture number and spacing, in Figure 4, we plot the AOT responses at different times. For the given injection rate, the minimum fracture number to extend the higher outlet temperature (>235 degree) for more than 20 years, is 5. Also, we can see that the AOT reaches the maximum performance if the spacing is equal to 50 meters when the fracture number is 5. Therefore we have a non-trivial solution that is required to satisfy given design requirements.
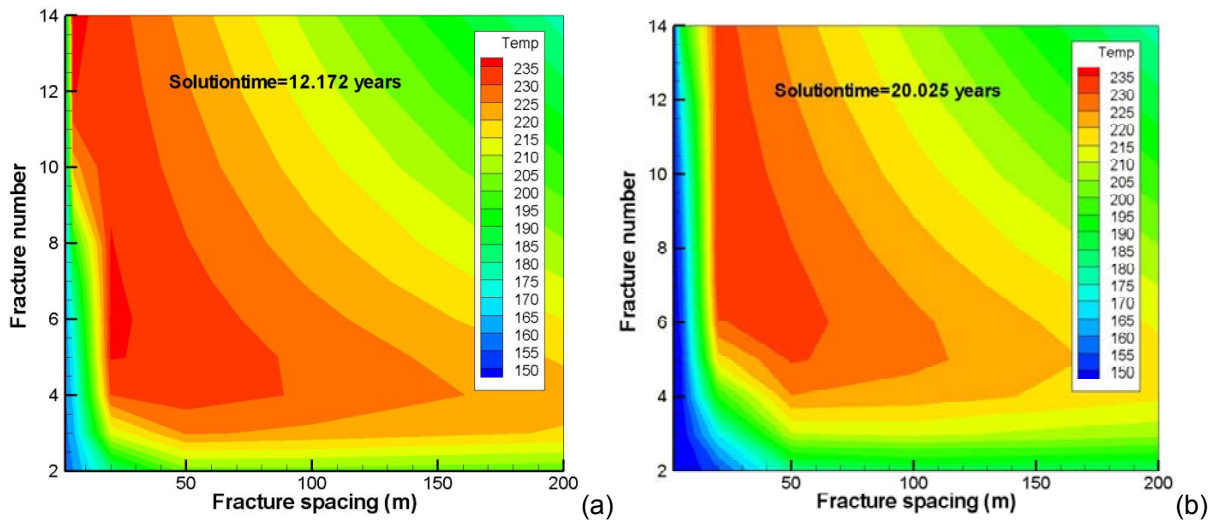
Figure 4: *AOT contour for case I where the depth of the bottom fracture is fixed and the fracture number and fracture spacing vary with fixed injection rates of 60 Kg/s. (a) is for t=12.172 years, (b) is for t==20.025 year.*
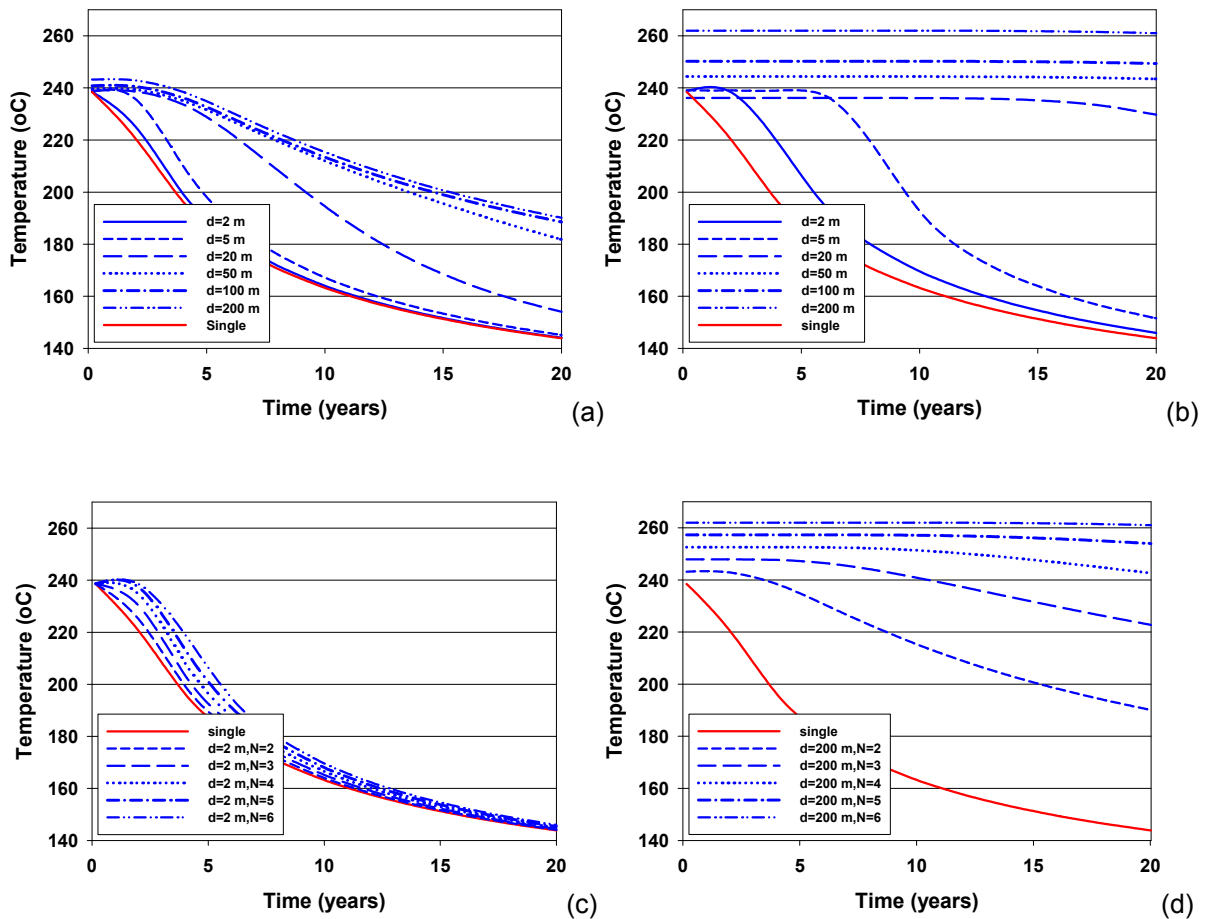
Figure 5: *AOTs under different numbers of fractures and fracture spacing for Case II. (a) for N=2 and (b) for N=6 with d varied; (c) for d=2m and (d) for d=200m with N varied.*
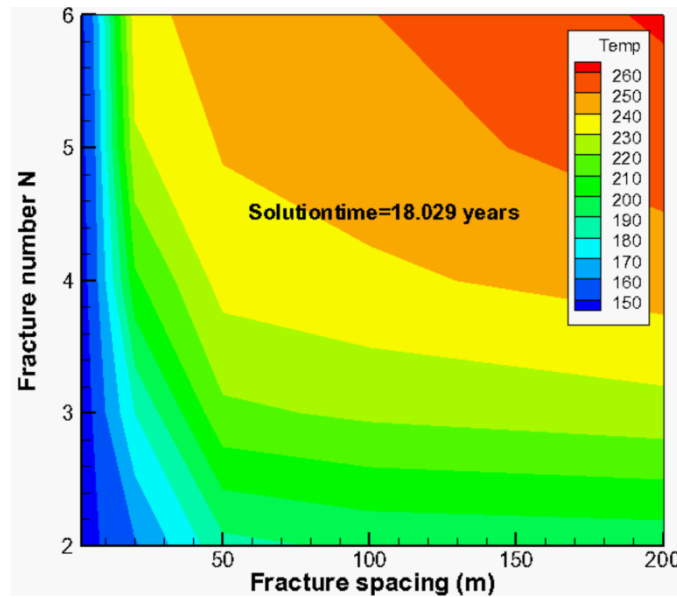
Figure 6: AOT contour at time=18 years for Case II where the depth of the top fracture is fixed.

Figure 5 and 6 plot the AOT results for Case II. For this case, it is easy to understand that the deeper the fractures, the higher the AOT. Also, if a greater number of deeper fractures are produced, the outlet temperature will accordingly increase. This is reflected in the contour plots for the AOT responses with the fracture number and spacing in Figure 6. Therefore, there is no optimal solution to choose under this monotonic situation. However, it is worth highlighting that the cost of creating deeper fractures also increases, so that a complete optimisation would need to consider economics.

Conclusions

This paper studies the effect of the fracture number and spacing on the average output temperature of an engineered geothermal system. Based on the calculations, the following conclusions are obtained:

- Fracture patterns including fracture number, spacing and the arrangement are important. More importantly, multiple fracture treatment can increase the lifetime of the system to produce a useful AOT level.

- For case I in Figure1 there is an optimal choice of fracture number and spacing to maximize outlet temperature at the given injection rate and expected lifetime for a engineered geothermal system. For case II in Figure 1 there is no optimal solution for the values tested.

Ongoing work includes extending the model to account for a single injection/producer pair and deriving scaling relations that will clarify the main parametric dependencies of the problem.

References

Abe, H, Mura,T., Keer, L.M., 1976. Heat extraction from a hydraulically fractured penny-shaped crack in hot dry rock. Proceedings Second Workshop Geothermal Reservoir Engineering, Stanford University, Stanford, California, December 1-3, 1976.

Abé, H., Sekine, H., Shibuya, Y., 1983. Thermoelastic analysis of a cracklike reservoir in a hot dry rock during extraction of geothermal energy. Journal of Energy Resources Technology, 105, 503-508,1983.

Cheng, A. H.D., Ghassemi, A., Detournay, E., 2001. Integral equation solution of heat extraction from a fracture in hot dry rock. International Journal for Numerical and Analytical Method in Geomechanics, 25:1327.

Ghassemi, A., Tarasovs, S., Cheng, A.H.D., 2005. Integral equation solution of heat extraction-induced thermal stress in enhanced geothermal reservoirs. International Journal for numerical and Analytical Methods in Geomechanics, 29:829-844.

Gringarten, A. C. and Sauty, J. P., 1975. A Theoretical Study of Heat Extraction from Aquifers with uniform regional flow. J. Geophys. Res., 80(35), 4956-4962.

Kolditz, O., 1995. Modelling flow and heat transfer in fractured rocks: conceptual model of a 3-D deterministic fracture network. Geothermics, 24(3), 421-437.

Lauwerier, H.A., 1955. The transport of heat in an oil layer caused by the injection of hot fluid. Applied Scientific Research, 5,145-150.

McFarland, R.D., 1975. Geothermal reservoir models: crack plane model. Technical Report , LA-5947-MS , Los Alamos Scientific Lab., New Mexico, USA.

M. Dopita, R. Williamson, Australia's renewable energy future, Australian Academy of Science, 2010.

Zhang, X, Jeffrey, R.G., Wu, B, Two basic problems for hot dry rock reservoir stimulation and production. 2009 Australian Geothermal Conference, Brisbane, 10-13 November, 2009.

Zyvoloski, G., 2005. Finite-element methods for geothermal reservoir simulation. International Journal for Numerical and Analytical Methods in Geomechanics 7: 75–86.

The Innamincka Enhanced Geothermal System (EGS) – Dealing with the Overpressures

Wyborn, D

Geodynamics Limited, Milton, Queensland, Australia,

doone.wyborn@geodynamics.com.au

Introduction

The Geodynamics EGS Project commenced in 2000 and targeted the Innamincka Granite following extensive research over a period of 8 years on international EGS projects. In 2002, the time of the Geodynamic public listing, EGS was referred to as Hot Dry Rocks. The Innamincka Granite over the depth interval 4-5km consists of 991 km^3 of granite with an average temperature of at least 250°C. This has an "in place" thermal energy resource of 185 exajoules (EJ) using a 165°C cut-off temperature (note: the world emits 21 billion tonnes of carbon dioxide per year by burning fossil fuels to produce 400 EJ of energy or 87% of all energy: Wikipedia). By way of comparison, the ultimate recoverable reserves of the Greater Gorgon gas field in Western Australia is 40 trillion cubic feet, which is roughly equivalent to 40 EJ. The granite is modelled by gravity to be about 10 km thick, and thermal modelling is consistent with a temperature at 18 km depth of 500°C.

Since the discovery of high fluid overpressures in the Habanero 1 well in May 2003 whilst drilling at a depth of 4,200 m, Geodynamics has had to contend with these pressures in all its wells into the Innamincka granite. The overpressures have allowed free flow of high pressure water and steam from the EGS reservoir and demonstration of the potential EGS energy available, but, in truth, they have resulted in difficult drilling operations, damage of the reservoir because of mud losses and more difficult management of hydraulic stimulation activities.

Origin of the overpressures

The fluid pressures in the natural granite fractures at Habanero are 34.47 MPa (5,000 psi) above hydrostatic with a stable column of fresh water in the well. Geodynamics has attributed the overpressures to a combination of (i) the recent increase in horizontal stresses in the Australian crust combined with (ii) a sedimentary caprock of impermeable shales and fine grained sandstones. The fine grained sandstones from the Patchawarra Formation to the top of the granite (about 3,200m to 3,700m depth) have been sealed by long-term (100 million years) conditions of high temperatures (>200°C) causing porosity and permeability destruction. This grain recrystallisation has been termed radiogenic metamorphism. The increase in horizontal stress would have compressed the natural rock porosity causing fluid pressure to increase. Normally this pressure increase would have bled off with upward fluid migration, but the caprock is too impermeable and the overpressure remains trapped, almost certainly for several millions of years.

Innamincka geology prior to drilling Habanero 1

Much was understood from existing oil and gas exploration drilling down to the top of the granite. The granite basement had been penetrated several times and its extent and thickness had been inferred by gravity mapping. Seismic reflection profiling had delineated the depth to the top of the granite. Temperatures in the granite had been measured and were extraordinarily high. The high temperatures were generated because of two independent geological conditions (i) a high heat flow from thick radiogenic basement granite, and (ii) the presence of quartz-poor low-conductivity sediments overlying the granite. The temperature at the top of the granite at around 3.7 km was known to be around 230°C. Such temperatures at this depth are unknown in any other location in the world outside volcanic areas.

In accord with the evidence from much of the Australian continental crust (Denham and Windsor, 1991), sediments in the deeper part of the Cooper Basin (known as the Nappamerrie Trough) above the granite were thought to have high horizontal stresses and this was likely to extend into the granite. The direction of the maximum horizontal stress was known to be approximately east-west. Much was made of the fact that stimulated reservoirs should have horizontal rather than vertical extent (Somerville et al., 1994) and such reservoirs could be stacked on one another to improve heat recovery and increase fluid flow. Since the granite had been exposed at the surface around 300 million years ago, and reburied to its current depth over the ensuing 200 million year period, then it was expected that there would be many horizontal unloading joints in the top of the granite, and that these joints would be available for stimulation.

Although there had been gas saturated overpressures recognised in the sediments above the granite, the thought at the time was that normal pressures would prevail in the water saturated granite beneath. The gas to water interface occurs a few hundred metres above the granite. This is based on electrical logs in the gas exploration wells.

Habanero 1 - discovery of the overpressures

Habanero 1 well was drilled into the granite in April 2003 and seven inch casing was set 471 m below the granite-sediment contact at a depth of 4,139 m. The drill mud weight was 14.5 ppg (1.74 SG) because of the need to counteract gas overpressures in the sediments above the granite. However during tripping before setting casing the well was flowing and the mud weight was increased to 15.0 ppg (1.80 SG). At the time of image logging above the 7 inch casing point it was not realised that the need to weight up the mud during the final bit trip was almost certainly caused by overpressures in what has been termed the upper fracture at a depth of 4,135 m.

Once casing was set, the mud weight was reduced considerably to 11.8 ppg (1.41 SG) on the assumption that the gas overpressures were cased off above. After a good bit run to 4,209 m a torque spike indicated that the bit should be pulled. It was found to have lost two cones and a flat bottom mill was deployed to clean up the cones. The subsequent operations over the next five days resulted in both water influx and mud losses and finally established a wellhead pressure equivalent to an overpressure of approximately 5,000 psi (34.47 MPa) assuming a water gradient. Important observations in this period included:

(i)   Any fracture at 4,209 m depth was initially showing no signs of overpressures being present (during bit trip and subsequent cone milling operations).

(ii)   After the initial influx during the tripping of the mill bit there was a reversal of pressure response and 425 barrels of 11.8 ppg mud was lost into the granite even though the final granite overpressure was established to require a mud weight of more than 15 ppg to hold it back. The reason for the losses has never been satisfactorily explained. One possibility is that a shear event on the exposed fracture created new fracture porosity and it was easier for the low pressure mud to fill this porosity than for higher pressure reservoir fluid to take up the space. Despite the higher pressure in the reservoir, the far field fracture conductivity in the immediate area was too low for the required flow into the newly sheared fracture.

(iii)   Subsequent water injection during the stimulation showed no evidence of a fracture being present at 4,209 m. The fracture at 4,209 m is known as the plugged fracture and is assumed to have been sealed by drill mud invasion.

The discovery of a 5,000 psi overpressure resulted in the suspension of drilling operations while a 10,000 psi blow out preventer was obtained from Singapore. The suspension lasted from 20 May 2003 to 30 June 2003.

The drilling below 4,209 m was continued with a heavy mud weight in the range 15.2 to 15.6. This weight ensured that losses would occur in any conductive fractures encountered. Indeed at one point at a depth of 4,254 m the driller reported that a fracture was encountered "Drilled thru fracture 13,956-7 ft - ROP 10 ft/hr from 5 ft/hr, torque spike, slight pressure loss and 10 bbl mud loss". This fracture,

estimated to be only 1 ft thick during drilling later turned out to be by far the dominant flow path during stimulation injection, and has been termed the main fracture.

After drilling through the main fracture drilling proceeded another 65 m to a depth of 4,319 m but during a bit change the well began to flow and at this time the float valve failed so that circulation could not occur. The well subsequently experienced trouble over the ensuing 6 weeks from 2 August 2003 to 14 September 2003 at this depth. Activities included influx, losses, bullheading, pumping of lost circulation material (LCM), float failure, running wireline and cleaning out drill pipe with coil tubing, stripping out of well, stripping with a snubbing unit, and mechanically stuck pipe. Total mud losses over this period were 1,582 bbl with mud weight mostly greater than 15 ppg (1.80 SG). In addition there were influxes amounting to 169 bbls of water. At one point during the pumping of an LCM pill the well was both gaining and losing during the operation. On 31 August 2003 after a 52 bbl influx the shut-in casing pressure was 3,600 psi indicating more than 50% of the well had filled with water. On 4 August 2003 the well flowed on open choke 17 bbls in 2 minutes (22.5 l/sec). Eventually the well was stabilized with a mud weight of 15.4 ppg (1.84 SG), and the well was completed to a depth of 4,421 m on 17 September 2003. The gains and losses whilst at 4,319 m cannot be attributed to a fracture at that depth. Rather known fractures at 4,209 m and 4,256 m are more likely to be implicated.

Circulation of influx from Habanero 1 whilst at 4,319 m allowed for the first time the collection of fluid from granite fractures. Analyses contained about 18,000 ppm total dissolved salts, a salinity that has remained for virtually all the fluids that have been produced from the granite since. Importantly the boron content of these fluids was 220 ppm indicating that there was very little drilling mud filtrate in the samples. The Na/K ratio of the fluid using the Fournier (1979) geothermometer indicates temperature of 240°C and 245°C for the two samples analysed. Fluid sampling from later wells had similar chemistry despite the addition of fresh water during stimulation operations.

Habanero 2 - drilling of multiple open fractures

The site for Habanero 2 was chosen 500m SSW of Habanero 1. In this direction seismicity during Habanero 1 stimulation indicated the presence of possible parallel multiple fracture layers, which were thought to provide greater chance of multiple flow paths and hence higher flow rate. Similar conditions occurred to the NW at another potential site, but it was thought that the seismicity in that direction was more complex and that reservoir impedance might be higher. In addition the seismicity grew to the SW at the start of the stimulation possibly indicating a more direct path in that direction.

The problem of drilling multiple fractures, or even a single highly conductive fracture with fully weighted mud at overpressured conditions was well understood from the drilling of Habanero 1. Consequently Geodynamics negotiated with a Shell subsidiary, Flow Drilling Engineering Ltd for a managed pressure drilling (MPD) package to be used during the drilling of the granite. The MPD equipment had been only used a few times in a testing environment, but was considered now ready for this particular issue. Bob Worrall (Shell E&P) provided guidance on the MPD operation.

Habanero 2 was spudded 500m SSW of Habanero 1 on 10 July 2004. The target was the main fracture predicted to be at a depth of 4,310 m on the basis of the microseismic data. Seven inch casing was set 240 m into the granite at 3,921 m depth. MPD was used in the granite section, and at a depth of 4,181 m influx from a flowing fracture was identified using the MPD Coriolis flow meter. Reservoir pressure was accurately assessed and the MPD system was adjusted to slightly higher pressure to stop the influx and drilling continued. The fracture was reasoned to be the upper fracture in Habanero 1, with fractures dipping gently to the west at around 10-20°.

After drilling a further 144 m to 4,325 m the well suffered total losses. The depth was 15 m deeper than the location predicted for the main fracture from seismic data. Five LCM pills of increasing severity were pumped. Only after the fifth pill consisting of 60 bbl of 5 ppb sandseal, 10 ppb calgrit fine, 10 ppb calgrit medium, 10 ppb calgrit coarse, 7 ppb quickseal and 7 ppb fracseal, were the losses cured. A total of 1359 barrels of mud and 185 barrels of LCM were lost into the fracture during the operation. Over the next few days a further 2951 barrels of mud and 490 barrels of LCM were lost in the well, as well as all cuttings from drilling blind for another 16 m to a total depth of 4,342 m. After the first curing of losses the bit was tripped and a new bit deployed. This bit reamed down to the main

fracture depth with full returns, but when it reached the fracture there were again total losses. The wellbore was plugged with LCM, not the fracture. Clearly the main fracture at this location was highly permeable. On a number of circulations during the period of losses into the main fracture there were also light mud returns from the depth of the upper fracture. The relatively small difference in fracture pressure, due entirely to hydrostatic head between the upper fracture and the main fracture resulted in influx from the upper fracture and major losses from the main fracture. As an example of the pressure sensitivity of the system, on 13 October 2004 when the new bit was run in for the 16 m of blind drilling, the mud weight was 14.9 ppg (1.773 SG). Light mud from influx from the upper fracture was circulated out. The pressure difference between the upper fracture and main fracture (144 m apart) at hydrostatic conditions (0.9 SG, temperature 250 degrees C, 20,000 TDS) is 188 psi (1.296 MPa; $144*0.9*10^{-3}$). In the well the pressure difference is 370 psi (2.553 MPa; $144* 1.773*10^{-3}$) with the higher density mud. Thus, assuming balance on the upper fracture, the over-pressure of the mud on the main fracture would only be 370-188 = 182 psi (1.255 MPa). This was clearly enough to result in complete losses.

During the pumping of five LCM pills five pressure spikes up to 17 psi were recorded at Habanero 1 indicating good communication along the fracture system between the two wells.

Following the blind drilling of the 16 m below the main fracture during reaming operations around the depth of the main fracture the torque became erratic. The string was pulled and it was found that a drill collar had parted 245 m up from the bit. The bit was caught in the main fracture it had not fallen to the bottom 16 m below. Although the fish was caught with a 5 ½ inch overshot grapple it was not possible to pull it with maximum pull. A sidetrack was called.

Habanero 2 Sidetrack 1 was drilled uneventfully down to a depth of 4,358 m. At 4,160 m the upper fracture was intersected when a clear influx was detected and managed with the MPD system. The depth was 21 m shallower than in the original hole. At a depth approximately equivalent to the depth of the main fracture there began to be small losses at a rate of 1-2 barrels per hour and at a depth of 4,345 m a 1.3 m drilling break from 8 ft/hour to 28 ft/hour suggested that this was the depth of the main fracture. It appeared that the main fracture was so damaged by mud losses from the original hole that there were no issues to drill it with the few hundred psi overbalance required to stop influx from the upper fracture.

When Sidetrack 1 was at 4,358 m it was decided that the main fracture must have already been penetrated so the well was called good and drilling ceased. A Halliburton bridge plug was installed at a depth of 920m, but was not able to be removed after installing the Christmas Tree. Finally after two separate attempts with two different coil tubing units (Halliburton and BJ) the bridge plug was lost down hole. It was proven to have gone past the upper fracture by later wireline logging but its actual location is not know.

It became clear from the flow testing of Habanero 2 that the well was impaired and this was put down to packing off of borehole breakout material around the lost bridge plug which must be lodge above the main fracture. Access to the main fracture was an imperative for future progress, but no drilling rig in Australia was available to do the job in late 2005. The rig that drilled Habanero 1 and 2 had moved to the Philippines. In addition the difficulty to control more than one fracture in an open hole became even more apparent. MPD alone was not sufficient. The only real alternative was to go to fully underbalanced conditions and drill with a water gradient, but with 5,000 psi (34.5 MPa) of back pressure at surface. A snubbing unit was available in Sale in Victoria, so it was decided that a second sidetrack (sidetrack 2) would be drilled in Habanero 2 to try to re-connect with the reservoir.

The snubbing operation lasted for more than 3½ months from 10 March to 30 June 2006. The operation was a failure, not because the snubbing unit could not do the job, but because of a number of down-hole failures. Initially two separate turbine bodies parted during drilling, requiring two additional side tracks (sidetracks 3 and 4). Finally the drill string became stuck when the well was approximately 120 m from the main fracture. The pipe was stuck 10 m off bottom (one joint), and circulation could not be established. The string had to be shot off above the drill collars at 12,415 ft (3,784 m), which is 77 m below top of granite.

Although the snubbing operation did not succeed in re-accessing the reservoir a number of important lessons were learnt.

- Snub drilling is certainly possible. Side tracks in granite using whipstocks or cement are possible. Impreg bits operated with turbines only work for a short time (1-2 hours) before the aggressive GHI diamond composite teeth flatten and then the bits stop drilling. The best performance with tricone bits were similar to the performance with mud, so high under-balance does not provide increased ROP.

- The drilling was mostly carried out with a low back pressure of only a few hundred psi. A high backpressure would only be required once a permeable fracture was encountered. The low back pressure caused massive breakout behind the bit so that the bit became stuck on virtually all connections. So long as circulation could be re-established this was not a problem. There was no trouble circulating the cuttings plus the breakout from the well using gel sweeps. Although higher back pressures up to 3,000 psi were tried it did not seem to affect the degree of breakout (this may have been an erroneous conclusion). It is likely that drilling with backpressure equivalent to the full reservoir overpressure would result in breakout of similar dimensions to drilling on-balance with mud.

- The breakout progressed down hole with drilling, such that the breakout above eventually stabilised over time. Once the well assumes some elliptical shape it no longer fails.

- During the operation water was flowing from sidetrack 1 past the sidetrack 2 whipstock. The flow rate was only a few kg/sec and gradually declined over the 3 month period. Interestingly as the flow rate declined the gas content seemed to increase. Samples of gas collected in the flow line at atmospheric pressure in early May 2006 contained 13% helium in a sample contaminated by 28% air. It appears that helium can transport somewhat independently of water in the upper reservoir once the water content of the fracture is depleted. During the snub drilling the reservoir pressure at Habanero 1 wellhead gradually fell from 4,990 psi (34.4 MPa) to 4,974 psi (34.3 MPa). Immediately after cessation of drilling at the end of June 2006 the pressure began to slowly rise. It took til September 2007 (15 months) for the Habanero 1 wellhead pressure to regain the 16 psi lost during Habanero 2 snubbing. There was clearly a tenuous connection between the upper fracture and the main fracture.

The two drilling reviews following the failed snubbing operation, one management initiated, and the other Board initiated, both concluded that drilling with a six inch bit and 3½ inch drill pipe was not robust for this environment. Wells would need to be drilled at a larger diameter (8½ inch bit and 5 inch drill pipe) for a low trouble well.

Habanero 3 - circulation testing, further recognition of drilling mud damage

The decision resulting from the Habanero 2 drilling reviews to drill the granite with 8½ bit and 5 inch drill pipe left Geodynamics with the problem that no land-based drilling rig in Australia could do this. Bringing a rental rig into the country with the guarantee of only one well (Habanero 3) meant that mobilisation costs were greater than the cost of the well. This was quite unpalatable and the hunt was on to purchase our own rig. Eventually the Le Tourneau "Lightening Rig" became the pick. It arrived in Brisbane on Sunday 1 July 2007 and Habanero 3 spudded on 15 August 2007.

Habanero 3 was drilled at a location away from Habanero 2 to minimise damage from lost drilling mud. A location 550 m NNE in approximately the opposite direction of Habanero 2 from Habanero 1 was chosen.

The well was drilled without difficulty notwithstanding the teething problems of the rig itself. One important aspect of the drilling at a larger diameter related to the reduced ROP in 12¼ inch hole compared to 8½ inch hole through the deeper formations of the Cooper Basin, in particular the thick Patchawarra Formation. In 8½ inch hole ROP was about 4 m/hr. However with 12¼ inch hole ROP was down to 1 m/hr. This considerably lengthened the drilling time over the interval. The granite was again drilled using a managed pressure drilling system. The location of the main fracture was determined from the seismic data at a depth of 4,160 m. The well head pressure at Habanero 1 was being monitored with a sensitive Quartzdyne pressure gauge. At a depth of 4,167 m increased

methane readings were detected and the MPD system adjusted. Then at a depth of 4,181 m the main fracture was intersected and the MPD system was substantially adjusted to counter the influx. At Habanero 1 the influx was seen as a drop in pressure of about 0.5 to 1 psi. The drilling mud weight was increased from 14.3 ppg (1.71 SG) to 14.8 ppg (1.77 SG) and the well was completed to a depth of 4,221 m giving a 40 m rat hole below the main fracture.

Habanero 3 - learnings from the well blowout

On 24 April 2009 at 10:48:44 UTC time (20:18:44 ADL time) there was a rupture of Habanero 3 casing in the top 6 m. Initially water and soon after steam flowed from the well and it took til 20 May 2009 (25 days) for the flow to be quelled. This was achieved by running coil tubing to a depth of 3,932 m and circulating 18 ppg (S.G. 2.16) mud. The casing failure was recorded on the Habanero microseismic network, and an almost identical event was also recorded 7 days earlier on 17 April 2009, at 15:45:07 UTC. The earlier event exhibited smaller signal amplitudes but was in other respects almost identical indicating that the failure took place in two stages. The failure resulted in an immediate response in the wellhead pressure at Habanero 1 with the pressure falling quite rapidly from around 4,790 psi (33.0 MPa) prior to the rupture to 4,570 psi (31.5 MPa) by 1 May 2009 and eventually 4,510 psi (31.1 MPa) by 20 May when the rupture was quelled. Total pressure loss in the reservoir was thus 1.9 MPa. Since that time the reservoir pressure has been rising to approach the original pressure of the reservoir determined when Habanero 1 was initially drilled in 2003. That pressure was 5016 psi (34.6 MPa) at the Habanero 1 wellhead with an approximate temperature equilibrated column of fresh water. On 28 September 2012 the pressure is 4,880 psi (33.65 MPa) prior to any activity in the newly completed Habanero 4. As of that date the well contains brine with a salinity of 20,000 ppm total dissolved salt, so reservoir pressure, as related to the Habanero 1 wellhead pressure with a column of fresh water would be underestimated by about 2% or about 100 psi. Hence the current (September 2012) reservoir pressure is probably only 20-30 psi lower than it was in 2003 when first encountered.

Jolokia 1 – proposal to seal overpressured fractures with cement

Jolokia 1 was located about 10 km west of Habanero close to where Burley 1-3 wells were drilled by Santos. Burley 2 drilled into the granite at a depth of 3,664 m and a temperature of 193°C was measured at a depth of 2,850 m during a cement bond log 9 years after completing the well. The temperature at Habanero at this depth is 183°C so the temperature in the vicinity of Jolokia 1 is possibly 10°C higher. Jolokia 1 was drilled as part of a program to extend the size of measured geothermal resources in the Innamincka granite by showing that similar reservoirs could be stimulated to the one at Habanero. In addition the reservoir development would be deeper and include stimulation of at least two separate reservoirs

The well was drilled from 15 March 2008 to 14 September 2008. In the granite section from a depth of 3,702 m equivalent mud weight was kept slightly below the reservoir pressure determined from Habanero using MPD equipment. The aim was to cement off each fracture as it was intersected and drill on. Only one relatively unproductive fracture was encountered (called the Dog Fracture) at 3,822 m depth. The Dog Fracture was determined to have approximately the same overpressure as that at Habanero, and its orientation was determined by an image log to be 20° to the WSW, an orientation optimal for slip during stimulation like the main fracture at Habanero. The Dog Fracture was cemented off because it was deemed too shallow to be of any use given that the aim was to develop deeper reservoirs than that at Habanero.

During the drilling of Habanero 1 the first detection of the reservoir pressure resulted from operating at mud pressures well below reservoir pressure and it took some time for the overpressure to show itself. In Jolokia mud weights were kept only slightly below reservoir pressure so once the well was completed at a depth of 4,911 m it was considered that permeable fractures below the dog fracture might still be present but not detected during drilling. Logging and drilling parameter variations of the deeper part of the well showed some evidence of fracture zones at around 4,400 m and again at 4,700 m, so a liner was planned to be set to around 4,350 m. Part of the design of Jolokia was to show that reservoirs could be created at deeper levels than the one at Habanero and also that multiple reservoirs could be created in the same well. The zones at 4,400 m and 4,700 m were targeted for the

formation of two reservoirs. However qualified high temperature open-hole packers were needed but not yet available. It was thought that such qualification was possibly within a short time (6-12 months) so it was decided that another well would be drilled before Jolokia 1 was stimulated. The rig was moved to Savina 1 a further 10 km west near the Santos well Bulyeroo 1. Later attempts to stimulate Jolokia 1 in October-November 2010 failed to indicate the presence of shallowly dipping fractures below the liner shoe set at 4,350 m. Only steeply dipping fractures were stimulated, and much higher pressures were needed since the stress normal to these fractures is higher than the vertical stress. The injectivity into these fractures is not sufficient for a viable EGS reservoir.

Savina 1 – more lessons on the overpressures

Savina 1 was located in order to extend the measured resource a further 10 km beyond Jolokia 1. The well was located prior to the Jolokia stimulation, so the concept of needing to identify locations where large shallowly dipping fractures might be present was not part of the thinking. At this time stimulation was thought to be possible in most places in the granite as fractures are likely to be common in granite at closely spaced (metre scale) intervals, as has been noted in granite drilling elsewhere in the world. The aim was to establish a Habanero-Jolokia-Savina corridor 20 km long and several kilometres wide through the centre of the Innamincka granite in which resources could be upgraded to "measured". It was envisaged that up to ten 50 megawatt power stations could be constructed along the corridor between Habanero and Savina.

Savina was located close to the Bulyeroo 1 well drilled by Santos in 1994 and intersected high heat production granite at a depth of 3,430 m on top of a basement hill. A temperature measurement of 222°C at 3,260 m was recorded at Bulyeroo 1 during a cement bond log 5 weeks after the well was last circulated. This temperature is 14 degrees hotter than Habanero at the same depth (208°C), so the area around Savina is considerably hotter than Habanero, and possibly even hotter than that at Jolokia.

Savina 1 was drilled from 17 October 2008 to 20 February 2009 using MPD equipment in the Cooper Basin and granite sections. Drilling was considerably underbalanced through the lower part of the Cooper Basin in an attempt to increase ROP in the 12¼ inch hole section. ROP in this section was better than Habanero 3 and Jolokia 1. The underbalanced drilling was continued into the granite which was encountered at 3,615 m. The mud weight was 11.4 ppg (S.G 1.366). In a drill-off test it was determined that rate of penetration (ROP) was greatest with no MPD back pressure so the granite was drilled with an equivalent mud weight of 11.4 ppg. Unfortunately a highly permeable fracture was intersected in the granite at 3,700 m which resulted in a strong influx that filled much of the well with water. The water was analysed and gave a composition similar to, but slightly more saline than, the Habanero water. The overpressure was calculated to be almost identical to the Habanero overpressure 18.5 km to the east. It is tempting to suggest that compartmentalisation, so common in oil and gas deposits, is not present in a fractured granite environment, and that there are fracture linkages from Habanero to Savina and beyond.

After the influx, during the weighting up of drilling mud to kill the well the drill string became differentially stuck on normally pressured sandstones at the top of the Toolachee Formation. There followed a normal operation of progressive washing down with an Overshot and back-off to eventually get below the differentially stuck zone. One back-off resulted in the fish top being located in the middle of a 5 m thick coal seam that was highly caved. Experts considered it would be impossible to get over the fish in such a large hole so the hole was abandoned. A cement plug was placed above the fish for a side track, but a change of plan resulted in the well being suspended on 2 March 2009 and efforts were reconcentrated on the stimulation of Jolokia 1 (see above).

Habanero 4

Habanero 4 became the replacement for Habanero 3, and like Habanero 3, it was designed to drill into only one main fracture so balancing more than one fracture was not necessary. The well was drilled with a mud weight close to balance while circulating. The reservoir could be tested by changing the mud circulation rate, with a low circulation rate giving a bottom hole pressure slightly lower than the

reservoir pressure and a high circulation rate resulting in a higher bottom hole pressure. A low-cost rotating head was used to allow back pressure to be applied up to 500 psi (3.45 MPa) so that the one connection to be made after penetrating the reservoir could be made with pumps off. The reservoir penetration and the trip following its drilling were made without difficulty.

Conclusions

Each of the wells drilled into the Innamincka Granite were drilled somewhat differently in order to overcome the problems of drilling highly conductive fractures filled with overpressured water. These differences resulted in different problems, and no one method has proved to be a panacea. They were:

Habanero 1: recognition of the overpressures resulting in large mud losses and multiple fluid influxes with multiple fractures open in the well. Loss of fracture conductivity due to mud losses.

Habanero 2: drilling with managed pressure drilling (MPD) to balance mud weights on fractures. Having two conductive fractures open in the same well section resulted in massive mud losses in the bottom fracture while balanced on the upper fracture to avoid fluid influx.

Habanero 2 sidetrack 1: no problems with MPD drilling because the bottom fracture was already significantly impaired by mud losses during drilling of the original hole

Habanero 2 sidetracks 2 to 4: drilling fully underbalanced with water using a snubbing unit so that hydrostatic pressure differences between fractures were the same in the well bore. No concern about mud damage. This method worked but had the problems of slow drilling, slow tripping and drilling small holes subject to mechanical failures. The operation failed to reach the main fracture.

Habanero 3: Drilling with MPD but expecting that only one fracture would be present in the well. Not suitable for creating multiple reservoirs to enhance output and heat recovery.

Jolokia 1: Drilling with MPD and cement squeezing any flowing fractures encountered. The aim was to access deeper fractures than that at Habanero. The drilling method worked but no productive deeper fractures could be stimulated.

Savina 1: Drilling underbalanced in order to increase penetration rate. This worked in the Cooper Basin sediments but could not be applied if a productive fracture was encountered.

Habanero 4: One major fracture drilled on-balance with pump rate variation dictating slight departure from reservoir pressure. A low pressure rated rotating head allowed connections to be made after the fracture had been penetrated.

A method to address the challenges of drilling multiple open overpressured fractures would be to use low mud weight or clear brine/water fluid. This requires controlling pressures of 34 MPa in the surface equipment with high temperature fluid (>200°C) returning to surface while drilling. These extreme conditions are not common in the oil and gas industry so equipment that can handle such high pressures and temperatures is not readily available. Some new experimental systems are currently under investigation including conventional rotary rig drilling and coil tubing drilling systems.

References

Denham, D., Windsor, C.R., 1991. The crustal stress pattern in the Australian Continent. Exploration Geophysics, 22, 101-105.

Fournier, R.O., 1979. A revised equation for the Na/K geothermometer. Geothermal Resources Council Transactions, 3, 221-224.

Somerville, M., Wyborn, D., Chopra, P.N., Rahman, S.S., Estrella D., Van Der Meulen, D.T., 1994. Hot Dry Rocks Feasibility Study, Energy Research and Development Corporation Report 94/243, pp. 133.

Subcritical Organic Rankine Cycles using Zeotropic Mixtures Working Fluids for Low Temperature Power Conversion

J. Zhang.[1], H. Gurgenci.[1], J. Czapla.[2], A. Rowlands 2, E. Sauret [2]

[1] Queensland Geothermal Energy Centre of Excellence, [2] The University of Queensland

j.zhang12@uq.edu.au

In recent years, much work has been undertaken to establish promising working fluids based on pure refrigerants for Organic Rankine Cycles (ORC) in order to optimize cycle performance at various conditions. The Queensland Geothermal Energy Centre of Excellence (QGECE) has been working on ORC power conversion systems with binary fluid mixtures to increase power generation from a given geothermal resource. At the moment, the Kalina cycle is the only commercially available mixed fluid cycle.

This paper focuses on exploring and optimizing zeotropic mixtures at low temperatures for geothermal energy conversion. An in-house developed Matlab ORC analysis program that makes use of Simulis thermodynamic database software was used to ascertain the performance of cycles of various mixture compositions. The specific brine benefit (β), a ratio of net work to hot resource mass flow, was used as the main metric to evaluate the performance depending on mixture composition, turbine inlet temperature and pressure. In this paper, several zeotropic mixtures are examined for a low-temperature geothermal power plant and are compared against the performance of each of the pure fluid components. At subcritical conditions, a fluid mixture of 50% R134a and 50% R245fa by mass fraction has the best performance (β =9.47 kJ/kg, at 90°C) without superheating at the same turbine inlet temperature, almost 50% higher than that of the pure fluids (β =7.63kJ/kg and β =4.19 kJ/kg, respectively, at 90 °C).

Key words: Zeotropic mixtures, Organic Rankine Cycle, Low temperature, Power conversion

Low-temperature binary geothermal power plant specification

Low to moderate-temperature water-dominated systems, with temperatures below 130°C, account for about 70% of the world's geothermal energy potential (Franco, 2011). In order to exploit these resources, binary power cycle technology have received much attention in recent years (Tchanche et al.,2011)(Chen et al.,2010).

For this study, the following parameters and conditions were assumed:

- Thermodynamic cycle: Organic Rankine Cycle without superheat;
- The system is at equilibrium and at steady-state;
- Pressure loss of pipes assumed negligible;
- Heat loss due to radiation from pipelines assumed negligible;
- Chemical exergies of the substances are neglected;
- The vapor quality at the turbine exit should be at least 90%;

The relative performance of cycles was measured using the metric β, specific brine benefit, a ratio of the network to mass flow rate of hot brine, as described in (Franco, 2011):

$$\beta = \frac{\dot{W}_{net}}{\dot{m}_{geo}} \quad (1)$$

The basic operation conditions are tabulated in Table 1 below.

Table 1: Standard parameters and boundary conditions of the geothermal ORC model

Parameter	
Turbine inlet temperature (T_5)	100°C
Geothermal water temperature (T_{ha})	T_5 +10°C
ΔT – Pinch – point (evaporation/condensation)	10°C
Cooling temperature (T_C)	27°C
Maximum pressure ORC	P_c *0.9
Isentropic efficiency of turbine	85%
Isentropic efficiency of pump	65%
Fixed turbine power output	100kW

As working fluids have a vital influence on the performance and the economics of the plant (Tchanche et al.,2011), for this case study, 5 promising refrigerants were investigated as 10 different combinations of binary zeotropic mixtures. Their basic physical and environmental data are tabulated in Table 2.

Table 2: Physical and environmental data of working fluids (Guo et al,2011)

Fluids	M kg/kmol	$T_{critical}$ °C	$P_{critical}$ MPa	Fluid Type	ODP	GWP (100yr)
R236ea	152.04	139.29	3.50	Dry	0	710
R134a	102.03	101.06	4.06	isentropic	0	1430
R152a	66.05	113.26	4.52	Wet	0	124
R245fa	154.01	153.87	3.64	Dry	0	1030
R227ea	170.03	102.8	3.00	Isentropic	0	2900

The performance of pure fluids and zeotropic mixtures

Combining these fluids results in 10 pairs of zeotropic mixtures that were investigated for a turbine inlet temperature of 363K: R245fa/R227ea, R134a/R236ea, R134a/R245fa, R245fa/R152a, R152a/R236ea, R245a/R236ea, R236ea/R227ea, R152a/R227ea, R134a/R227ea, R134a/R152a.

Figures 1(a) and (b) shows the results of the simulation for these mixtures; the data have been split across two figures for clarity. Based on the results for the zeotropic mixtures, it can be seen that R134a-R245fa has the highest β of any of the mixtures across a mass fraction composition range of 10-90% at 90 °C. Interestingly, a mass composition of 50/50[2] R134a/R245fa has the highest β (9.47 kJ/kg), almost 50% higher than that of either pure R134a (7.63 kJ/kg) or pure R245fa (4.19 kJ/kg) at the same conditions. R245fa/R152a also has relatively high β at the same conditions. Figure 1(c) and (d) shows that out of all the mixtures investigated, R245fa/R152a and R245fa/236ea have highest first law efficiencies (thermal efficiency, η) whilst overall, pure R245fa has best first law efficiency.

The performances of pure fluids and best zeotropic mixture are listed in Table 3. It can be seen from Figure 1 and Table 3 that the best mixture investigated (50/50 R134a/R245fa) does not simultaneously produce the highest β and the highest thermal efficiency. This highlights the importance of using β as a performance metric rather than relying on thermal efficiency, which does not best describe the cycle that makes optimal use of available energy.

Interestingly, for any given pure fluid pair at any mass fraction composition, the mixture will always produce a higher β than either the pure fluids. Mixtures can therefore be utilized to extend the range and power output of commonly investigated working fluids.
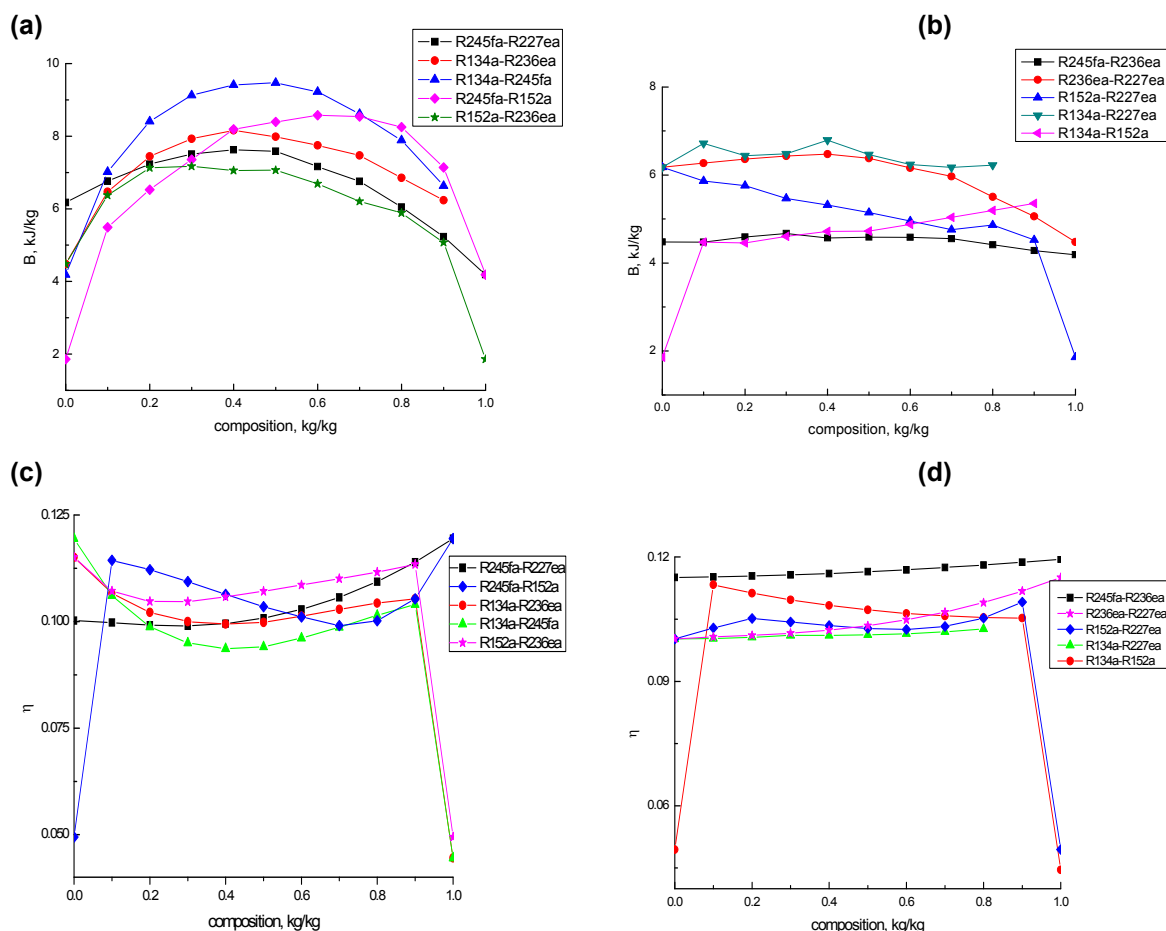

Figure 1: *the specific brine benefit and efficiencies depending on the composition at 90 °C for all mixtures.*

2 This presents the mass fraction composition of the mixture

Table 3: The performances of pure fluids and the best zeotropic mixture

	R236ea	R134a	R152a	R245fa	R227ea	0.5R134a/0.5R245fa
β (kJ/kg)	4.48	7.63	1.86	4.19	6.18	9.47
η	11.51	4.46	4.95	11.95	10.02	9.41

Now, as known from simulation, 50/50 R134a/R245fa may be the most competitive option. The three pairs of mixtures (namely 40/60 R134a/R245fa, 50/50 R134a/R245fa and 60/40 R134a/R245fa) are tested by ORC loop in QGECE Lab to validate the simulation results.

The use of working fluid mixtures benefits the design and costs of the power plant due to: the variation of mixture compositions can improve design parameters of cycle components; with suitable mixtures, the volume flow ratio of turbine is lower. This will have an influence in designing a turbine; because of the temperature glide in VLE of mixtures, the irreversibilities of the condenser visibly decrease (Heberle.F et al., 2012). Blends of refrigerants are commonly used in commercial refrigeration and air-conditioning facilities without difficulty. The ORC should not offer an extra challenge.

References

Franco, A.(2011). Power production from a moderate temperature geothermal resource with regenerative Organic Rankine Cycles. Energy for Sustainable Development, 15(4), 411-419.

Tchanche, B.F., et al.(2011). Low-grade heat conversion into power using organic Rankine cycles – A review of various applications. Renewable and Sustainable Energy Reviews, 15(8), 3963-3979.

Chen, H., D.Y. Goswami, and E.K. Stefanakos (2010). A review of thermodynamic cycles and working fluids for the conversion of low-grade heat. Renewable and Sustainable Energy Reviews, 14(9), 3059-3067.

Guo, T., H.X. Wang, and S.J. Zhang (2011). Selection of working fluids for a novel low-temperature geothermally-powered ORC based cogeneration system. Energy Conversion and Management, 52(6), 2384-2391.

Heberle.F et al. (2012), Zeotropic mixtures as working fluids in Organic Rankine Cycles for low-enthalpy geothermal resources. Renewable Energy, 37, 364-370.